GEOCHEMICAL ELUCIDATION OF GNEISS - HOSTED MASSIVE SULFIDE DEPOSITS

by

Bernard E. Gaboury

A thesis
presented to
the University of Manitoba
in partial fulfillment of the
requirements for the degree of
Master of Science
in
Department of Earth Science

Winnipeg, Manitoba, 1986

ISBN Ø-315-33599-8

GEOCHEMICAL ELUCIDATION OF GNEISS - HOSTED MASSIVE SULFIDE DEPOSITS

BY

BERNARD EMILE GABOURY

A thesis submitted to the Faculty of Graduate Studies of the University of Manitoba in partial fulfillment of the requirements of the degree of

MASTER OF SCIENCE

I hereby declare that I am the sole author of this thesis.

I authorize the University of Manitoba to lend this thesis to other institutions or individuals for the purpose of scholarly research.

Bernard E. Gaboury

I further authorize the University of Manitoba to reproduce this thesis by photocopying or by other means, in total or in part, at the request of other institutions or individuals for the purpose of scholarly research.

Bernard E. Gaboury

The University of Manitoba requires the signature of all persons using or photocopying this thesis. Please sign below, and give address and date.

ABSTRACT

Massive sulfide deposits in gneissic terrains are hosted by rocks which have a greater proportion of sedimentary component than comparable deposits located in adjacent greenstone terrains.

Wall - rock petrography and 223 chemical analyses for six gneiss - hosted deposits are presented. Four deposits are situated in the Canadian Shield (Sherridon, Manitoba; Geco, Ontario; Montauban, Quebec and New Calumet, Quebec); one is in the Proterozoic core of the Colorado Front Ranges, U.S.A. (North Maysville) and one is in the Willyama Structural Province of the Australian Shield (Broken Hill, N.S.W.). The high metamorphic grades involved in these gneiss-hosted ore deposits mask the original characteristics of the host rocks.

Chemical variation diagrams indicate that the sillimanite - bearing gneisses and schists common to all the deposits are rocks with low quantities of K_2O, CaO, Na_2O and TiO_2, geochemically similar to the less altered volcanic rocks found at the outer margins of the alteration pipes associate with some volcanogenic massive sulfide deposits of greenstone terrane. Cordierite - anthophyllite rocks have some of the attributes of iron formations, and also some of the attributes of those rocks found at the cores of the alteration pipes associated with volcanogenic massive sulfide deposits of greenstone terranes. They are enriched, with respect to other enveloping rocks, in MgO and FeO and contain low quantities of Na_2O, CaO, K_2O, Ni and TiO_2. Results indicate that the metamorphic host rocks of gneiss - hosted ore deposits represent physical mixtures of epiclastic sediments (some of which may be altered volcanic material erupted from a hydrothermal vent) and chemical sediments (whose source is the same hydrothermal vent).

ACKNOWLEDGEMENTS

The author would like to express gratitude to Selco Inc. and Noranda Ltd. (Geco Division) for their aid in acquiring data for this study. The author is indebted to Dr. P. Laznicka for his supervision of this study.

A word of thanks to Dr. C.D. Anderson and Irene Berta for their moral support.

The author would like especially to thank his family for their support; both material and spiritual.

"The heavens declare the glory of God, and the firmament proclaims His handiwork... "

Psalm 19

TABLE OF CONTENTS

Page

CHAPTER I

STATEMENT OF THE PROBLEM

1.1 Introduction

Although the known occurrences of base metal (Cu, Zn, Pb) massive sulfide deposits in gneissic terrain are fewer in comparison with similar deposits in greenstone terrain, some of the largest deposits of this class (Broken Hill, N.S.W.; Gamsberg, South Africa and Prieska, South Africa) are found in this setting. The origin and depositional environment of these deposits are enigmatic.

The mutual relationship of granite - greenstone and granulite - gneiss terrains is a research problem of long standing, but is still inconclusively interpreted. Beakhouse (1985) has put foreward a model which portrays the relationship of the English River Gneiss Belt and the greenstone - tonalite paragneisses adjacent to its northern and southern contacts as a former lithofacies change between fundamentally different depositional environments. He has suggested that the sedimentary precursors of the Ear Falls - Manigotogan paragneisses were deposited synchronously with the volcano - sedimentary precursors of the adjacent greenstone - tonalite terrains. A similar genetic relationship has been ascribed to the Kisseynew Gneiss Belt and the flanking Flin Flon - Snow Lake Greenstone Belt in the Churchill Structural Province of the Canadian Shield (Gale et al, 1980; Bailes and McRitchie, 1978) and to the Quetico Gneiss Belt and its flanking greenstone belts in the Superior Structural Province of the Canadian Shield (Goodwin et al,

1972; MacKasey, Blackburn and Trowell, 1974). If greenstone and adjacent gneissic terrains developed contemporaneously, an analogy or correlation may be drawn between those massive sulfide deposits of greenstone terrain and those of gneissic terrains. Such a correlation has in fact been made for massive sulfide deposits of the volcano - sedimentary "exhalative" type (Fe Cu Zn $\pm$ Pb composition) (Gale et al, 1980) and may be expanded to include other massive sulfide deposits generated in a comparable geotectonic setting elsewhere (i.e. at convergent plate boundaries).

1.2 Scope of the Thesis

Table 1-1 is a compilation of data on selected massive sulfide deposits, grouped according to ore metal composition. Included with some of the more pertinent characteristics of these deposits are some conclusions on their possible genesis, summarized from the literature. This compilation includes the five North American massive sulfide deposits which are further treated in this study plus other deposits, all of which have been subjected to various degrees of metamorphism.

The five North American deposits considered here are located in the Churchill Structural Province of the Canadian Shield (Sherridon area of Manitoba); in the Grenville Province of the Canadian Shield (New Calumet and Tetreault Mines, Quebec); in the Superior Structural Province of the Canadian Shield (Geco Mine, Manitouwadge, Ontario); and in the Precambrian basement of the Colorado Front Ranges (N. Maysville deposit, Colorado). The general setting of all these deposits fits the general model of gneiss belt stratigraphy suggested by Wilson et al (1976).

TABLE 1-1 Compilation and Brief Description of Selected Massive Sulfide Deposits of the World Arranged by Ore Metal Composition.

METAL TYPE	EXAMPLE	REGION	GEOLOGY	HOST LITHOLOGY	TONNAGE (tonnes) & GRADE	PROPOSED ORIGIN	REFERENCE
Fe,Zn,Pb (Cu)	Falun, central Sweden	Bergslagen	concordant sulfide mineralization occurs within a series of felsic to intermediate volcanics and associated sedimentary rocks metamorphosed to amphibolite facies	mineralization is hosted by quartz-feldspar gneisses referred to as "leptites". Intercalations of metalimestone, & iron formation occur within the metavolcanics which are overlain by metamorphosed pelites, and greywackes.		metamorphogenic or chemical-sedimentary	Magnusson (1950) Magnusson
	Sullivan south central B.C. Canada	base of the upper Proterozoic Purcell Supergroup	well laminated massive sulfide orebody occurs within greywakes & argillites of the Lower Aldridge Fm. Orebodies are concordant and stratigraphically underlain by an alteration pipe	footwall rocks consist of tourmalinized breccia & stockwork. Argillites occur as interbands within the well-banded massive lead, zinc and iron sulfides. Hanging wall argillites & greywackes are locally albitized.	155 M 6.6% 5.7 Zn 68 g.Ag	exhalative-sedimentary origin associated with basin development	Gustafson & Williams (1981)
	Broken Hill Main Lode N.S.W. Australia	Broken Hill Block of the Willyama Complex	6 large productive Ag-Pb-Zn lodes concordant with the metamorphic fabric are located in a small drag fold on the east flank of a major syncline	metamorphic rocks that host the orebodies consist of felsic gneises overlain by banded iron formation & amphibolite. The "Potosi Gneiss" (meta-rhyolite), amphibolite, banded iron formation & psammopelitic gneisses are rock units most closely associated with the ore lenses	180 M 11.3% Pb 9.8% Zn 75 g.Ag	mineralization is spatially & probably genetically related to banded iron formations	Gustafson & Williams (1981)
	Tetreault Mine Montauban Quebec Canada	Grenville structural province	massive sulfide bodies concordant with the local tectonic fabric occur within Proterozoic metavolcanic & metasedimentary gneisses of the Grenville Supergroup	host rocks include a cordierite-anthophyllite rock, meta-carbonate, calc-silicate and quartz-feldspar-biotite gneiss	2.4 M 4.53% Zn 1.54% Pb 75 g.Ag .6 g.Au	volcanic-exhalative	Stamatelopoulou-Seymour & MacLean (1977) McAdam & Flannagan (1976)
	New Calument Mine Calumet Island, Quebec, Canada	Grenville Structural Province	massive sulfide bodies concordant with tectonic fabric of host gneisses	host rocks include a cordierite-anthophyllite rock, calc-silicate gneiss amphibolites, metaquartzites & quartz-feldspar-biotite gneisses	4 M 6.5% Zn 1.8% Pb 40 g.Ag	?	Moorhouse (1941) McAdams & Flannagan (1976)
Fe,Cu (Zn)	N.Maysville near Salida, Colorado U.S.A.	Proterozoic core of the Colorado Front Ranges	several small tabular bodies of massive & disseminated sulfides concordant with the local tectonic fabric	series of quartz-feldspar-(biotite) gneisses and schists, iron formation and amphibolites	55,000 5% Cu	volcanic-exhalative	Knight (1981)
	Coronation Mine S.W. of Flin Flon, Canada	Flin Flon Greenstone belt Churchill Province	three concordant orebodies of massive and/or disseminated sulfides within volcanic flows pyroclastics with subordinate amounts of clastic sediments of the Amisk Super-group	ore is hosted predominantly by a cord.-anth. rock. Other rocks include biotite gneisses, amphibolities and felsic gneisses of volcanic origin	1.4 M 4.2% Cu	volcanogenic "similar to Flin Flon"	Whitmore (1968)

TABLE 1 - 1 (cont'd)

METAL TYPE	EXAMPLE	REGION	GEOLOGY	MOST LITHOLOGY	TONNAGE (tonnes) & GRADE	PROPOSED ORIGIN	REFERENCE
Fe,Cu (Zn) cont'd	Millenbach Mine, 8 km. N.of Noranda	Abitibi Greenstone Belt	concordant lenses of massive sulfides with underlying alteration pipes are usually associated with small domes of massive rhyolite	the ore lenses & their associated alteration pipes are hosted by rhyolites and andesites of a thick multi-cycle volcanic pile. Massive sulfides grade laterally into a siliceous tuff.	2.7 M 3.5% Cu 4.5% Zn	volcanogenic, partially exhalative	Large (1977) Knuckey et al. (1982)
Fe,Cu, Zn	Ruttan Mine 20 km. east of Leaf Rapids, Canada	Rusty Lake Greenstone Belt	massive sulfide bodies occur at the contact between volcaniclastics and greywackes within and "exhalite" horizon in a series of basaltic flows, andesitic volcaniclastics, "exhalites" and greywacke sediments	thick greywackes form the footwall strata', the orebody itself grades laterally in to a felsic volcaniclastic while the hanging wall sequence consists of greywacke, conglomerate, iron formation & a few mafic flow units	45.5 M 1.4% Cu 1.6% Zn	volcanogenic	Speakman et al (1982)
	Brittania Mine 40 km N. of Vancouver Canada	The Brittania roof pendant of the Coast Plutonic Complex.	concordant massive sulfides occur in a series of mid-Mesozoic volcanic and associated sedimentary rocks	ore is situated at an unconformity (representing a hiatus) which separates a tuff breccia from a dacitic volcano-sedimentary rock.	50 M 1.1% Cu. .65% Zn 6 g.Ag .6 g.Au	sedimentary-volcanogenic "similar to other base metal camps of Canadian greenstone belts	Payne et al (1980)
	Pyhasalmi-Pielavesi district of central Finland	Svecofennides of Scandanavia	several massive sulfide orebodies occur in a series of volcanic and related metasedimentary rocks, concordant with the local tectonic fabric	host rocks include mafic to intermediate volcaniclastics, "carbonate exhalites" and aluminous greywacke sediments (biotite-plagioclase gneisses)		volcanic-exhalative	Sangster & Scott (1976)
	Geco 5 km east of Manitouwadge, Canada	boundary of the Wawa & Quetico subprovinces of the Superior province	concordant massive and disseminated sulfide bodies occur in an overturned sequence of sedimentary & volcanic rocks metamorphosed to almandine-amphibolite grade	stratigraphic footwall rocks are a biotite-garnet-cordierite-anthophyllite gneisses of possible sedimentary origin. Hanging wall rocks include iron formation, quartz-feldspar-biotite gneiss, & hornblende-plagioclase gneiss.	Production: 26.9M of 1.97% Cu 4.01% Zn 61.4 g.Ag	sedimentary-volcanogenic	Friesen et al. (1982) Hutchinson (1982)
	Sherridon deposits of Sherridon, Manitoba, Canada	Kisseynew gneiss belt	two thin but extensive tabular massive sulfide orebodies occur at the same stratigraphic horizon in a series of highly metamorphosed shelf sediments of the Sherridon Group	a cordierite-anthophyllite unit occurs in the footwall of both deposits. The Jungle & Park Lake deposits, also, within the Sherridon Structure, occur at the same horizon. Other host-rocks include siliceous pelitic and calc-silicate gneisses & amphibolites.	7 M 2.37% Cu 2.78% Zn	chemical sedimentary	Goetz (1980) Goetz & Froese (1982) Hutchinson (1982)
	Prieska 50 km SW of Prieska S. Africa	Namaqua-Natal Mobile belt	concordant sulfide bodies occur in highly metamorphosed fine clastic & chemical sedimentary rocks in a sequence of mafic to felsic volcanics	carbonate, calc-silicate & mica-rich zones are closely associated with ore. The orebody is enveloped by a meta-quartzite & is hosted by a series of calc-alkaline meta-basalt, andesite, dacite, & rhyolite flows & pyroclastics	42.7 M 1.7% Cu 3.8% Zn	syngenetic pyroclastic	Middleton (1973) Anhaeuser et al. (1976)

They are all hosted by, or are closely associated with, a sillimanite - bearing light colored schist or gneiss and a cordierite - anthophyllite bearing schist or gneiss. Both of these rock types are characterized by imbalances of alkalies and CaO in comparison with unaltered volcanic rocks formed in an island arc setting, as is the case attributed to the origin of the deposits of the Noranda camp or Flin Flon. It would appear that if these rocks were volcanic in origin, they have been altered or modified during or after deposition.

The purpose of this thesis is to contribute to the determination of the origin of gneiss - hosted massive sulfide deposits using petrography and bulk chemistry. Chemical variation diagrams are used to characterize enveloping host rocks of these deposits and to compare them to normal unaltered igneous and sedimentary rocks selected from the literature (listed in Appendix B-1). A comparison is also made with altered volcanic rocks from two volcanogenic massive sulfide deposits of greenstone terrains selected from the literature (listed in Appendices B-8 and B-9). Finally, a comparison is made with the hydrothermal alteration resulting from hot spring activity in felsic igneous environments (Appendix B-6 and B-7). An attempt has been made to determine whether the chemically anomalous schists and gneisses are hydrothermally altered products or whether they are, in part, rocks augmented during the time of deposition by a chemical sedimentary component.

CHAPTER 2

SAMPLING METHODS AND FIELD RECONNAISANCE

2.1 Sampling Methods

Localities investigated for this study were selected on grounds of presence in Precambrian gneiss belts and their general compatibility with the stratigraphic model discussed by Wilson (1976). The selection was limited to deposits of at least amphibolite facies metamorphism, and characterized by sillimanite - bearing units closely associated with ore. The sillimanite - bearing gneisses or schists were considered of particular interest since it has been postulated that these may represent, in whole or in part, metamorphosed aluminous chemical sedimentary products (Stanton 1979, 1984). Each of the deposits investigated is associated with a complex folded synformal structure in which the original strata are now steeply dipping.

Due to the frequently intimate interlamination of ore and host gneiss or schist, detailed sampling was required (when possible) in order to detect fine scale chemical variations which would aid in determining the original composition and relationship of host rocks and ore. Care was taken to avoid sampling proximal to rocks displaying signs of anatexis, because partial melting of rocks would alter their pre-metamorphic composition and this would render determination of precursor composition impossible. The assumption that metamorphism has been isochemical has been made (Stanton, 1979). Samples collected in

the field were approximately two kilogram unweathered pieces, with the exception of diamond drill core samples, which were, obviously, smaller. A total of 223 samples were collected from the field, and 274 analyses were obtained from the literature. These are listed, respectively, in Appendices A and B.

2.2 Field Reconnaisance

Fig. 2-1 shows sampling sites in the metasedimentary rocks of the Ear Falls gneiss belt in the English River Subprovince in Ontario. The area contains iron - enriched, sulfide - bearing metasedimentary rocks hosted in quartz - feldspar - biotite paragneisses. The metasedimentary rocks of the Ear Falls area were studied with the purpose of determining the relationship between the ferruginous, presumably chemical sedimentary rocks, and their clastic sedimentary hosts, both presently metamorphosed to amphibolite facies metamorphism.

An examination of orebodies in the Grenville Province at Montauban and New Calumet was completed during a field trip in October 1979, sponsored by Selco Inc. Samples, in the form of diamond drill core were recovered at the former Tetreault mine site. Additional hand samples of the cordierite - anthophyllite schist and calc - silicate gneiss were taken from locations depicted in Fig. 2-2. Samples from each major stratigraphic unit were from drill core from the Bowie deposit on Calumet Island, Quebec. At both localities, the drill samples were tentatively identified both megascopically and under the microscope, and

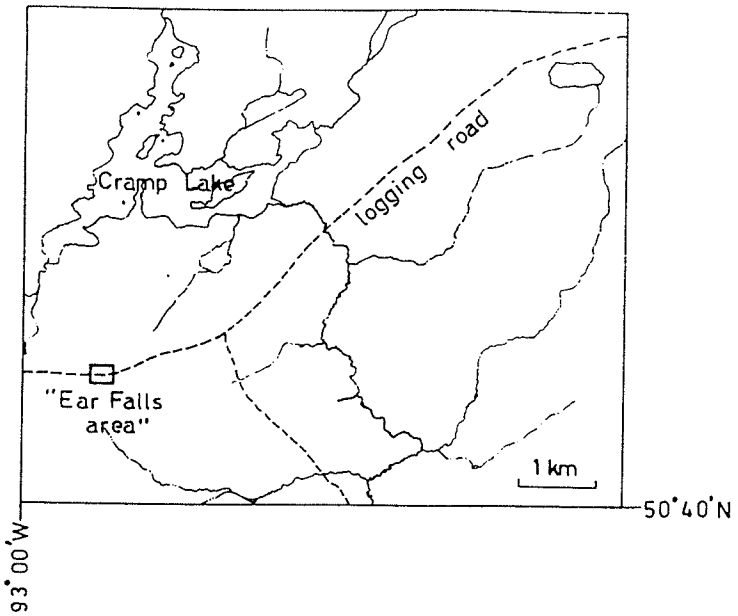

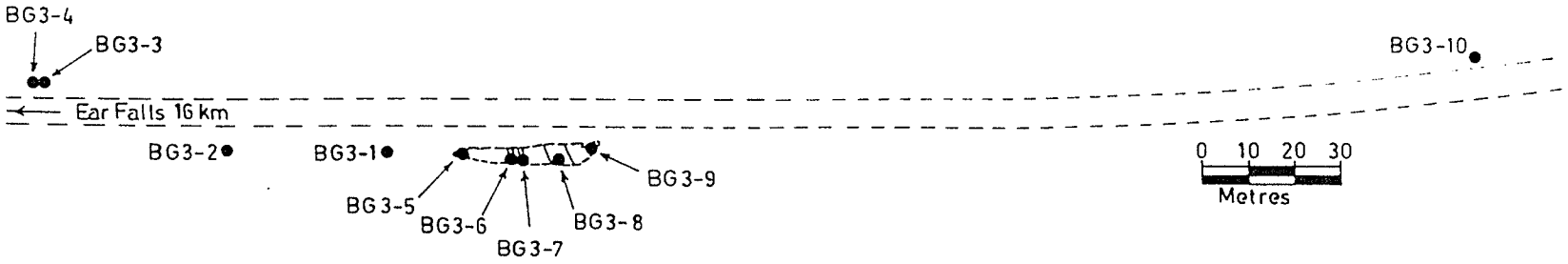

FIGURE 2-1 TOP: Sample localities in the Ear Falls area
BOTTOM: Detail of sample sites along the Reed Paper Co. logging rd.

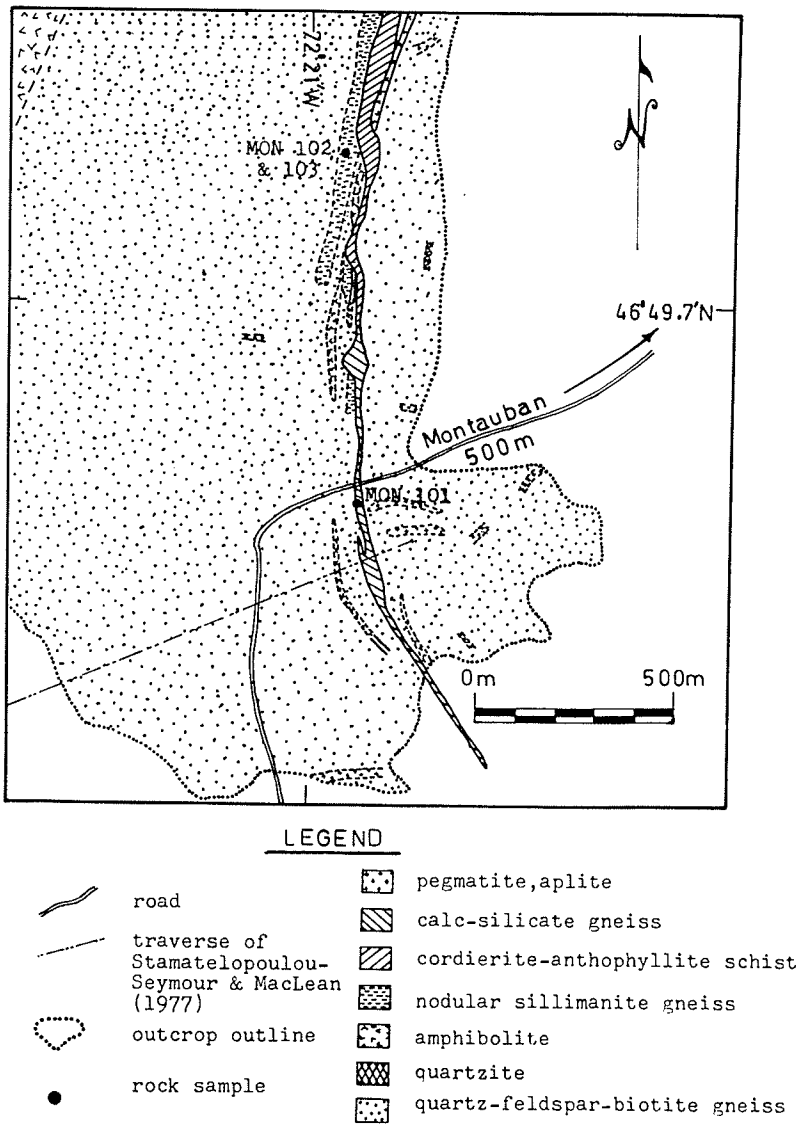

FIGURE 2-2 Local geology of the Montauban deposit with sample locations. Also shown is the traverse of Stamatelopoulou-Seymour and MacLean (1977).

assigned to the local stratigraphic units on the basis of published mine maps and descriptions. The rock types sampled are listed in Table 2-1.

Table 2-1: Rock types selected from the diamond drill core at New Calumet, Quebec (Fig. 3-12).

Sample numbers	Rock type
Clm 1 to Clm 5	amphibolite
Clm 6 to Clm 31	sillimanite gneiss
Clm 32 to Clm 35	metacarbonate (marble)
Clm 36 to Clm 45	garnet - sillimanite gneiss

Field studies made in April 1980 and December 1982 at the Geco Mine, Manitouwadge (Fig. 2-3) consisted of a traverse across the local stratigraphy to the south of the orebody (Fig. 2-4) followed by detailed sampling of the "Sericite Schist group" and "Granite Gneiss group" (informal terms employed locally by the Geco geological staff). Samples taken in the surface traverse utilized the rock - unit subdivision given by Milne (1969), and located in Fig. 2-4. Figs. 2-5, 2-6, 2-7, and 2-8, indicate the locations of samples collected underground. This was carried out with the aid and assistance of the Geco Mine geological staff.

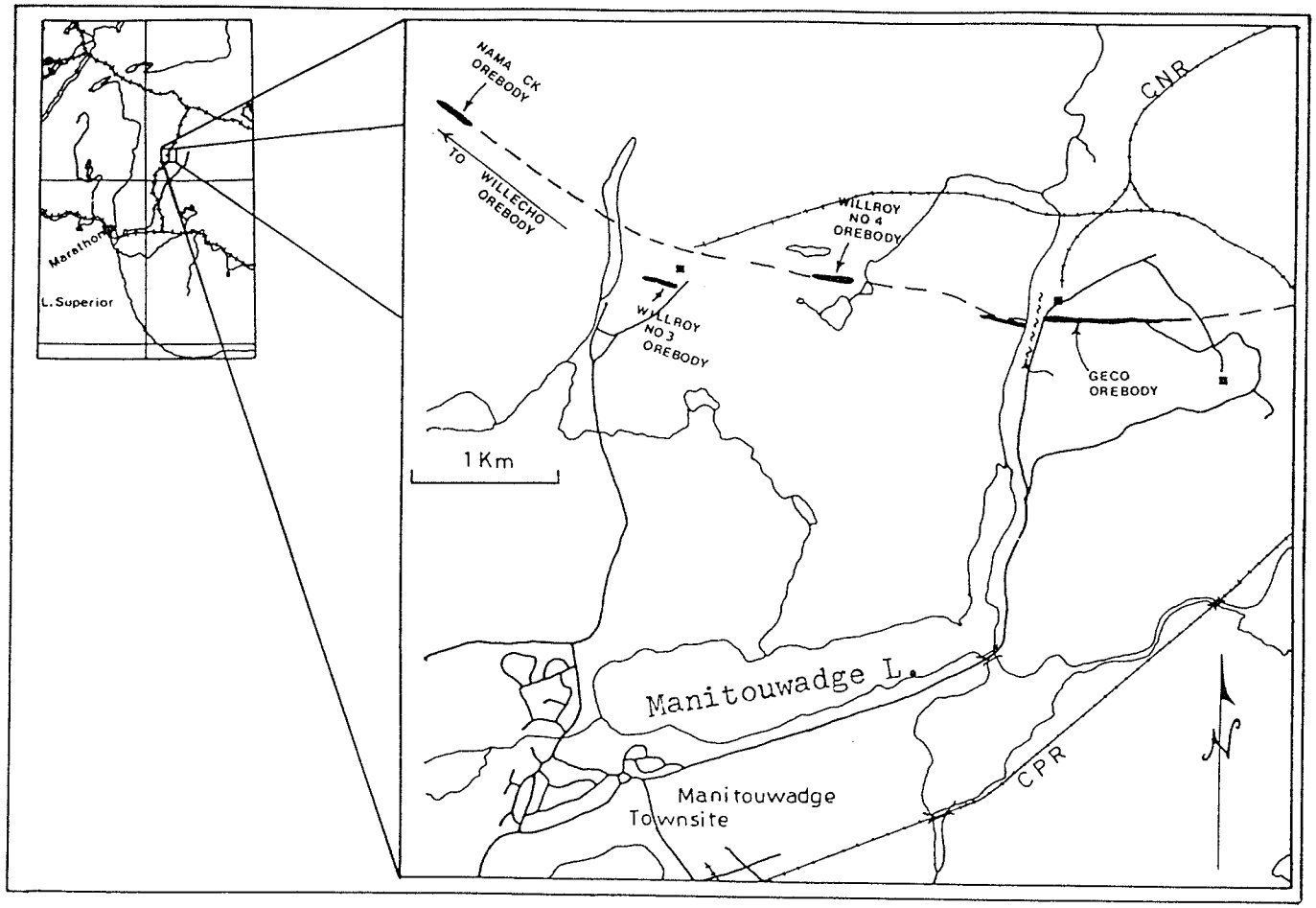

FIGURE 2-3 Location map for the Manitouwadge area showing the Geco Mine and some of the smaller neighboring deposits.

FIGURE 2-4 Geology of the area surrounding t Geco Mine (modified after Milne, 1969). Also depicted are location of samples collected along a surface traverse to the south of mine.

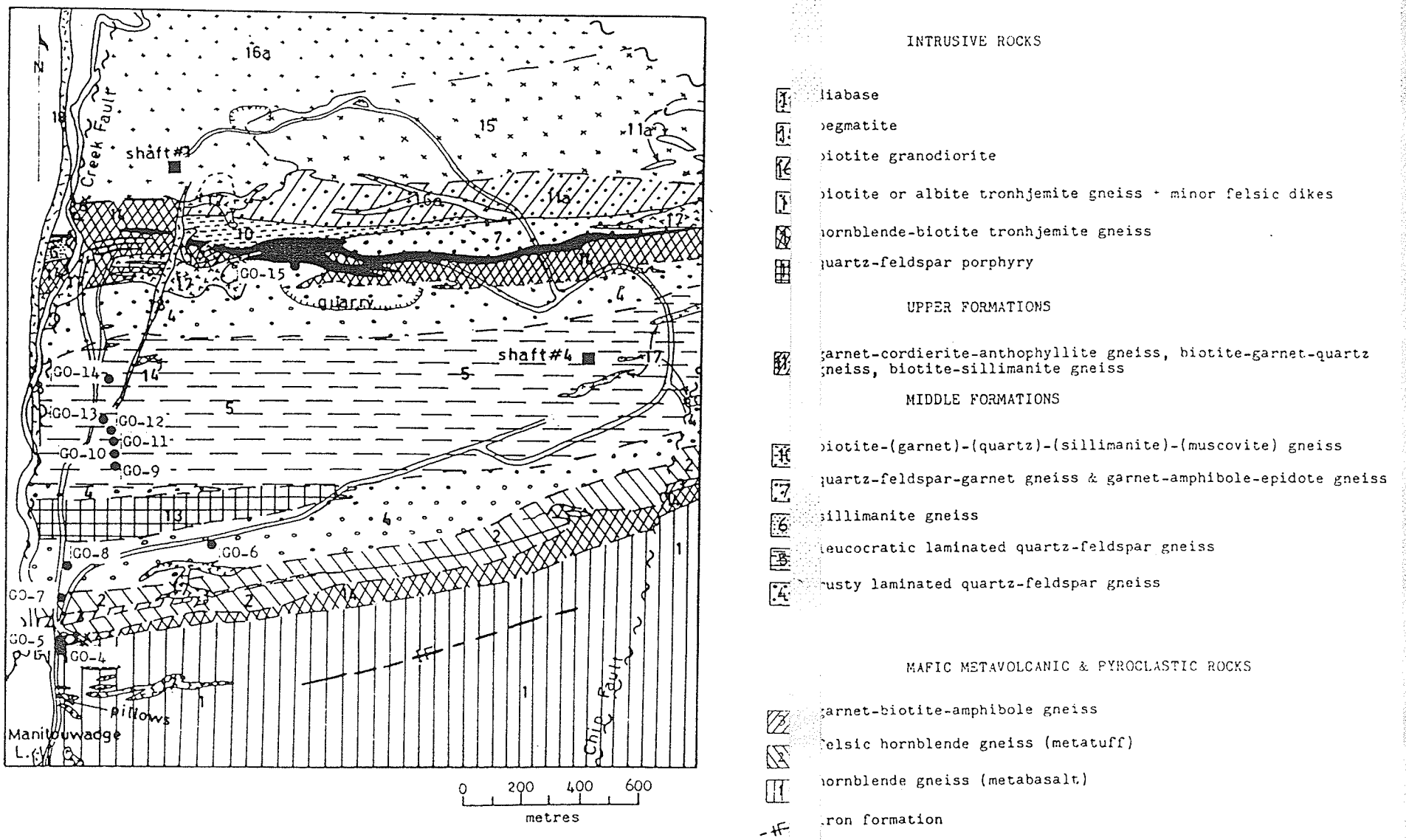

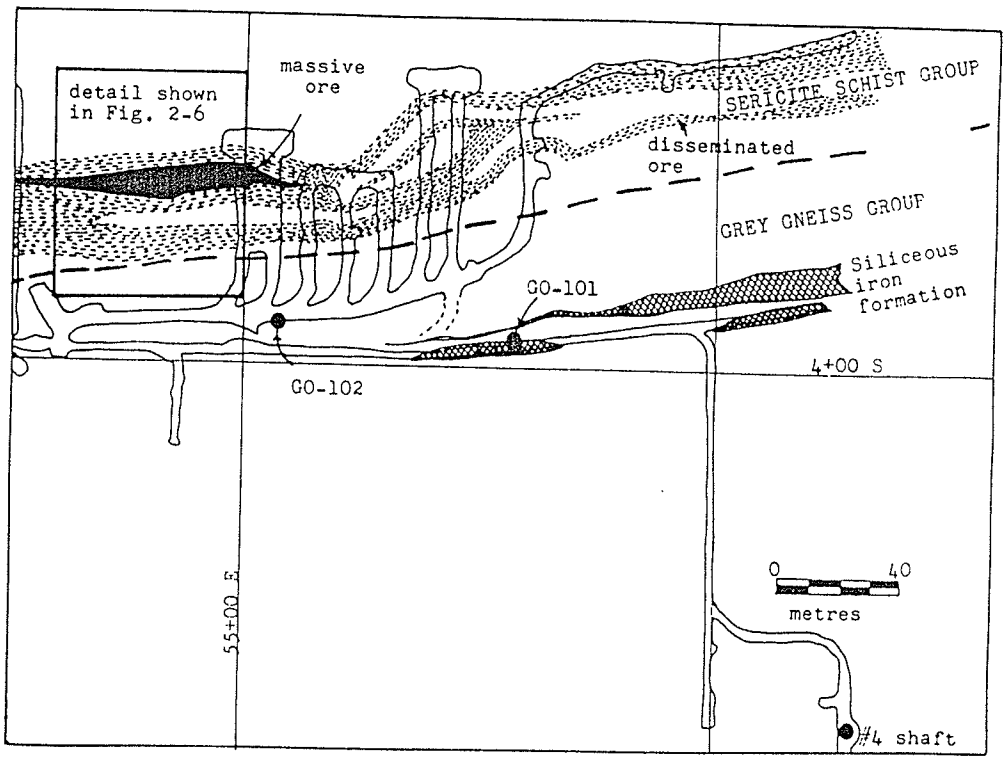

FIGURE 2-5 Geology of the 2450 level at the Geco Mine showing area depicted in Figure 2-6. (based on mapping by Geco geological staff)

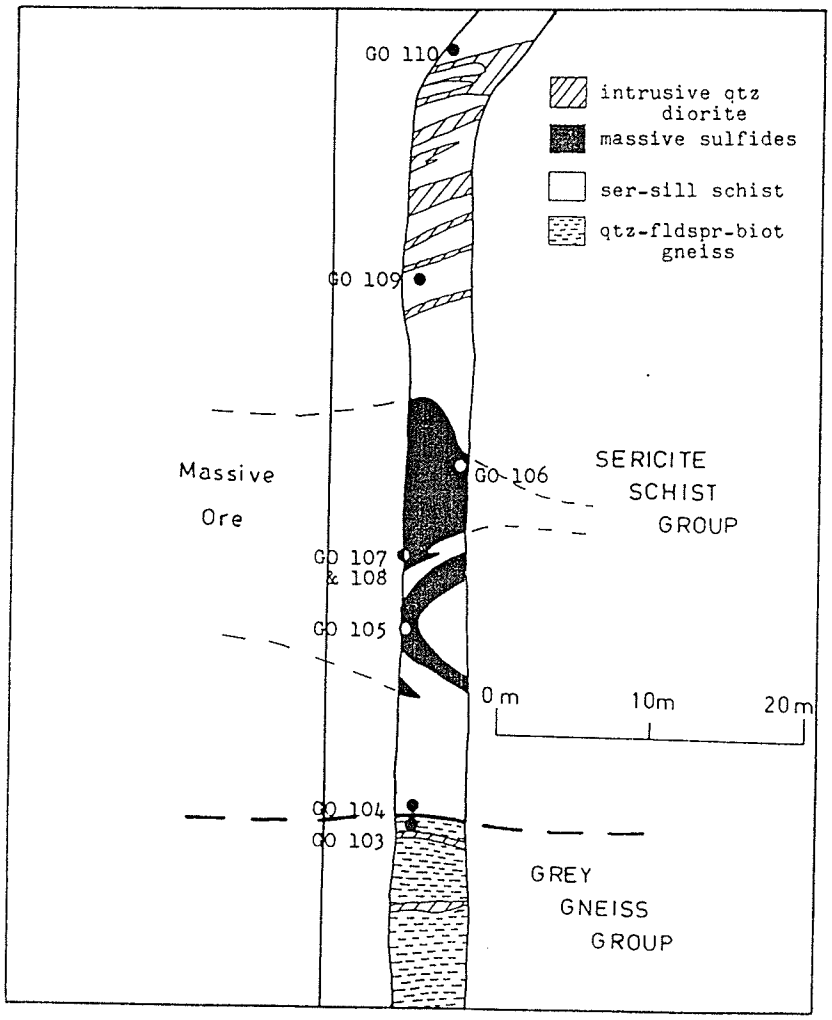

FIGURE 2-6 Geology and sample locations along the 23-54 cross-cut (see location of this section in Fig. 2-5)

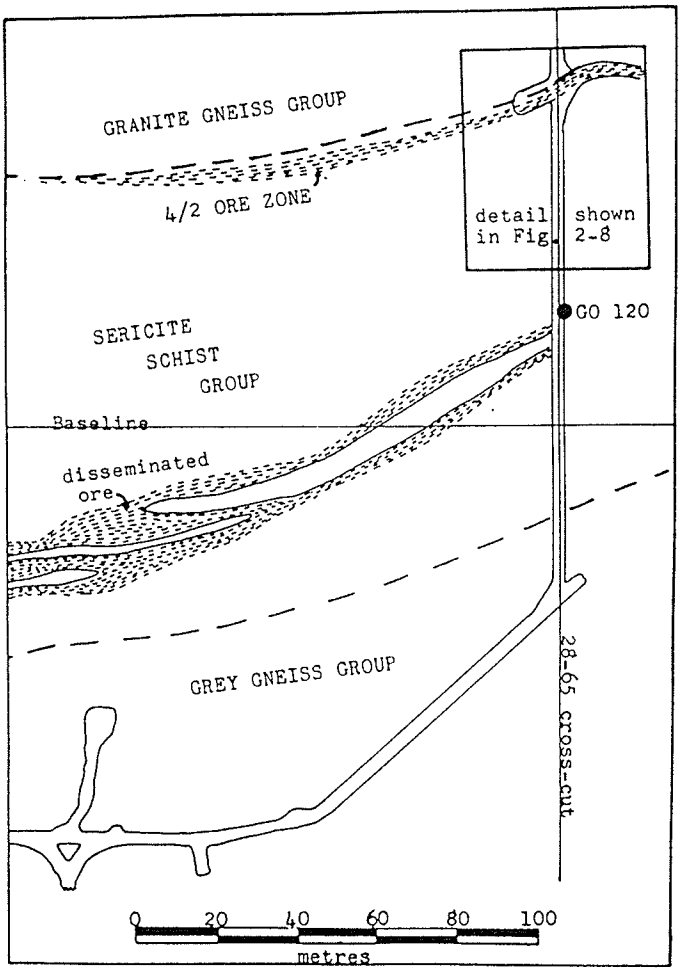

FIGURE 2-7 Geology of the 2850 level of the Geco Mine showing the area depicted in Figure 2-8 (based on mapping of Geco geological staff)

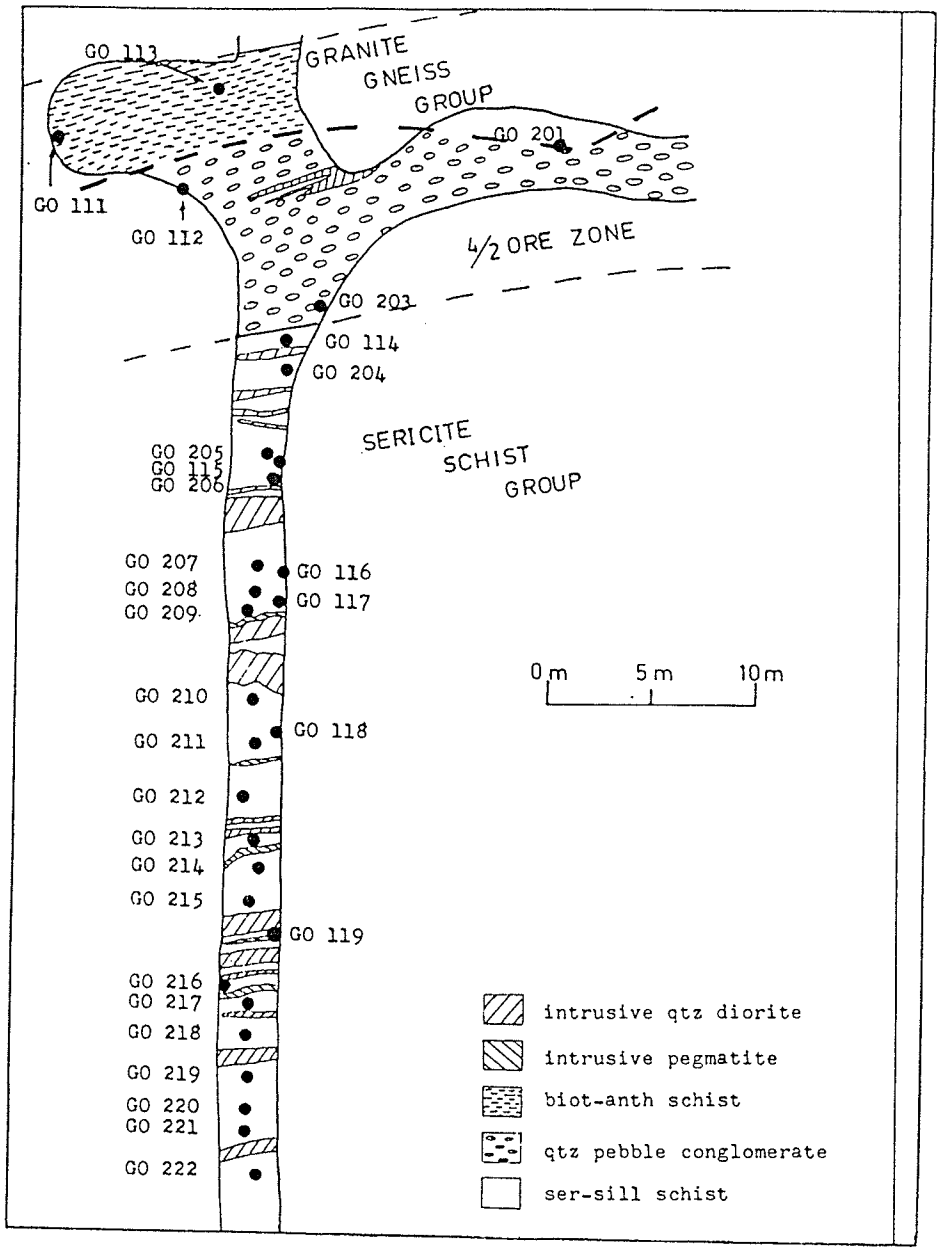

FIGURE 2-8 Geology and sample locations along the 28-65 cross-cut at the Geco Mine. (based on the mapping of Geco geological staff)

Field studies made on Yakushavitch Island in the Sherridon area of Manitoba, consisted of examination and sampling of diamond drill core made available by Selco - B.P., Ltd. This trip took place in March 1982 and was the last field trip made for the purpose of this thesis. Locations of two diamond drill holes sampled are shown in Figs. 2-9, 2-10, 2-11, and 2-12.

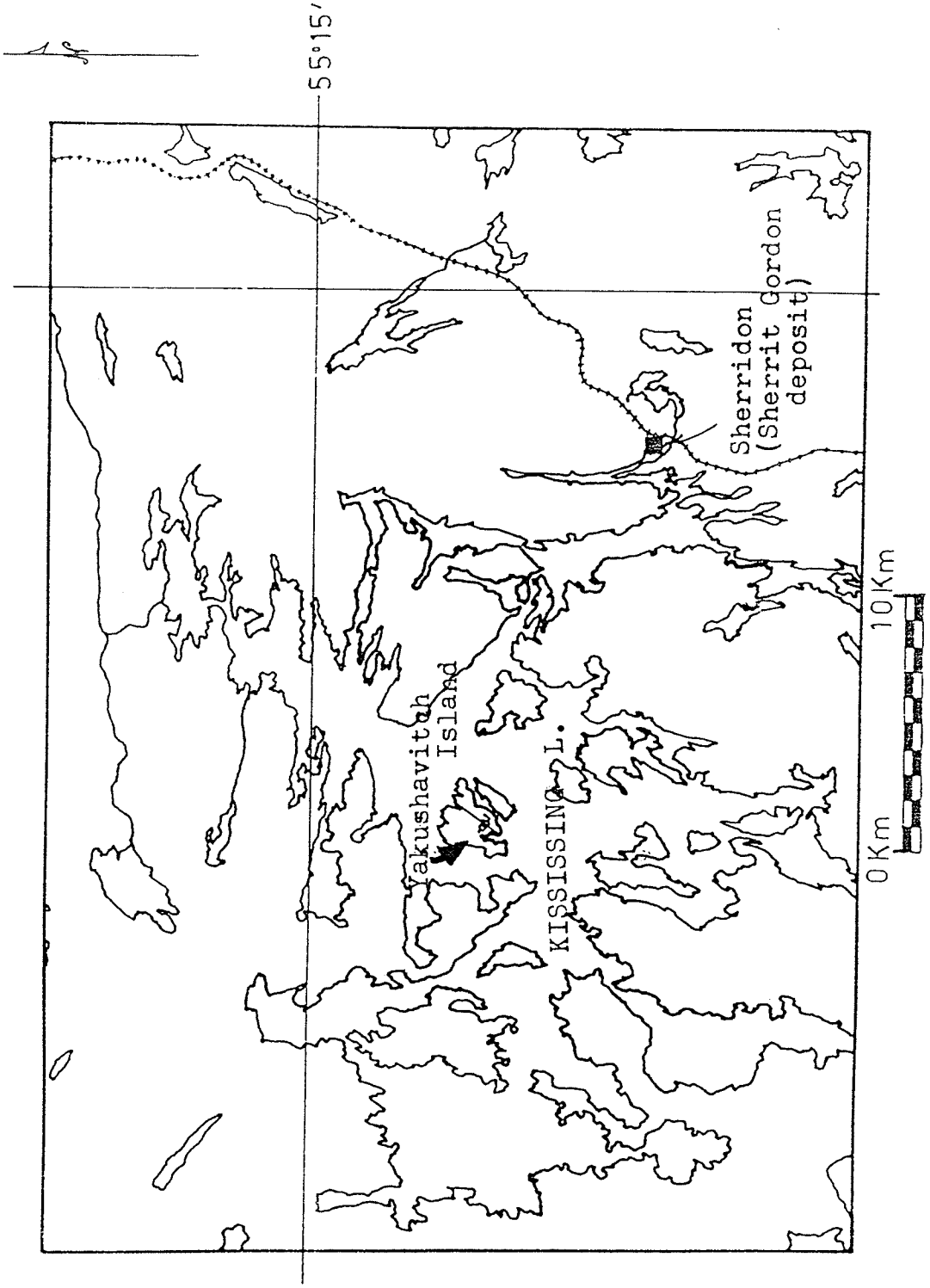

FIGURE 2-9 Location map, Sherridon area, Manitoba

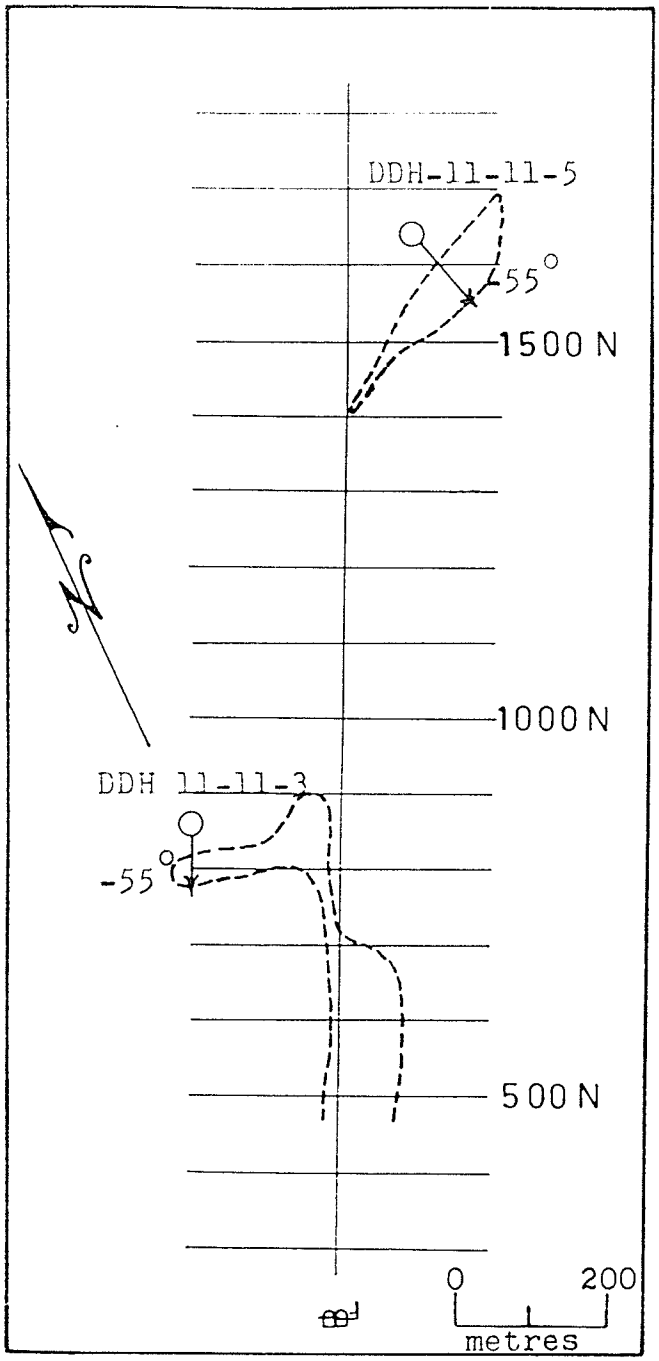

FIGURE 2-10 Detailed location of the diamond drill holes sampled on Yakushavitch Island, Kississing Lake, Manitoba. Modified after Desnoyers, 1981.

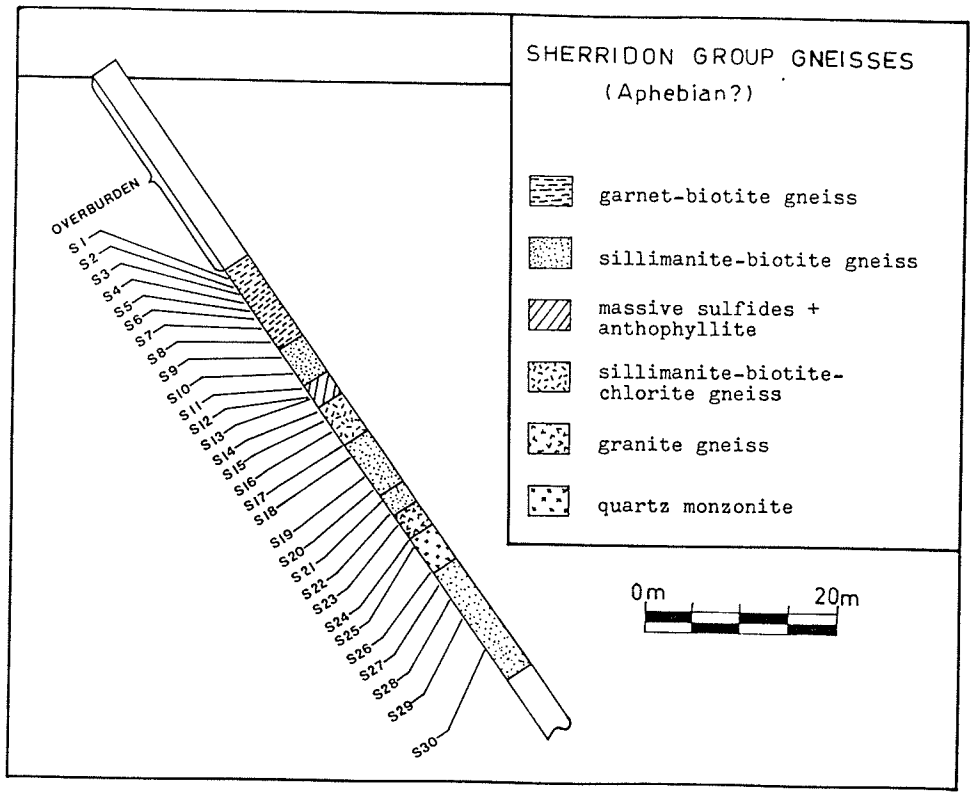

FIGURE 2-11 Diamond drill section of DDH-11-11-5, Yakushavitch Island, showing geology and sample locations.

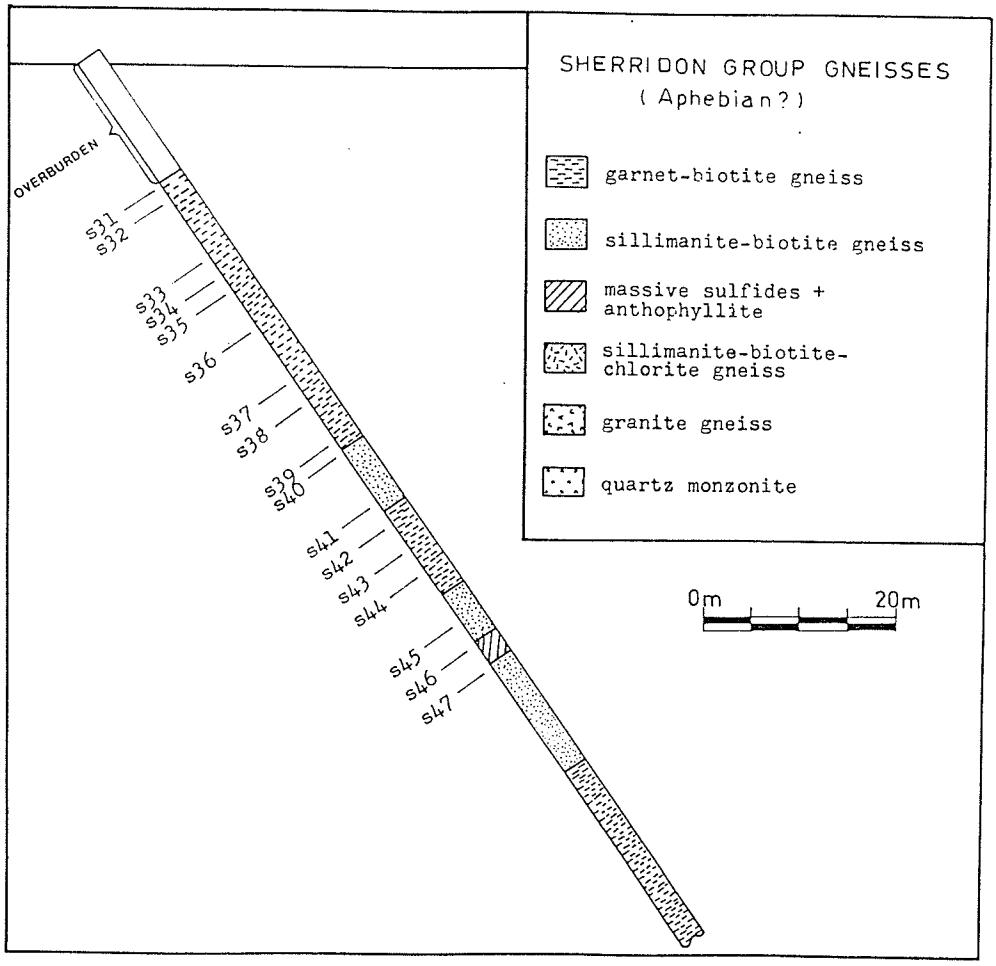

FIGURE 2-12 Diamond drill section of DDH 11-11-3, Yakushavitch Island, showing geology and sample locations.

CHAPTER 3

GEOLOGY OF THE DEPOSITS STUDIED: BRIEF INTRODUCTION

3.1 "Ear Falls area", Ontario

The Ear Falls Gneiss Belt is a series of highly metamorphosed sedimentary rocks which forms part of the English River Subprovince (Beakhouse, 1985) (Fig. 3-1). Metamorphic grades within these sedimentary rocks vary from amphibolite to granulite facies (Beakhouse, 1985). The English River Subprovince is characterized by belts of metamorphosed basic lavas, intermediate to felsic lavas and pyroclastics, greywacke and shale, whose boundaries are faults or metamorphic gradients (Wilson, 1971). This succession is conformable and the basic lavas dominate the basal section (Douglas, 1976). The metasedimentary rocks of the Ear Falls Gneiss Belt (Beakhouse, 1985) are folded about easterly trending axes which are locally cross-folded about north trending axes (Douglas 1976). Easterly - striking faults and small ultramafic intrusive bodies, are also characteristic of the English River Subprovince (Douglas, 1976).

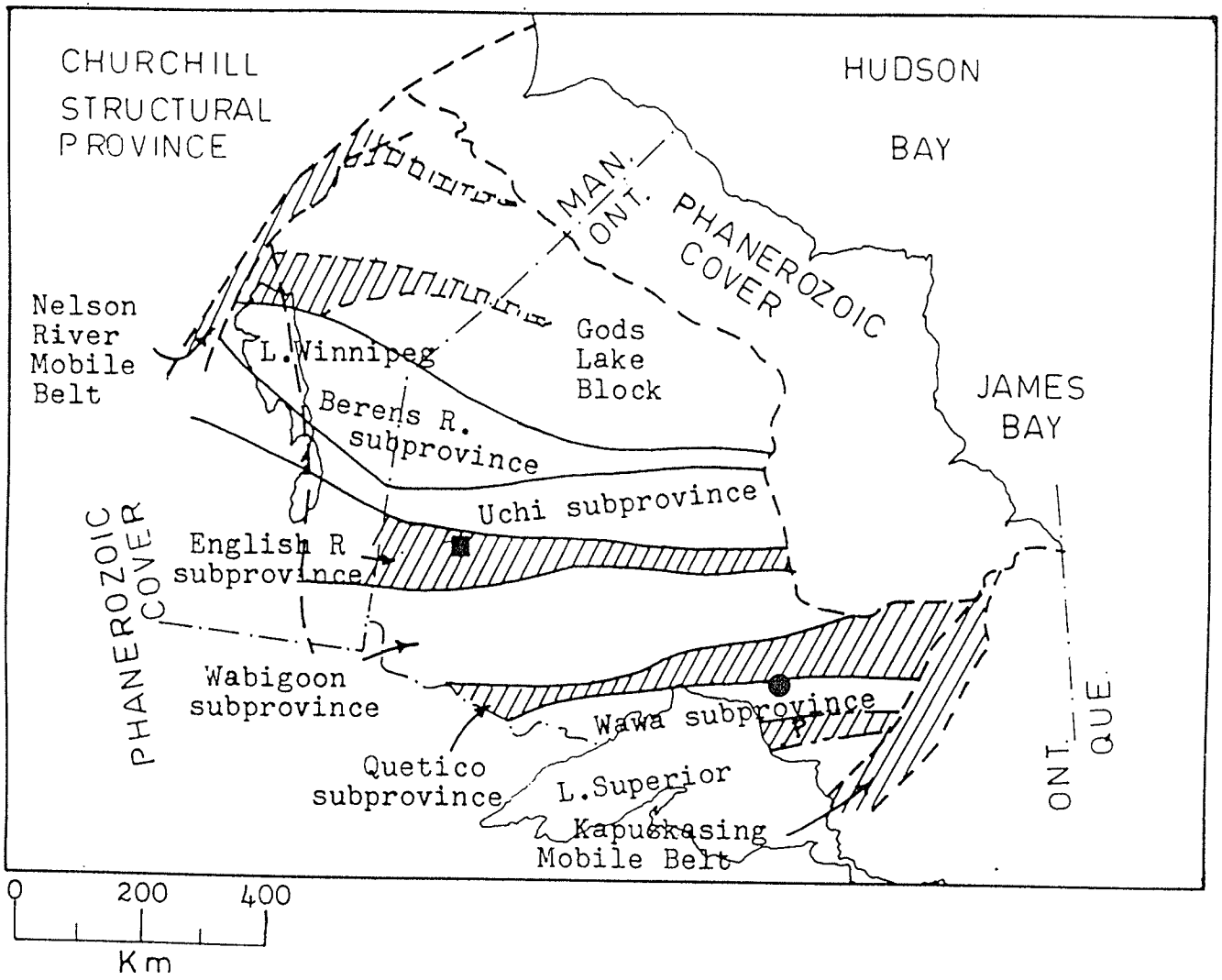

FIGURE 3-1 West half of the Superior structural Province of the Canadian Shield. Gneissic subprovinces are indicated by cross-hatching. The solid square shows the location of the Ear Falls area while the solid circle shows the location of the Manitouwadge area. Modified after Wilson et al.,1976.

3.1.1 Petrography of Massive Sulfide - Bearing Units

Locations of samples of ferruginous metasedimentary rocks ("lean iron formations") plus metasedimentary gneisses hosting sulfide mineralization in the Ear Falls area are shown in Figs. 2-1 and 3-1. Chemical analyses and mineralogical compositions of these samples are listed in Appendix A-1.

Garnetiferous sulfide and magnetite - bearing ferruginous metasedimentary rocks are enveloped by poorly to fairly well foliated gneisses. The gneiss layers consist of biotite, quartz, plagioclase (An15 - An30) and K-feldspar. Sillimanite, garnet, pyrite and muscovite are rare. Except for adjacent to iron - rich units, the mineralogical composition of the enveloping quartz - feldspar - biotite gneisses shows little variation. They do, however, possess gradational contacts with the iron - rich units, marked by increasing garnet and sulfide content. Garnet contents up to 50% are encountered within the iron - rich units, which may contain clinopyroxene and retrograde hornblende. Although these garnets are rounded, fractured and contain many quartz and chlorite inclusions, they do not appear to be rolled to any extent. These garnetiferous bands may, in addition, contain up to 35% hornblende as fractured, chloritized, crushed and altered prismatic grains.

The abundance of garnet and the lack of cordierite in both the host gneisses and the ferruginous bands indicate pressures in excess of 6 kbars (Winkler, 1976) (Fig. 3-2). Sillimanite indicates metamorphic temperatures in excess of 600°C (using the aluminosilicate triple point which is an average of those reported by Althaus, 1967, 1969 and

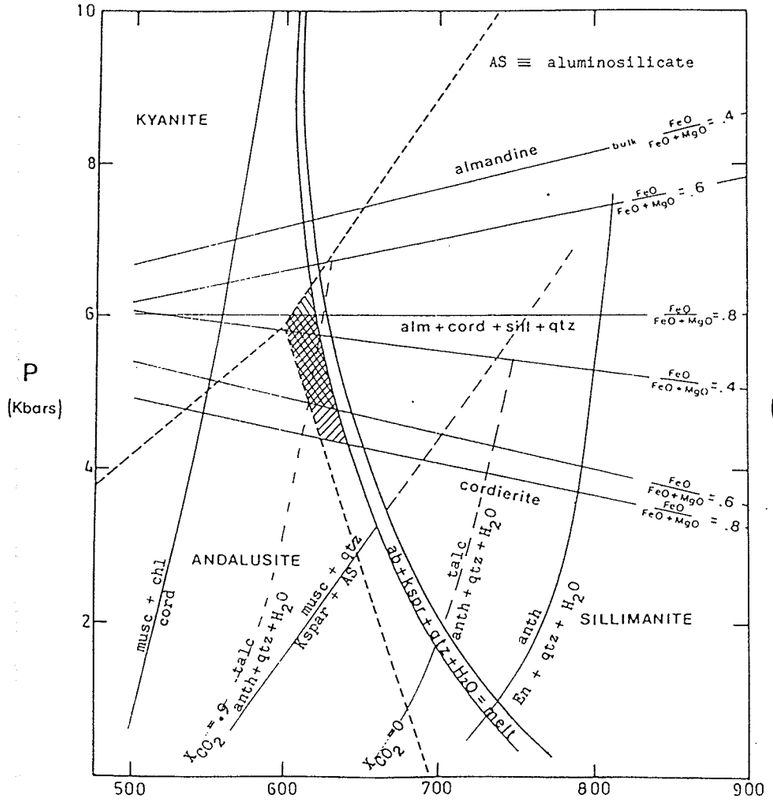

range of P-T indicated by the mineral assemblage in the ferruginous metasedimentary gneisses

range of P-T indicated by the mineral assemblage in the quartz-feldspar-biotite gneisses

FIGURE 3-2 Metamorphic pressure-temperature regime for some iron-rich metasedimentary gneisses and their enveloping quartz-feldspar-biotite gneisses from the English River gneiss belt (Ear Falls area). Data obtained in this study are incorporated into the diagram of Winkler (1976, p230, 238 & 242). The approximate boundaries of the aluminoslilicate polymorphs' stability fields represent values intermediate between those given by Althaus (1967, 1969) and by Richardson et al. (1968, 1969).

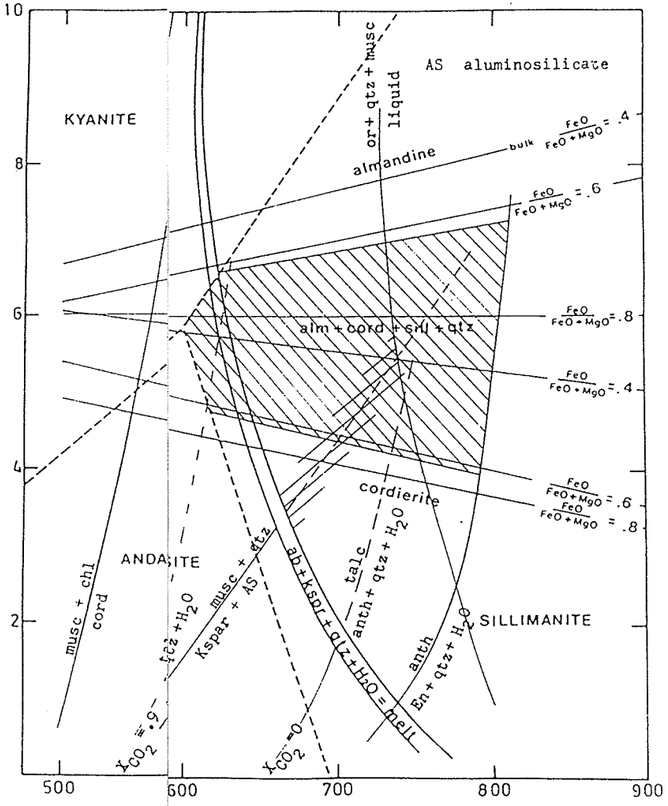

Pressu emperature range indicated by the mineral assemblage of the dierite-anthophyllite rocks at the Geco Mine

Pressu emperature range indicated by the mineral assemblage of the limanite bearing rocks of the Sericite Schist group he Geco Mine

FIGURE 3-3 Metamo c pressure-temperature regime indicated by mineral assemb s at the Geco Mine, Manitouwadge, Ontario. Data o ned during this study are incorporated into the P-T di m of Winkler (1976, p230, 238 & 242)

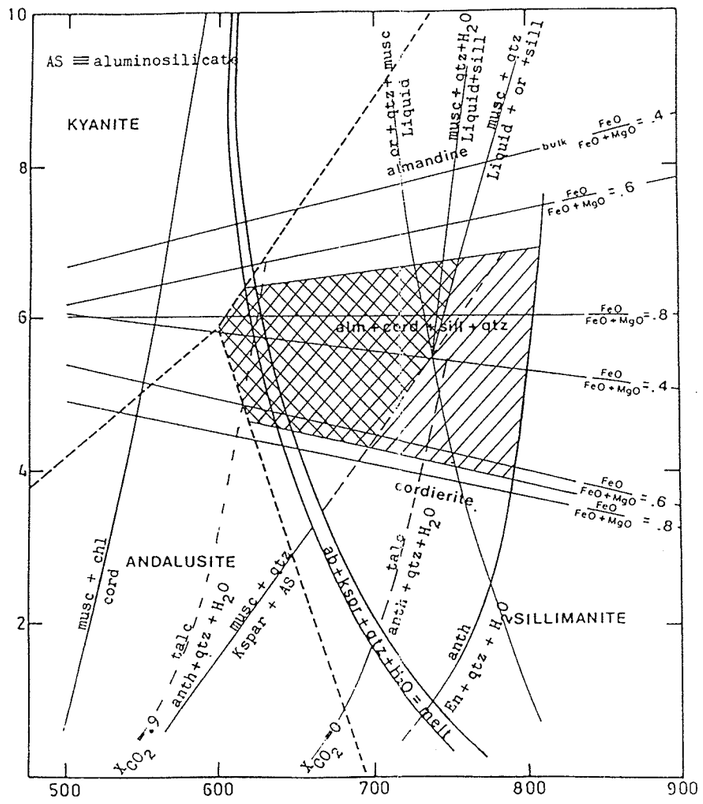

conditions indicated by assemblages present in the anthophyllite bearing schist

conditions indicated by assemblages present in sillimanite bearing gneisses, assuming anhydrous conditions.

FIGURE 3-4 Metamorphic conditions indicated by assemblages in diamond drill core recovered on Yakushavitch Island, Kississing Lake, Manitoba.
Data obtained during this study are incorporated into the P-T diagram of Winkler (1976, p230, 238 & 242).

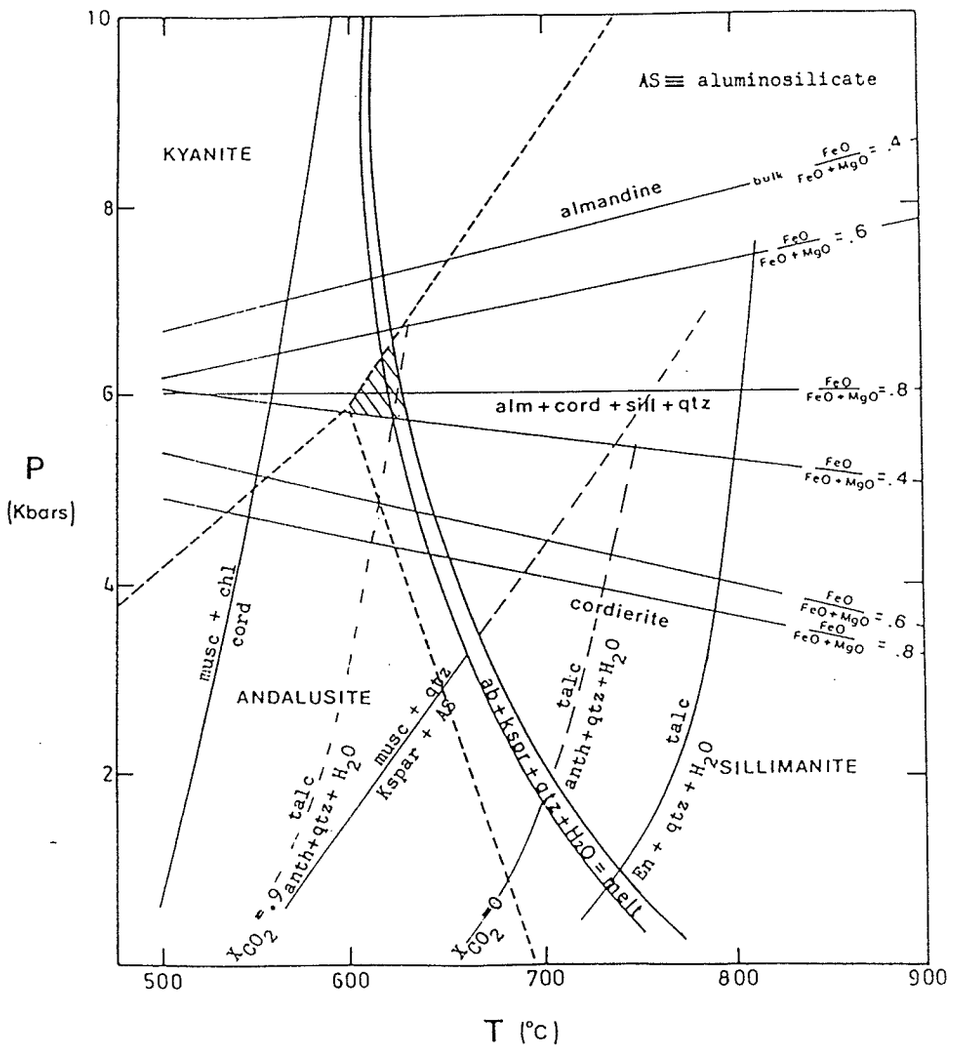

▨ conditions indicated by mineral assemblages present in the cordierite-anthophyllite rocks at Montauban, Quebec. It is assumed that X_{CO_2} is in excess of 0.9.

FIGURE 3-5 Metamorphic conditions indicated by mineral assemblages present at Montauban, Quebec. Data obtained during this study are incorporated into the P-T diagram of Winkler (1976, p230, 238 & 242).

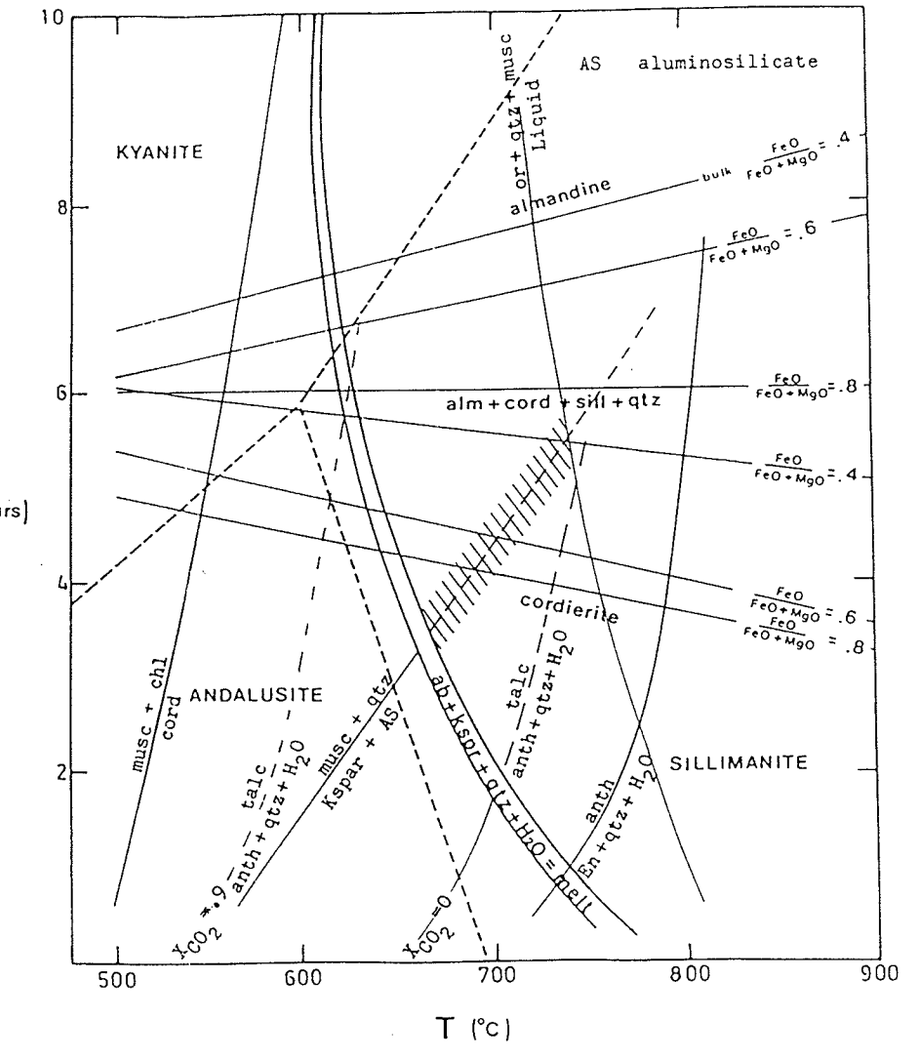

▨ conditions indicated by the mineral assemblages present in the sillimanite bearing gneisses/schists of the New Calumet deposit, Calumet Island, Quebec.

FIGURE 3-6 Metamorphic conditions indicated by mineral assemblages present at the New Calumet deposit, Calumet Island, Quebec. Data obtained during this study are incorporated into the P-T diagram of Winkler (1976, p230, 238 & 242).

Richardson et al., 1968, 1969). Fig. 3-2 illustrates the effect of bulk ratios of FeO to FeO + MgO on the range of pressure - temperature stability for coexisting almandine, cordierite, sillimanite and quartz. This ratio varies from roughly 0.6 in the host gneisses to over 0.8 in the ferruginous metasedimentary units (Appendix A-1). This relationship would indicate that metamorphic pressures in the range of 4.8 to 6.0 kbars were prevalent. The upper temperature limit is based on the lack of evidence for anatexis. Therefore, the temperatures of metamorphism shown in Fig. 3-2 are 600°to 650°C

3.2 Geco Mine Area, Manitouwadge, Ontario

The Manitouwadge area, which contains the Geco deposit as well as a number of smaller Cu-Zn dominated massive sulfide deposits, is situated in the Wawa Greenstone Belt, 8km south of the Quetico Gneiss Belt (Stanton, 1984). It is located 84 km N.E. of Marathon and 105 km S.E. of Geraldton, Ontario, in the Superior Province. Figures 2-3 + 2-4 show the location of the Geco deposit. Pye (1957) described a section consisting of four groups of Precambrian rocks folded into a large synclinal structure. However, this has been interpreted as being a possible overturned anticline with rocks younging in a southward direction at Geco (Sangster and Scott, 1976). Although the Manitouwadge structure is within the Wawa Subprovince, rocks within the immediate vicinity of the Geco deposit are predominantly gneisses and schists of amphibolite facies of metamorphism (Gale et al, 1980; Stanton, 1984)

which appear to be similar to those of the Quetico Subprovince to the north. It would appear that Geco host rocks would be of a provenance more closely related to that of rocks of the Quetico Subprovince rather than that of the greenstone of the Wawa Subprovince, or at least a provenance transitional between the two. Douglas (1976) has remarked that the marginal areas of the Quetico Subprovince are marked by a gradational decrease in the degree of metamorphism and granitization and that more relict textures and generally more of the original character of the rocks are discernable.

Geco is the largest of several Cu-Zn massive sulfide deposits in the Manitouwadge area. Other major deposits of the area include Willroy, Willecho and Nama Creek. The combined production of the Manitouwadge area, up to 1980, is reported to be approximately seventy million metric tons of ore (Gale et al., 1980).

Fig. 3-7 represents the metamorphic stratigraphy of the Archean rocks at Geco as interpreted by Sangster and Scott (1976). At Geco the orebody is hosted by a biotite - sillimanite - quartz schist enveloped by a muscovite - quartz schist (Fig. 2-5). It extends along the south contact of a thick garnet - amphibole - biotite schist unit which extends across the Geco and adjoining Wilroy Mines properties. The sillimanite - biotite schist forms a fairly continuous unit reaching thicknesses in excess of 100 metres. It is commonly found intercalated with biotite gneiss or quartz - feldspar - biotite gneiss and demonstrates a gradation from a porphyroblastic to an equigranular fabric. Porphyroblasts are felted lenses or ovoid patches of sillimanite up to 1 cm long, commonly found in the more biotite - rich bands.

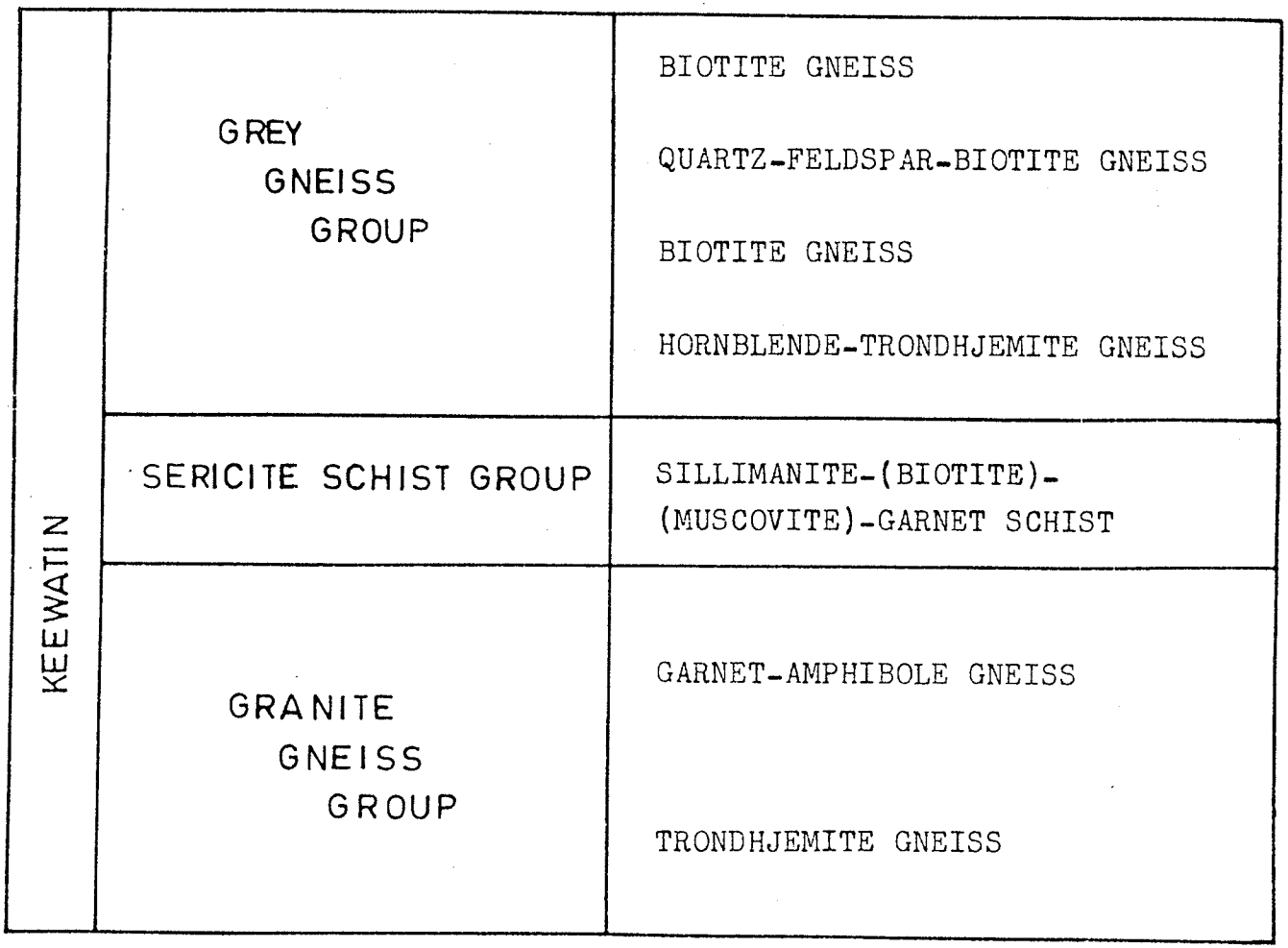

FIGURE 3-7 Metamorphic stratigraphy of Archean rocks at Geco Mine; based on the structural interpretation of Sangster & Scott (1976)

A band of muscovite - quartz schist separates the biotite - sillimanite - quartz schists from the Grey Gneiss unit in the south. The Grey Gneiss unit consists of quartz - feldspar - biotite gneiss, iron formation, biotite quartzite and hornblende gneiss which grade southward into amphibolite and hornblende gneisse. The Grey Gneiss unit is noted for intercalations of magnetite - rich units (iron formations) which may attain thicknesses in excess of 30 metres (Pye, 1957).

The main orebody at Geco may be subdivided into two types of ore:

(1) massive sulfide ore rich in zinc;

(2) disseminated ore, poor in zinc but containing copper and silver.

Pye (1957) subdivided the massive ore again into three types:

(1) a copper rich variety which is dominant on the west side of the massive ore zone;

(2) a zinc-rich (up to 10% Zn) type which becomes dominant in the central section of the massive sulfide zone;

(3) a barren pyrite, pyrrhotite ore which becomes dominant towards surface and the east.

The disseminated ore is hosted by a muscovite - quartz schist which contains barren interbands of biotite - quartz - feldspar - (hornblende) gneiss.

3.2.1 Petrography of Rock Samples from the Geco Mine Area

Petrographic data and chemical analyses of samples from the Geco

Mine area are listed in Appendix A-4.

Amphibolite from Milne's unit #1 (Milne, 1969) consists mainly of hornblende, clinopyroxene and plagioclase (An45 to An55) and often displays a relict subophitic texture.

Feldspar - bearing gneisses and biotite schists immediately south of the mine sequence are marked, at many places, by a fine scale banding and grain size variations which may represent relict sedimentary structures. In addition to plagioclase (An20 to An30) these gneisses contain variable amounts of hornblende, biotite and K-feldspar as well as minor amounts of muscovite and sericite. The quartz - feldspar groundmass of these gneisses is typically granoblastic and exhibits sutured or curved grain boundaries. Hornblende, when present, occurs as isolated lozenge - shaped crystals or aggregates of aligned crystals within the quartz - feldspar groundmass, thus contributing, with biotite, to the lepidoblastic texture of these rocks.

The iron formation in the updip continuation of the Geco orebody (Fig. 2-4) is represented by sample numbers GO-15f to GO-15j inclusive. These samples show a compositional variation ranging from siliceous to sulfide - rich and to garnetiferous iron formation. All contain abundant quartz (>50% and often up to 80%), variable amounts of sulfide (primarily pyrite) and Fe, Ti oxides.

The rock enveloping the Geco iron formation is unit 4 of Milne, 1969, a biotite - rich garnetiferous schist represented by samples GO-15a to GO-15e inclusive. It is petrographically similar to the other intermediate to mafic schists encountered in the Grey Gneiss group. It has a fine scale banding and an overall gradational increase in quartz towards the iron formation. This may be a consequence of fine

interbanding or dilution of the original muddy clastic sediments by more siliceous hydrothermal sediments, the siliceous sediments gradually becoming more dominant as one approaches the iron formation. The petrographic and chemical analytical data listed in Appendix A-4 lends support to this.

Rocks from the Sericite Schist group, sampled underground, are generally well foliated, leucocratic and more siliceous than those of the Grey Gneiss group to the immediate south. They commonly consist of a polygonal quartz - feldspar groundmass with bands of sillimanite, biotite and muscovite. Sillimanite is conspicuously scarce or nonexistent when plagioclase is present in any appreciable amount. This is demonstrated in Fig. 3-8. Fig. 3-8 also shows a gradual decrease in both biotite and sillimanite as one approaches the north contact of the biotite - anthophyllite schist at the stratigraphic base of the 4/2 ore zone (distance = 0 metres corresponds to the north contact of the anthophyllite schist and distances are measured south of this point).

Rocks from the massive sulfide ore zone at Geco are generally more quartz - rich and feldspar deficient. Biotite still persists in small amounts, but sillimanite and muscovite are practically non-existent. The host rock to mineralization in the 4/2 ore zone on the 2850 level is given the name "quartz pebble conglomerate" by Geco geologists, based on megascopic textural features. This rock is composed of quartz, cordierite and anthophyllite, the latter two minerals being concentrated in the interstitial areas between stretched quartz fragments. In thin section cordierite occurs as large irregular crystals engulfing and replacing biotite. In addition to inclusions of biotite and quartz the cordierite contains small euhedral crystals of gahnite. Anthophyllite

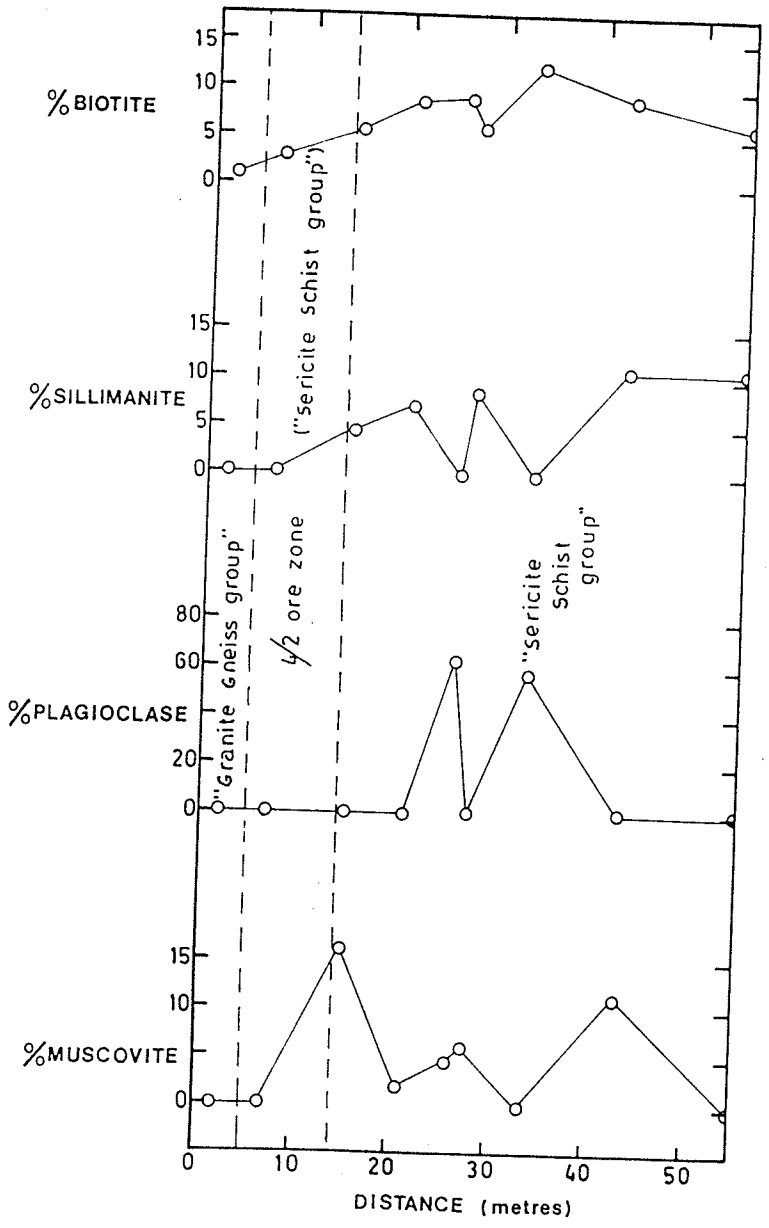

FIGURE 3-8 Variation in mineralogical composition across the Sericite Schist Group along the 28-65 crosscut at the Geco Mine

occurs as lozenge-shaped crystals and aggregates which are aligned to give the rock its fabric. Cordierite and anthophyllite show some alteration to chlorite whereas biotite, when present, is lightly sericitized.

A rock composed almost exclusively of cordierite and biotite occurs near the massive ore of the 8/2 group at Geco. It is represented by samples GO-109 and GO-109b. Geco geologists have named this rock a staurolite - cordierite - biotite hornfels. Rather than staurolite, this rock was found to contain kyanite. It also does not possess the attributes of a hornfels. Staurolite was observed in parts of the 4/2 ore zone (4/2 ore zone is a term employed by Geco mine site geologists to describe a small zinc - rich sulfide - bearing zone characterized by an anthophyllite - bearing schist).

The assemblage quartz - K-feldspar - muscovite - sillimanite - biotite is ubiquitous in the Sericite Schist group on the 2850 level at Geco. Plagioclase (An20 to An30) is also present in similar schists which envelope the massive ore zone on the 2350 level. Muscovite occurs as large undeformed flakes with interpenetrating masses of sillimanite needles replacing it. It does not appear to be of retrograde metamorphic origin. The pressure-temperature regimes for the assemblages existing in the Sericite Schist group rocks at the 2350 and 2850 levels are shown in Fig. 3-3. Assuming a pelitic origin, the coexistence of muscovite - quartz - K-feldspar - sillimanite is possible (Winkler, 1976) within the range of $650^{\circ}C<T<740^{\circ}C$ and 2.9 kbars$<P<$5.7 kbars. The additional presence of plagioclase in similar schists on the 2350 level further restricts the metamorphic conditions into the range of $645^{\circ}C<T<660^{\circ}C$ and 2.8 kbars$<P<$3.2 kbars.

Assuming, again, a pelitic origin for the cordierite - anthophyllite schists of the 4/2 ore zone, the coexistence of garnet - cordierite - sillimanite - quartz restricts the metamorphic conditions to those depicted in Fig. 3-3. This range agrees fairly closely with that determined for the adjacent sillimanite - bearing schists of the 1850 level. Using the FeO/FeO+MgO ratio one may further narrow down metamorphic conditions to the range $680°C<T<740°C$ and $4.5 \text{ kbars}<P<5.8 \text{ kbars}$.

Since the stability of anthophyllite - bearing assemblages are sensitive to mole fraction of CO_2(Johannes, 1969) and the contribution of CO_2 during metamorphism cannot be evaluated, the presence of anthophyllite is insufficient to determine metamorphic conditions.

3.3 Sherridon Area, Manitoba

The former Sherritt Gordon Mine near Sherridon is located on the east shore of Kississing Lake, approximately 160 km north of The Pas, Manitoba (Fig. 2-9). It is situated within the Kisseynew Gneiss Belt of the Churchill province less than 30 km north of the boundary of the Kisseynew and Flin Flon-Snow Lake Subprovinces (Gale et al., 1981). Ore was produced from two orebodies known respectively as the East and West, both hosted by rocks of the Sherridon Group.

The Aphebian Sherridon Group is underlain by the Nokomis Group which in turn is underlain by the Amisk Supergroup (Goetz, 1980). The

Sherridon and Nokomis Groups are dominantly metasedimentary in nature as opposed to the Amisk Supergroup which is chiefly metavolcanic. Sherridon Group rocks have been subdivided into quartz - rich gneisses and hornblende gneisses with minor amounts of calcitic marble, calc - silicate gneiss and anthophyllite - bearing schist (Robertson, 1953). An interpretation of the stratigraphy at Sherridon and its relationship to mineralization is given by Goetz (1980). Fig. 3-9 is a simplified outline. Goetz (1980) basically utilized Robertson's (1953) subdivision of the Sherridon Group but he also genetically subdivided the metamorphic rocks into a sequence of pillowed and fragmental mafic metavolcanic rocks and another sequence of lithic meta-arenites and meta-carbonates. His interpretation of the metasedimentary subdivision is shown in Fig. 3-10.

The Sherridon orebodies are associated with a garnet - biotite - sillimanite schist and anthophyllite schist of the Lower Arenite unit. These rocks are characterized by their larger grain size and more aluminous constituents (Goetz, 1980). They are usually well banded with sharp contacts.

Massive sulfide ore was mined from two adjacent orebodies situated at roughly the same stratigraphic horizon marked by a thin but almost continuous anthophyllite schist. This extends around the entire Sherridon structure. The Sherridon structure is a roughly NW - SE trending complexly deformed anticlinal structure very similar to the Manitouwadge structure described earlier. It is possible that, due to the similar structural features produced by the steeply dipping rocks of both of these localities, they may share similar metamorphic histories. Several smaller Cu-Zn occurences are found around the structure along

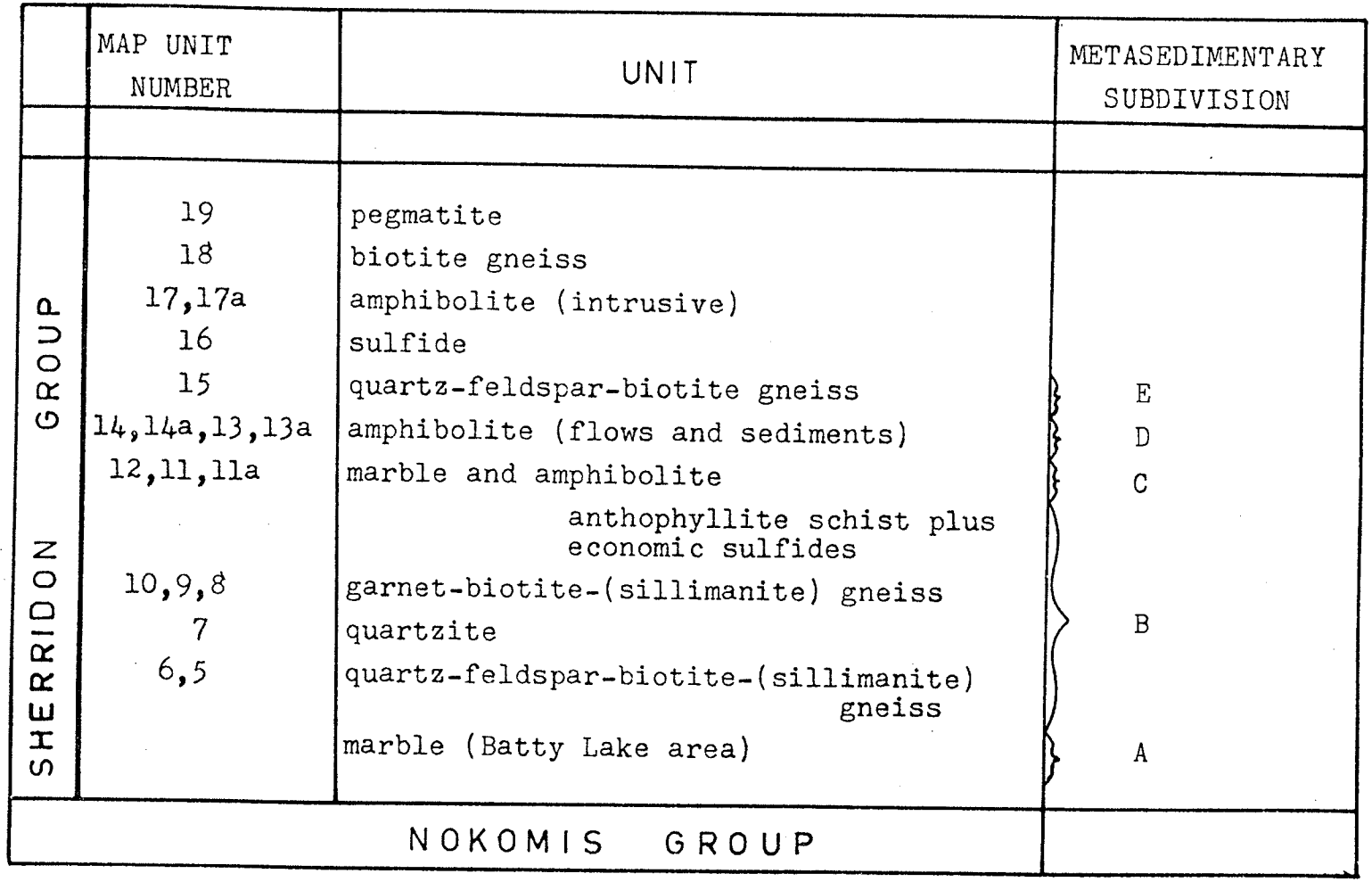

FIGURE 3-9 Metamorphic stratigraphy of the Sherridon Group, Sherridon-Kississing Lake area, Manitoba. Modified after Goetz (1980)

SUBDIVISION	UNIT	PROTOLITH INTERPRETATION
E	biotite gneiss	Upper Arenite
D	biotite-garnet gneiss	Greywacke
C		Arenaceous Limestone
B	biotite gneiss	Lower Arenite
A	calc-silicate	Calcarenite

FIGURE 3-10 Interpretation of pre-metamorphic rock compositions of the Sherridon Group, Kississing Lake, Manitoba, after Goetz (1980).

the anthophyllite schist unit contact but the Sherridon East and West orebodies are the largest. These orebodies are separate but each is laterally contiguous. Their combined strike length exceeds 8 km but their thickness rarely exceeds 2 metres. The West orebody containing less zinc than the East orebody, is underlain by the anthophyllite schist and overlain by a minor metapelite unit (Bateman and Harrison, 1946). The western part of the East orebody is zinc rich and is hosted by a sillimanite - bearing meta-arenite whereas its eastern section, which is more copper rich, is hosted by a more complex association including the anthophyllite schist and meta-carbonate. Although the two orebodies occur at the same stratigraphic horizon they are not linked by an iron formation as are the Geco and Wilroy #1 orebodies in the Manitouwadge district.

Cu-Zn mineralization on Yakushavitch Island occurs in a metasedimentary package similar to that hosting the Sherridon deposit. The rocks occur within a smaller synformal structure similar to the Sherridon structure. Selco Ltd's properties in the Sherridon area include Yakushavitch Island located approximately 32 km W.N.W. of Sherridon on Kississing Lake (Fig. 2-9). Rock types encountered in diamond drill holes on Yakushavitch Island include garnet - biotite gneiss, sillimanite - biotite gneiss and the anthophyllite schist of the Sherridon Group. Diamond drill holes were located along a N-S trending grid extending across the island (Fig. 2-10). They intersected small pods of mineralization hosted by the rock types listed above. Copper and zinc sulfides were encountered in the two drill holes sampled for this study (DDH-11-11-3 and DDH-11-11-5). In addition, significant gold values were detected in DDH-11-11-1 on the south end of the same

mineralized zone extending from DDH-11-11-3.

3.3.1 Petrography of Core Samples Taken from Diamond Drill Holes on Yakushavitch Island

Petrographic data and chemical analyses of diamond drill core samples from the drill holes on Yakushavitch Island are listed in Appendix A-5.

Host rocks to the mineralization on Yakushavitch Island are mostly quartz - feldspar - biotite gneisses with minor amounts of sillimanite, muscovite and garnet. Plagioclase (An30 to An40), quartz and K-feldspar exhibit a granoblastic texture with well sutured grain contacts. The weak to moderate foliation is due to their biotite content. Biotite is usually present as stubby shredded flakes frequently partly altered to chlorite. Sillimanite is present as individual fibres or as spindle - shaped masses associated with sericite, biotite and/or muscovite. Sericite and chlorite appear to be of retrograde metamorphic origin.

A banded quartz - sericite - sillimanite schist (sample #S-11) was encountered in the diamond drill core immediately above the mineralized anthophyllite - rich section in the drill hole. Within the mineralized horizon plagioclase and biotite disappear, as shown in Fig. 3-11. Quartz is present in lesser quantities and it displays a polygonal texture. Talc accompanies anthophyllite in the moderately schistose mineralized section along with small amounts of carbonate (sample #S-14). At the lower contact of the anthophyllite - bearing section,

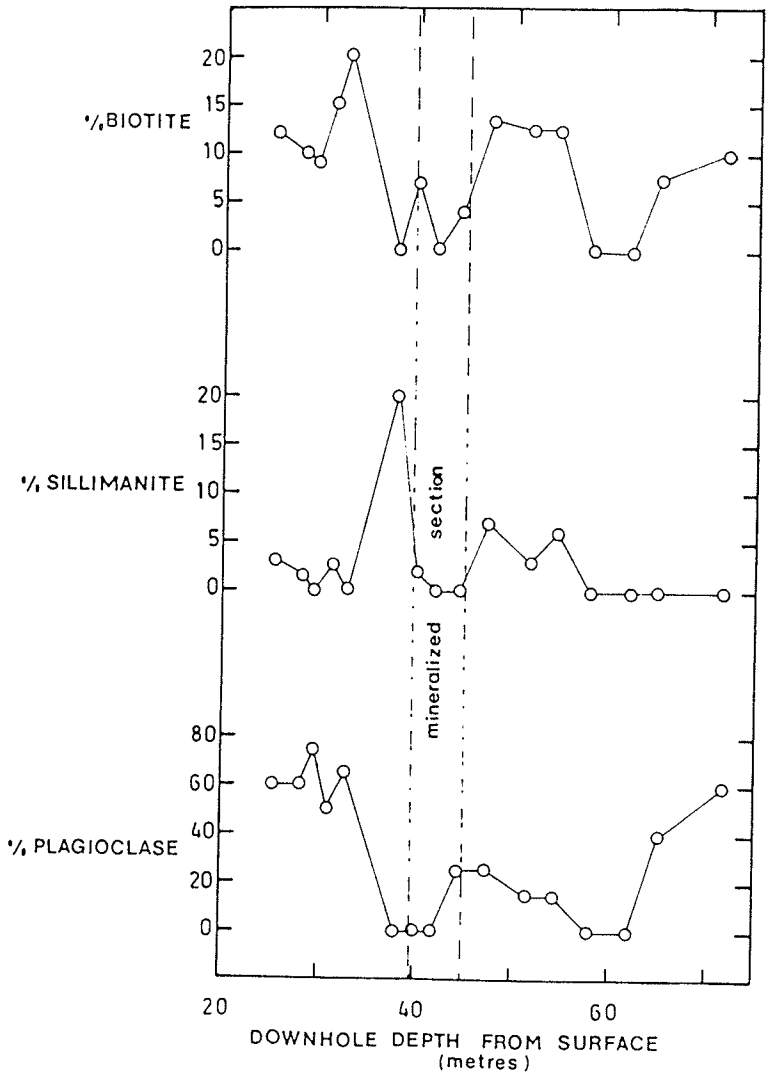

FIGURE 3-11 Variation of mineralogical composition in diamond drill hole DDH-11-11-5, Yakushavitch Island, Kississing Lake, Manitoba.

sulfide mineralization no longer occurs and plagioclase, biotite and eventually sillimanite is present again. Apart from a section rich in clinopyroxene, the gneisses below the mineralized interval are very similar to those above it.

Sample S-20, taken 9.5 metres downhole from the mineralized interval in diamond drill hole DDH-11-11-5, contains the assemblage quartz - biotite - plagioclase - sillimanite - garnet - cordierite. FeO/(FeO+MgO) ratios are in the range of 0.6 to 0.8, so the conditions during metamorphism would likely have been restricted to those depicted in Fig. 3-4 (Winkler, 1976). The coexistence of muscovite and quartz in sample S-18, sets the upper temperature during metamorphism to about 750° C (Fig. 3-9). On the basis of the work of Richardson (1968) and Schreyer (1968), the existence of staurolite in sample S-16, from the lower part of the mineralized interval in DDH-11-11-5, may set the upper temperature limit to no more than approximately 700°C. Metamorphic conditions may thus be narrowed down to the range 6.3 kbars>P>4.3 kbars and 700°C>T>600°C.

3.4 Montauban Area, Quebec

The Tetreault Pb - Zn - Ag deposit at Montauban - Les - Mines is located 84 km west of Quebec City in Portneuf County, Quebec (Fig. 2-2). Sulfide mineralization consists of coarse grained galena and sphalerite pods and lenses hosted by coarse carbonate and calc-sillicate gneiss (Stamatelopoulou - Seymour and MacLean, 1977). Other host rocks include

quartz - feldspar gneisses and amphibolites of the Grenville Supergroup. Stamatelopoulou - Seymour and MacLean (1977), utilizing field relationships in the amphibolites to the west of the deposit, determined that the hanging wall rocks, which they have designated "The Composite Gneisses", are the youngest rocks in the vicinity of the deposit. This Composite Gneiss, to which they ascribe a meta-volcanic origin, is overlain to the west by a series of quartz - feldspar gneisses collectively termed "Leptites" (Stamatelopoulou - Seymour and MacLean, 1977). The "leptites" are then further subdivided into three categories:

(1) quartz - feldspar - biotite gneiss;

(2) quartz - feldspar - biotite - hornblende gneiss;

(3) quartz - biotite - muscovite - sillimanite - (garnet) gneiss.

Although the chemical evidence indicates a likely volcanic origin similar to deposits in the Noranda Camp, Stamatelopoulou - Seymour and MacLean (1977) suggest that some very siliceous members of the rock association at Montauban appear to be metaquartzites.

The Pb - Zn - Ag ore occurs in the basal portion of the "leptite" unit, closely associated with a thin band of cordierite - anthophyllite schist which is itself mineralized (McAdam and Flannagan, 1976). The old Anacon workings occur within a calc - silicate gneiss horizon which is enveloped by a cordierite - anthophyllite - bearing sillimanite gneiss. Although the calc - silicate gneiss becomes less significant northwards along strike, the cordierite - anthophyllite assemblage persists and carries significant Au - Cu values (McAdam and Flannagan, 1976; Ledoux and Assad, 1979).

3.4.1 Petrography of Rock Samples Collected in the Montauban Area

Petrographic data and chemical analyses of samples from the Montauban area are listed in Appendices A-2 and B-4.

Sillimanite - bearing gneisses at Montauban are relatively low in plagioclase. They typically consist of micaceous bands alternating with quartz - felspar bands. The micaceous bands consist of an intergrowth of biotite and muscovite, and up to 8% sillimanite occurs as individual fibres and spindle shaped masses frequently replacing the biotite. The anthophyllite - bearing schists at Montauban are represented by three associations:

(1) a talc - anthophyllite schist (represented by sample #MON 6);

(2) a cordierite - rich, anthophyllite poor rock (represented by sample #MON 7);

(3) a cordierite - anthophyllite schist (represented by sample #MON 103).

Anthophyllite occurs as lozenge-shaped crystals with biotite and sillimanite in micaceous bands separated by interbands composed of irregular to polygonal crystals of quartz and cordierite.

Muscovite, quartz, K-feldspar and sillimanite were observed to coexist together in only one sample of the sillimanite - bearing schist. Schists containing muscovite are usually sillimanite - free whereas schists containing sillimanite usually lack muscovite. Metamorphic conditions would therefore appear to extend throughout the sillimanite

field of Fig. 3-5 on the curve representing the univariant reaction:

muscovite + quartz $\rightleftharpoons$ k-feldspar + sillimanite.

Bulk FeO/(FeO + MgO) ratio of 0.4 to 0.5 and the presence of plagioclase in the cordierite - anthophyllite schist would restrict metamorphic conditions to the field outlined in Fig. 3-5 (Winkler, 1976). The presence of kyanite in two samples of cordierite - anthophyllite schist substantiates the relatively high pressures indicated in Fig. 3-5. This suggests that higher pressures possibly existed in localized areas within the ore zone during metamorphism at Montauban.

3.5 New Calumet Deposit, Calumet Island, Quebec

The New Calumet deposit is located in rocks of the Proterozoic Grenville Supergroup (Douglas, ed., 1976) on Calumet Island, on the Ottawa River, 85 km west of Ottawa (Fig. 3-12). Osborne (1944) outlined a mineralized area, approximately 2 km x 0.8 km in size, containing one major economic orebody ("the Bowie") plus several smaller ore occurrences. The deposits occur in a "cylindrical prism" (Osborne, 1944) of biotite gneiss and amphibolite enveloped by migmatitic rocks. This resembles the antiformal structures encountered at the other localities previously discussed.

The Bowie orebody is immediately overlain by a carbonate-containing amphibolite according to the interpretation of Moorhouse (1941) (Fig. 3-13). Host rocks to the ore consist mainly of intercalated siliceous biotite gneiss, carbonate and calc - silicate gneiss. Two other

FIGURE 3-12 Local geology of Grenville Supergroup metamorphic rocks in the vicinity of the New Calumet deposit, Calumet Is., Quebec. The solid square indicates the former location of the Bowie Mine while the solid circles indicate the locations of other smaller occurences; modified after Osborne (1944).

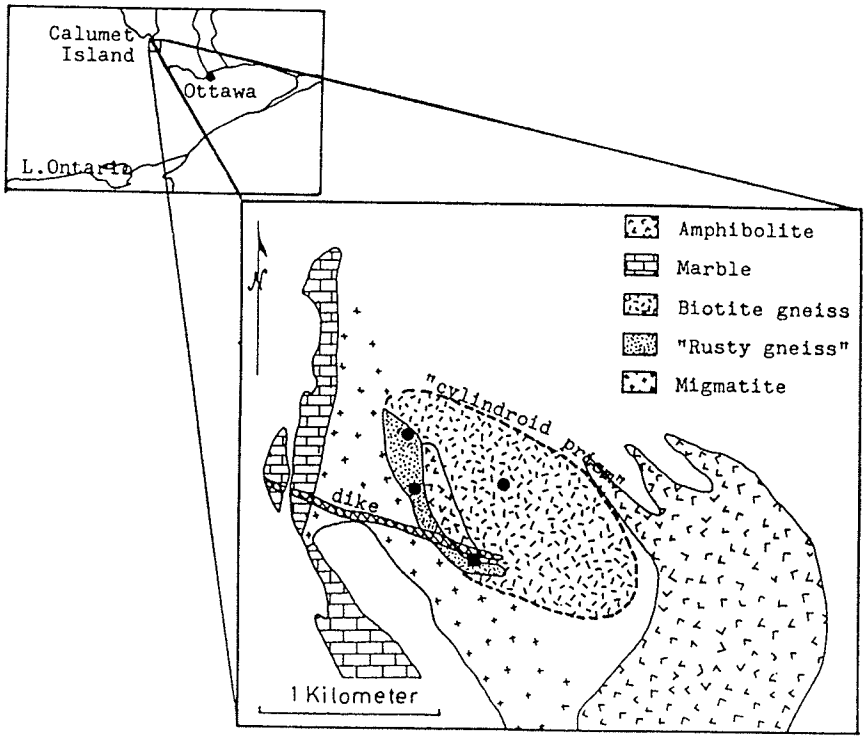

FIGURE 3-13 Metamorphic stratigraphy of the Proterozoic rocks in the area of the New Calumet deposit, after Moorhouse (1941).

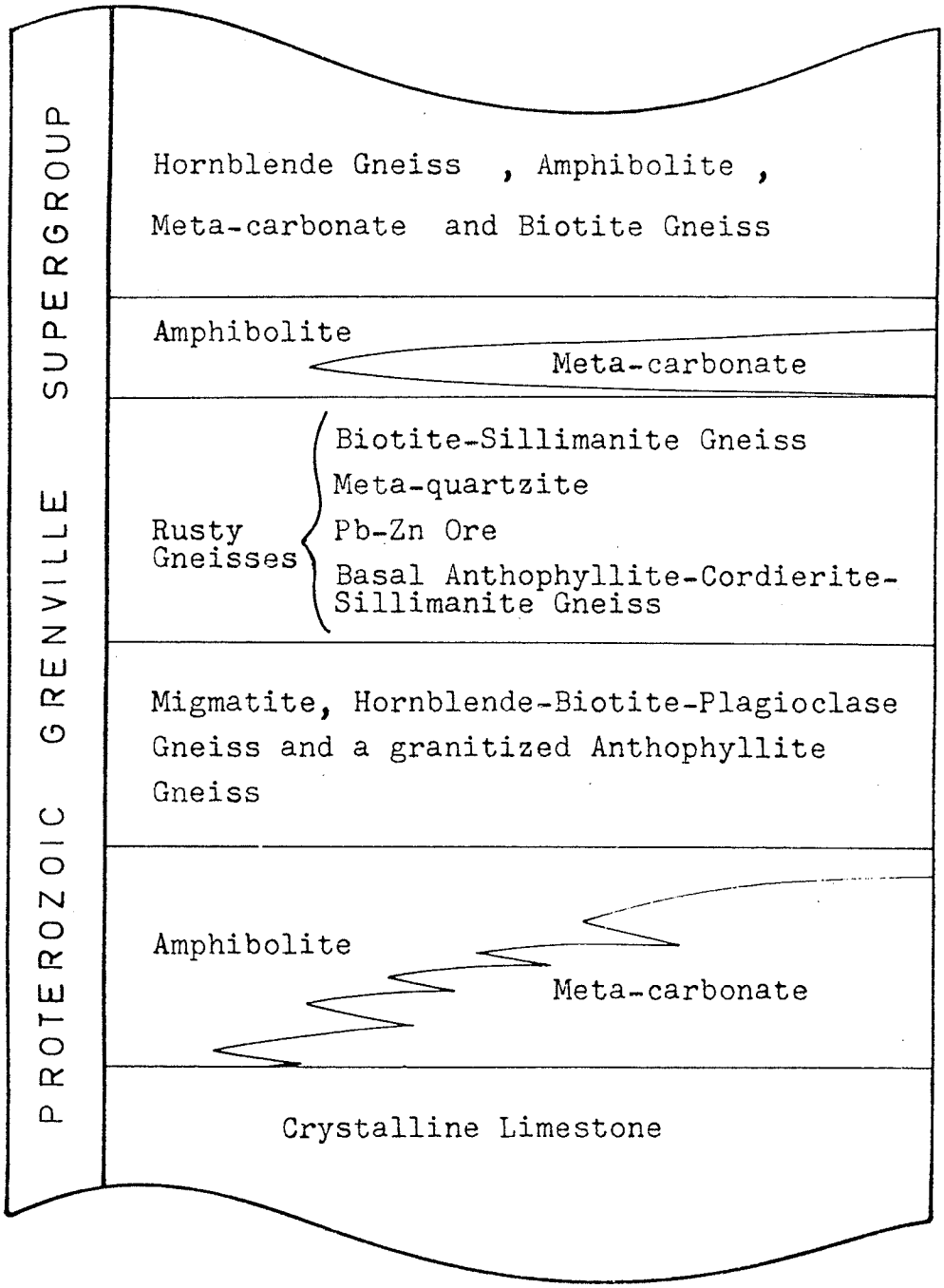

principal deposits at the Russel and McDonald showings occur somewhat stratigraphically lower within the "Rusty Weathering Gneisses" (Moorhouse, 1941). They are also extensive blanket-like bodies, peneconcordant with foliation, but are considerably smaller than the Bowie deposit.

Amphibolite in the area has a high carbonate content and tends to grade into metacarbonate. This is particularly apparent in the footwall amphibolite. Osborne (1944) suggested that this represents a series of originally intercalated calcareous and argillaceous metasedimentary rocks. The footwall amphibolite and carbonate are separated from the "Rusty Gneisses" by a series of migmatitic gneisses including an irregular band of pargasite - anthophyllite gneiss (Moorhouse, 1941). Osborne (1944) has reported that some original sedimentary features are discernable within portions of the migmatites.

The "Rusty Weathering Gneisses" contain sulfide-bearing quartzitic horizons as well as biotite gneiss layers containing sillimanite, minor sphalerite, galena, and sometimes cordierite. The most strongly recrystallized portions of the biotite - (sillimanite) gneiss become microcline rich (Moorhouse, 1941). Finer grained layers may contain sericite and/or graphite which Moorhouse (1941) has suggested may indicate a sedimentary origin for these gneisses. In analogy with Montauban, lead - zinc mineralization in the New Calumet orebodies is associated with significant gold values (Moorhouse, 1941).

3.5.1 Petrography of Samples Taken from the New Calumet Deposit

Petrographic data and chemical analyses of samples for the New Calumet deposit are listed in Appendix A-3.

Sillimanite - bearing schists at New Calumet are medium to fine-grained equigranular lepidoblastic rocks composed typically of K-feldspar, plagioclase (An20 - An30), biotite, sillimanite and muscovite. As much as 15% sillimanite occurs as individual fibres and interwoven masses intimately intergrown with biotite and muscovite in micaceous bands, alternating with quartz - felspar bands. Biotite and muscovite are present as well formed undeformed foliation - parallel flakes which are usually embayed and penetrated by sillimanite needles. Plagioclase occurs as large, irregular, sericitized laths, which may represent original plagioclase phenocrysts or fragments. Samples examined in which plagioclase content increased to near 50% are strongly depleted in sillimanite and K-feldspar. Conversely those samples rich in K-feldspar and sillimanite are practically devoid of plagioclase. Although Moorhouse (1941) and Osborne (1944) reported anthophyllite and cordierite, these minerals were not observed within the sillimanite gneisses at New Calumet during my sampling.

Although rather uncommon, coexisting muscovite, K-feldspar, quartz, sillimanite and plagioclase restrict metamorphic conditions to the univariant reaction:

muscovite + quartz $\rightleftharpoons$ k-feldspar + sillimanite

shown in Fig. 3-6 (Winkler, 1976). Since micas present in this assemblage are sufficiently hydrated, conditions of metamorphism would

be restricted by the wet solidus curve to the range: 2.9 kbars<P<3.4 kbars and 645°C<T<665°C.

3.6 North Maysville Deposit, Central Colorado, USA

The Maysville deposit occurs in Precambrian rocks (1.7-1.8 Ga) (Knight, 1981) of the Sangre de Cristo Range, Chaffee County, 16 km west of Salida, Colorado (Fig. 3-14). Knight (1981) described the results of a detailed stratigraphic study of the ore-bearing quartz - feldspar - biotite - sillimanite gneiss unit in this area. The relative position of this unit in the local stratigraphic column is depicted in Fig. 3-15. Analyses of samples collected by Knight (1981) from the sillimanite gneiss along a 120 m long traverse centered over the Bon Ton Mine are utilized in this study. Table 3-1 is a simplification of the stratigraphic section with sample locations, reported by Knight (1981). Chemical analyses of these samples are listed in Appendix B-11. Distance = 0 corresponds to the west contact of the sillimanite gneiss unit which hosts the Bon Ton deposit. Knight (1981) subdivided the sillimanite gneiss into three subunits:

(1) major quartz - feldspar - biotite - sillimanite gneiss and quartz - feldspar - (biotite) gneiss;

(2) quartz - magnetite banded iron formation;

(3) anthophyllite - (gahnite) gneiss with biotite - garnet gneiss.

The iron formation is usually found in gradational contact with the

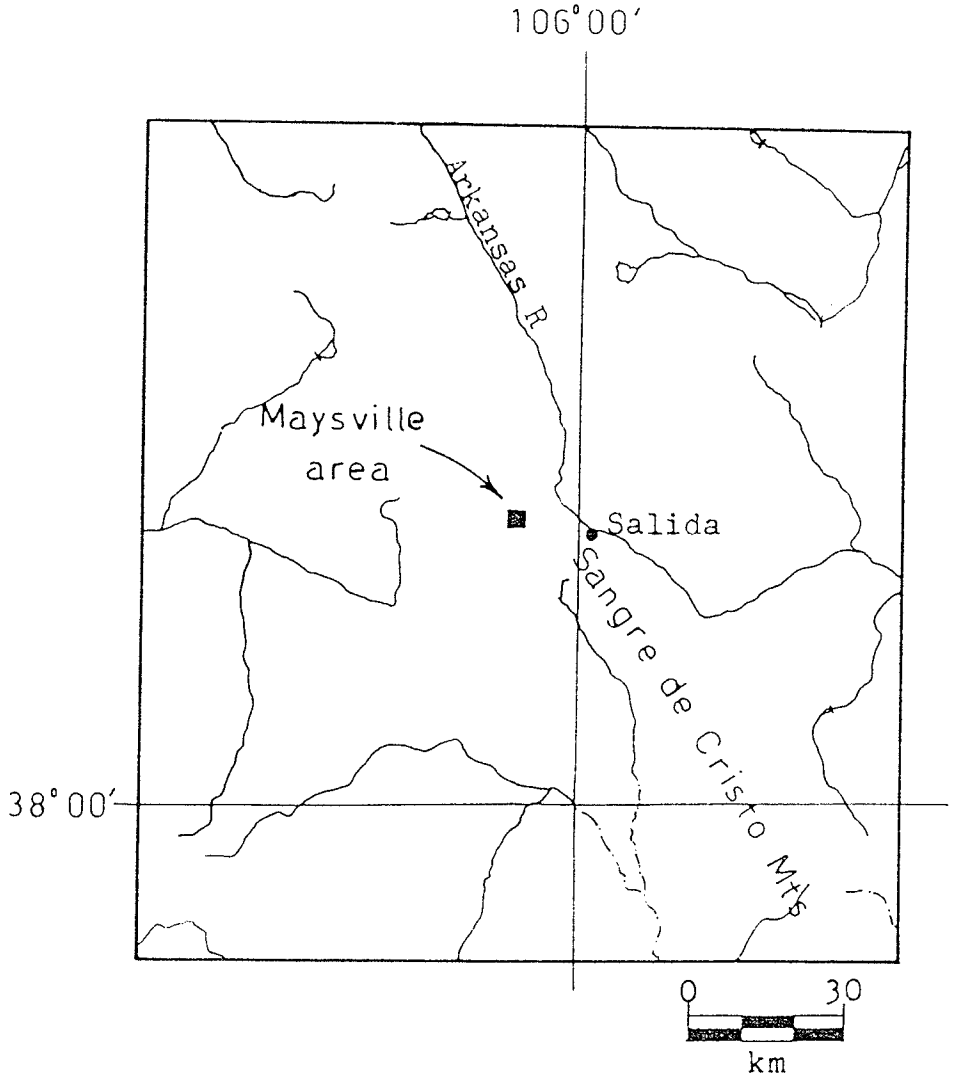

FIGURE 3-14 Location of the Maysville area, Colorado.

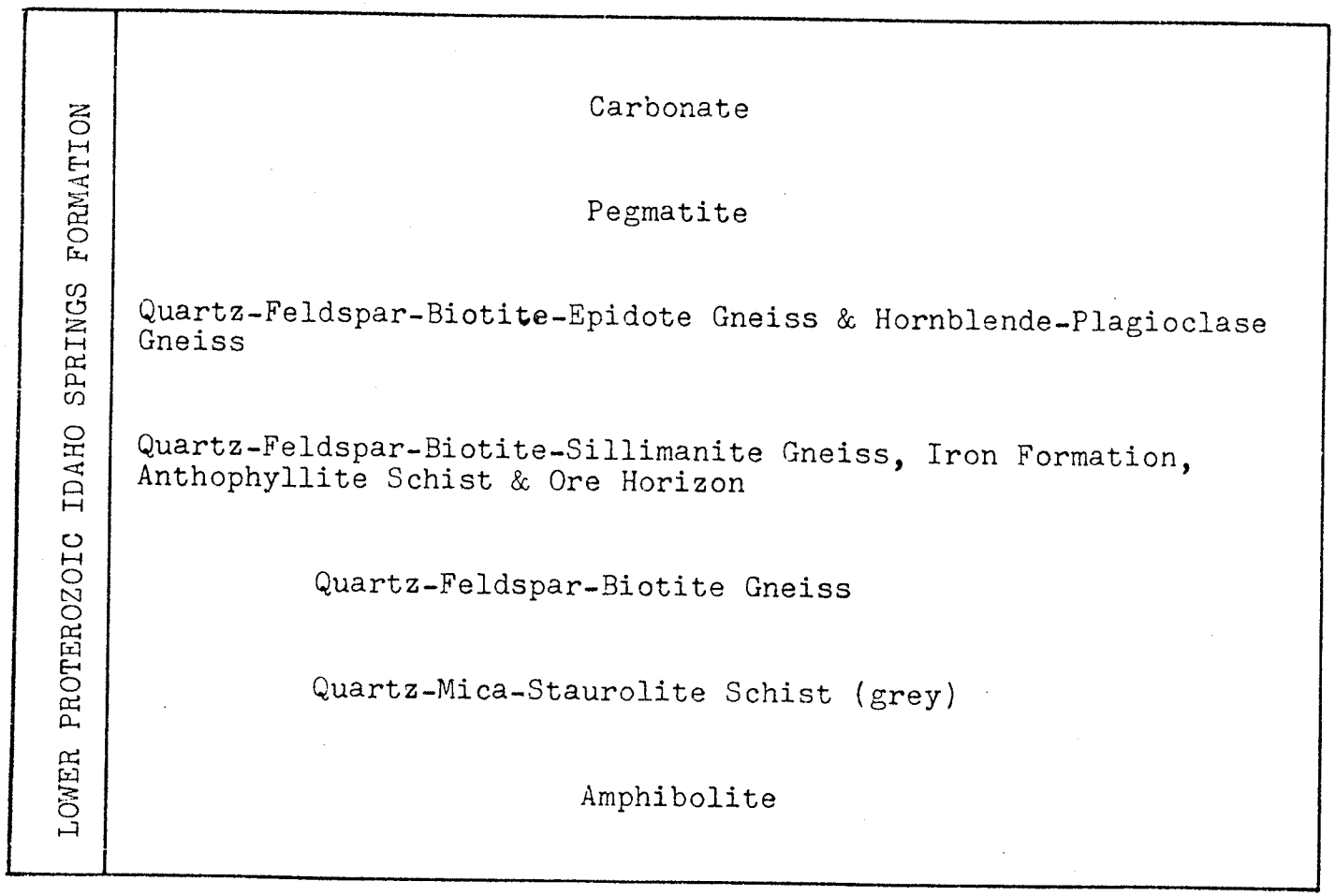

FIGURE 3-15 Metamorphic stratigraphy of the Proterozoic rocks of the Maysville area of central Colorado; after Bradshaw (1978)

TABLE 3-1

Locations of rock samples collected along an east-west traverse through the Bon Ton Mine in the Sillimanite Gneiss Unit at North Maysville, Colorado (modification after Knight,1981). Distance = 0 corresponds to the west contact of the Sillimanite Gneiss Unit, and distances increase eastward.

DESCRIPTION	SAMPLE NO	DISTANCE (metres)
qtz-fldspr-biot-musc-sill gneiss	DKG101	0
qtz-fldspr-biot-sill-garn gneiss	DKG102	.75
qtz-fldspr-biot-ser-sill gneiss	DKG103	1.3
qtz-fldspr-biot-musc-sill-garn-mgt gneiss	DKG104	2.0
qtz-biot-sill-musc gneiss	DKG105	3.0
mgt-qtz-biot gneiss	DKG106	3.7
qtz-fldspr-biot schist	DKG107	5.8
qtz-fldspr-biot-epid schist/gneiss	DKG201	8.3
qtz-fldspr-biot-musc gneiss	DKG202	12.2
amph-biot-mgt-(garn) schist	DKG203	15.8
amph-biot-mgt-garn schist	DKG204	16.4
qtz-biot-sill-fldspr-garn gneiss	DKG205	16.9
biot-qtz-garn-sill-musc schist	DKG206	17.4
qtz-biot-garn-sill-fldspr-musc schist	DKG207	20.8
amph-biot-mgt-garn-qtz schist	DKG208	24.9
qtz-biot-garn-mgt schist	DKG209	25.3
qtz-biot-mgt gneiss	DKG210	25.7
sulfide lens biot-qtz-ser-mgt	DKG211	26.1
fldspr-qtz-biot-garn-epid schist/gneiss	DKG212	26.8
qtz-fldspr-biot-(mgt)-sill schist	DKG213	31.9
amph-plag-epid gneiss (metabasalt)	DKG215	35.2
amph-plag-epid gneiss (metabasalt)	DKG216	36.7
amph-plag gneiss (metagreywacke or metabasalt)	DKG217	39.1
amph-plag gneiss (metagreywacke or metabasalt)	DKG308	48.1
anth-garn-carb gneiss	DKG307	59.3
sulfide lens (mgt-biot-qtz-chl-sill)	DKG306	60.0
qtz-biot-epid-ser gneiss	DKG305	60.75
qtz-biot-sill-mgt gneiss	DKG304	61.8
epid-biot-qtz-fldspr-sill-ser schist	DKG303	62.6
qtz-biot-garn-mgt schist	DKG302	63.0
qtz-biot gneiss	DKG301	63.4

anthophyllite subunit. The mineralized version of this couple repeats itself several times in the North Maysville section (Table 3-1).

3.7 Broken Hill Main Lode Deposit, NSW, Australia

The Broken Hill Main Lode Deposit occurs within the Broken Hill Antiform of the lower Proterozoic Willyama Complex of western New South Wales, Australia (Fig. 3-16). The Broken Hill block is one of many blocks of metamorphic and subordinate igneous rocks in the complex. It is composed dominantly of metasedimentary schists and lesser amounts of quartz - feldspar rocks interpretted as being of migmatitic derivation (Stevens et al., 1979). Metamorphic grades are estimated to vary from low pressure greenschist (andalusite being the stable aluminosilicate polymorph) up to granulite facies (Phillips, 1977).

Sulfide and gahnite mineralization, peneconcordant with the local tectonic fabric at Broken Hill, occurs as disseminations or pods of galena, iron rich sphalerite and other sulfides in the upper portion of the "Mine Sequence" (Stevens et al., 1979; Laing, 1979) (Fig. 3-17). The Mine Sequence suite consists of various types of metasedimenary gneisses intercalated with leucocratic quartz - feldspar gneiss, amphibolite and a quartz - feldspar - biotite - (garnet) gneiss called the Potosi Gneiss. Mineralized horizons are reported to be composed essentially of a quartz - gahnite or quartz - garnet rock (Barnes, 1979). Other gangue minerals include calcite, fluorite and manganese and calcium silicates. Relict graded bedding is reported to be common

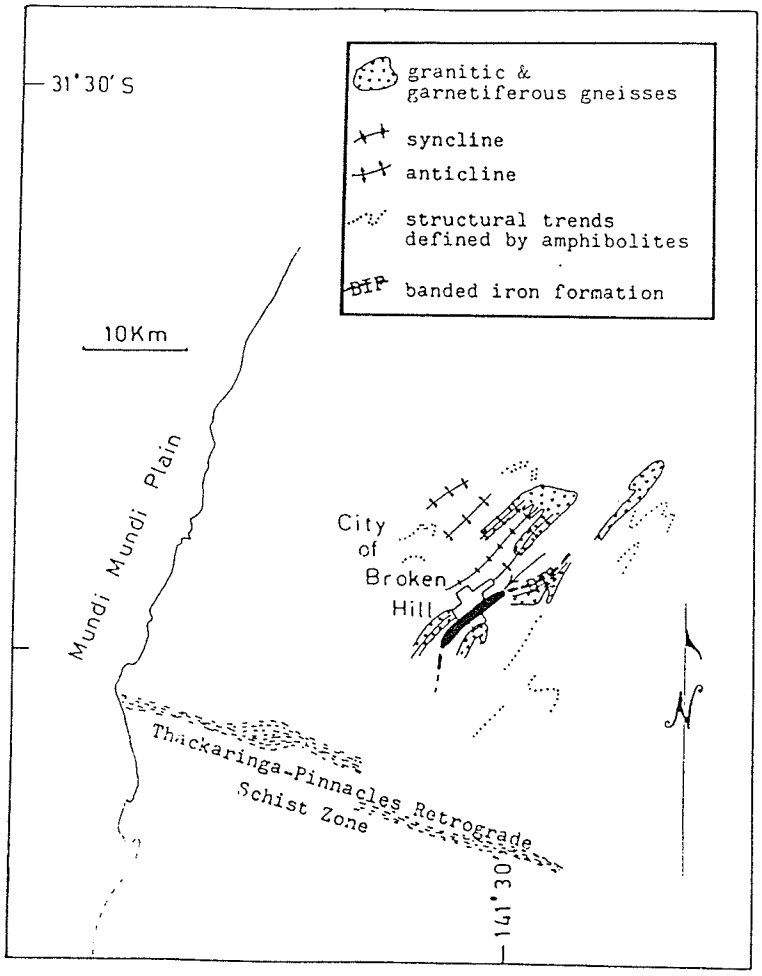

FIGURE 3-16 Location of the Broken Hill Main Lode, Broken Hill, N.S.W., Australia. Modified after Both and Rutland (1976).

FIGURE 3-17 Local stratigraphy of rocks of the lower Proterozoic Willyama Supergroup in the Broken Hill area, N.S.W., Australia, showing setting of ore lenses.

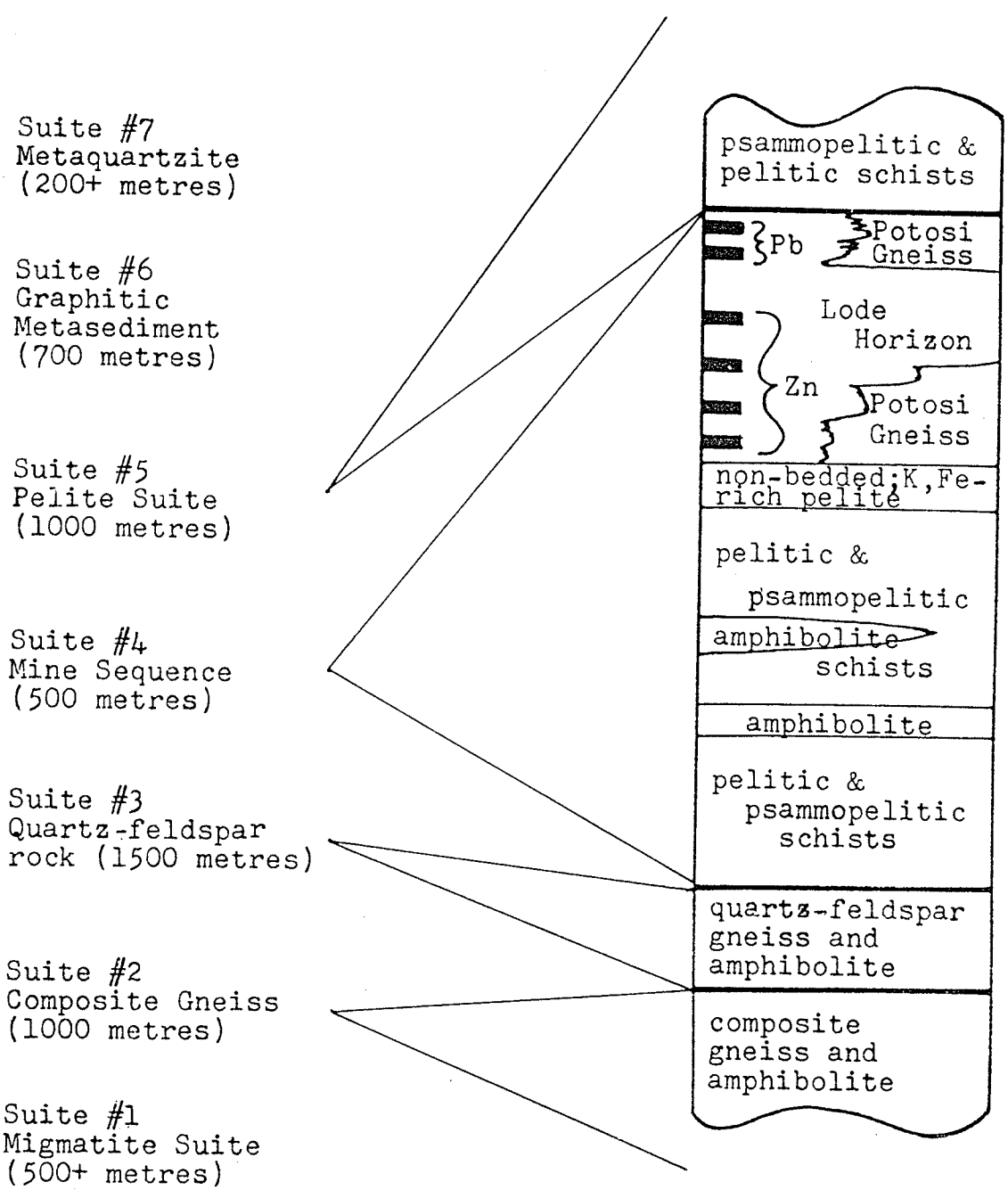

in the underlying pelite and psammopelite schists of the Pelite Suite (Laing, 1979). A non-bedded potassic, iron-rich pelite schist occurs at the base of the Potosi Gneiss. It typically contains abundant biotite, sillimanite, orthoclase and garnet.

Six rich, massive Pb - Zn - Ag ore lenses occur in the productive ore horizon. The top two are known collectively as the Lead Lodes and the bottom four as the Zinc Lodes. Continuity of the ore horizon appears to exist on the opposite limb of the Broken Hill Antiform where iron formations are found in place of the Pb - Zn - Ag ore in the Potosi Gneiss (Laing et al., 1979). No anthophyllite unit related to mineralization has been reported but the banded iron formations do contain minor grunerite. The four major components of the iron formations are quartz, magnetite, garnet and apatite. Chemical analyses of selected iron formations and enveloping rocks at Broken Hill, N.S.W. are listed in Appendix B-3.

CHAPTER 4

DATA PROCESSING AND INTERPRETATION

4.1 Sampling Methods and Geochemical Discrimination Techniques Utilized

Although the deposits subject to this study are classified as massive sulfide deposits, every locality studied also contains significant disseminated ore zones in which sulfide mineralization is intimately associated with sillimanite or cordierite - anthophyllite - bearing schists or gneisses (as shown by mineralogical data in Appendix A). Due to this repeated and intimate association between ore and host rock it is assumed that the mineralization was coeval with the geochemical activity also affecting the host rocks, either resulting from chemical sedimentation or post-depositional hydrothermal alteration. The purpose of the present data interpretation based on major element geochemical variations and mutual relationships has been to determine whether the host rocks acquired their present composition

(a) originally during sedimentation;

(b) by post - depositional hydrothermal alteration;

(c) during metamorphism.

The problem of chemical homogenization and/or differentiation produced through metamorphism has been studied several times in considerable detail but so far there are no universally applicable results. Stanton (1979) pointed out that the widely accepted concept of geochemical diffusion over large distances during metamorphism has been

greatly exaggerated. Electron microprobe studies of metamorphic minerals indicated that diffusion of most elements was generally restricted to distances of the order of millimetres (Stanton, 1979; Carmichael, 1969). Stanton (1979) has also stated that certain stratiform ores and their alteration envelopes often provide striking examples of the preservation of compositional inhomogeneities over small distances. La Roche (1974) has stated that greywackes and arkoses (coarse grained immature sediments) have a tendency to preserve the essential geochemical characteristics of their parent rocks (which were usually igneous). Problems are, however, encountered with mature sediments. For example, one often encounters problems of chemical convergence of amphibolites derived by metamorphism of calcareous pelitic sediments and basaltic igneous rocks. La Roche (1974) successfuly utilized the triangular "silicoaluminate" diagram (used in section 4.3 of this study) to differentiate between amphibolites from high metamorphic grade terrains. Similarly Van de Kamp (1970) successfully used methods based on Niggli values in an investigation of highly metamorphosed mafic sediments of the Scottish Dalradian Series.

A set of discrimination techniques that may differentiate between metamorphic rocks of sedimentary and igneous origin has been selected from the literature. Analytical results listed in Appendix A and Appendix B have been numerically processed, evaluated and compared using the petrochemical discrimination techniques listed below:

(1) $\log_{10} SiO_2/Al_2O_3$ vs. $\log_{10} (Na_2O + CaO)/K_2O$ (Garrels and MacKenzie, 1971);

(2) Silicoaluminate triangle (La Roche, 1965, 1974);

(3) Niggli k vs. mg (Leake, 1964);

(4) Niggli al - alk vs. c (Van de Kamp, 1970);

(5) Niggli al + alk vs. c (used strictly as a discriminant plot with no implied relationship to modal composition);

(6) log [Ni] vs. Niggli mg (Van de Kamp, 1970);

(7) Niggli ti vs. al + alk (a modification after Leake, 1964; Van de Kamp et al., 1976) with no implied correlation to be made with modal composition.

Niggli values are calculated according to the procedures outlined in Appendix C. The original raw data listed in Appendices A and B were subjected to these calculations. Appendix C also outlines calculations of the parameters for the methods of Garrels and MacKenzie (1971) and La Roche (1974).

4.2 The Discrimination Method of Garrels and MacKenzie (1971)

4.2.1 Introduction

Garrels and MacKenzie (1971) subdivided the compositional fields of sedimentary rocks and modern day unconsolidated sediments on the basis of their alkali ratios and silica : alumina ratios (Fig. 4-1). Siliceous sediments are characterized by a high silica : alumina ratio, calcareous sediments by a high $(CaO+Na_2O)/K_2O$ ratio and pelitic sediments by their more aluminous and potassic nature (low SiO_2/Al_2O_3 and low $(Na_2O+CaO)/K_2O$). When igneous rock compositions are plotted on the same graph, a continuous, relatively narrow banana - shaped field

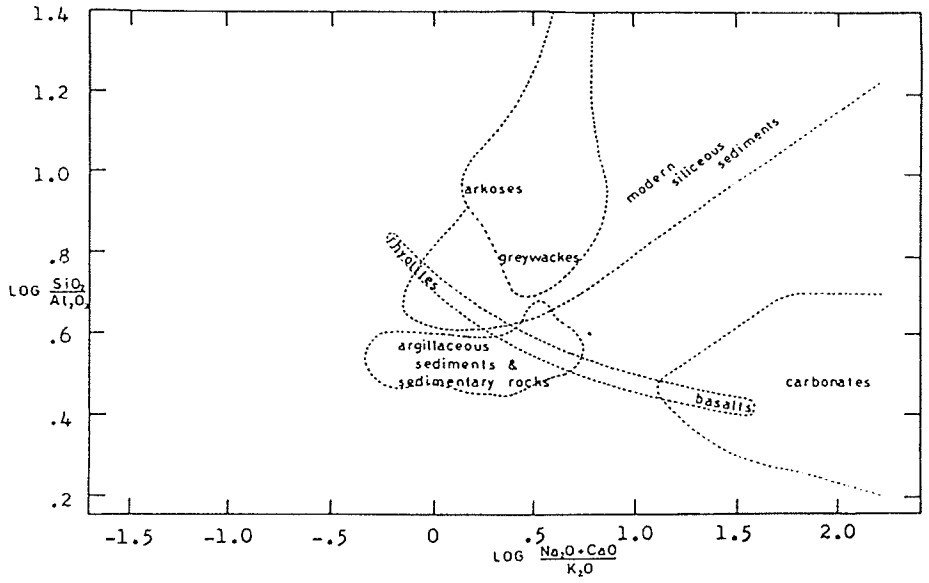

FIGURE 4-1 Compositional plot of consolidated and unconsolidated sediments and volcanics according to the method of Garrels and MacKenzie, (1971).

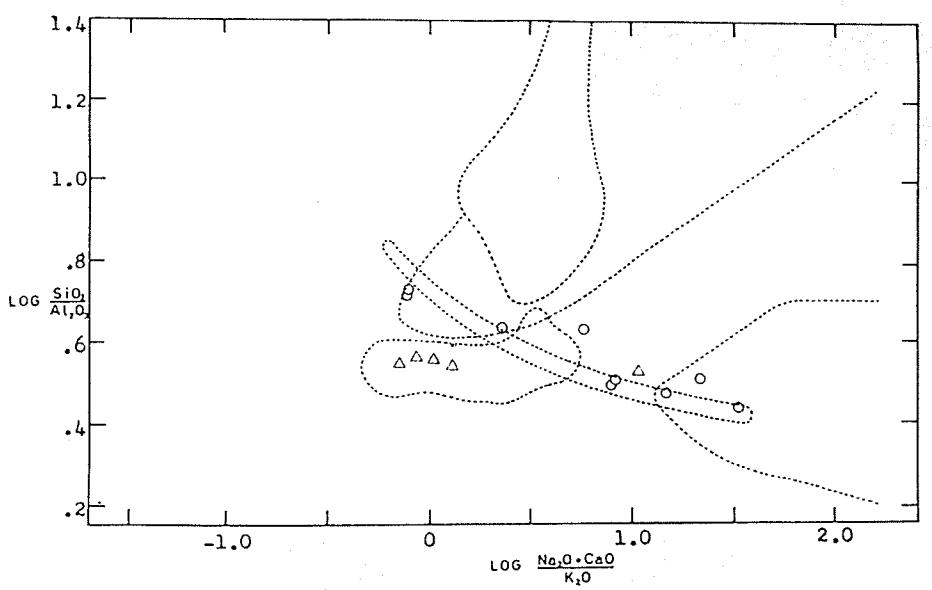

FIGURE 4-2 A test plot of several averaged analyses of unaltered igneous and sedimentary rocks (obtained from the literature; see Appendix B) into the sedimentary and volcanic compositional diagram of Garrels and MacKenzie, (1971).

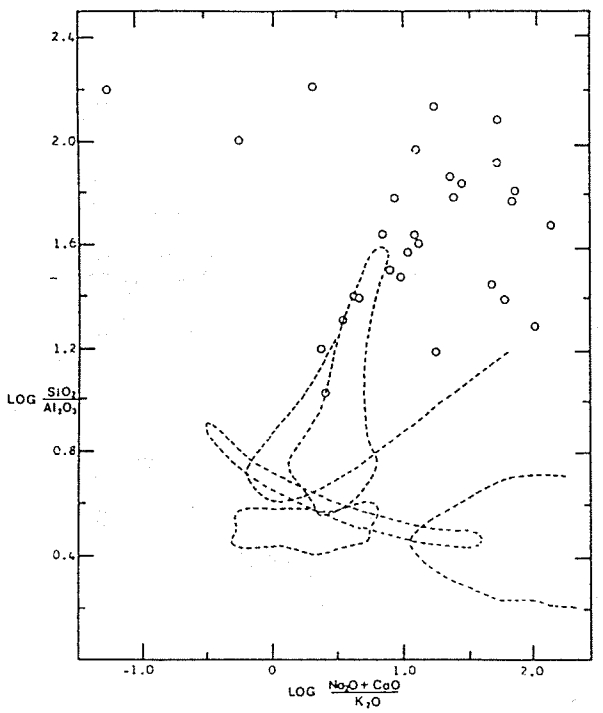

FIGURE 4-3 Plot of selected literature data on composition of iron formations (see Appendix B) according to the method of Garrels and MacKenzie, (1971).

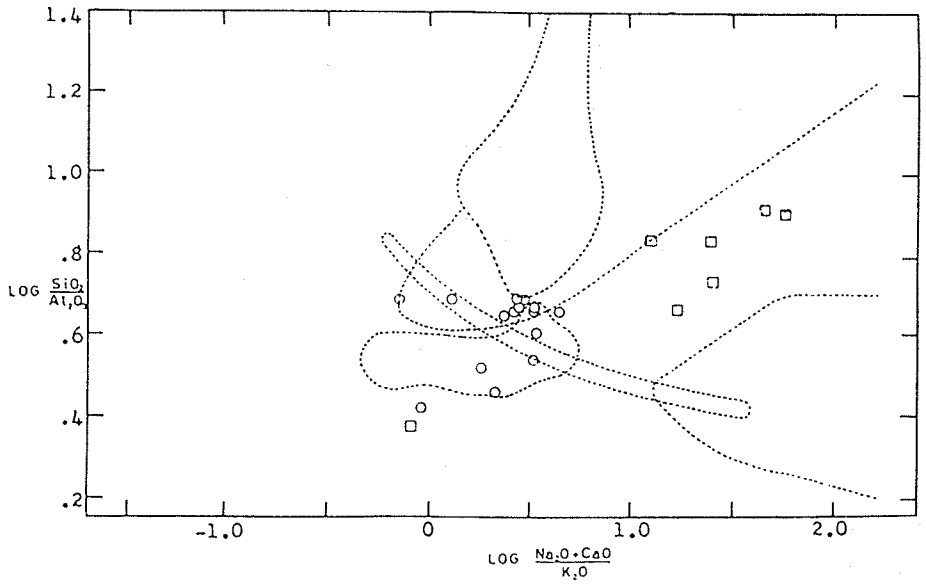

FIGURE 4-4 Garrels and MacKenzie (1971) plot of iron-rich metasedimentary rocks from the Ear Falls area, Ontario. Iron-rich gneisses are represented by squares and enveloping quartz-feldspar-biotite-(hornblende) gneisses by circles.

extending from silicic, potash - rich felsic rocks to more calcic, silica deficient mafic rocks. Fig. 4-2 demonstrates the application of this method to selected averaged analyses of normal igneous and pelitic rocks from the literature. Generally the fields outlined by Garrels and MacKenzie (1971) appear reasonably accurate, only minor departures from the narrow banana - shaped igneous field exist. Overlap of rock types, however, restricts the application of this method for protolith discrimination. Another weakness of this method is its inability to indicate low overall levels of all alkalies and calcium, as is the case in cherty iron formations (Fig. 4-3).

An investigation of the bulk compositions of numerous Algoma and Superior type iron formations based on data taken from the literature (listed in Appendix B-2), was made in order to compare iron formations and cordierite - anthophyllite schists occuring in the orebodies under consideration. Fig. 4-3 demonstrates that most iron formations fall within the siliceous sediment field outlined by Garrels and MacKenzie (1971) (Fig. 4-1).

4.2.2 Potash Enrichment, as Indicated by the Method of Garrels and MacKenzie, 1971

A small section of quartz - feldspar - biotite gneiss containing iron - rich (garnet - pyrite - pyrrhotite) bands in an area within the English River Gneiss Belt NE of Ear Falls, Ontario, was investigated to test the idea that these high grade metamorphic rocks had originally

been chemical sediments. Also tested was their relationship with enveloping clastic metasedimentary host gneisses. In the Garrels and MacKenzie (1971) diagram (Fig. 4-4), the host rocks cluster tightly within the lower arenaceous field close to the intermediate igneous field and may therefore represent greywacke metasediments. Iron enrichment is coupled with low levels of soda and potash; hence, iron - enriched rocks are displaced towards the right (higher values of log (Na_2 O+CaO)/K_2 O) on the diagram. Very little silica enrichment is apparent and given the marginal iron levels (<15 wt % FeO) one would assume the original sediments to have been ferruginous mudstones rather than members of a true siliceous iron formation.

A study of the ore zone and surrounding host rocks at the Geco Mine has demonstrated the anomalous geochemical character of the Sericite Schist group which hosts the orebody (Fig. 4-5). Rocks immediately south of the orebody appear to correspond to intermediate and mafic metavolcanic and associated metasedimentary rocks. Fig. 4-5 also gives a breakdown of Sericite Schist group rocks, and cordierite - anthophyllite schists of the 4/2 ore zone. Sericite Schist group metamorphic rocks fall, in part, within the same field as Grey Gneiss group metamorphic rocks but the former are characterized by a more potassic nature and slight silica enrichment in comparison with Grey Gneiss group samples. This skewing to the left on the Garrels and MacKenzie (1971) diagram is due not only to potash enrichment but also to severe calcium depletion within the Sericite Schist group (Appendix A-4).

Fig. 4-5 also indicates the less potassic nature of the cordierite - anthophyllite schists of the 4/2 ore zone at the northern contact of

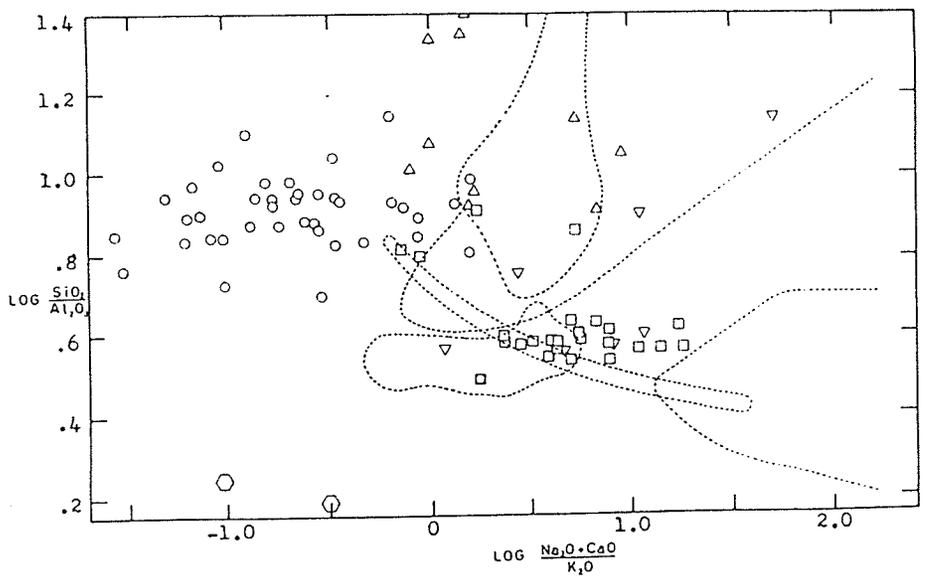

FIGURE 4-5 Plot of Grey Gneiss Gp and Milne Sequence rocks at the Geco Mine, Manitouwadge, against the background of the compositional fields of Garrels and MacKenzie, (1971). Grey Gneiss Gp rocks (excluding iron formations) are represented by squares, Grey Gneiss Gp iron formations by interted triangles, sillimanite-bearing Sericite Schist Gp rocks by circles, cordierite-anthophyllite rocks by triangles and "biotite-staurolite hornfels" by hexagons.

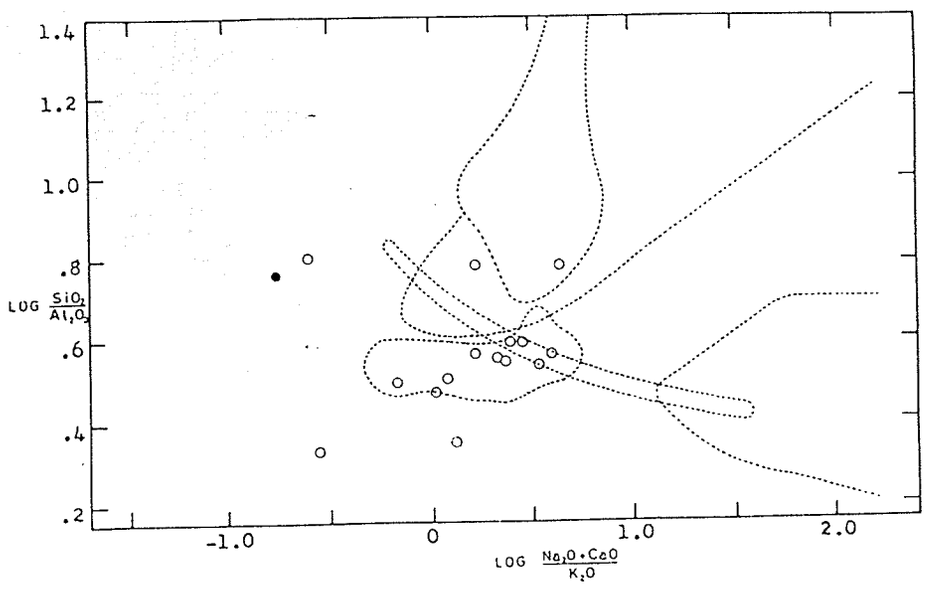

FIGURE 4-6b Garrels and MacKenzie (1971) plot of rocks encountered in diamond drill hole DDH-11-11-3 on Yakushavitich Island, Kississing Lake, Manitoba. Quartz-feldspar-biotite-sillimanite gneisses are represented by circles. The solid circle indicates anomalous levels of Cu and Zn (greater than 500 ppm).

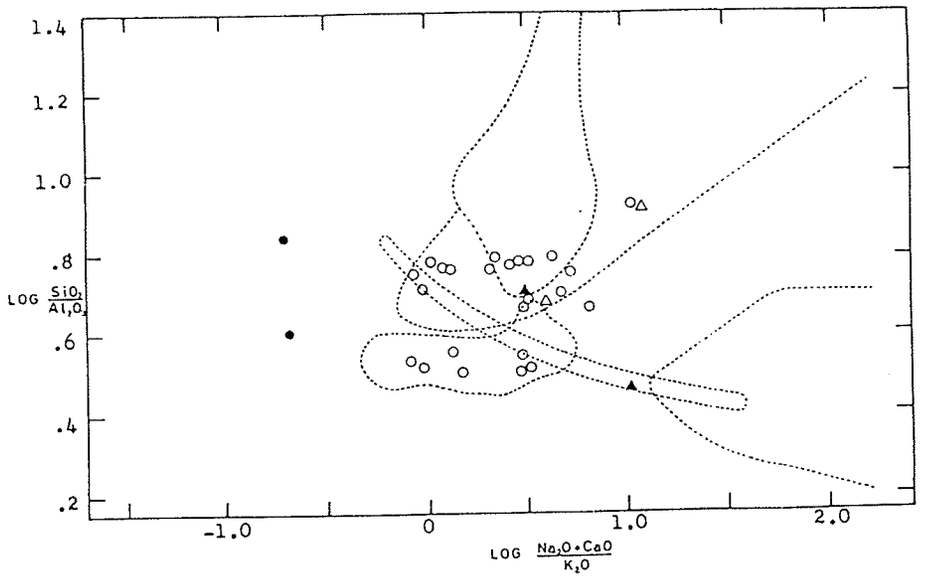

FIGURE 4-6a Garrels and MacKenzie (1971) plot of for rocks encountered in diamond drill hole DDH-11-11-5 on Yakushavitch Island, Kissi ssing Lake, Manitoba, Quartz-feldspar-biotite-sillimanite gneisses are represented by circles and anthophyllite-bearing roacks by triangles. Solid figures indicate Cu/Zn mineralization (greater than 500 ppm Cu or Zn).

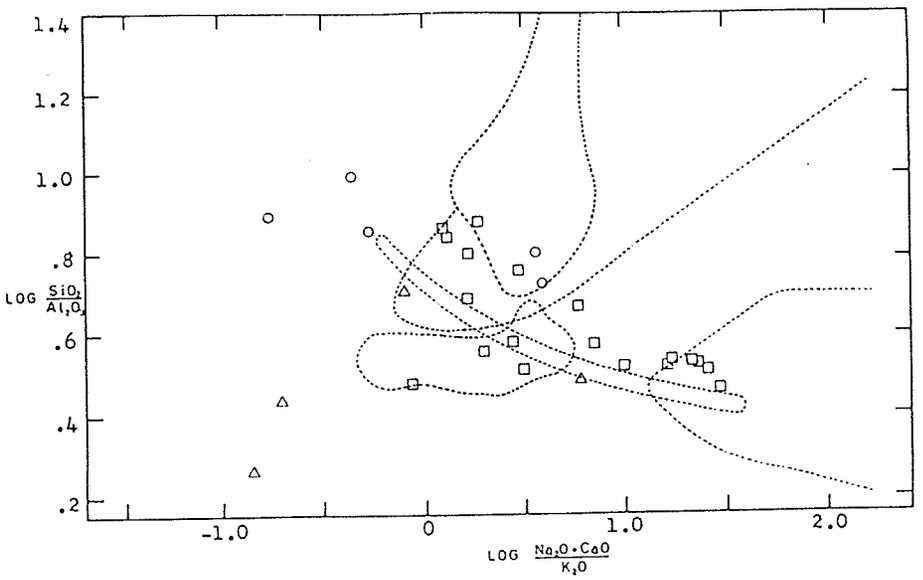

FIGURE 4-7 Garrels and MacKenzie (1971) plot of rocks from the Sherridon deposit, Sherridon,Manitoba,Quartz-feltspar-biotite-(hornblende) gneisses are represented by squares, biotite-sillimanite gneisses by circles and anthophyllite-bearing rocks by triangles (analyses from Goetz, 1980; see Appendix B).

the Sericite Schist group. The most notable characteristic of these rocks is depletion of all alkalies and calcium (Appendix A-4). Finally, Fig. 4-5 shows the nature of the iron formations between shafts #1 and #4. These iron formations, which vary from sulfide - rich to silicate - rich and to an oxide - enriched facies, and the immediately adjacent biotite - rich schists (Milne's unit 4) demonstrate variable ($Na_2O+CaO)/K_2O$ ratios, analogous to 4/2 cordierite - anthophyllite schists. They are, however, often slightly more aluminous. Coupled with the higher calcium contents (Appendix A-4), Geco Mine iron formations occupy a field to the right of that occupied by the cordierite - anthophyllite schists. Although the host rock (Milne's unit 4) is more aluminous, many of the samples of the iron formation itself are definitely siliceous with log $(SiO_2/Al_2O_3)>1.0$. Some of the samples of the iron formation demonstrate intermediate values of log (SiO_2/Al_2O_3) that could be explained by physical mixing of epiclastic and chemical sedimentary material.

The relationship between potash-enriched rocks and mineralization on the 2850 level at Geco Mine is demonstrated in Fig. 4-12; a modification of the Garrels and MacKenzie (1971) diagram. This section of the Sericite Schist group represents the down-dip extension of the main orebody. The 4/2 ore zone is a smaller economically exploitable ore mass consisting of a cordierite - anthophyllite - quartz groundmass containing stretched, rounded, pebble to cobble sized quartz fragments and hence designated "Quartz Pebble Conglomerate" by Geco Mine geological staff, plus a basal cordierite - anthophyllite - biotite rock. It can be noted that south of the 4/2 zone, despite fluctuations, $\log_{10}((Na_2O+CaO)/K_2O)$ remains below -0.4. Since this is a logarithmic

plot the effect of soda - potash variation is subdued and it is significant that drastic alkalies variations are occuring over relatively short distances, as this indicates that the rocks are not monotonous, as their outward appearance suggest.

Garrels and MacKenzie diagram for diamond drill core from Yakushavitch Island on Kississing Lake (Figs. 4-6a + 4-6b) indicates that the quartz - feldspar - biotite - sillimanite gneisses hosting Cu - Zn mineralization are likely greywacke metasediments in analogy with Sherridon itself (Bateman and Harrison, 1946; Froese and Goetz, 1979). Mineralized sections on Yakushavitch Island are small but as one can see in Fig. 4-13, Cu - Zn enrichment correlates with potash enrichment and sodium - calcium depletion. Fig. 4-13 also shows some degree of metal zonation (copper grades reaching a maximum at 40 metres and zinc at 42 metres).

Fig. 4-7 is an application of Garrels' and MacKenzie's method to selected averaged rock compositions for several members of the metamorphic association at Sherridon itself (from Goetz, 1980). It demonstrates the problems arising from the averaging of rock compositions when small scale chemical fluctuations may exist, as appears to be the case within the Sericite Schist group at the Geco Mine (Fig. 4-50.

Generally the anthophyllite - bearing schists at Sherridon and on Yakushavitch Island demonstrate potash enrichment, as opposed to those at the Geco Mine. One must again bear in mind, however, that all alkalies and calcium are depleted in the anthophyllite - bearing schist (Appendix A-5) so this means only that potash is not as depleted as within the anthophyllite schists at Geco.

Knight (1981) described a similar section of sillimanite and fibrous amphibole - bearing gneisses at Selco's North Maysville property in central Colorado (Fig. 4-8). Mineralization once again correlates with potash enrichment (Fig. 4-14). Two major mineralized sections were encountered, separated by a barren amphibole gneiss unit. Both sections appear to show some metal zonation with copper concentrated lower down in the section (towards the right in Fig. 4-1). Alkali fluctuations at North Maysville are even more extreme than those observed at Geco.

Relatively unmineralized samples such as DKG-202 and DKG-205 possess alkali ratios characteristic of normal igneous rocks and since there is a clustering of data points in the field of normal felsic igneous rocks, Knight (1981) concluded that these likely originally represented normal felsic volcanic rocks (tuffs). Departure to the left of this field occurs in the rocks which are mineralized, or immediately adjacent to mineralized rocks. Potash enrichment in DDH-11-11-5 on Yakushavitch Island (Fig. 4-13) in the Sherridon area does not reach its maximum within the mineralized section itself but in the rocks immediately uphole of the mineralization. A similar, although much broader, potash "envelope" occurs at the Geco Mine (Fig. 4-12). It becomes apparent that this effect may have practical application because it increases target size in exploration for similar orebodies.

Geochemical comparison of the rocks hosting the Broken Hill orebody in New South Wales, Australia with rocks hosting the orebodies discussed earlier is of interest in order to explore the possibility of genetic similarity.

Several reported analyses (Joplin, 1963) (listed in Appendix B-3) of different stratigraphic units at Broken Hill indicate a potash

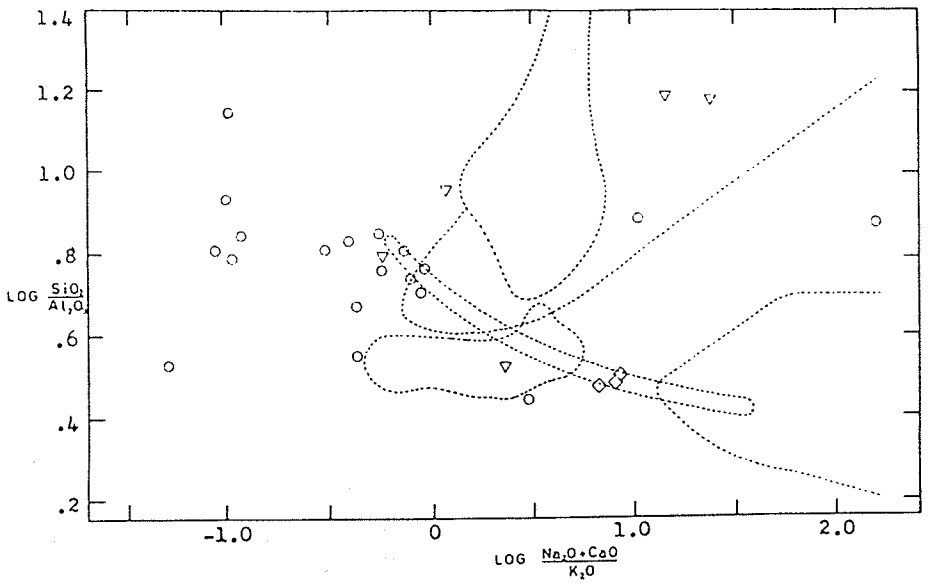

FIGURE 4-8 Garrels and MacKenzie (1971) plot of rocks from the Sillimanite Gneiss Unit at N. Maysville, Colorado based on data in Knight (1981). Amphibolities are represented by diamonds, sillimanite-bearing rocks by circles, iron formations and fibrous amphibole-bearing rocks by inverted triangles.

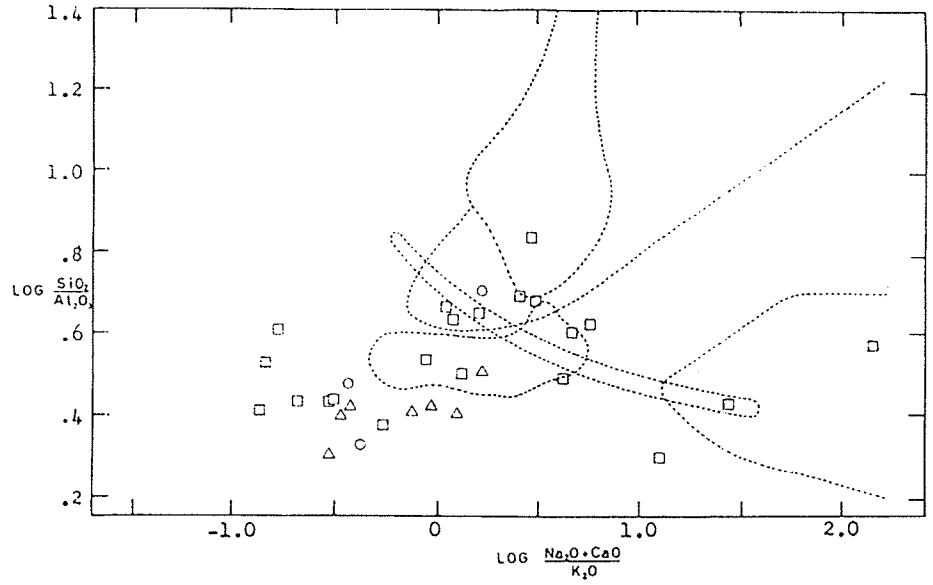

FIGURE 4-9 Garrels and MacKenzie (1971) plot of rocks from the Broken Hill Main Lode, Broken Hill, N.S.W., Australia (analyses from Joplin, 1963; see Appendix B). Sillimanite-cordierite gneisses are represented by triangles, other sillimanite-bearing gneisses by circles and other non-sillimanite felsic gneisses by squares.

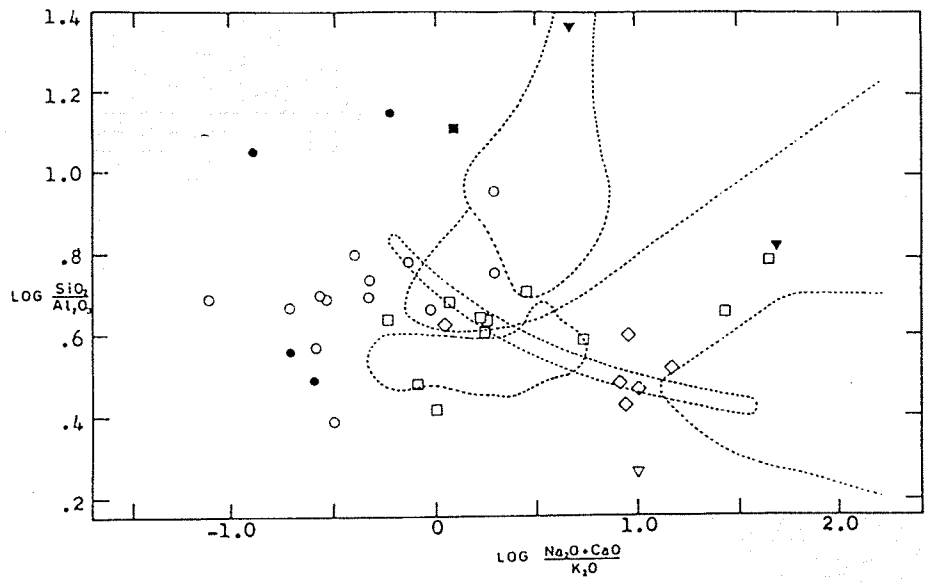

FIGURE 4-10 Garrels and MacKenzie (1971) plot of rocks from the New Calumet deposit,Calumet Island, Québec. Non-sillimanite gneisses and schists are represented by squares, sillimanite-bearing roacks by circles, amphibolities by diamonds, calc-silicate gneisses and carbonates by inverted triangles. Solid figures indicate Cu or Zn ⩾ 500 ppm.

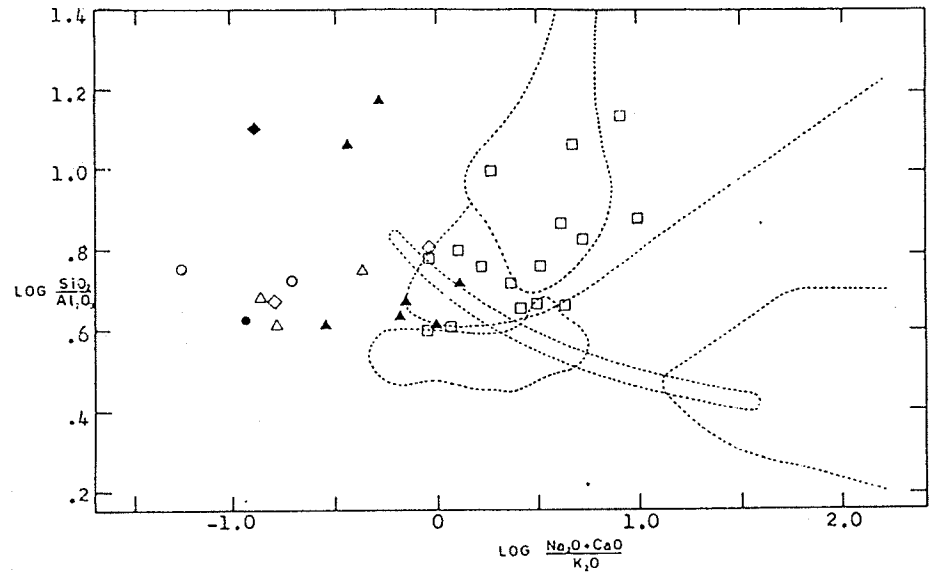

FIGURE 4-11 Garrels and MacKenzie (1971) plot of rocks from the Tetréault Mine and vicinity, Montauban,Québec. "Leptites" (analyses from Stamatelopoulou-Seymour and MacLean, 1977; see Appendix B), are represented by squares, calc-silicate gneisses and carbonates by inverted triangles, amphibolities by diamonds, sillimanite-bearing rocks by circles and cordierite-anthophyllite rocks by triangles. Solid figures indicate Cu or Zn ⩾ 500 ppm.

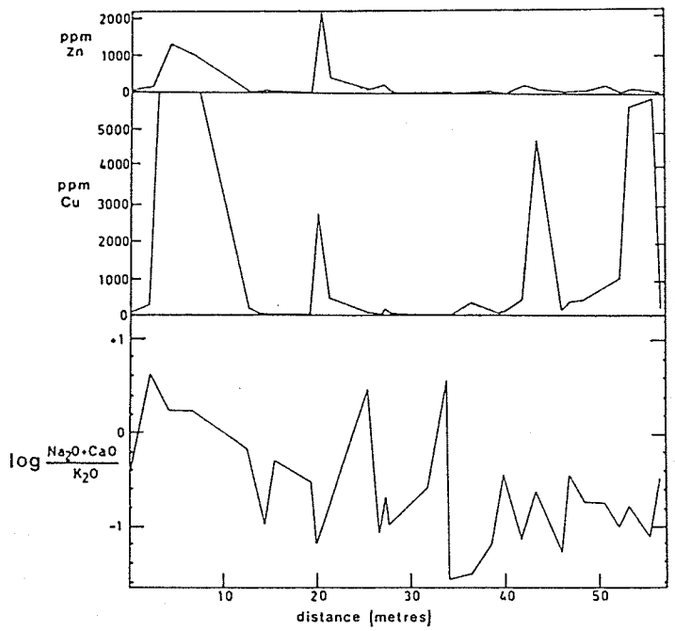

FIGURE 4-12

Relationship of potassium enrichment and mineralization with distance along the 28-65 cross-cut at the Geco Mines, Manitouwadge. Distance is measured south from the Stratigraphic base of the 4/2 ore zone. Based on the method of Garrels and MacKenzie, (1971).

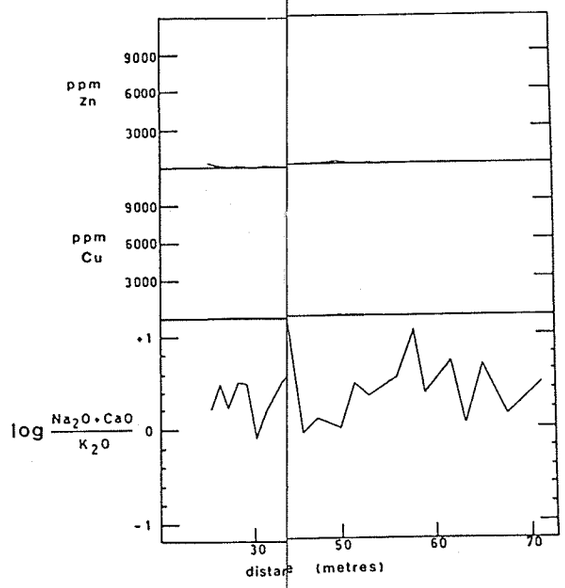

F

Re of potassium
end Cu/Zn
mion with down-
hde in diamond
drDH-11-11-5 on
Ya Island,
Kiake, Manitoba.
Ba method of
GaMacKenzie (1971).

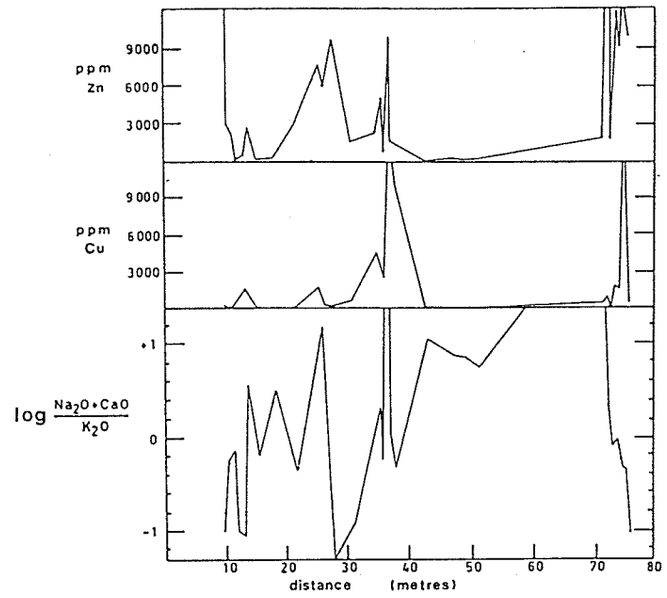

FIGURE 4-14

Relationship of potassium enrichment and Cu/Zn mineralization with distance across the Sillimanite Gneisse Unit at N. Maysville,Colorado. Distance is measured east from the west contact of the Sillimanite Gneiss Unit. Based on the method of Garrels and MacKenzie, (1971).

enrichment similar to those encountered at Geco, Sherridon and North Maysville (Fig. 4-9). But some differences are also apparent. Whereas Geco, Sherridon and North Maysville exhibit silica : alumina ratios comparable to those of normal felsic to intermediate igneous rocks, Broken Hill gneisses are somewhat more aluminous (silica : alumina ratios being equal to or less than those characteristic of normal shales). Secondly, although not apparent on Garrels' and MacKenzie's diagram, the calcium depletion observed at Broken Hill (Appendix B-3) is not as severe as other localities discussed earlier. The higher calcium contents of Broken Hill gneisses are also responsible for masking, to some extent, their potassic nature on the Garrels and MacKenzie diagram. The weakness of the Garrels and MacKenzie method manifests itself in its inability to portray calcium deficiencies and therefore the more calcic nature of Broken Hill gneisses (in comparison with those of Geco, Sherridon and North Maysville).

Gneissic sillimanite - bearing diamond drill core from the New Calumet deposit on Calumet Island, Quebec (Fig. 4-10) again demonstrates the same type of potash enrichment observed at the other previously discussed localities. Calcium depletion exists at New Calumet despite the occurence of dominant carbonate and calc-silicate gneiss units within the ore zone (samples clm 30, clm 31, clm 32 and clm 33). The cordierite - anthophyllite gneisses were not sampled but are reported by Moorhouse (1941) to exist. Variable potash enrichment is observed within the quartz - feldspar gneisses. Some of these plot within the field of normal felsic to intermediate igneous rocks while others plot to the left of them. They have silica : alumina ratios comparable or slightly lower than those within the igneous field. Generally, all the

sillimanite gneisses show potash enrichment. Of the samples taken, copper mineralization is restricted to more sillimanite - rich hosts whereas zinc is more commonly concentrated in calc-silicate rocks. In both cases the silica : alumina ratio is usually elevated (Fig. 4-10). Moorhouse (1941) has reported that significant gold mineralization exists at New Calumet but he does not specify whether it occurs within the cordierite - anthophyllite schist, sillimanite - bearing felsic gneiss or carbonate.

Plots of some of the New Calumet amphibolites are shown in Fig. 4-10. The bulk of the amphibolites at New Calumet has been interpreted to be of sedimentary origin. The Garrels and MacKenzie plot, however, demonstrates clustering around the mafic end of the sausage-shaped igneous field and the carbonate field. Although the origin of the amphibolites is nebulous according to this method, intimate field relationships of the amphibolites and carbonates would appear to indicate that the amphibolites may be meta-carbonates.

In analogy with New Calumet the sillimanite - bearing gneisses at Montauban occupy a region to the left of the field of normal felsic to intermediate igneous rocks (Fig. 4-11). Some of the "Sodic Leptites" described by Stamatelopoulou - Seymour and MacLean (1977) are also represented. These rocks, located to the west of the ore-bearing horizon, generally occupy a field with $\log_{10}((Na_2O+CaO)/K_2O)>=0$. Stamatelopoulou - Seymour and MacLean (1977), on the basis of normative corundum contents, interpreted the sixteen leptites depicted in Fig. 4-11 to be of felsic volcanic origin. The generally higher values of $\log_{10}((Na_2O+CaO)/K_2O)$ in the leptites are, once again, partly the result of elevated calcium contents. Table 4-1 demonstrates increasing potash

TABLE 4-1 Variation of alkalies, calcium and silica:alumina ratio within the "Leptites" (data from Stamatelopoulou-Seymour and MacLean, 1977), Montauban, Quebec. Distance is measured west from the Calc-silicate Unit or the Cordierite-Anthophyllite Unit (which both occur at the same stratigraphic level).

SAMPLE NUMBER	DISTANCE (metres)	CaO	Na_2O	K_2O	$\log\left[\frac{Na_2O+CaO}{K_2O}\right]$	$\log\left[\frac{SiO_2}{Al_2O_3}\right]$
A133	0	1.25	0.32	3.59	-.359	0.750
A101	0	0.29	0.02	0.87	-.448	1.06
A31	30	4.61	0.81	1.03	.721	0.822
A33	120	0.28	2.48	0.69	.674	1.06
A34	170	0.65	4.41	1.23	.614	0.866
A35	240	1.04	0.85	1.01	.272	0.991
A38	420	3.83	3.29	1.66	.632	0.655
A39	430	2.81	2.93	4.81	.077	0.604

enrichment as the ore-bearing calc - silicate / cordierite - anthophyllite unit is approached. It is possible that intermixing of felsic volcaniclastic rocks and sediments such as clay and/or some carbonate has produced these CaO contents which are atypical of normal felsic volcanic rocks. Although some leptites cluster near the intermediate section of the igneous field (Fig. 4-11), many are displaced upwards toward high $\log_{10}(SiO_2/Al_2O_3)$ values. This also indicates departure from a purely volcanic origin unless the metamorphics represent normal intermediate volcanic rocks which were subsequently silicified. Assuming the stratigraphic interpretations of Stamatelopoulou - Seymour and MacLean (1977) are correct, these silicified rocks could be a result of late stage deposition of minor amounts of chemically precipitated silica considered in the volcanogenic massive sulfide model proposed by Large (1977). According to the data of Stamatelopoulou - Seymour and MacLean (1977), the most silicic leptites occur within an area of 120 to 240m west of the ore-bearing calc - silicate unit. Sample A31 (Table 4-1), located about 30m west of the orebody, occurs approximately 10m east of an amphibolite unit which may be a metabasalt. The proximity of the amphibolite may be responsible for the lower SiO_2/Al_2O_3 ratio of sample A31.

Anomalous zinc levels are found within the sillimanite - cordierite - anthophyllite gneisses and calc - silicate gneisses (Fig. 4-11). McAdams and Flannagan (1976) have also reported copper grades approaching 3% and gold grades up to 0.7 oz/ton within the cordierite - anthophyllite gneiss at Montauban.

4.2.3 Discrimination Results Based on the Garrels and MacKenzie (1971) Method: a Discussion

Experimental studies have indicated that alteration of regular greywacke sediments by heated seawater or solutions equivalent to hydrothermal brines (Bischoff et al., 1981) causes a slight potash enrichment over soda and calcium oxide. Potassium metasomatism occurs in the more severely hydrothermally altered rocks at Steamboat Springs, Nevada (Sigvaldson and White, 1962; Parry et al, 1980). Fig. 4-15 shows the effects of the alteration which occurs in a granodiorite at Steamboat Springs, Nevada (data from Sigvaldson and White, 1962). Some of the data points are displaced towards the left in the Garrels and MacKenzie plot indicating that potash enrichment over Na_2O + CaO has occured in these rocks. Similarly Fig. 4-16 indicates potash enrichment in a quartz monzonite at Roosevelt Spgs., Utah (data from Parry et al., 1980). A similar type of potassium metasomatism is reported to occur in rhyolites in the Sinai Peninsula (Agron and Bentor, 1981). The effects of this alteration are also shown on the Garrels and MacKenzie plot in Fig. 4-16. The direction of increasing alteration is based upon data from the literature, listed in Appendices B-6 and B-7.

Potassium metasomatism has also been frequently recorded within the alteration pipes of volcanogenic massive sulfide deposits. Fig. 4-17 depicts the progressive alteration of felsic host rocks at the Millenbach Mine and the Mattagami Lake Mine. Again, the direction of increasing alteration is based upon data from the literature, listed in Appendices B-8 and B-9. These deposits are both situated in the

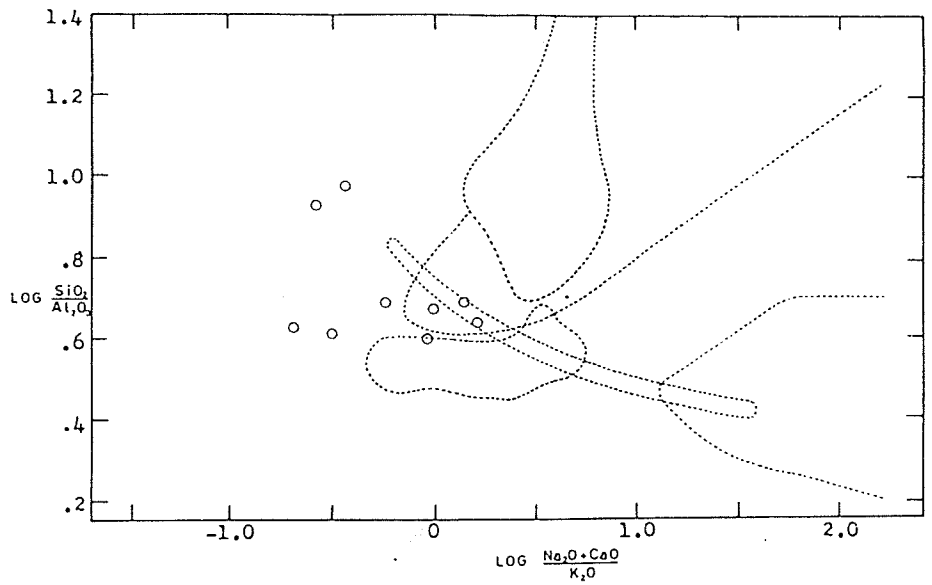

FIGURE 4-15 Application of the method of Garrels and MacKenzie (1971) to some hydrothermally altered felsic igneous rocks from Steamboat Springs, Nevada (data from Sigvaldson and White, 1962; see Appendix B).

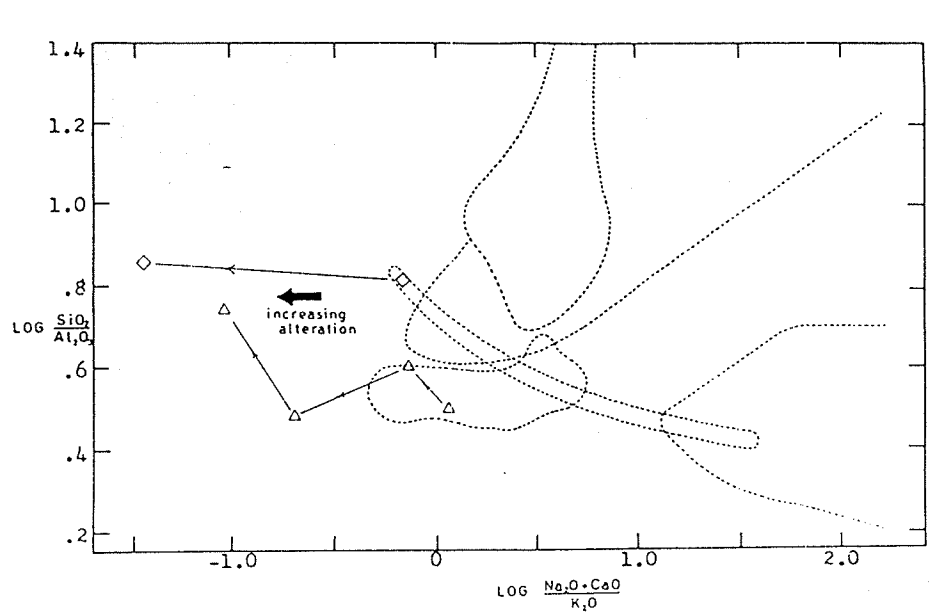

FIGURE 4-16 Garrels and MacKenzie (1971) diagram showing the effects of prograde hydrothermal alteration on some felsic igneous rocks. Diamonds represent alteration of rhyolities from Biq'at Hayareah, Sinai (data from Agron and Bentor, 1981; see Appendix B); and triangles represent alteration of a quartz monzonite at Roosevelt Hot Springs, Utah (data from Parry et al., 1980; see Appendix B).

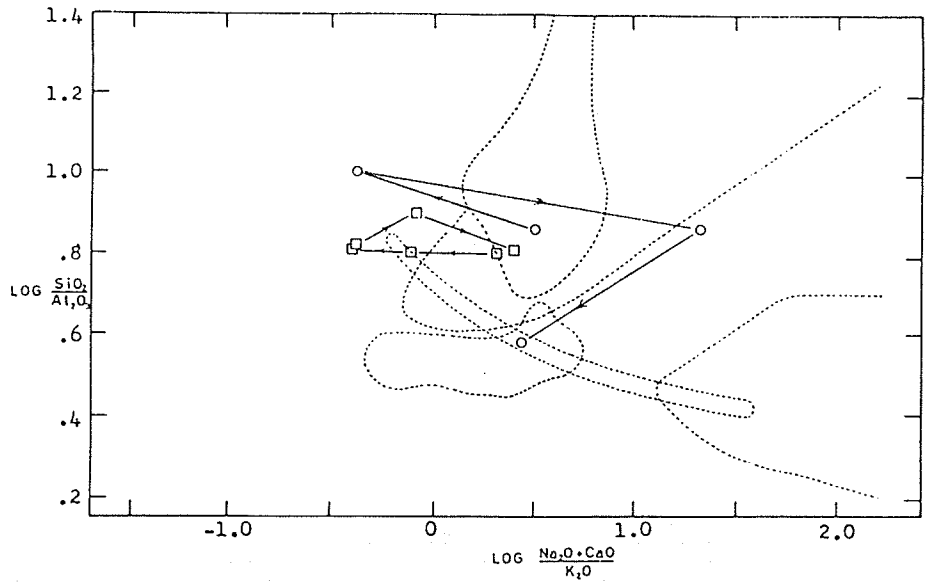

FIGURE 4-17 Garrels and MacKenzie (1971) diagram showing plots of hydrothermally altered rocks from the alteration pipes of selected massive sulfide deposits. Squares represent rocks from the Millenbach Mine (data from Riverin and Hodgson, 1980; see Appendix B) and circles represent rocks from the Mattagami Lake Mine (data from Roberts and Reardon, 1978; see Appendix B). Arrows indicate increasing alteration.

Superior structural Province of the Canadian Shield in Quebec. In both instances an initial depletion of Na_2O becomes more extreme, as one approaches the core of the pipe, and K_2O is also leached. In the plot of an altered rhyodacitic tuff at Mattagami Lake, one data point is situated a fair distance towards the right of the others (Fig. 4-17), indicating a substantial re-introduction of calcium, a similar case has not been observed at any of the localities subject to the present study. The most altered rocks at both Mattagami Lake and Millenbach are found at the cores of the alteration pipes. They are depleted in all alkalies and CaO, and are enriched in magnesium and iron. Geochemically they are similar to the cordierite - anthophyllite rocks which occur at each of the localities discussed thus far.

If one tries to draw an analogy with the alteration pipes of volcanogenic massive sulfide deposits, assuming alteration is responsible for the compositional departure of metamorphic rocks out of the field of "normal" rocks, the potash enrichment which occurs in the sillimanite - bearing host rocks at Geco, Sherridon, N. Maysville, New Calumet and Montauban would bear closest resemblance to the moderately altered host rocks at the Millenbach and Mattagami Lake Mines. For example, samples LT 150 and LT 151 (Appendix B) at Millenbach, which correspond to the best developed "dalmatianite" (Riverin and Hodgson, 1980), show the greatest enrichment of K_2O over Na_2O and CaO.

4.3 Geochemical Discrimination Based on the La Roche (1974) "Silicoaluminate" Triangle

4.3.1 Introduction

La Roche (1974) utilized a very simple triangular plot of Na_2O, K_2O and MgO in order to outline fields of magmatic rocks and several types of sedimentary rocks. Fig. 4-18 demonstrates the adherance of selected, "normal" igneous and sedimentary rocks from the literature to the fields generated by LaRoche (1974).

Application of this plotting method to various iron formations (Fig. 4-19) produces a clustering near the MgO apex of the diagram. Since this diagram may be considered to be a projection of the tetrahedral diagram K_2O - MgO - Na_2O - SiO_2 on to the K_2O - MgO - Na_2O plane, variations in silica are not portrayed.

4.3.2 Alkalies Enrichment as Shown by the "Silicoaluminate" Diagram of La Roche (1974)

Iron - rich metasedimentary rocks from the Ear Falls area demonstrate enrichment of magnesia over soda and potash (Fig. 4-20). Their host rocks plot within La Roche's greywacke field, thus supporting the results of the Garrels and MacKenzie (1971) method (Fig. 4-4). Fig.

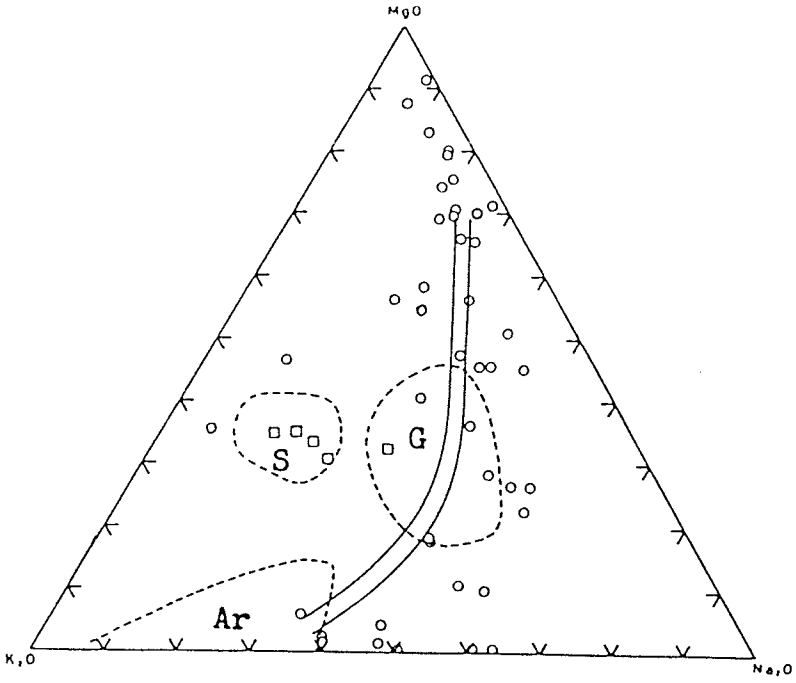

FIGURE 4-18 Silicoaluminate diagram (La Roche,1974) for several common igneous and sedimentary rocks selected from the literature (see Appendix B). Igneous rocks are represented by circles and sedimentary rocks by squares. Key to fields bounded by dashed lines (from La Roche, 1974): Ar = arkose field, G = greywacke field, S = shale field. The igneous field of La Roche (1974) is bounded by solid lines.

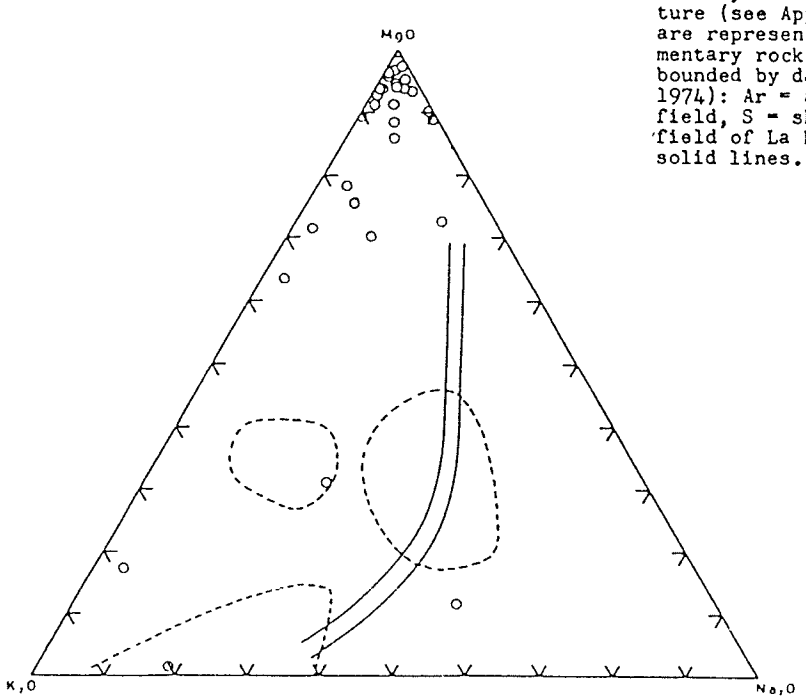

FIGURE 4-19 Silicoaluminate diagram (La Roche, 1974) showing plots of several iron formations based on worldwide literature data (see Appendix B).

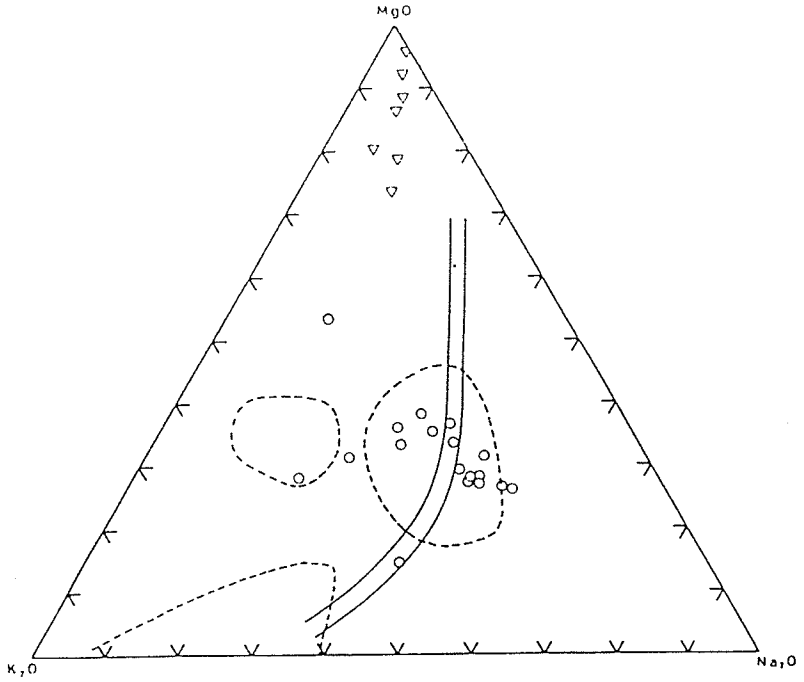

FIGURE 4-20 Silicoaluminate diagram (La Roche, 1974) for ferruginous metasedimentary rocks (inverted triangles) and enveloping quartz-feldspar-biotite-(hornblends) gneisses (circles) of the Ear Falls area, Ontario.

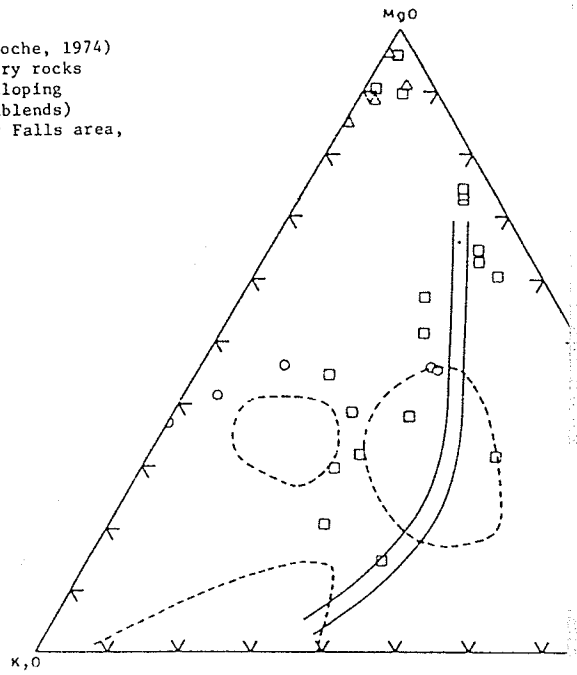

FIGURE 4-22 Silicoaluminate diagram (la Roche, 1974 for selected metamorphics from the Sherridon deposit, Manitoba (analyses from Goetz,1980). Cordierite-anthophyllite rocks are represented by triangles, biotite-sillimanite gneisses by circles and other quartz-feldspar gneisses by squares.

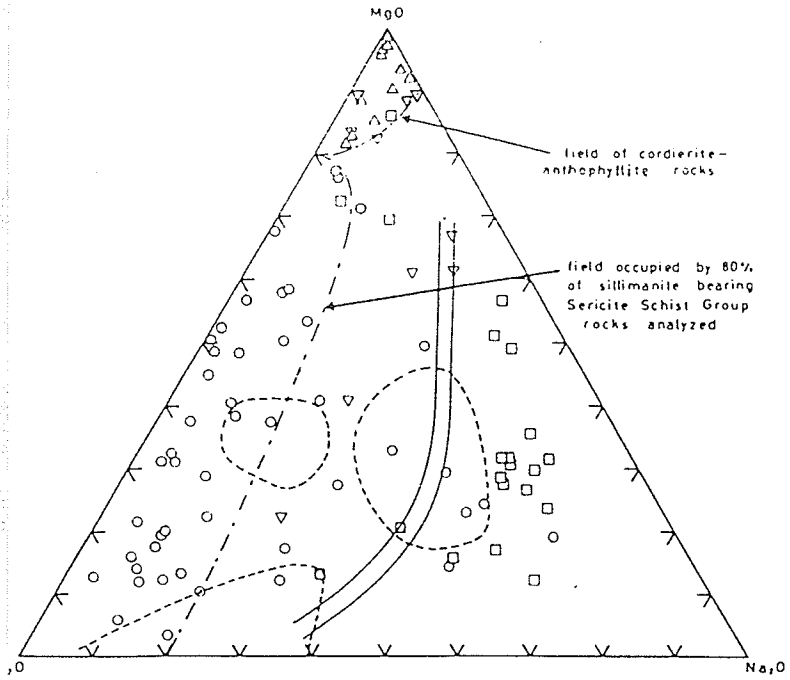

FIGURE 4-21 Silicoaluminate diagram (La Roche, 1974) for rocks from the Geco deposit and vicinity. Grey Gneiss Gp rocks (with the exception of iron formations) are represented by squares, Grey Gneiss Gp iron formations (and intercalated meta-sedimentary rocks) are represented by inverted triangles, sillimanite-bearing rocks of the Sericite Schist Gp are represented by circles and cordierite-anthophyllite rocks from the 4/2 ore zone are represented by triangles.

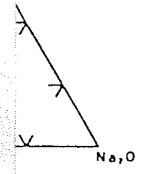

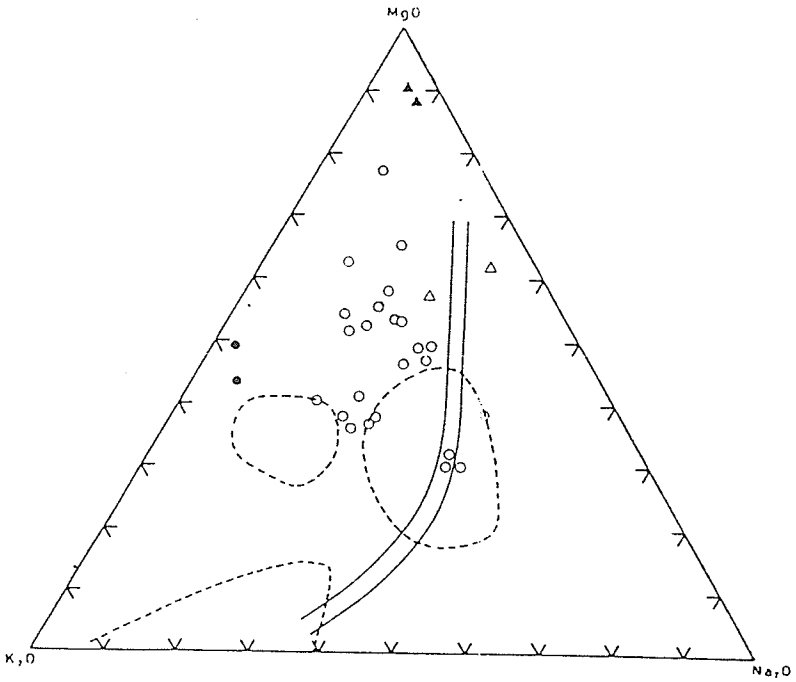

FIGURE 4-23 Silicoaluminate diagram (La Roche, 1974) for ore-bearing rocks encountered in diamond drill hole DDH-11-11-5 on Yakushavitch Island, Kissinssing Lake, Manitoba. Anthophyllite-bearing rocks are represented by triangles and enveloping quartz-feldspar-biotite-(sillimanite) gneisses and schists by circles. Solid figures indicate greater than 500 ppm Cu or Zn.

4-20 also suggests a gradational contact between sulfide - bearing host rocks and the iron enriched sediment.

Grey Gneiss group rocks at Geco, Manitouwadge (Fig. 4-21) are found to cluster along the right edge of La Roche's (1974) greywacke field and to a lesser extent along the right edge of the mafic igneous field. This being the case, if progenitors of grey gneiss rocks are igneous in origin, some soda enrichment is indicated. Sericite Schist group rocks which host the orebody, on the other hand, indicate soda depletion, plotting along the MgO - K_2O leg of the diagram. Members of the Sericite Schist group at the 2850 level are found to become gradually enriched in MgO as one approaches the 4/2 ore zone. Cordierite - anthophyllite - rich schists of the 4/2 ore zone, and Sericite Schist group rocks hosting massive sulfides on the 2350 level at Geco are found to cluster near the MgO apex of the diagram in much the same way the iron formations were found to (Figs. 4-19 and 4-20).

Fig. 4-22 shows the distribution of sillimanite - bearing gneisses and anthophyllite schists of the Sherridon area (analyses from Goetz, 1980). The potassic nature of some of the sillimanite - bearing host gneisses at Sherridon is obscured by averaged analytical results. A wide range of Na_2O values is demonstrated by these gneisses but averaging causes the data to plot within the field of normal shales and greywackes.

A similar wide range in Na_2O is again demonstrated by host gneisses for mineralization on Yakushavitch Island, Kississing Lake, Manitoba (Fig. 4-23). Soda enrichment, however, does not extend beyond the right side of the igneous field generated by La Roche (1974). Therefore, if the host rocks to the ore are of igneous origin (tuffs of intermediate

composition), the wide range of Na_2O values shown may well indicate varying degrees of potash enrichment and soda depletion. This is discussed in greater depth in Section 4.3.3. Additionally, MgO enrichment (in comparison with quartz - feldspar host gneisses) appears to accompany mineralization, in analogy with the Sherridon deposit.

Gneisses from the N. Maysville prospect in Colorado (Fig. 4-24) fall roughly within the same field as do the Sericite Schist group rocks at the Geco Mine (Fig. 4-21). Again, mineralized schists and gneisses cluster near the MgO apex of the diagram.

Broken Hill host rocks also show an excess of potash over soda (Fig. 4-25). They do not, however, plot in the same field as the sillimanite - bearing gneisses at Geco, North Maysville or Sherridon. As a result, there does not appear to be a gradation between these gneisses and iron formations at Broken Hill.

A plot of sillimanite gneisses from the New Calumet Mines area in Quebec (Fig. 4-26) produces a dispersed field generally centered on the shale field outlined by La Roche (1971). There are, however, a few soda - enriched samples. Calcareous and calc - silicate rich gneisses plot near the MgO apex of the diagram. Although sillimanite - bearing gneisses of the plot coincide roughly with the shale field, a sufficiently large percentage fall into the same soda - depleted region demonstrated by similar gneisses at the Geco Mine.

If Stamatelopoulou - Seymour and MacLean's (1977) assumption concerning the stratigraphy at Montauban is correct, samples taken from the upper section of the "Leptite" unit appear to fall within La Roche's greywacke and arkose fields (Fig. 4-27). Due to the overlap of fields, they may also represent intermediate tuffaceous rocks. As one

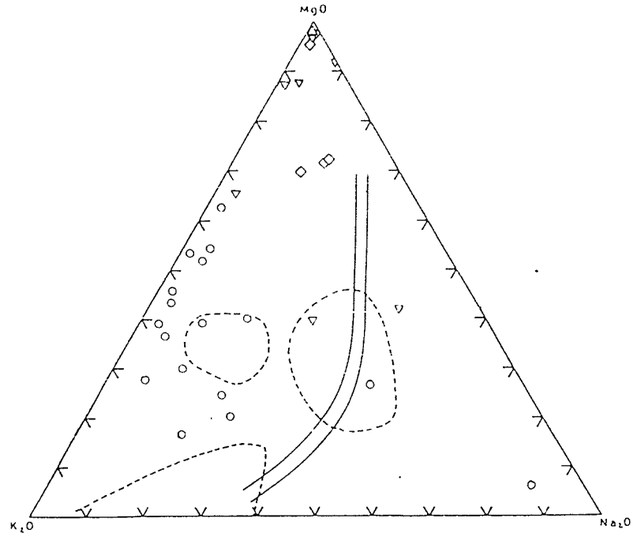

FIGURE 4-24 Silicoaluminate diagram (La Roche, 1974) for rocks from the Sillimanite Gneiss Unit at N. Maysville, Colorado (after Knight, 1981). Metabasalts are reprsented by diamonds, iron formations and other "exhalities" (Knight, 1981) by inverted triangles, anthophyllite-bearing rocks by triangles, and sillimanite-bearing rocks by circles.

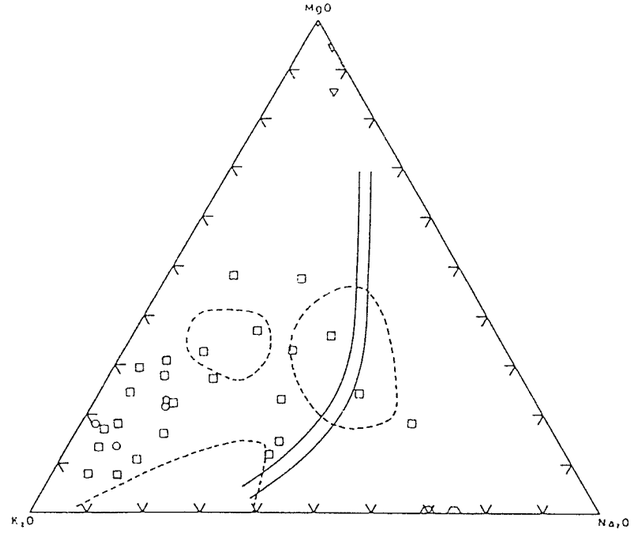

FIGURE 4-25 Silicoaluminate diagram (La Roche, 1974) for selected representative rocks from the Broken Hill Main Lode, Broken Hill, N.S.W., Australia (analyses from Joplin, 1963; see Appendix B). Iron formations are represented by inverted triangles, sillimanite-bearing gneisses by circles, barium-rich gneisses by hexagons and other gneisses by squares.

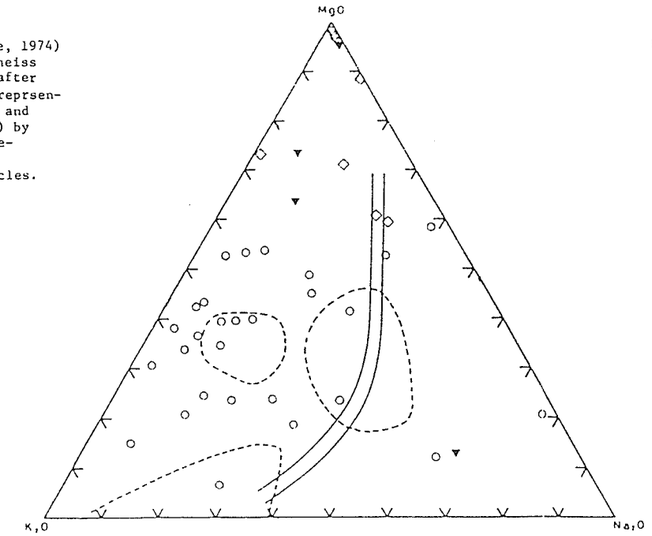

FIGURE 4-26 Silicoaluminate diagram (La Roche, 1974) for ore-bearing gneisses and schists from the New Calumet deposit, Calumet Island, Quebec. Quartz-feldspar-biotite-(sillimanite) gneisses and schists are represented by circles, amphibolities by diamonds, carbonates by inverted triangles and calc-silicates by solid inverted triangles.

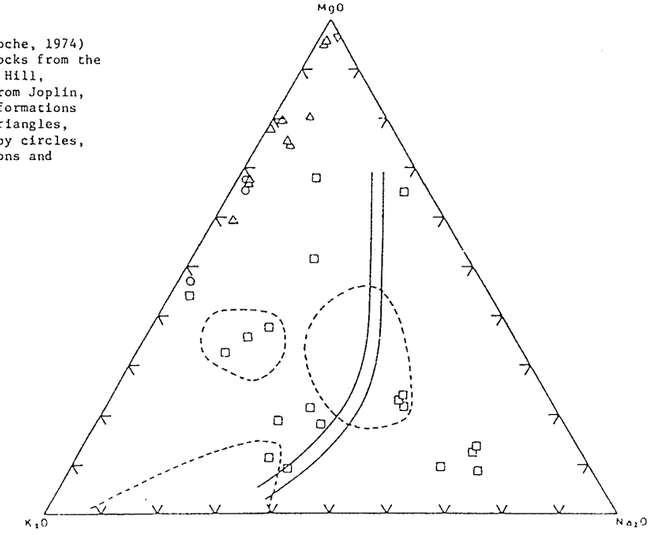

FIGURE 4-27 Silicoaluminate diagram (La Roche, 1974) for ore-bearing gneisses and schists from the Tétreault Mine, Montauban, and vicinity, Quebec. Cordierite-anthophyllite rocks are represented by triangles, carbonates and calc-silicate gneisses by inverted triangles, sillimanite-bearing rocks by circles and "leptite" (data from Stamatelopoulou-Seymour and MacLean, 1977) by squares.

approaches the lower section of the Leptite unit there is a distinct soda enrichment (Appendix B). In the immediate vicinity of the ore zone, however, soda drops off to near zero and quartz - feldspar - biotite - sillimanite - (cordierite) - (anthophyllite) gneisses begin to show the same potash and magnesia enrichments observed in sillimanite and anthophyllite - cordierite - bearing schists investigated at Geco, Sherridon, Maysville and New Calumet.

4.3.3 Geochemical Discriminations Based on the "Silicoaluminate" Diagram of La Roche (1974): a Discussion

Hydrothermally altered felsic intrusive rocks at Steamboat Springs, Nevada (Fig. 4-28) and at Roosevelt Springs, Utah (Fig. 4-29) all demonstrate the same soda depletion which exists in host rocks at the various localities covered in this study. A subtle difference does, however, occur. Alteration in the hydrothermal areas mentioned above results in a crude shifting of data points towards the K_2O apex of the diagram. In contrast, the anomalous rock types at the localities subject to this study produce a field hugging the K_2O - MgO leg of the diagram. This would indicate that in contrast with hydrothermal spring alteration some MgO enrichment has occurred in the host rocks of these orebodies. MgO concentrations in the cordierite - anthophyllite schists of the orebodies studied (Appendix A), being considerably higher than in any "normal" igneous rock, indicate that some MgO enrichment did occur. Geco sillimanite gneisses (Fig. 4-21) very definitely demonstrate an MgO

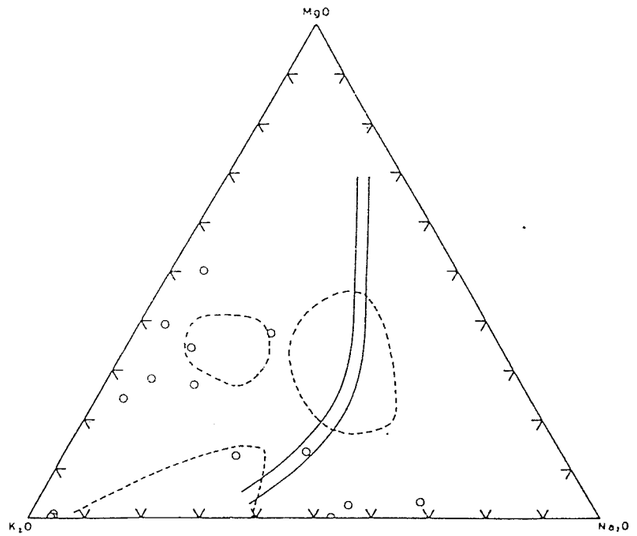

FIGURE 4-28 Silicoaluminate diagram (La Roche, 1974) for hydrothermally altered felsic and intermediate igneous rocks at Steamboat Springs, Nevada (analyses from Sigvaldson and White, 1962; see Appendix B). (rocks encountered in diamond drill hole GS-7).

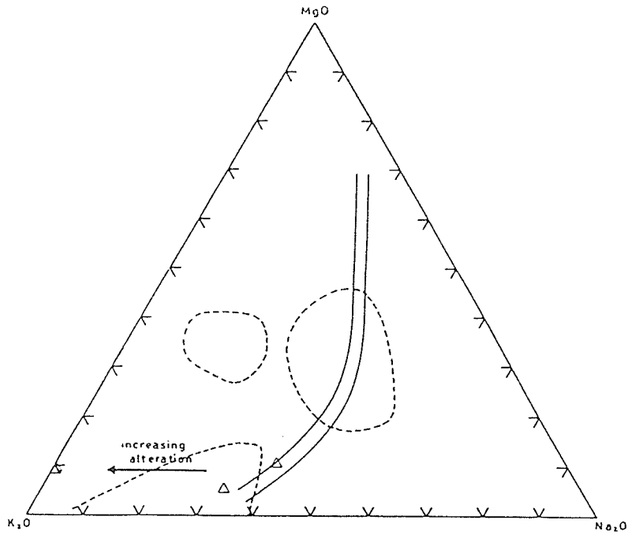

FIGURE 4-29 Silicoaluminate diagram (La Roche, 1974) for hydrothermally altered quartz monzonite at Roosevelt Hot Springs, Utah (analyses from Parry et al.,1980; see Appendix B).

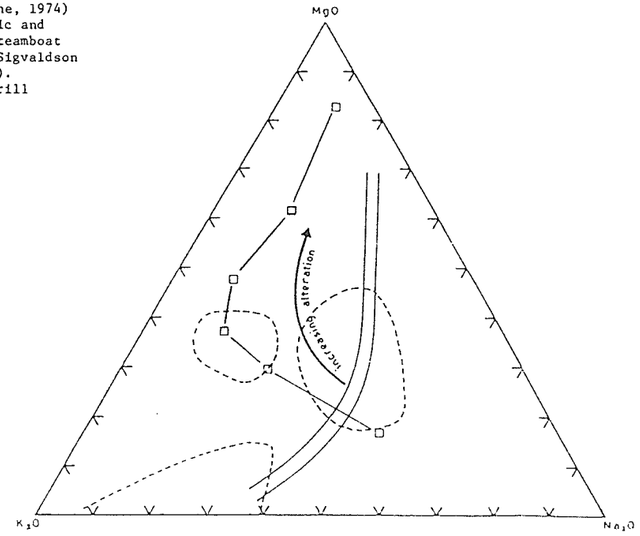

FIGURE 4-30 Silicoaluminate diagram (La Roche, 1974) for hydrothermally altered rocks from the alteration zone at the Millenbach Mine, Noranda area, Quebec analyses from Riverin and Hodgson, 1980; see Appendix B). The arrow indicates increasing intensity of alteration towards the core of the zone.

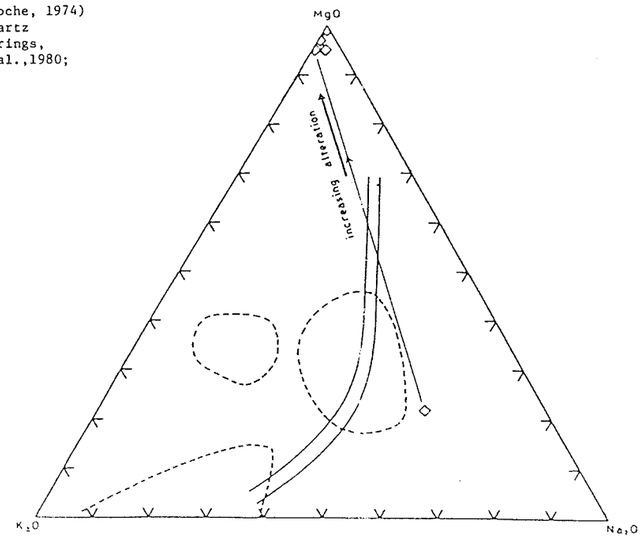

FIGURE 4-31 Silicoaluminate diagram (La Roche, 1974) for hydrothermally altered rocks from the alteration zone of the Mattagami Lake Mine, Quebec (analyses from Roberts and Reardon, 1978; see Appendix B). The arrow indicates increasing intensity of alteration towards the core of the zone.

enrichment as one approaches the 4/2 ore zone on the 3850 level.

Felsic volcanic rocks at Millenbach Mine and Mattagami Lake Mine demonstrate the same coincident soda depletion and MgO enrichment observed in sillimanite and cordierite - anthophyllite - bearing rocks of the orebodies under investigation (Figs. 4-30 and 4-31). Although the MgO enrichment at the Millenbach, Mattagami Lake and other volcanogenic massive sulfide deposits is very likely due to magnesium metasomatism, the same increase in Fe and Mg may be produced by addition of Mg - Fe-bearing chemical precipitates to a normal or altered (soda depleted - potash enriched) clastic sediment (i.e. a tuff of felsic to intermediate composition).

As stated earlier this diagram fails to take into account the role of silica. A tetrahedral plot of SiO_2 - MgO - K_2O - Na_2O might prove to be more useful in separating iron formations and other siliceous chemical sedimentary rocks from mafic and ultramafic igneous rocks.

4.4 Geochemical discrimination based on the Niggli k : mg Diagram

4.4.1 Introduction

Leake (1964) utilized a plot of Niggli k as a function of Niggli mg to distinguish amphibolites of sedimentary origin from those of igneous origin. He found that pelitic rocks fell largely within the range of k = 0.5 to k = 0.8. But Van de Kamp (1970) extended this slightly to

cover a field $0.45 < k < 1.00$ and $0 < mg < 0.5$ as is demonstrated in Fig. 4-32.

The solid dark lines on this diagram outline the field for normal igneous rocks. The validity of this field is somewhat verified in that 87% of the 75 samples of Karoo dolerites analyzed by Leake (1964) fall within it.

Fig. 4-33 demonstrates the confinement of various iron formation plots to a field with highly variable Niggli k but with Niggli $mg < 0.2$.

4.4.2 Potash Enrichment as Shown on the Niggli k : mg Diagram

The iron - rich metasedimentary rocks in the Ear Falls area fall within the same restricted field as the plots of iron formations of world wide occurrence, obtained from the literature (Fig. 4-34). Host rocks are of greywacke association and cluster within the intermediate igneous to shaley fields initially depicted in Fig. 4-32. Niggli k values for host rocks to the sulfides or of the iron - rich metasediments are found not to extend much above 0.6.

Grey Gneiss group rocks to the south of the Geco Mine (Fig. 4-35) were found to plot largely within the field of intermediate to mafic volcanic and sedimentary - volcanic rocks. Rocks from the ore zone, however, demonstrate notably increased k values although mg values remain the same as those demonstrated by rocks to the south of the deposit. Different samples from the large iron formations, which occur on surface above the Geco deposit, are also depicted in Fig. 4-35. Most

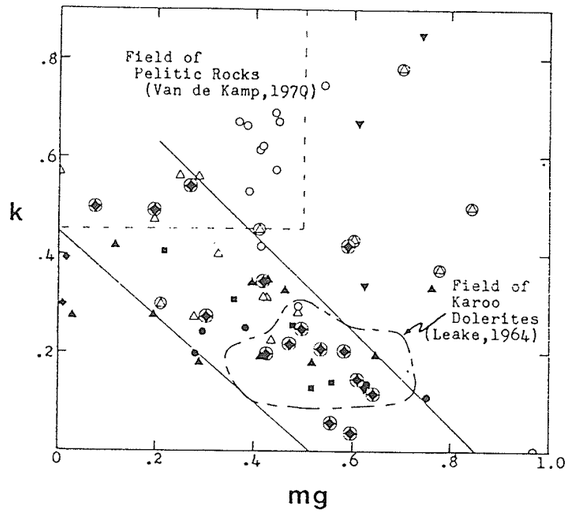

FIGURE 4-32 k-mg diagram for various common igneous and sedimentary rocks selected from the literature (see Appendix B). Key to rock types: solid diamonds = peralkaline igneous rocks; solid triangles = alkaline-olivine basalt series volcanics; solid squares = calc-alkaline series volcanics; solid circles = tholeiitic series volcanics; solid inverted triangles = nephelinites etc., solid circled diamonds = other igneous rocks; open circles = argillaceous sedimentary rocks; open triangles = greywackes; open circled triangles = calcareous greywackes. The field bounded by solid lines is that occupied by most igneous rocks.

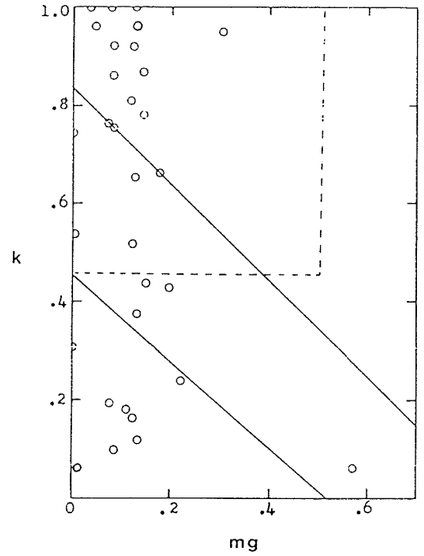

FIGURE 4-33 k-mg diagram showing field occupied by various iron formations from around the world (based on analyses from the literature, listed in Appendix B).

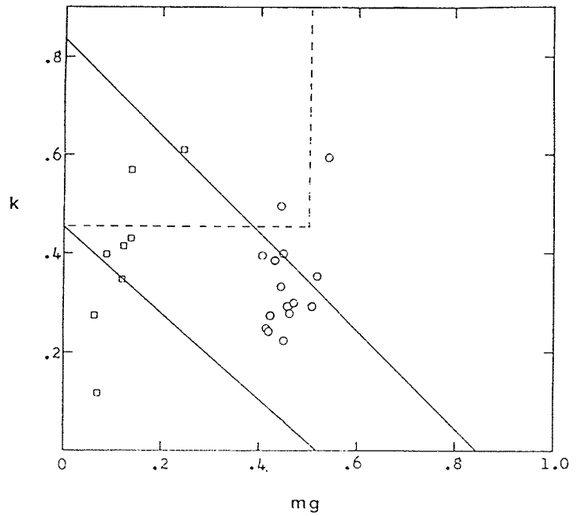

FIGURE 4-34 k-mg diagram for rocks of the Ear Falls area, Ontario. Ferruginous metasedimentary rocks are represented by squares and the enveloping quartz-feldspar-biotite-(hornblende) gneisses by circles.

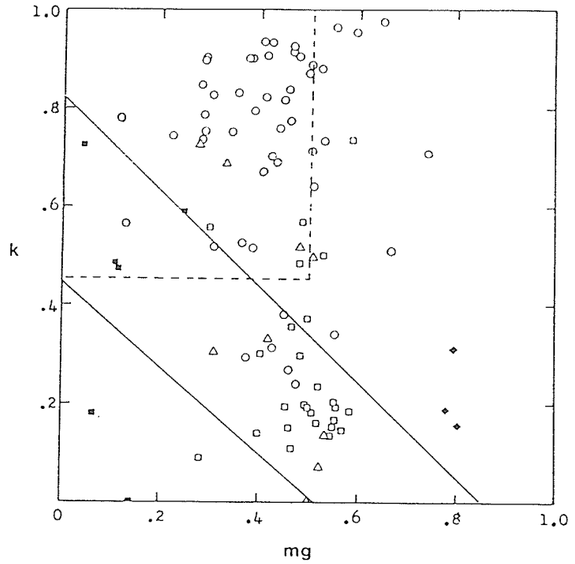

FIGURE 4-35 k-mg diagram for rocks from the Geco Mine and the surrounding area, Manitouwadge, Ontario. Grey Gneiss Gp rocks from a surface traverse to the south of the mine (excluding iron formations) are represented by open squares, Grey Gneiss Gp iron formation by solid squares, Grey Gneiss Gp rocks which occur as intercalations within the iron formations by solid diamonds, sillimanite-bearing Sericite Schist Gp rocks by circles and cordierite-anthophyllite rocks from the stratigraphic base of the 4/2 ore zone by triangles.

of these fall in the same field occupied by various types of iron formations in Fig. 4-33. Some members of this diverse iron formation, however, represent a transition from Milne's (1969) Unit 4 into the iron formation, and demonstrate fairly high Niggli mg values. An additional feature is that the highest K values are not demonstrated by rocks of the 4/2 or Sericite Schist (8/2) massive ore zones themselves, but rather by sillimanite - rich host schists.

Host rocks from two diamond drill holes on Selco's Yakushavitch Island Property on Kississing Lake, Manitoba, occupy a fairly dispersed field (Fig. 4-36) centered on the intermediate igneous field outlined earlier in Fig. 4-32. Niggli k values extend up into the shale field and, therefore, support the interpretted origin of these rocks as being sediments (Goetz, 1980). Analysis of core from the narrow mineralized horizons indicate similar mg values in the non-mineralized portions but with substantially elevated k values.

The result of a similar analysis of data from the Sherridon area, reported by Goetz (1980), is depicted in Fig. 4-37. Goetz (1980) has averaged the analyses for different rock types and this has had the effect of masking anomalous alkalies values in the biotite - sillimanite gneisses. Fig. 4-37 also indicates the potassic nature in the anthophyllite - bearing gneisses of the Sherridon area in analogy with the anthophyllite - bearing mineralized sections encountered on Yakushavitch Island (Fig. 4-36). The anthophyllite - bearing gneisses of the Sherridon area appear to be somewhat more magnesian and potassic than those of Geco.

Fig. 4-38 represents the k : mg diagram for rocks from the detailed stratigraphic section of North Maysville. Knight (1980) recognized a

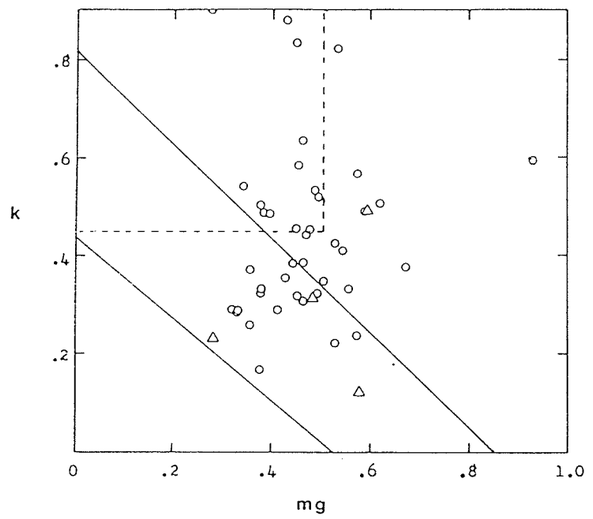

FIGURE 4-36 k-mg diagram for Sherridon Gp rocks on Yakushavitch Island, Kississing Lake, Manitoba. Quartz-feldspar-biotite-(sillimanite) gneisses/schists are represented by circles and anthophyllite-bearing rocks by triangles.

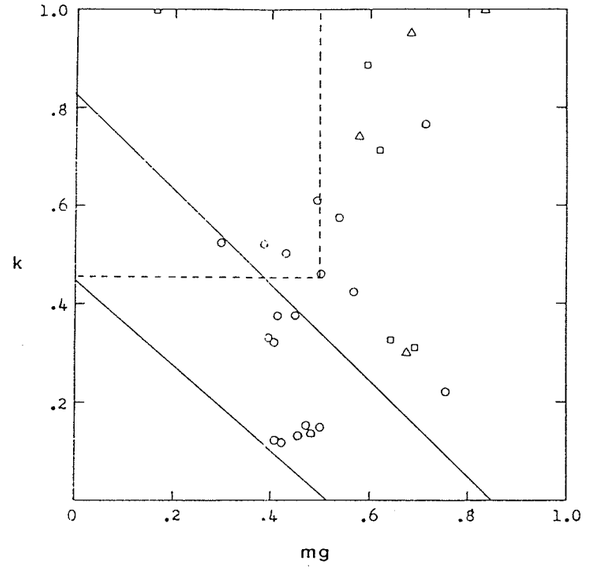

FIGURE 4-37 k-mg diagram for Sherridon Gp rocks from the Sherridon deposit, Sherridon Manitoba. (analyses from Goetz, 1980, see Appendix B) Unaveraged analyses of sillimanite-bearing gneisses are represented by squares, quartz-feldspar-biotite-(sillimanite) gneisses by circles and anthophyllite-bearing rocks by triangles.

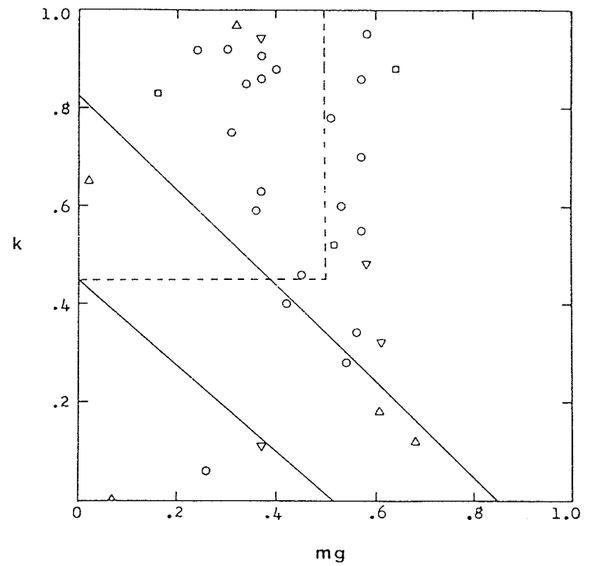

FIGURE 4-38 k-mg diagram for rocks from the Sillimanite Gneiss Unit at N.Maysville, Colorado, (after Knight, 1981). Sillimanite bearing gneisses/schists are represented by circles, anthophyllite-bearing rocks by squares, amphibolites by inverted triangles and "exhalative metasediments" by triangles.

dominant chemical sedimentary component supported by the setting of copper - bearing quartz - magnetite - rich gneisses in and near the iron formation field outlined earlier in Fig. 4-33. Some sillimanite - bearing gneisses adjacent to these iron rich, cupiferous sections are also skewed toward the iron formation field. Several of these gneisses resemble the more magnesia - rich transitional metasedimentary rocks found within the iron formation, which is found along the surface extension of the Geco orebody, Manitouwadge (Fig. 4-35). Both sillimanite - bearing gneisses and the iron formation demonstrate wide variations in alkalies, and Niggli k values often extend beyond 0.7.

One immediately notes that, in comparison with the other localities investigated thus far, Broken Hill gneisses are widely dispersed throughout the field of Niggli mg < 0.4 (Fig. 4-39). Almost half the analyses considered, including the Broken Hill iron formations themselves, fall within the same field outlined for various iron formations earlier in Fig. 4-33, whereas most other rocks plot within the pelite field of Van de Kamp (1976). In analogy with North Maysville, sillimanite gneisses were found to plot close to this iron formation field.

New Calumet amphibolites (Fig. 4-40) show a dispersed pattern to the right of the igneous field outlined earlier in Fig. 4-32. The bulk of the New Calumet amphibolites therefore appear geochemically consistent with a predominantly sedimentary origin. This is also supported by the textural and structural evidence utilized by Osborne (1944). They may, however, be in part derived from volcanic material (mafic pyroclastic).

Felsic rusty gneisses closely associated with ore at New Calumet

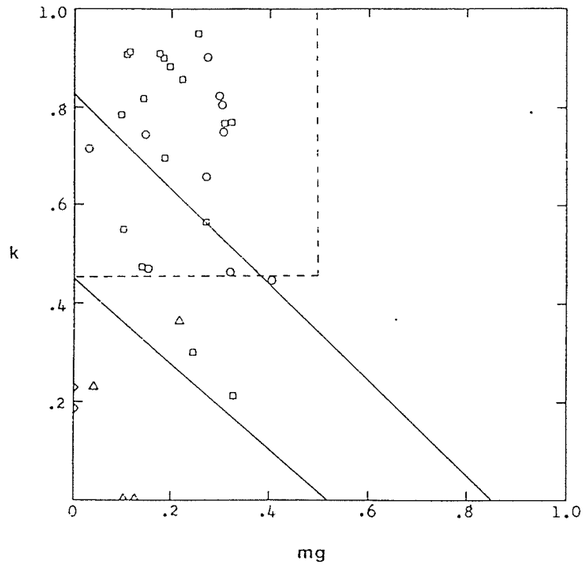

FIGURE 4-39 k-mg diagram for selected representative rocks from the Broken Hill Main Lode, Broken Hill, N.S.W., Australia (analyses from Joplin, 1963; Richards, 1966; see Appendix B). Sillimanite-bearing gneisses are represented by circles, iron formations by triangles, barium-rich gneisses by diamonds and other quartz-feldspar gneisses by squares.

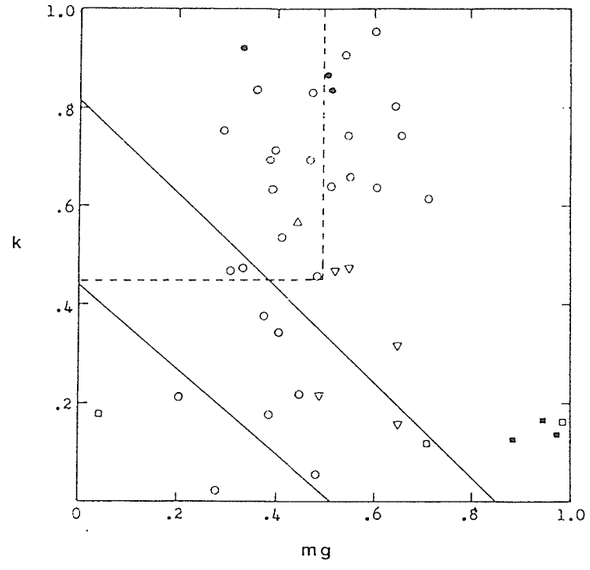

FIGURE 4-40 k-mg diagram for rocks from the New Calumet deposit, Calumet Island, Quebec. Sillimanite-bearing rocks are represented by circles, amphibolites by inverted triangles, carbonates by squares, and calc-silicate gneisses by triangles. Solid figures represent rocks with greater than 500 ppm Cu or Zn.

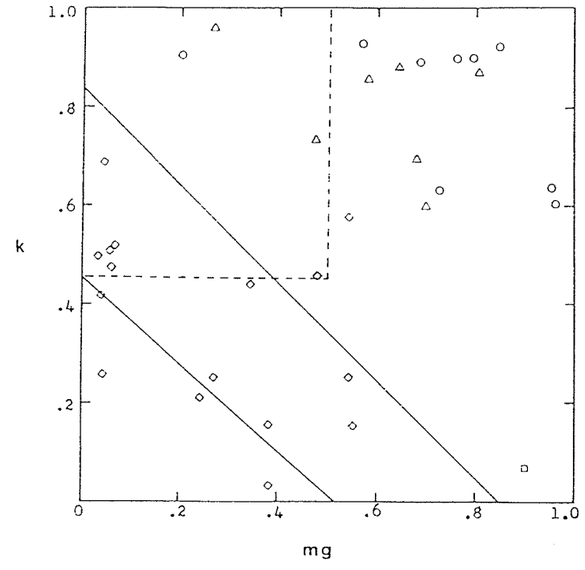

FIGURE 4-41 k-mg diagram for rocks from the vicinity of the Tetreault Mine, Montauban, Quebec. "Leptities" (analyses from Stamatelopoulou-Seymour and MacLean, 1977; see Appendix B) are represented by diamonds, calc-silicates by squares, sillimanite-bearing rocks by circles and cordierite-anthophyllite rocks by triangles.

plot largely in a diffuse field of high Niggli k and are restricted largely to Niggli mg values between 0.3 and 0.75, within the pelitic field. Mineralized versions of sillimanite - bearing gneisses generally demonstrate k values > 0.7, whereas mineralized calcareous gneisses are understandably marked by depressed k values.

Analyses from Stamatelopoulou - Seymour and MacLean (1977), plus data from diamond drill core collected at the Montauban deposit, are represented in Fig. 4-41. "Leptites" further removed from the orebody are found to plot roughly in the region of felsic igneous rocks outlined earlier in Fig. 4-32. As one approaches the orebody from the west, Niggli mg is found to increase steadily indicating an enrichment of Mg over Fe oxides. Quartz - feldspar gneisses enclosing the orebody demonstrate a further enrichment of magnesium and potash. In the vicinity of the Anacon orebody and North Gold Zone Niggli k values, for the most part, remain above 0.6 and often exceed 0.85. The Montauban anthophyllite schists demonstrate fairly wide variations in Niggli mg ($0.2 < mg < 0.7$).

4.4.3 Niggli k : mg Discrimination Technique: a Discussion

Without regarding the possible effects of alteration, the fields outlined in Figs. 4-32 and 4-33 indicate that the Sericite Schist Group rocks at Geco (Fig. 4-35) plot into the category of potassic metapelites whereas Grey Gneiss group rocks to the south of the orebody demonstrate a likely volcanic origin (e.g. flows and volcaniclastics).

Plots of Sherridon host rocks (Fig. 4-37) and unmineralized gneisses on Yakushavitch Island (Fig. 4-36) straddle the igneous and pelitic fields substantiating the interpretation (Goetz, 1980; Gale et al., 1980) that they likely represent normal greywacke metasediments.

Sillimanite - bearing gneisses at North Maysville, Colorado (Fig. 4-38) and New Calumet Mines, Ontario (Fig. 4-40) plot within the same field as Sericite Schist group gneisses at Geco. These often appear to be more potash enriched than normal pelitic rocks.

Sillimanite - bearing gneisses at Montauban (Fig. 4-41), however, are displaced to the right of the pelitic field occupied by sillimanite - bearing gneisses at Geco and North Maysville. This indicates an enrichment of MgO over iron oxides. Leptites located about 400 metres east of the Montauban orebody plot within the felsic end of the field produced by normal igneous rocks. They demonstrate a gradual enrichment of MgO over iron oxides as one approaches the orebody. This may be explained as;

1) an effect of alteration;
2) a result of increasing quantites of dolomitic mud, or;
3) chemical sediment composed of magnesium and iron hydroxides, deposited contemporaneously with the leptite progenitor.

Considerable carbonate and calc-silicate gneiss horizons do occur within the immediate vicinity of the old Anacon workings.

It is also possible that the observed increase in Niggli mg, as one approaches the orebody, is due to an overall change from felsic to more mafic volcaniclastics. The leptites appear to be confined to the

igneous field outlined earlier in Fig. 4-32 and deviation to high values of Niggli k are not observed until one is within the ore zone.

As was demonstrated earlier, Broken Hill gneisses do not behave as do the gneisses of other orebodies considered. Using the fields outlined in Figs. 4-32 and 4-33, Broken Hill gneisses would appear to be mixtures of chemical and pelitic metasediments. There does not seem to be stronger evidence supporting the involvement of rocks of volcanic origin, as appears to be the case with each of the other localities studied.

Hydrothermally altered granodiorite from Steamboat Springs, Nevada is plotted in Fig. 4-42. They occur in a dispersed field extending towards higher Niggli k and mg values originating from the field of intermediate igneous rocks. This parallels the behaviour of the host gneisses at Montauban. A similar trend has been observed at Roosevelt Springs, Utah (Fig. 4-43).

Similarly, hydrothermal alteration of rhyodacitic tuffs from the Mattagami Lake Mine (Fig. 4-44) causes a shift, with increase in the degree of alteration toward higher Niggli k + mg values. Roberts and Reardon (1978) also reported an analysis for the unaltered version of a rhyodacitic tuff and this is also represented in Fig. 4-44.

Alteration of a quartz-feldspar porphyry at the Millenbach Mine in the Noranda Camp (Fig. 4-45) is marked by an initial increase in Niggli k values followed by a decrease of the same, as the core of the alteration pipe is approached. In contrast with Mattagami Lake and Montauban, however, Niggli mg does not increase substantially with the degree of alteration. This being the case, one might be able to determine the composition of the progenitor simply by projecting

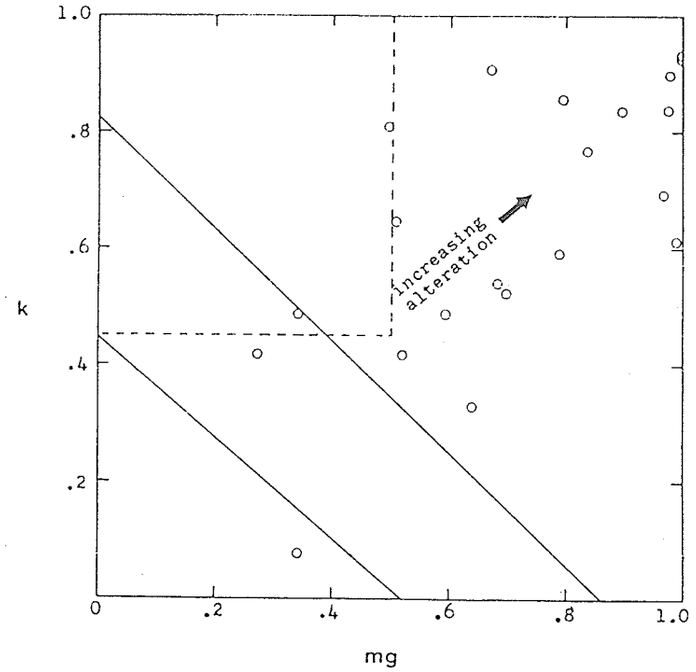

FIGURE 4-42 k-mg plot of hydrothermally altered granodioritic rocks from Steamboat Springs, Nevada (analyses from Sigvaldson and White, 1962; see Appendix B)

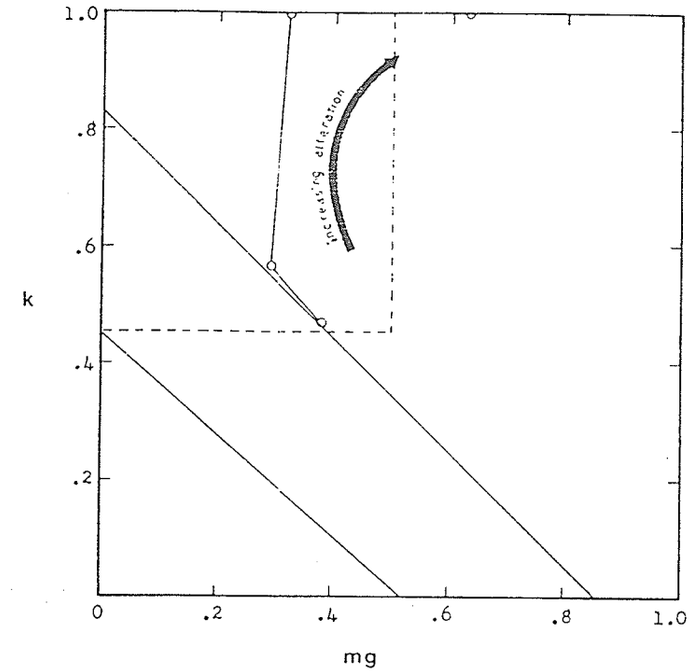

FIGURE 4-43 k-mg plot of hydrothermally altered quartz monzonite at the Roosevelt Hot Springs thermal area, Utah (analyses from Parry et al., 1980; see Appendix B).

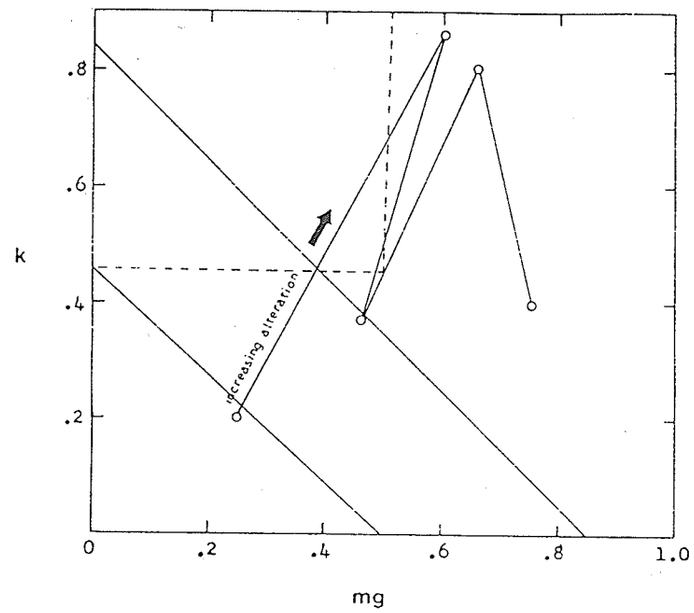

FIGURE 4-44 k-mg plot of hydrothermally altered rocks from the alteration pipe of the Mattagami Lake Mine, Quebec (analyses from Roberts and Reardon, 1978; see Appendix B).

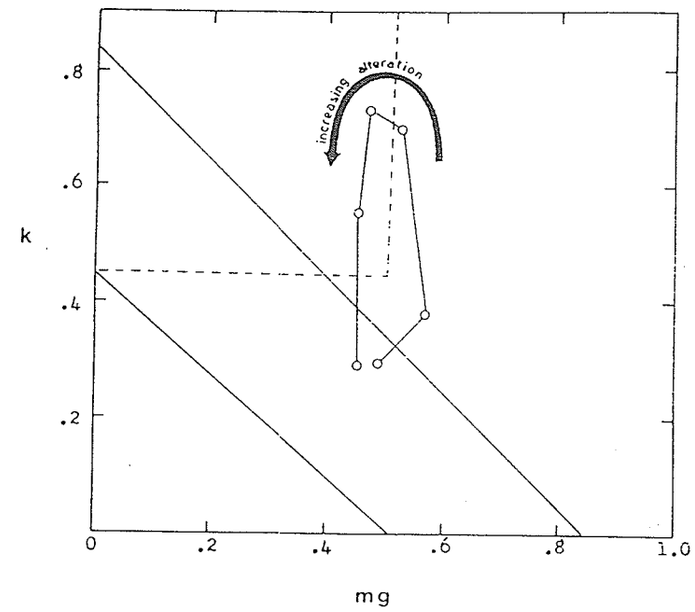

FIGURE 4-45 k-mg plot of hydrothermally altered rocks from the alteration pipe of the Millenbach Mine, Noranda area, Quebec (analyses from Riverin and Hodgson, 1980; see Appendix B).

individual data points (representing altered metamorphics) downwards, parallel to the Niggli k axis, to the field for normal igneous rocks. This would indicate that the progenitor of the Millenbach quartz - feldspar porphyry was originally andesitic in composition.

4.5 Geochemical Discrimination Based on the Niggli al-alk : c Diagram

4.5.1 Introduction

Van de Kamp (1970) and Leake (1969) utilized a plot of Niggli al-alk against Niggli c to separate metamorphic rocks of igneous origin from those of sedimentary origin. The value al-alk indicates available alumina present in excess of that used to produce all micaceous minerals and feldspars. Small variation of al-alk with composition produces a broad igneous field (of positive slope) which overlaps other fields.

4.5.2 Plots of Sillimanite and Cordierite - Anthophyllite - Bearing Metmorphics on the Niggli al-alk : c Diagram

Grey Gneiss group rocks located to the immediate south of the Geco orebody at Manitouwadge, Ontario, fall entirely within the low al-alk, low c portion of the igneous field outlined by Leake (1969) (Fig. 4-46). They would therefore correspond to rocks of intermediate to felsic

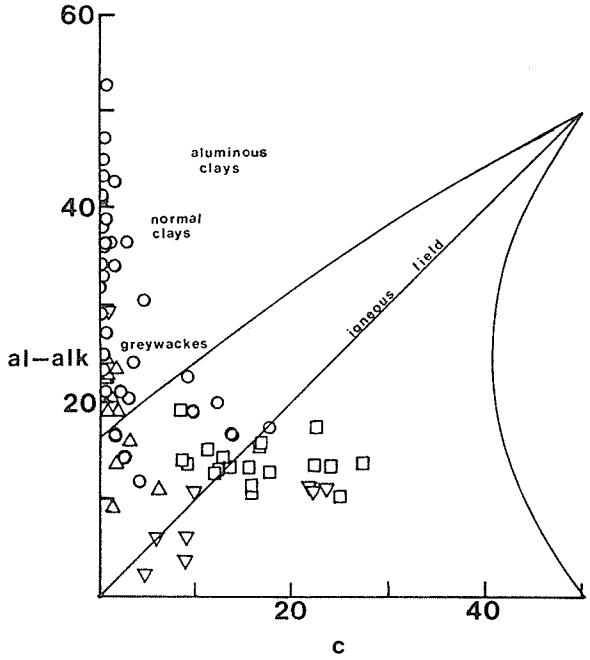

FIGURE 4-46 al-alk:c diagram for host rocks of the Geco deposit, Ontario. Iron formations are represented by inverted triangles, Grey Gneiss Gp. rocks by squares, Sericite Schist Gp. rocks by circles, and cordierite-anthophyllite rocks by triangles. Method of Leake, 1964.

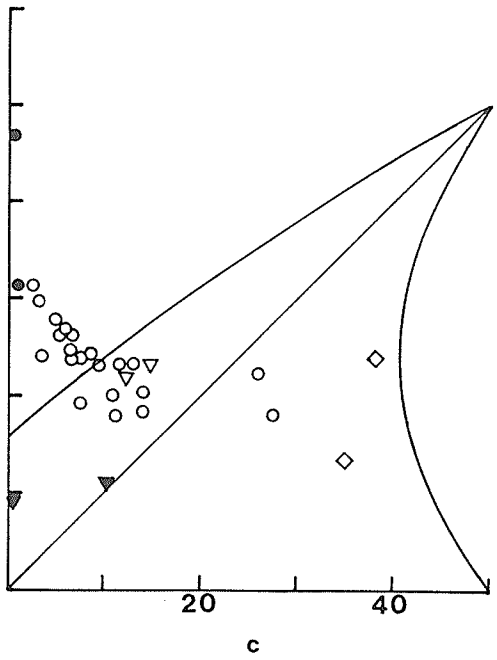

FIGURE 4-47 al-alk:c diagram for rocks encountered in DDH 11-11-5 on Yakushavitch Is., Man. Quartz-feldspar-biotite-(sillimanite) gneisses are represented by circles, anthophyllite-bearing rocks by inverted triangles and calc-silicate gneisses by diamonds. Solid figures indicate Cu or Zn 500 ppm.

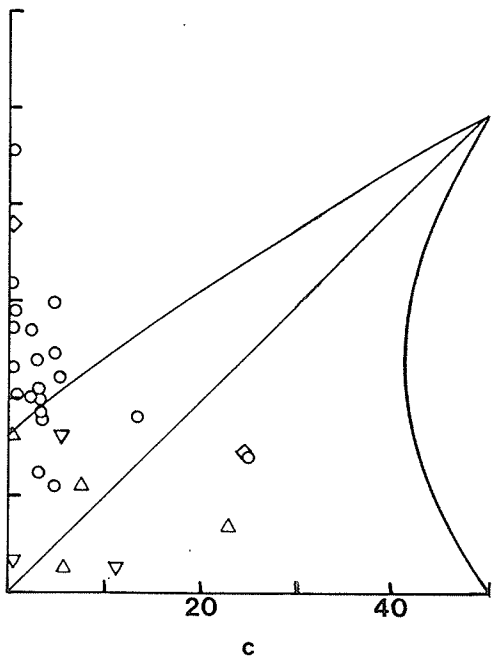

FIGURE 4-48 al-alk:c diagram for host rocks of the N.Maysville deposit of Colorado. Quartz-feldspar-biotite-(sillimanite) gneisses/schists are represented by circles, ferruginous chemical sedimentary rocks by triangles, and amphibolites by diamonds.

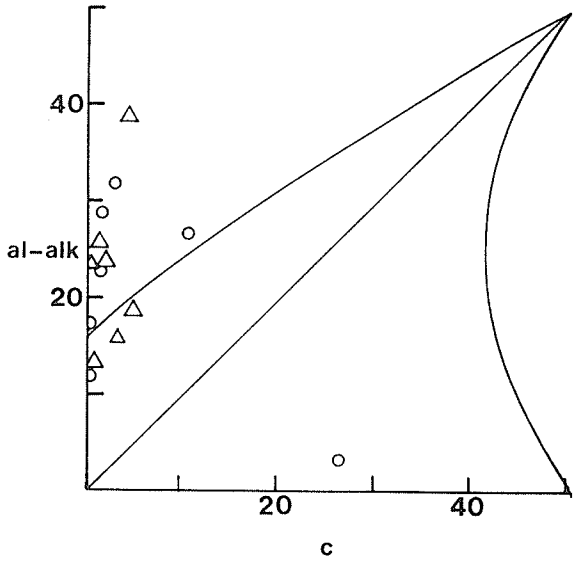

FIGURE 4-49 al-alk:c diagram for host rocks of the Montauban deposit, Quebec. Quartz-feldspar-biotite-(sillimanite) gneisses/schists are represented by circles and cordierite-anthophyllite rocks by triangles. Method of Leake, 1964.

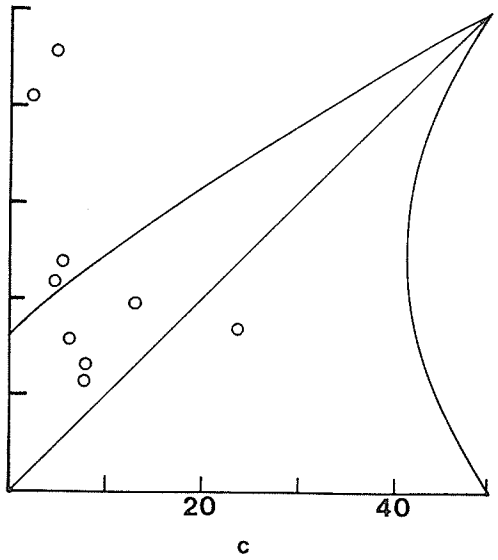

FIGURE 4-50 al-alk:c diagram for hydrothermally altered igneous rocks at Steamboat Springs, Nevada.

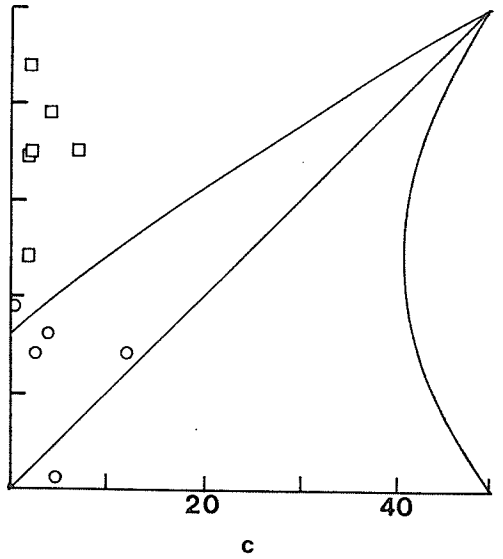

FIGURE 4-51 al-alk:c diagram for hydrothermally altered volcanic rocks at the Millenbach Mine, Quebec (squares) and the Mattagami Lake Mine, Quebec (circles).

igneous origin. Cordierite - anthophyllite rocks from the 4/2 ore zone at the north contact of the Sericite Schist group occupy a field with c $\leq$ 5 and 25 > al-alk $\geq$ 9 and consequently fit into the fields of felsic igneous rocks and greywackes. Sillimanite - bearing Sericite Schist group rocks also show strong calcium deficiency with c < 5. They occupy a field corresponding to greywackes and clays.

In analogy with the Geco orebody, sillimanite - bearing rocks encountered in diamond drill hole DDH 11-11-5 on Yakushavitch Island, Manitoba (Fig. 4-47) exhibit low values of Niggli c and plot within the fields of greywackes and clays. Anthophyllite - bearing rocks correspond to felsic igneous rocks. Similar trends were observed at Maysville (Fig. 4-48) and Montauban (Fig. 4-49).

4.5.3 Discussion of the al-alk : c Method

Very low calcium levels comparable to those observed at such localities as Geco, Yakushavitch Island, Maysville and Montauban are not observed in the hydrothermally altered rocks associated with hot spring activity at Steamboat Springs, Nevada (Fig. 4-50). Hydrothermally altered host rocks associated with base metal mineralization at the Mattagami Lake and Millenbach Mines are, however, geochemically analogous to the host rocks at Geco, Yakushavitch Island, Maysville and Montauban (Fig. 4-51). Altered rocks at Mattagami Lake fall into the same field as some of the cordierite - anthophyllite rocks at the above localities while the altered rocks at Millenbach correspond more closely

to the sillimanite - bearing rocks there.

Apart from showing the similarity of sillimanite and cordierite - anthophyllite - bearing rocks near the gneiss - hosted orebodies to hydrothermally altered rocks of several volcanogenic massive sulfide deposits, the al-alk : c diagram is redundant in its portrayal of excess alumina (since aluminosilicates and/or garnets were observed in thin section). This plot fails to separate the broad igneous field from that occupied by cordierite - anthophyllite rocks and iron formations. This is important since it has been speculated that cordierite - anthophyllite rocks may represent altered mafic volcanic rocks (Stamatelopoulou - Seymour and MacLean, 1977).

4.6 A Discriminant Plot of Niggli al + alk Against Niggli c

4.6.1 Introduction

In order to distinguish between igneous precursors and chemical sedimentary precursors to metamorphics, a discriminant plot of Niggli al + Niggli alk vs. Niggli c was developed. Niggli al + alk (an approximation of 100-[fm+c]) decreases and Niggli c increases with an increase in ferromagnesian minerals and calcic plagioclase as one progresses from felsic to more mafic igneous rocks. The result is a narrow field of negative slope (Fig. 4-52). Fig. 4-52 also displays a more shallow negatively sloping field corresponding to sedimentary rocks of shale and greywacke composition. The validity of the igneous field

FIGURE 4-52 Plot of Al+alk:c for various igneous and sedimentary selected from the literature (see Appendix B). Key to rock types: open diamonds = alkaline olivine basalt series volcanics; open squares = calc-alkaline series volcanics; open circles = tholeiite series volcanics; open triangles = peralkaline volcanics; open inverted triangles = nephelinites etc.; open hexagons = other igneous rocks; solid squares = greywackes + lith-arenities + arkoses; solid triangles = mudstones + shales + slates; solid inverted triangles = carbonates.

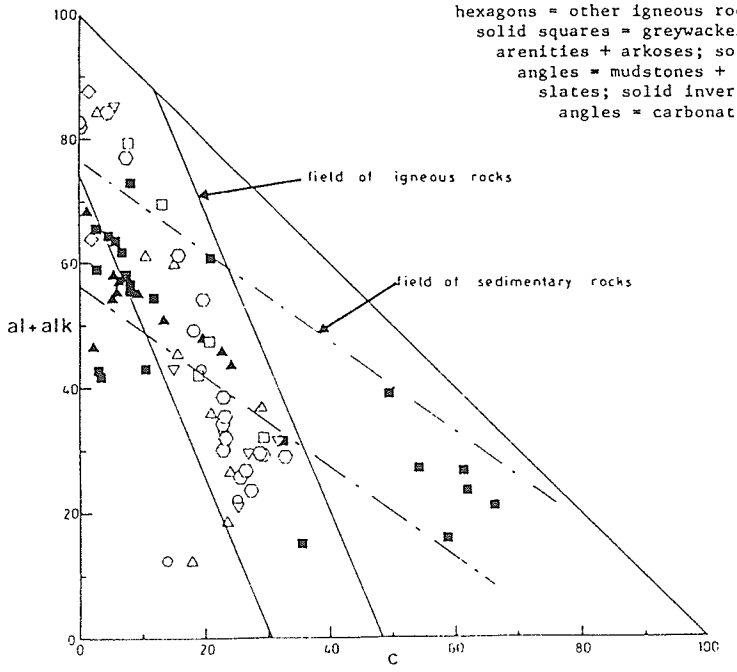

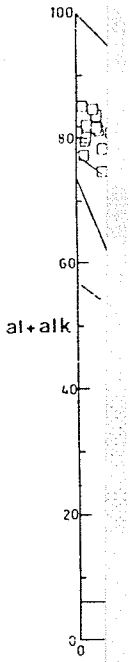

FIGURE

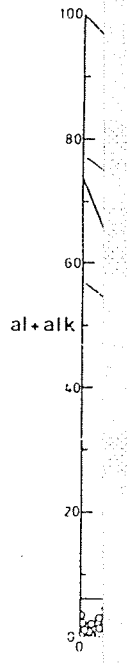

53 Plot of Niggli al+alk:c for some felsic intrusive and extrusive igneous rocks of the Katharina Province of North Africa (data from Agron and Bentor, 1981; see Appendix B).

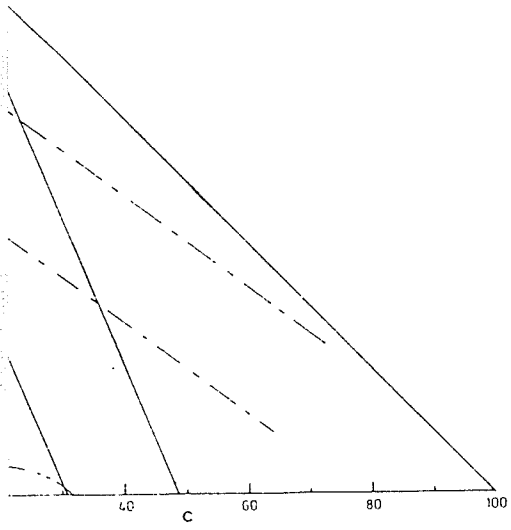

FIGURE 4-54 Plot of Niggli al+alk:c for rocks from the Green Beds of the Scottish Dalradian Series (data from Van de Kamp, 1970; see Appendix B).

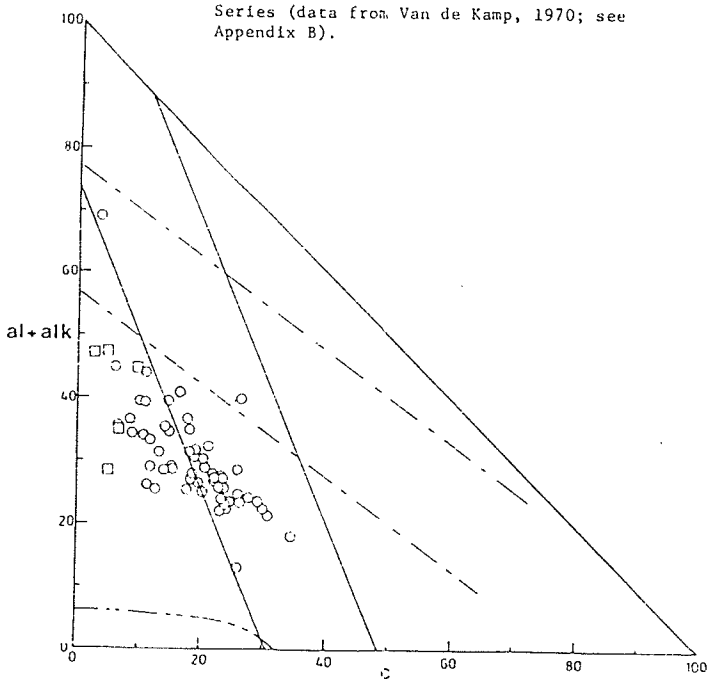

ɔt of Niggli al+alk:c for various iron ːmations of the world (analyses obtained ɔm the literature; see Appendix B).

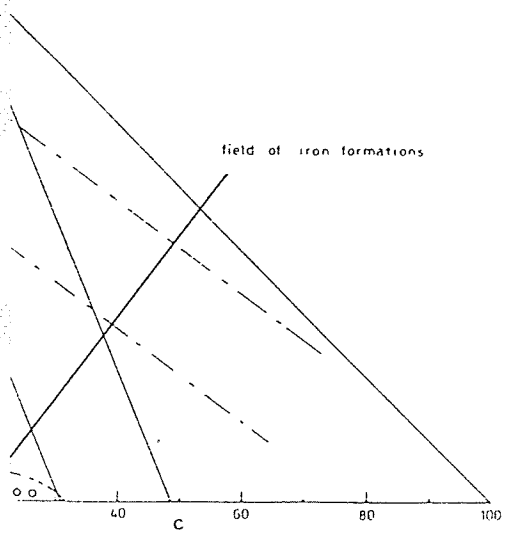

FIGURE 4-56 Niggli al+alk:c plot for rocks from the Ear Falls area, Ontario. Iron-rich metasedimentary rocks are represented by inverted triangles and enveloping quartz-feldspar-biotite -(hornblende) gneisses by squares.

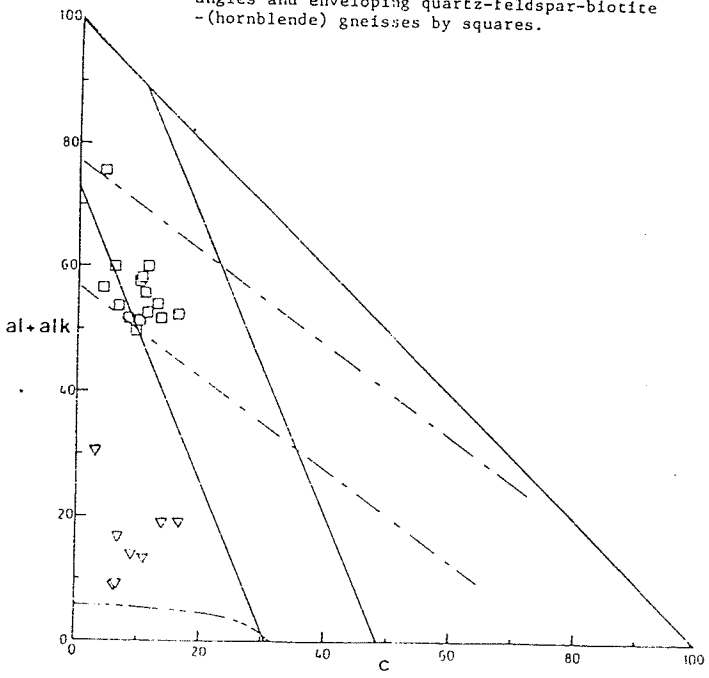

is further verified in Figs. 4-53 and 4-54. Fig. 4-53 shows plots of analyses reported by Agron and Bantor (1981) for the Katharina alkalic volcanics and intrusives of North Africa. Fig. 4-54 portrays analyses of mafic volcaniclastics and interbanded pelites from the Scottish Dalradian Series (Van de Kamp, 1970). Over 60% of these fall within the mafic igneous field outlined by Van de Kamp (1970). Displacement of the remaining data to the left of the igneous field may be due to alteration (leaching of CaO, etc.) during or shortly after deposition. Alternatively simple dilution of mafic pyroclastics by fine (pelitic) epiclastic sediments would produce the observed skewing of these "anomalous" green beds toward the shale-greywacke field. In fact, even the rocks Van de Kamp (1970) classified as pelites appear, from their position on the diagram, to have been possibly derived from the volcanic rocks.

Iron formations, due to their high iron content and low alumina and alkali contents, cluster tightly near the origin (Fig. 4-55) with Niggli al + alk generally <5 and Niggli c <27. It should once more be noted that the al + alk : c diagram is a discriminant plot and no correlation with modal composition is implied.

4.6.2 Application of the Niggli al + alk vs c Variation Diagram to the Deposits Studied.

Iron - rich metasedimentary rocks and their host rocks from the Ear Falls area are shown in Fig. 4-56. The host gneisses, which are

interpretted to have originally been greywackes, cluster tightly within the common field of shales and greywackes and intermediate igneous rocks depicted earlier in Fig. 4-52. The iron - rich metasedimentary rocks, however, do not plot within the field of true iron formations but rather somewhat above it. This may be explained as being due to a mixing of chemical sedimentary material with the clastic greywacke detritus responsible for producing the host gneisses.

Amphibolites from the east side of Manitouwadge Lake (Fig. 4-57) plot within the mafic igneous field outlined earlier in Fig. 4-52.

The Grey Gneiss group rocks located to the immediate south of the orebody cluster fairly tightly within the field of felsic to intermediate igneous rocks and the shale - greywacke field. On this basis and on the basis of field textural and structural observations these rocks are interpretted to be a series of interlayered felsic to intermediate metavolcanic and related metasedimentary rocks.

The fields of Sericite Schist group rocks and cordierite - anthophyllite rocks from the 4/2 ore zone are shown in Fig. 4-58. They indicate fairly severe calcium depletion by their displacement toward the al + alk axis. Some Sericite Schist group rocks also demonstrate an increase in al + alk which may be attributed to a decrease in Mg and Fe oxides. Geco iron formations either plot within or slightly above the field of iron formations outlined in Fig. 4-55. On this basis, there appears to be some similarity between anthophyllite schists of the 4/2 ore zone and some members of the iron formation which is located on surface above the Geco orebody.

Rocks hosting mineralization on Yakushavitch Island, Kississing Lake in Northern Manitoba (Fig. 4-59 and Fig. 4-60) were found to

FIGURE 4-57 Niggli al+alk:c plot for rocks from the Geco Mine and vicinity, Manitouwadge, Ontario. Grey gneiss Gp rocks (with the exception of iron formations) are represented by squares, Grey Gneiss Gp iron formations by inverted triangles, sillimanite-bearing Sericite Schist Gp rocks by circles, and cordierite-anthophyllite rocks from the 4/2 ore zone by triangles.

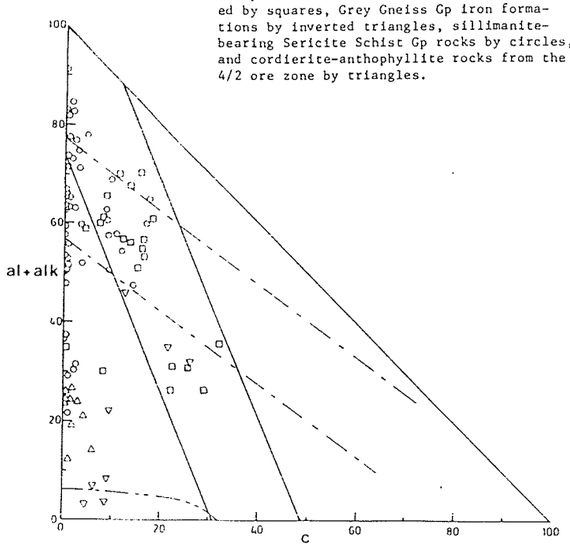

FIGURE 4-58 Niggli al+alk:c plot for rocks from the Mine Sequence at Geco, Manitouwadge, Ontario. Sillimanite-bearing rocks from the Sericite Schist Gp are represented by circles and cordierite-anthophyllite rocks from the 4/2 ore zone by triangles.

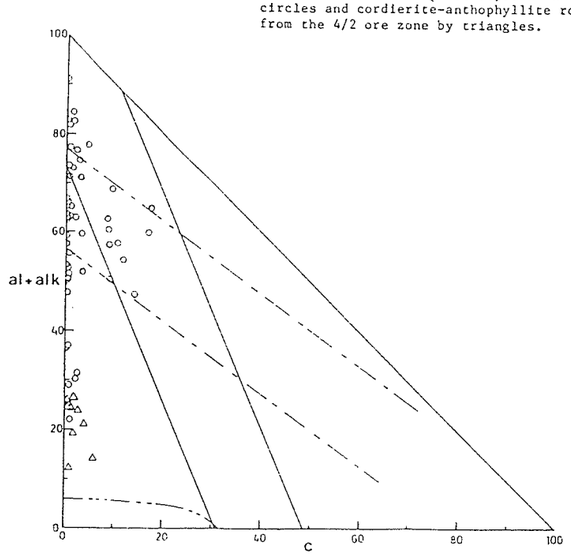

FIGURE 4-59 Niggli al+alk:c plot for rocks encountered in diamond drill hole DDH-11-11-5 on Yakushavitch Island, Kississing Lake, Manitoba. Quartz-feldspar-biotite-(sillimanite) gneisses are represented by circles, and anthophyllite-bearing rocks by triangles. Solid figures indicate Cu or Zn levels in excess of 500 ppm.

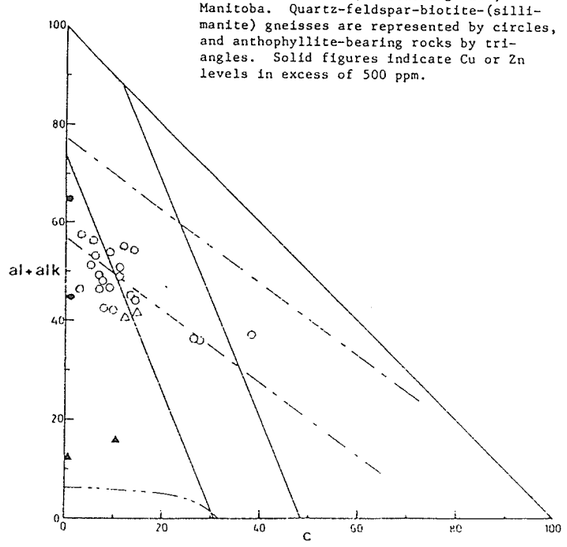

FIGURE 4-60 Niggli al+alk:c plot for quartz-feldspar-biotite-(sillimanite) gneisses encountered in diamond drill hole DDH-11-11-3 on Yakushavitch Island, Kississing Lake, Manitoba. The solid circle indicates greater than 500 ppm Cu and Zn.

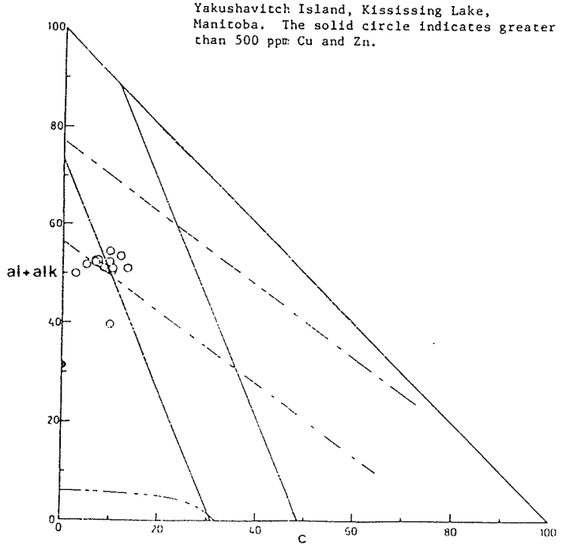

FIGURE 4-61 Niggli al+alk:c plot for rocks hosting the Sheridon deposit, Sherridon, Manitoba, (analyses from Goetz, 1980; see Appendix B). Sillimanite-bearing rocks are represented by circles, other quartz-feldspar gneisses and schists by squares, and anthophyllite-bearing rocks by triangles.

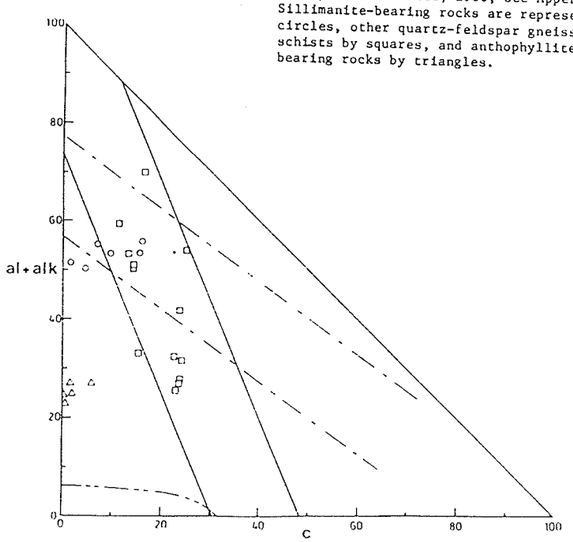

cluster tightly within the common field occupied by argillaceous and greywacke sedimentary rocks as well as intermediate igneous rocks depicted in Fig. 4-52. Sample S-46 represents a mineralized section from DDH 11-11-3 (Fig. 4-60). It plots within the same field as the Geco anthophyllite - bearing rocks. Similarly, samples S-13 and S-14 from DDH 11-11-5 (Fig. 4-59) plot within the same field as Sericite Schist group rocks at Geco. Fig. 4-61 demonstrates that the same situation occurs in the Sherridon area itself. There, anthophyllite - bearing gneisses demonstrate low al + alk and very low Niggli c, while sillimanite - bearing gneisses demonstrate al + alk values comparable to surrounding greywacke metasediments of the Sherridon Group, but with depressed Niggli c values.

Fig. 4-62 demonstrates the rather severe calcium depletion which is characteristic of gneisses hosting mineralization in the North Maysville area described by Knight (1981). Once again iron - enriched members do not generally show the same low values of al + alk demonstrated by iron formations (Fig. 4-55), but al + alk values are depressed to levels displayed by the ocherous metasediments in the Ear Falls area (Fig. 4-56) and the cordierite - anthophyllite schists of "4/2 Zone" ores at Geco (Fig. 4-58). Similarly al + alk values decrease not strictly as a result of decreasing alumina and alkalies but also as a result of increased Niggli fm (higher levels of Mg and Fe).

Broken Hill host rocks characteristically demonstrate slightly higher calcium levels than those observed at the other localities and tend to fall within the shale - greywacke field (Fig. 4-63). Sillimanite gneisses which stratigraphically underlie the ore lenses, however, are calcium - poor in analogy with the sillimanite - bearing

FIGURE 4-62 Niggli al+alk:c plot for rocks from the Sillimanite Gneiss Unit at N.Maysville, Colorado (after Knight, 1981). Rocks interpreted by Knight (1981) to be metabasalts are represented by diamonds, those interpreted to be iron formations or exhalative metasedimentary rocks are represented by inverted triangles, sillimanite bearing rocks are represented by circles and anthophyllite-bearing rocks by triangles.

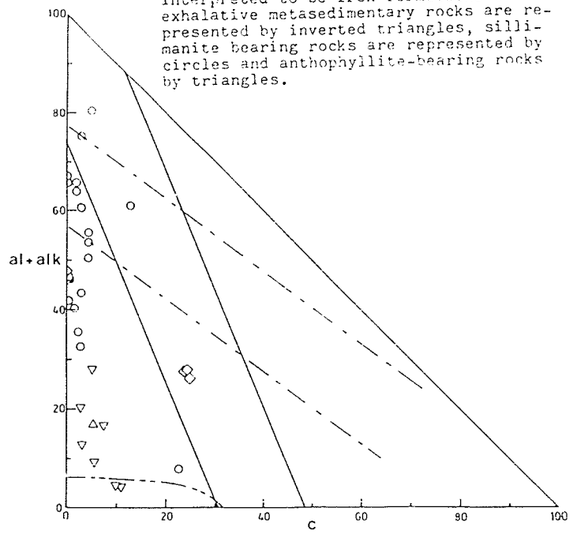

FIGURE 4-63 Niggli al+alk:c plot for some representative rocks from the Mine Sequence at the Broken Hill Main Lode, Broken Hill, N.S.W., Australia (data from Joplin, 1963; see Appendix B). Sillimanite-bearing rocks are represented by circles, other felsic rocks by squares, iron formations by inverted triangles and barium-rich gneisses by hexagons.

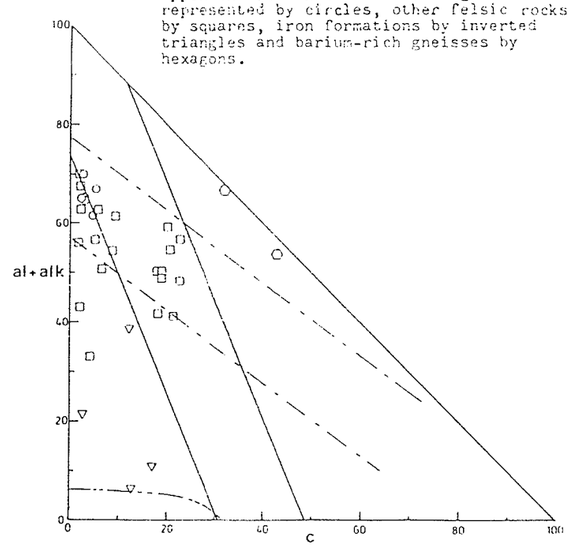

FIGURE 4-64 Niggli al+alk:c plot for rocks from the New Calumet deposit, Calumet Island, Quebec. Sillimanite-bearing rocks are represented by solid circles, sillimanite-deficient rocks by open circles, amphibolites by diamonds, calc-silicates by triangles and carbonates by inverted triangles.

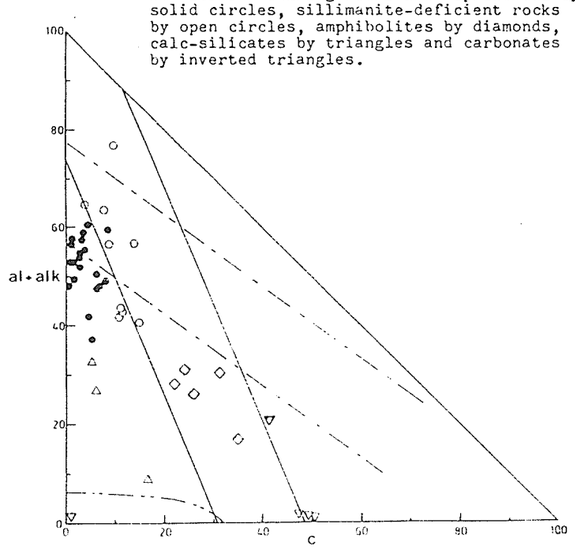

FIGURE 4-65 Niggli al+alk:c plot for rocks from the Tetreault Mine and vicinity, Montauban, Quebec. "Leptites" (data from Stamatelopoulou-Seymour and MacLean, 1977; see Appendix B) are represented by squares, sillimanite-bearing rocks by circles, and cordierite-anthophyllite rocks by triangles.

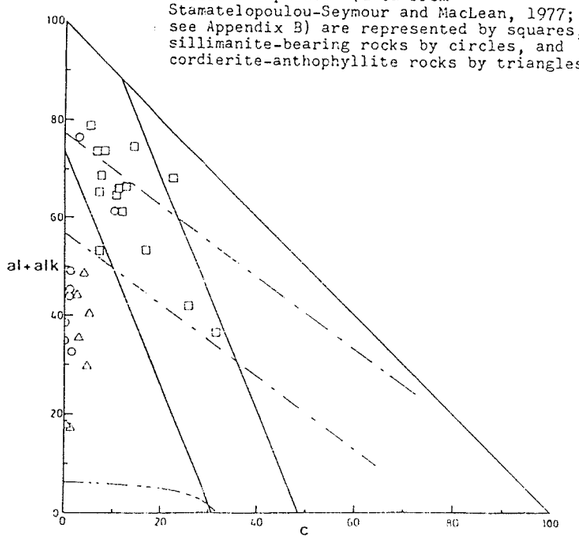

rocks of the other localities. Ore at Broken Hill is associated with magnetite - garnet - quartz iron formations shown in Fig. 4-63. There is no report of a major anthophyllite - bearing unit at Broken Hill but some of the iron formations which host the ore plot in the same general field as the anthophyllite - bearing host rocks at Sherridon and Geco. This, however, is misleading since the Broken Hill iron formations do not contain the magnesia enrichment observed at Geco, Sherridon, New Calumet, Montauban and N. Maysville. According to the fields defined in Fig. 4-52, many of the Broken Hill gneisses may have been derived from felsic to intermediate volcanics or related sedimentary rocks (greywackes or transported tuffs). Due to the overlap of the sedimentary shale - greywacke field and the felsic to intermediate igneous field, the al + alk : c diagram can not offer a distinction.

Analysis of several samples of sillimanite - bearing gneisses in DDH core from the Bowie Orebody at New Calumet demonstrates calcium depletion comparable to sillimanite - bearing gneisses at Geco and North Maysville, regardless of the presence of abundant carbonate units within the immediate vicinity of the orebody (Fig. 4-64). Amphibolites plot within the mafic igneous field while sillimanite gneisses plot to the left of the felsic to intermediate igneous field (which also coincides with the sedimentary field). Fig. 4-64 indicates that the New Calumet sillimanite gneisses may be either altered felsic to intermediate volcanic rocks or a series of calcium-deficient metapelites. One sample of the sillimanite - deficient gneisses analyzed falls above the field of sedimentary rocks shown in Fig. 4-52. The sillimanite - deficient gneisses contain appreciable plagioclase (ranging in composition from An20 to An50) and usually less than 20% quartz. They are suspected to

represent intermediate to felsic volcanic or volcaniclastic rocks. The sillimanite - bearing gneisses may then represent altered equivalents of the same.

As is the case at Geco, Sherridon and North Maysville, anthophyllite gneisses at Montauban are characterized by calcium depletion and low Niggli al + alk values (Fig. 4-65). The sodic leptites described by Stamatelopoulou - Seymour and MacLean (1977) do not demonstrate a calcium depletion and plot within the field of intermediate to felsic igneous rocks. This is consistent with the Conclusions of Stamatelopoulou - Seymour and MacLean (1977) concerning their origin. Quartz - feldspar - biotite - (sillimanite) gneisses, in analogy with the other localities, exhibit depressed Niggli c values. In analogy with New Calumet they may represent the altered equivalents of the "leptites".

4.6.3 Discussion of the Results of the al + alk : c Discrimination Method

This diagram basically demonstrates that calcium depletion is inherent in sillimanite - bearing members of the ore zones at Geco, Sherridon, North Maysville, New Calumet, Montauban and to some degree the aluminous schists at Broken Hill. It also demonstrates the elevated levels of Mg and Fe oxides within the cordierite - anthophyllite gneisses at Geco, Sherridon, N. Maysville, New Calumet and Montauban. Niggli c and al + alk for some of the ore - bearing iron formations at

Broken Hill are found to be roughly the same as those for cordierite - anthophyllite gneisses at Geco, Sherridon, North Maysville and Montauban. Figs. 4-66 and 4-67 demonstrate the effects of prograde hydrothermal alteration on the Niggli c and al + alk values for rocks from the alteration zones of the massive sulfide orebodies at the Millenbach Mine and the Mattagami Lake Mine. In both cases increased alteration, as one approaches the core of the alteration pipe, is marked by decreasing al + alk and depressed values of Niggli c. It should be noted that the decrease in Niggli al + alk is due not only to alkali depletion, but also to dilution by MgO and FeO.

Hydrothermal alteration at Roosevelt Springs (Fig. 4-68), however, demonstrates no Mg/Fe metasomatism within the host quartz monzonite. Niggli al + alk increase due to this leaching out of CaO, Fe oxides, Na_2O and MgO with the resultant concentration of alumina in the residuum. The trend, as opposed to that observed in the alteration pipes of volcanogenic massive sulfide bodies and within sillimanite gneisses of the orebodies subject to this investigation, is toward an increase of Niggli al + alk and a decrease of Niggli c with the degree of alteration. Generally this same trend appears to exist in altered granodiorites at Steamboat Springs, Nevada (Figs. 4-69 + 4-70). In addition to the decrease in Niggli c generally observed, there also appears to be some localized calcium enrichment within certain sections of the altered granodiorite.

If the anomalous rock types (sillimanite gneisses and cordierite - anthophyllite gneisses) at Geco, N. Maysville, New Calumet, Montauban and Sherridon were derived by alteration of normal volcanic rocks, they appear to have followed a genetic pathway similar to the rocks of

FIGURE 4-66 Niggli al+alk:c plot for rocks from the alteration zone at the Millenbach Mine, Noranda area, Quebec. The direction of the arrow indicates increasing intensity of alteration towards the core of the pipe (analyses from Riverin and Hodgson, 1980; see Appendix B).

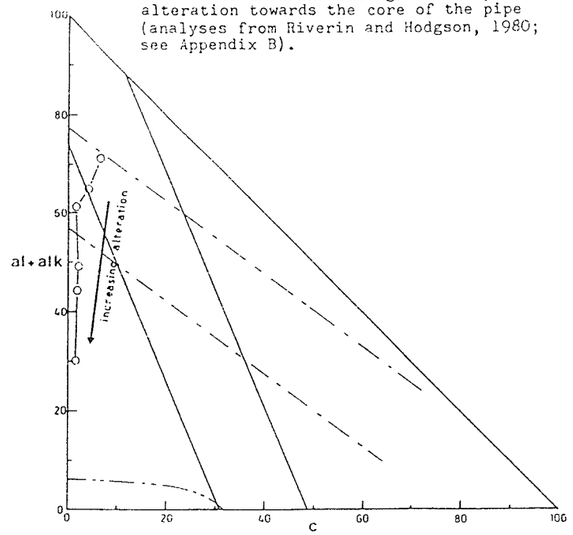

FIGURE 4-67 Niggli al+alk:c plot for rocks from the alteration zone of the Mattagami Lake Mine, Quebec. The direction of the arrow indicates increasing intensity of alteration towards the core of the pipe (analyses from Roberts and Reardon, 1978; see Appendix B).

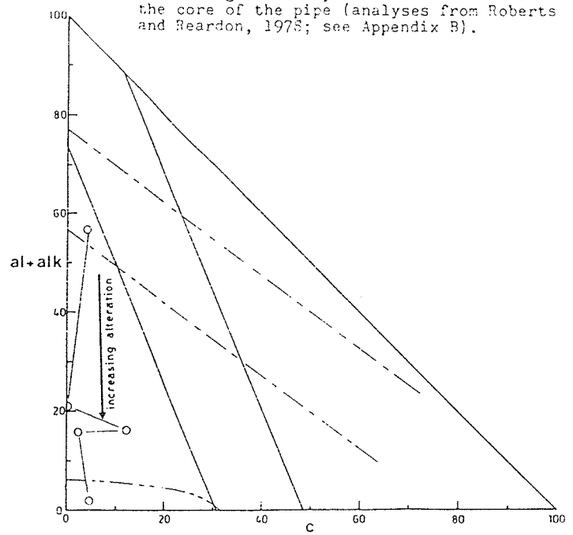

FIGURE 4-68 Niggli al+alk:c plot for hydrothermally altered quartz monzonite at Roosevelt Springs, Utah (analyses from Parry et al.,1980; see Appendix B).

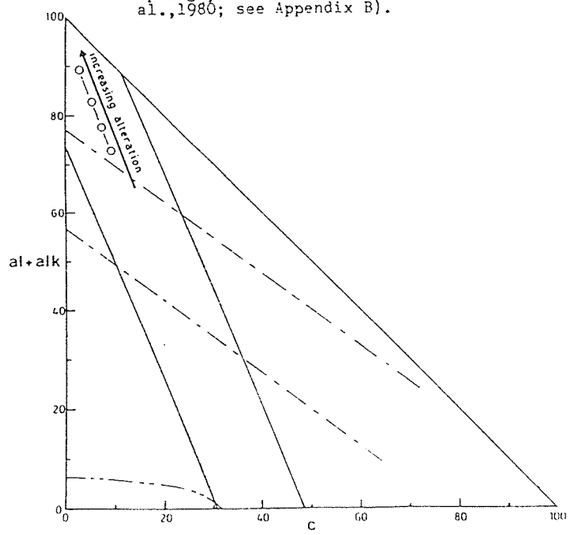

FIGURE 4-69 Niggli al+alk:c plot for hydrothermally altered felsic and intermediate igneous rocks in diamond drill hole GS-5 at Steamboat Springs, Nevada (analyses from Sigvaldson and White,1962; see Appendix B).

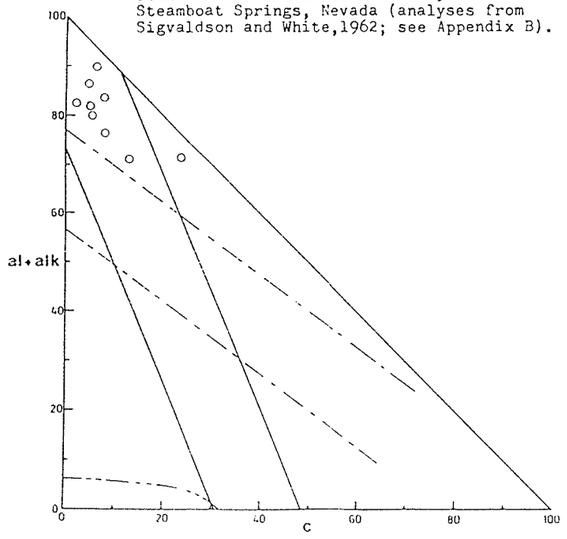

FIGURE 4-70 Niggli al+alk:c plot for hydrothermally altered felsic and intermediate igneous rocks in diamond drill hole GS-7 at Steamboat Springs, Nevada (analyses from Sigvaldson and White, 1962;see Appendix B).

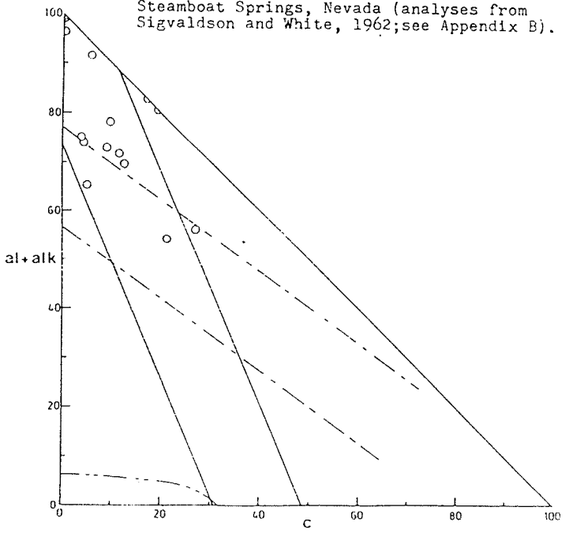

volcanogenic massive sulfide alteration pipes.

4.7 Nickel - Cobalt Trace Contents and their Use in Progenitor Determination

4.7.1 Introduction

In accordance with the expected positive correlation of nickel content and the ferromagnesian mineral content of igneous rocks, Table 4-2 lists the approximate ranges of Ni and Co in "normal" igneous rocks (summarized from Rankama and Sahama, 1952; Krauskopf, 1970).

ROCK TYPE	RANGE OF Ni (ppm)	RANGE OF Co (ppm)
Ultramafic rocks	800+	200+
Mafic rocks	50-800	25-200
Intermediate rocks	8-50	11-25
Felsic rocks	0-8	0-11

TABLE 4-2 Nickel and cobalt contents of common igneous rocks. (modified after Rankama and Sahama, 1952).

Ni demonstrates a broad range of stability and one expects nickel to mobilize under oxidizing or reducing conditions (Krauskopf, 1979).

Outside of tropical regoliths both nickel and cobalt have a strong affinity for sulfur. They also readily form organic complexes and so both should precipitate readily in a euxenic environment. Both are also removed from solution by adsorption in oxidate and hydrolyzate sediments. Nickel is preferentially adsorbed by hydrolyzates while cobalt prefers oxidates. In other words nickel would prefer adsorption to hydrothermal clays, etc., while cobalt prefers adsorption to freshly precipitated iron hydroxide. Chemically, cobalt is similar to iron and tends to accumulate in hydrothermally precipitated pyrite.

Van de Kamp (1970) used a plot of log [Ni] (ppm) as a function of Niggli mg to distinguish between metamorphic rocks of volcanic and sedimentary origin. Fig. 4-71 is a modification of his diagram demonstrating, in addition to his shale - carbonate field, approximate fields for iron formations and different igneous rocks. These fields are based upon Niggli mg ranges determined and the ranges of nickel contents depicted in Table 4-2. The shale carbonate field is one of negative slope whereas the igneous field demonstrates positive slope.

4.7.2 Nickel Contents of Ore - Bearing Metamorphic Host Rocks.

Gneisses from the Ear Falls area demonstrate a clustering within the common area shared by shale - carbonate rocks and intermediate igneous rocks (Fig. 4-72). The iron - rich rocks of this area are displaced towards the iron formation field outlined in Fig. 4-71. There is little difference between the nickel content of the iron - enriched

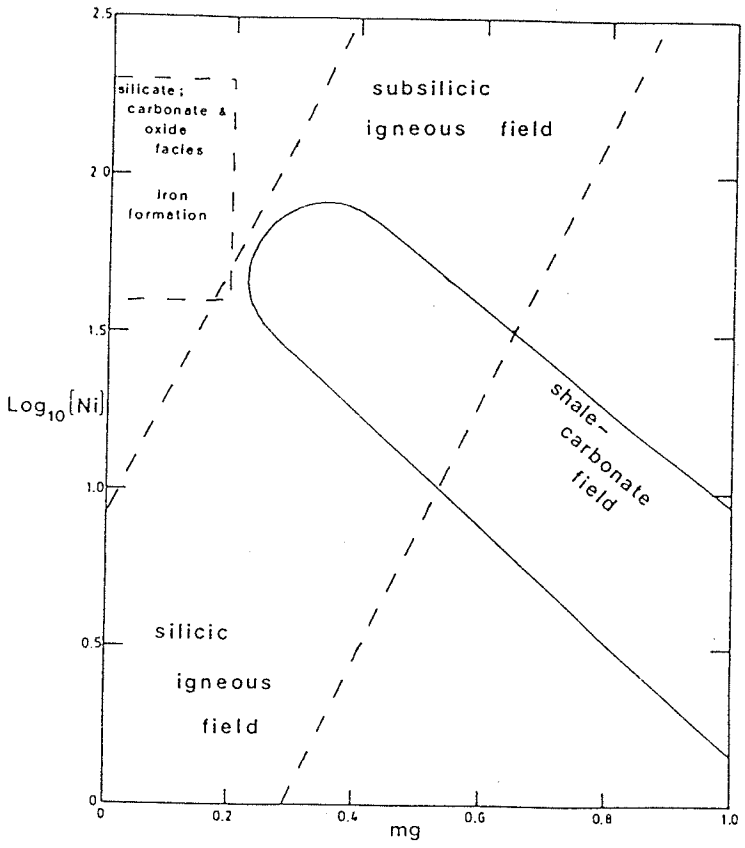

FIGURE 4-71 Plot of log (Ni) against Niggli mg (Van de Kamp,1970) showing the fields of common igneous and sedimentary rocks.

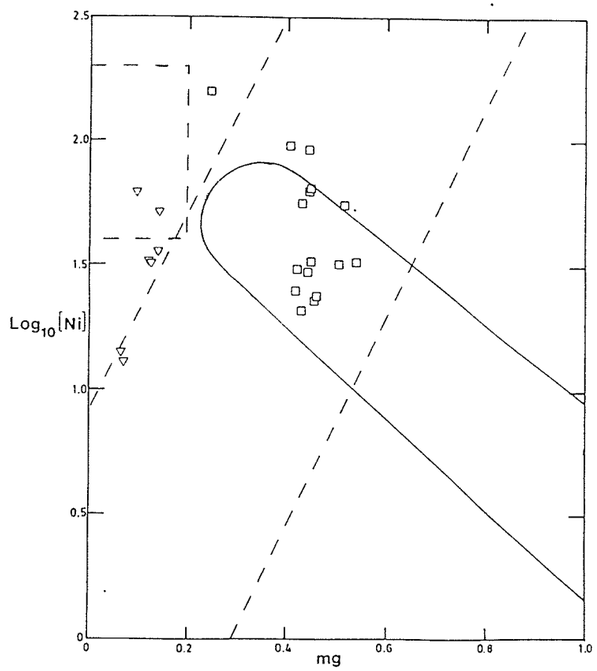

FIGURE 4-72 Plot of log (Ni) against Niggli mg (Van de Kamp,1970) for ferruginous metasedimentary rocks (represented by circles) and enveloping quartz-feldspar-biotite-(hornblende) gneisses (represented by inverted triangles) from the Ear Falls area, Ontario.

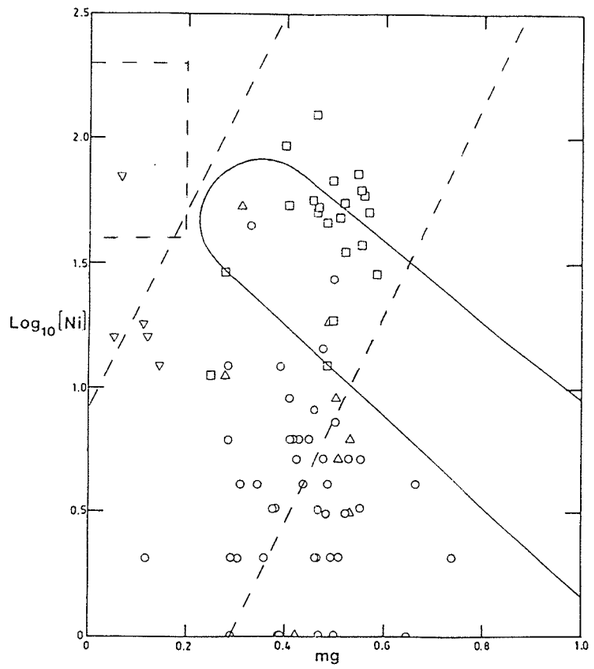

FIGURE 4-73 Plot of log (Ni) against Niggli mg (Van de Kamp,1970) for ore-bearing rocks from the Geco Mine, Manitouwadge, Ontario. Grey Gneiss Gp rocks (with the exception of iron formations) are represented by squares, Grey Gneiss Gp iron formations (plus intercalated metasedimentary rocks) are represented by inverted triangles, sillimanite-bearing Sericite Schist Gp rocks are represented by circles and cordierite-anthophyllite rocks from the 4/2 ore zone by triangles.

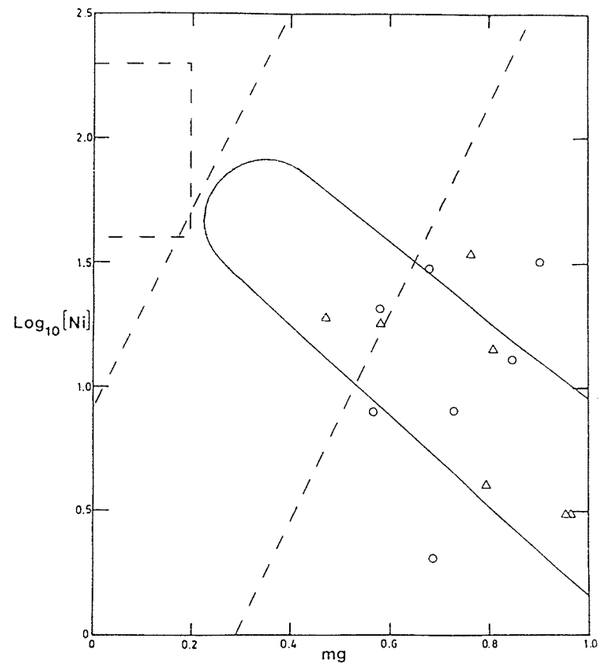

FIGURE 4-74 Plot of log (Ni) against Niggli (Van de Kamp,1970) for ore-bearing rocks from the Tetreault Mine, Montauban, Quebec. Sillimanite-bearing rocks are represented by circles and cordierite-anthophyllite rocks by triangles.

metasedimentary rocks and their host rocks, but there is enough to account for dilution by a non nickeliferous chemical sediment.

The intermediate to mafic volcanic rocks of the Grey Gneiss group at Geco, Manitouwadge (Fig. 4-73) plot within a field at the upper end of the shale - carbonate field corresponding to the subsilicic to intermediate igneous field outlined in Fig. 4-71. Sericite Schist group rocks, although having the same range of Niggli mg, demonstrate nickel levels up to a hundred times lower than Grey Gneiss group rocks. If volcanics such as Grey Gneiss group rocks are the progenitors of Sericite Schist group rocks, then this strong nickel depletion may have been brought about by either leaching and/or dilution. They may, however, represent more felsic rocks which have been altered through Mg-Fe metasomatism in analogy with some volcanogenic massive sulfide deposits (e.g. Millenbach Mine).

Niggli mg values for some cordierite - anthophyllite and sillimanite schists at Montauban-Les-Mines, Quebec are equivalent to those of ultramafic or magnesia - rich carbonate rocks. Nickel values, however, are almost a hundred times lower than those expected for ultramafic rocks, and are even too low for gabbroic rocks (Fig. 4-74). One also notes that nickel contents within the ore zone demonstrate variations of up to two orders of magnitude. Carbonate units are common within the immediate vicinity of the Montauban orebody and a dolomite component would shift the "Sodic Leptites" described by Stamatelopoulou - Seymour and MacLean (1977) towards higher mg values. Bearing in mind the effects of dilution, extrapolation of the data points in Fig. 4-74 back towards mg values displayed by the sodic leptites ($0<mg<0.55$) would produce a result in agreement with intermediate to mafic volcanic

progenitors. Lack of carbonate in the anthophyllite schists is still a problem, however, if one is to consider a diluent of dolomitic composition. This may be resolved if the diluent is a hydrothermal Mg chlorite devoid of nickel.

Quartz - feldspar - biotite - sillimanite gneisses and amphibolite at New Calumet, Calumet Island, Ontario, produce a field of roughly positive slope corresponding to intermediate to mafic igneous rocks (Fig. 4-75). Some carbonates at New Calumet fit well into the shale - carbonate field of Van de Kamp (1970), while others fit well into the field of subsilicic igneous rocks. Ore - bearing gneisses and gneisses with anomalous copper and zinc contents generally demonstrate a slight skewing towards lower nickel contents. Although these are generally more sulfide - rich, there is no enrichment of nickel or cobalt (Appendix A-3).

Skewing towards lower nickel contents is, once again, demonstrated by mineralized sillimanite - bearing gneisses on Yakushavitch Island, Kississing Lake, Manitoba (Figs. 4-76 and 4-77). Host gneisses are confined entirely to the shale - carbonate field of Van de Kamp (1970) which is in accordance with the interpretation that these gneisses represent an original greywacke assemblage. The skewing of mineralized gneisses toward lower nickel contents may be due to leaching of the nickel and/or dilution by other components. Mineralized gneisses are enriched in anthophyllite and talc, which may have been derived by metamorphism of a chloritic component. This again may have been a hydrothermally precipitated component devoid of nickel or it may have been produced by Mg-Fe metasomatism in analogy with volcanogenic massive sulfide deposits.

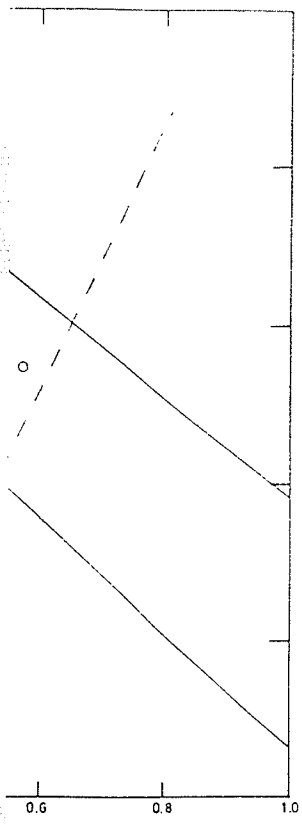

nst Niggli mg (Van de
aring rocks encountered
DDH-11-11-3 on
Kississing Lake, Man.
te-(sillimanite)
are represented by
s indicate greater than

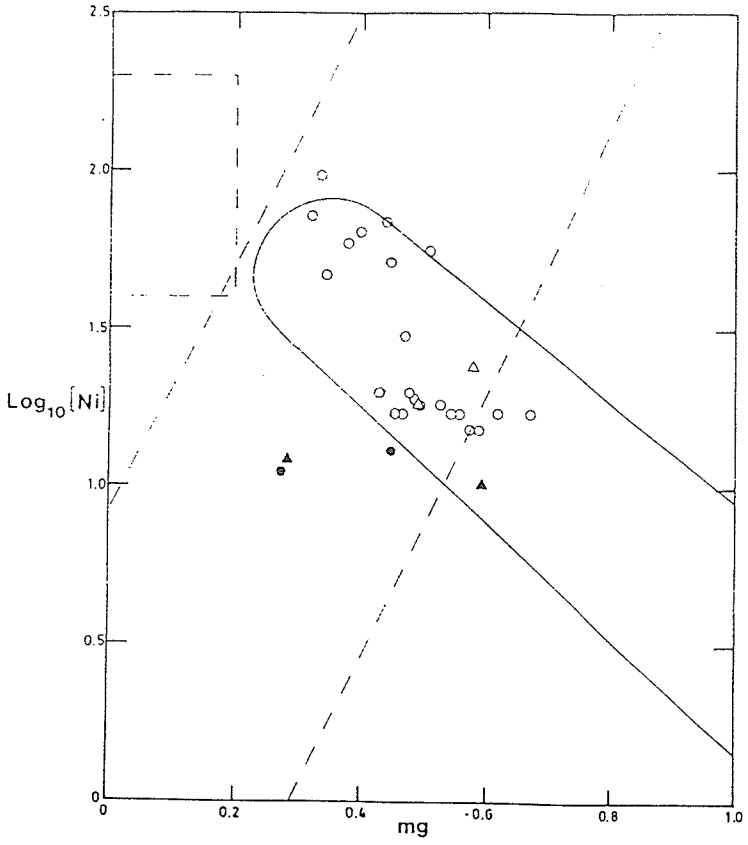

FIGURE 4-77 Plot of log (Ni) against Niggli mg (Van de Kamp,1970) for ore-bearing rocks encountered in diamond drill hole DDH-11-11-5 on Yakushavitch Island, Kississing Lake, Man. Quartz-feldspar-biotite-(sillimanite) schists and gneisses are represented by circles and anthophyllite-bearing rocks by triangles. Solid figures indicate greater than 500 ppm Cu or Zn.

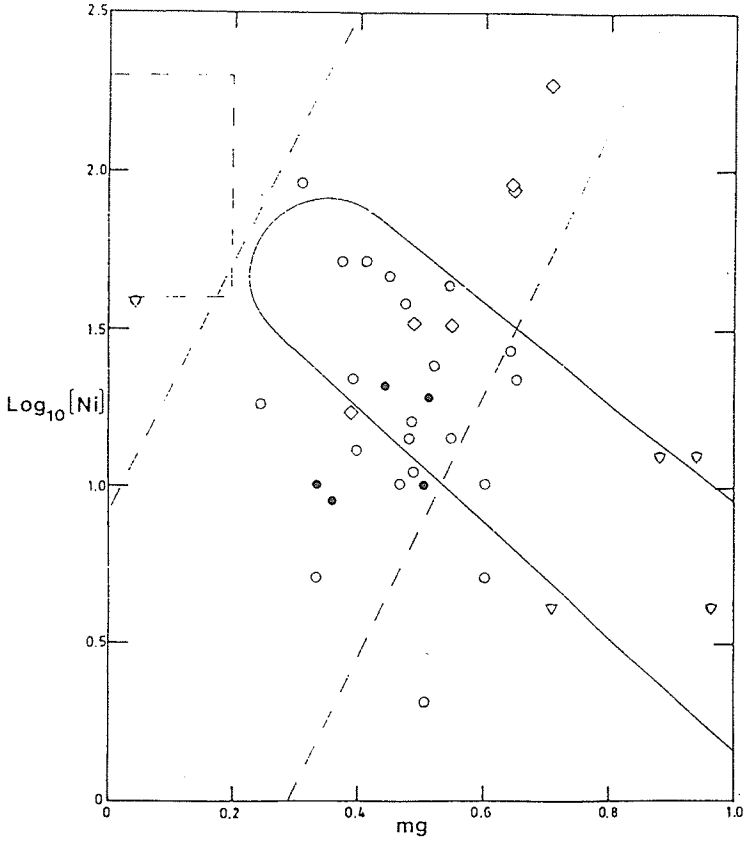

FIGURE 4-75 Plot of log (Ni) against Niggli mg (Van de Kamp,1970) for ore-bearing rocks from the New Calumet deposit, Calumet Island, Quebec. Amphibolites are represented by diamonds, quartz-feldspar-biotite-(sillimanite) rocks by circles, and carbonates and calc-silicates by inverted triangles. Solid figures indicate greater than 500 ppm Cu or Zn.

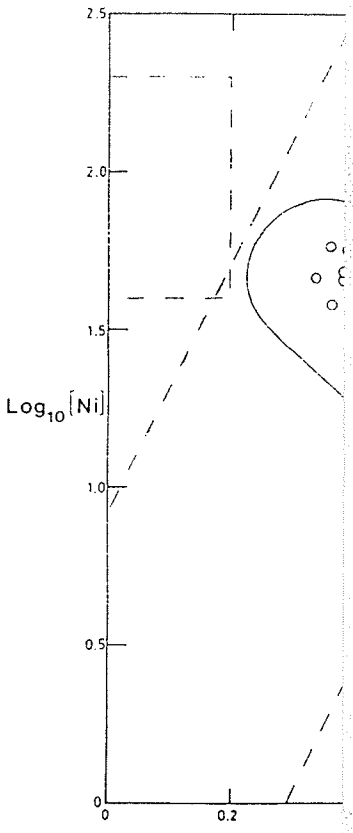

FIGURE 4-76 Plot of log
Kamp,1970) f
in diamond d
Yakushavitch
Quartz-feldsp
gneisses and
circles. Soli
500 ppm Cu o

4.7.3 Nickel and Cobalt Contents of the Metamorphic Host Rocks bearing Mineralization: a Discussion

Normal metamorphosed igneous and sedimentary rocks appear to fall within the field generated in Fig. 4-71. The overlap of the shale - carbonate field and the intermediate igneous field, however, does not allow one to use nickel contents to determine the origin of a rock falling into this common field.

Detailed examination of host rocks at Geco, N. Maysville and to a lesser extent Montauban and New Calumet, does indicate that a fairly severe depletion of nickel occurs within the ore zones. Cobalt is sporadic in its occurrence. For example, within the Sericite Schist group at Geco some rocks demostrating nickel depletion may show a depletion or enrichment of cobalt (appendix A). If leaching was solely responsible for the nickel depletion, all Sericite Schist group rocks should demonstrate an even more severe cobalt depletion, since cobalt is even more mobile (Rankama and Sahama, 1952). The information revealed in Table 4-3, although nebulous, indicates that ratios do appear to roughly reflect original rock types, according to the ratios listed by Rankama and Sahama (1952). In the case of Geco, Milne's (1969) unit 1a should fall in the field of normal basaltic rocks, but the actual average ratio is somewhat high at 0.875. The low average Co/Ni ratio of Milne's unit 5 indicates nickel predominates over cobalt in these rocks. Much of unit 5 appear to be interbedded argillaceous and arenaceous

TABLE 4-3 AVERAGED COBALT/NICKEL RATIOS IN METAMORPHICS (THIS STUDY), COMPARED WITH THE CO AND Ni RANGES REPORTED BY RANKAMA AND SABAMA, 1952.

LOCATION	ROCK TYPE	AVERAGE Co RANGE (ppm)	AVERAGE Co/Ni	INTERPRETATION MOST CONSISTENT WITH BOTH Co RANGE AND Co/Ni (based on ranges reported by Rankama and Sahama, 1952)
EAR FALLS AREA	qtz-fldspr-biot-(hbde) gneisses	20-25	0.45	shale-sandstone mixture (greywacke ?)
	ferruginous qtz fldspr-biot-(garn) gneisses	0-10	0.32	same field occupied by Geco iron formations
GECO MANITOUWADGE	hbde gneiss (unit 1a; Milne, 1969) Grey Gneiss Gp	50-60	0.88	mafic igneous rock
	qtz-fldspr-biot gneiss (unit 2; Milne, 1969) Grey Gneiss GP	10-20	0.66	shale-sandstone mixture (greywacke ?)
	biot schist (unit 4;Milne, 1969) Grey Gneiss GP	30	0.81	intermediate igneous rock
	qtz-fldspr-biot-(hbde) gneiss (unit 5;Milne, 1969) Grey Gneiss GP	15-25	0.31	mafic to intermediate igneous rock
	qtz-fldspr-biot-sill gneiss Sericite Schist Gp	0-10	1.45	consistent with felsic igneous origin
	cord-anth rocks at base of 4/2 ore zone	0-10	2.01	consistent with felsic igneous origin
	iron form (Milne, 1969)	0-10	0.25	
YAKUSHAVITCH ISLAND SHERRIDON AREA	qtz-fldspr-biot-sill gneisses	20-30	0.49	consistent with a shale-sandstone mixture
	qtz-fldspr-biot-anth-(sill) - (talc) gneiss/ schist	4-83 (drastic variations)	2.7	partially consistent with a felsic igneous origin & partially with some iron formations
MONTAUBAN	qtz-fldspr-biot-sill gneisses	3-5	0.81	somewhat consistent with a felsic igneous origin
	cord-anth rocks	3-5	0.63	somewhat consistent with a felsic igneous origin
NEW CALUMET	hbde gneisses	30-40	0.63	intermediate to mafic igneous origin
	plag-biot-(qtz)	10-20	0.64	somewhat consistent with an intermediate to felsic igneous origin
	qtz-fldspr-biot-sill gneisses	0-10	0.77	felsic to intermediate igneous origin

rocks with considerable mafic mineral content. Goldschmidt (1937) has stated that nickel's predominance over cobalt in hydrolyzate sediments produces Co/Ni ratios of about 0.40. The production of hydrolyzate sediments upon weathering of mafic rocks (e.g. basalts of unit 1a) may be responsible for the low average Co/Ni ratio of Unit 5. It should be noted that Table 4-3 indicates drastic variations of cobalt in the anthophyllite - bearing rocks at Yakushavitch Island. These rocks are characterized by wide variations of Co over short distances.

The high average value of Co/Ni for Milne's (1969) unit 11a may reflect hydrothermal sulfide addition to these rocks (Rankama and Sahama, 1952). But upon examination of the sulfur contents of the samples demostrating the highest ratios (appendix A) one finds no direct correlation. For example, sample GO-113 d1 contains 0.081% S and has a Co/Ni ratio of 7.0 whereas sample GO-113 d2 contains 1.392% S and has a Co/Ni ratio of 0.278. These discrepancies may, however, be the result of metamorphic reactions involving sulfides. The maximum possible Co/Ni ratio for rocks of igneous origin is 4.00 (Rankama and Sahama, 1952). Oxidate sediments including oxide and carbonate facies iron formation and manganiferous marine sediments do have the ability to produce Co/Ni ratios in excess of 4.00 (Rankama and Sahama, 1952). Therefore, the high average Co/Ni ratio of the Sericite Schist group (Milne's Unit 11a) may be due to the involvement of fairly felsic material such as rhyolitic tuffs while occasional very high Co/Ni ratios may be due to intercalations of ferruginous, siliceous exhalative metasediments.

4.8 A Discriminant Plot of Niggli ti Against the Sum of Niggli al and Niggli alk.

4.8.1 Introduction

The use of a discriminant plot of the value Niggli ti against the value al plus Niggli alk offers some aid in the determination of igneous and, to some degree, sedimentary progenitors by virtue of the reported immobility of titanium under even the most extreme conditions (Finlow-Bates and Stumpfl, 1981; Roberts and Reardon, 1978). Niggli al + alk is used along the x-coordinate to produce a broad igneous spectrum with felsic rocks of high al + alk values and mafic rocks of low al + alk values (high fm + c).

Van de Kamp et al. (1976) in an investigation of some California arkoses have reported Niggli ti values of 0.75 and greater. This would place the lower limit of arkosic sediments (al + alk ranging from 50 up) in the same position as that of normal igneous rocks. Although difficult to separate rocks of sedimentary origin from those of igneous origin with this method, the great variability of titanium in bedded sediments (due to concentration of the resistate minerals rutile and sphene) helps to explain this problem somewhat. One may then suspect that a rock which demonstrates high and/or highly variable Niggli ti may be of sedimentary origin. Felsic igneous rocks demonstrate little variability (Fig. 4-78), Niggli ti varying from a low of 0.85 for alkaline granitic rocks to no greater than 1.5 for calc-alkaline granitic rocks. Mafic rocks demonstrate Niggli ti values as low as 1.35

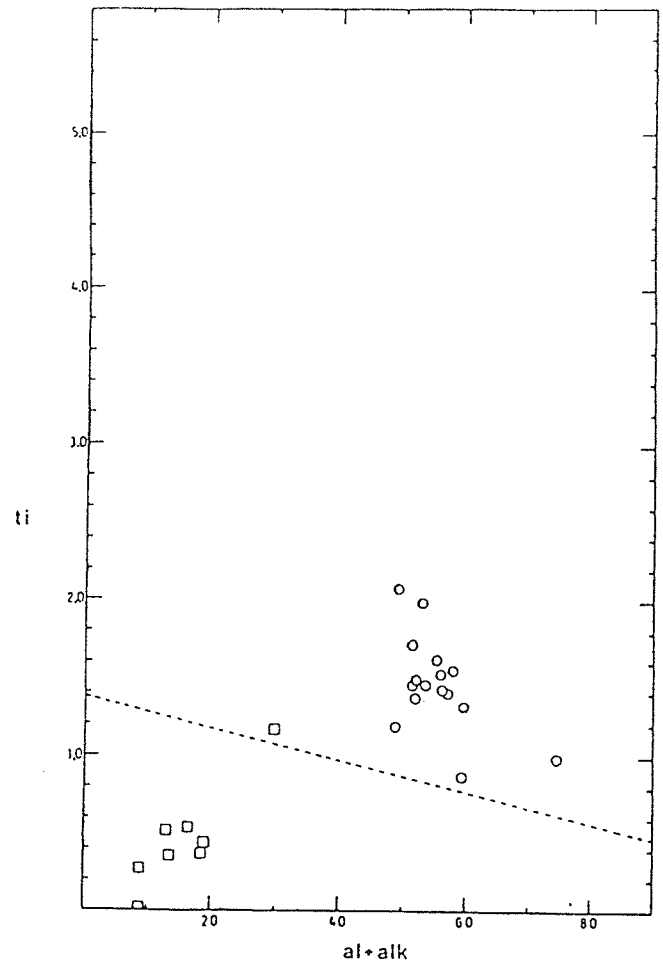

FIGURE 4-80 Niggli ti:al+alk diagram for ferruginous metasedimentary rocks (represented by squares) and enveloping quartz-feldspar-biotite-(hornblende) gneisses (represented by circles) from the Ear Falls area, Ontario.

for several
id the world,
ure (see

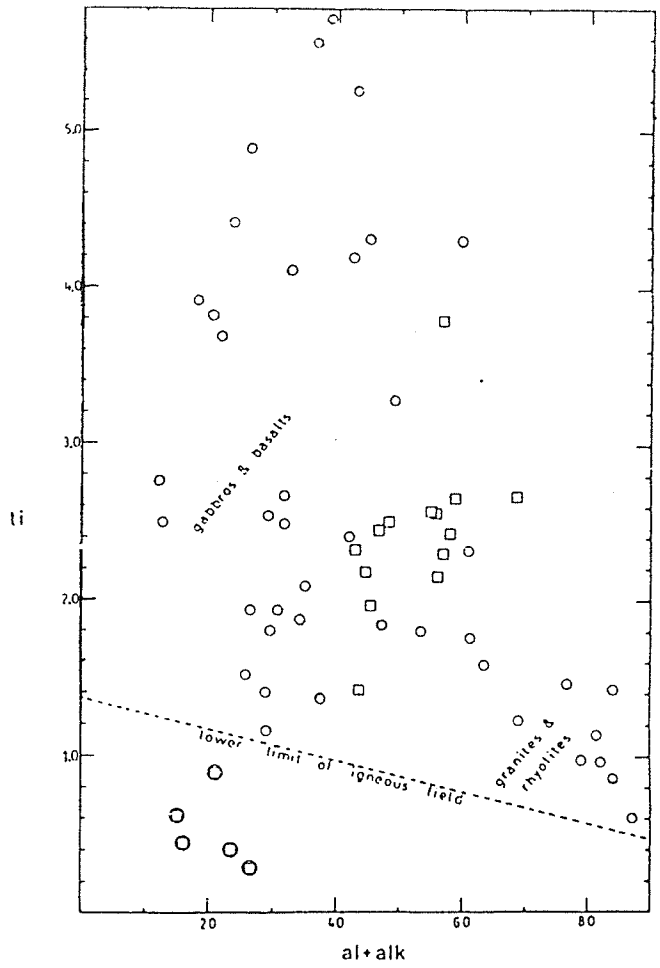

FIGURE 4-78 Niggli ti:al+alk diagram for some common igneous and sedimentary rocks selected from the literature (see Appendix B). Key to rock types: igneous rocks are represented by circles and sedimentary rocks by squares. Circled squares represent calcareous greywackes.

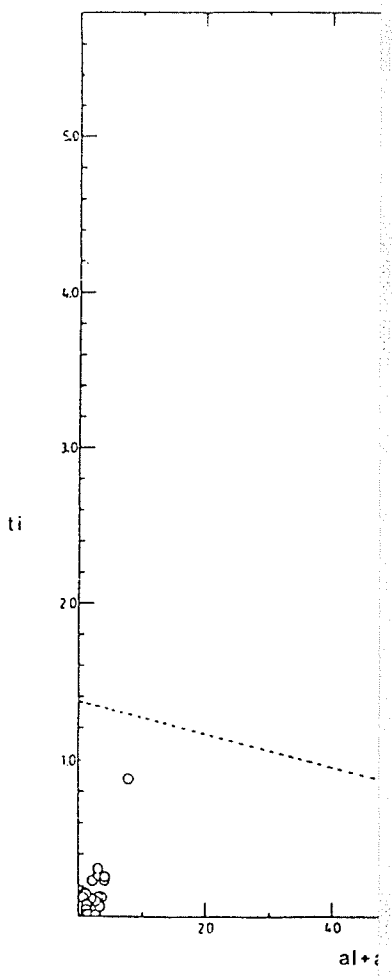

FIGURE 4-79 Niggli ti:al+alk
iron formations f
selected from the
Appendix B).

for low titanium basalts such as those found in the Flin Flon area (Stauffer et al., 1975). Upper values for basalts may, however, exceed 4.0, but average ti values for basalts commonly hover around 2.0. Although this diagram demonstrates the increase of Niggli ti as one progresses from felsic to mafic members of the igneous spectrum, the effect of changing titanium concentration is diminished since Niggli ti is a molecular ratio of titanium to iron plus magnesium plus manganese (and all four of these elements increase towards the mafic end of the igneous spectrum).

4.8.2 Titanium Contents of Metamorphic Ore Bearing Host Rocks as Depicted by the Niggli ti : al + alk Diagram

The relative immobility of titanium is suggested by Fig. 4-79 where Niggli ti values rarely exceed 0.3 in iron formations. The iron - rich metasedimentary gneisses of the Ear Falls area (Fig. 4-80) demonstrate Niggli ti values slightly elevated with respect to this field of iron formations. This is very likely due to intermixing of chemical and epiclastic material. The host sediments in this area cluster within the field bounded by $60 > al + alk > 50$ and $1.8 > ti > 1.3$ with no drastic variations in Niggli ti. This would suggest that the progenitors were immature sediments, where little time was allowed for resistate minerals to separate out and accumulate as accessories in more mature sediments. This substantiates the interpretation that the host gneisses are of greywacke/volcaniclastic affiliation (Bond et al., 1975).

Mafic and intermediate volcanic rocks of the Grey Gneiss group at Geco conform well to the igneous field depicted in Fig. 4-81. The Grey Gneiss group also contains some garnetiferous biotite schists exhibiting some relict clastic textures and relatively high Niggli ti values. Although bedded concentrations of resistate titanium minerals are common in mature sedimentary rocks, similar high titanium levels may be produced by chemical weathering of basalt. Goetz (1980) has reported such an instance in the Flin Flon area, where high titanium levels occur in a regolith on an old basaltic land surface.

Niggli al + alk values of the Sericite Schist group are slightly greater than those of the Grey Gneiss group rocks to the immediate south. Niggli ti values, however, are generally half as high as those demonstrated by the Grey Gneiss group rocks. Some Niggli ti values fall below the lowest levels observed in the most felsic igneous rocks, and approach levels comparable to those demonstrated by iron formations in Fig. 4-79.

Rocks of the 4/2 ore zone have the low al + alk values characteristic of ultramafic rocks but Niggli ti values are half as high as those expected in the most felsic rocks (ti < 0.5). This same combination of low al + alk and low Niggli ti is again observed in Milne's unit 4 (Milne, 1969), near the contact with the iron formation between Geco shafts #1 and #4. This behaviour, in the proximity of the iron formation, indicates that unit 4 may have been "modified" (by addition of certain chemical sedimentary components) rather than chemically altered. That is, the contact zone may have formed during a period of waning chemical sedimentation at the onset of deposition of unit 4. This would produce a hybrid sediment partially of chemical

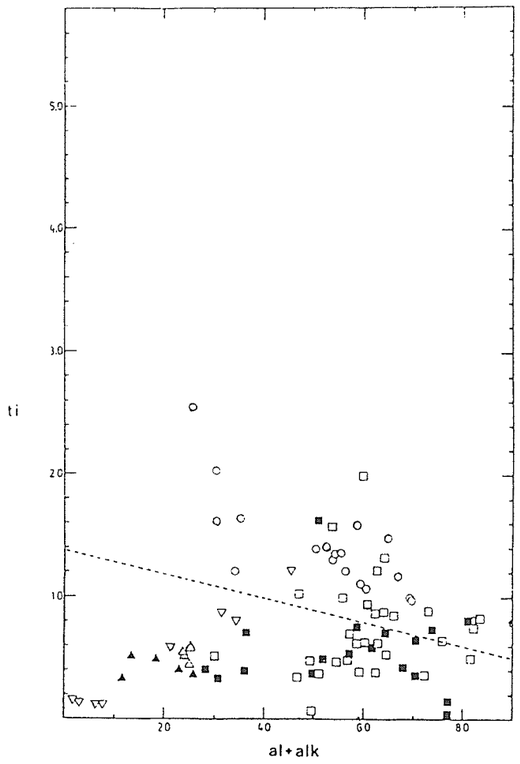

FIGURE 4-81 Niggli ti:al+alk diagram for ore-bearing rocks from the Geco Mine and vicinity, Manitouwadge, Ontario, Grey Gneiss GP rocks (with the exception of iron formation) are represented by squares, Grey gneiss Gp iron formation (plus intercalated metasedimentary rocks) are represented by inverted triangles, sillimanite-bearing Sericite Schist Gp rocks by circles, and cordierite-anthophyllite rocks of the 4/2 ore zone by triangles. Solid figures indicate greater than 500 ppm Cu or Zn.

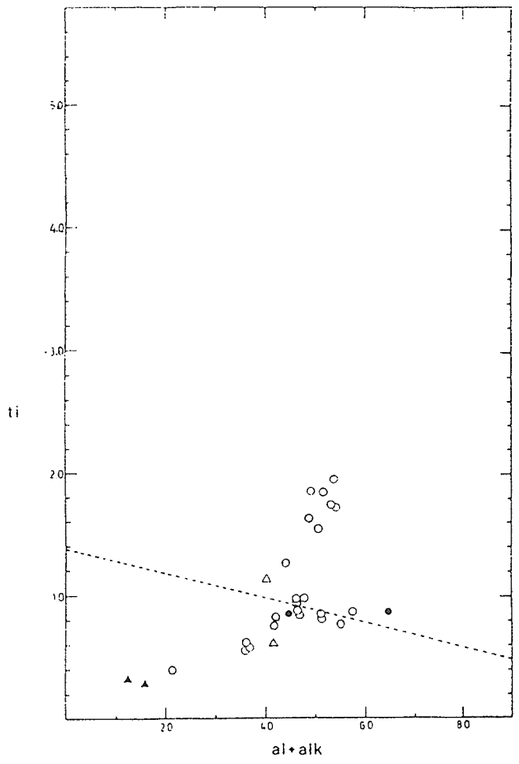

FIGURE 4-82 Niggli ti:al+alk diagram for ore-bearing rocks encountered in diamond drill hole DDH-11-11-5 on Yakushavitich Island, Kississing Lake, Manitoba, Quartz-feldspar-biotite-(sillimanite) gneisses are represented by circles and anthophyllite-bearing rocks by triangles. Solid figures indicate greater than 500 ppm Cu or Zn.

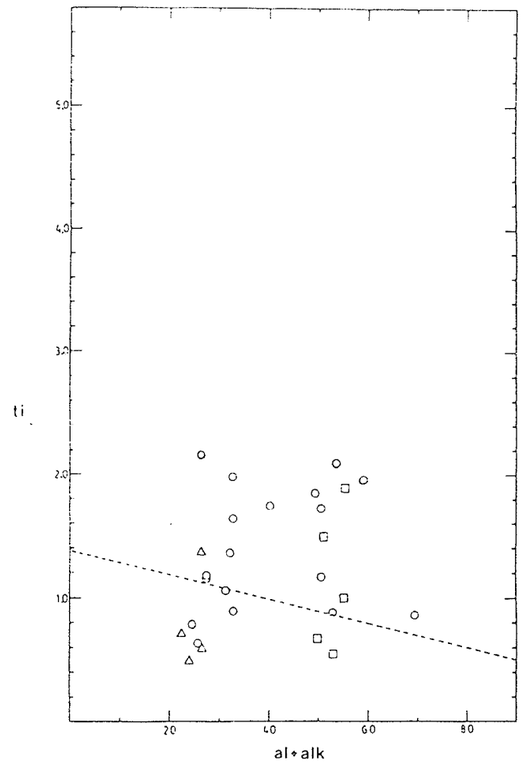

FIGURE 4-83 Niggli ti:al+alk diagram for some representative rocks from the Sherridon deposit at Sherridon, Manitoba (analyses from Goetz, 1980; see Appendix B). Cordierite-anthophyllite rocks are represented by triangles, sillimanite-bearing rocks by squares and other quartz-feldspar schists and gneisses by circles.

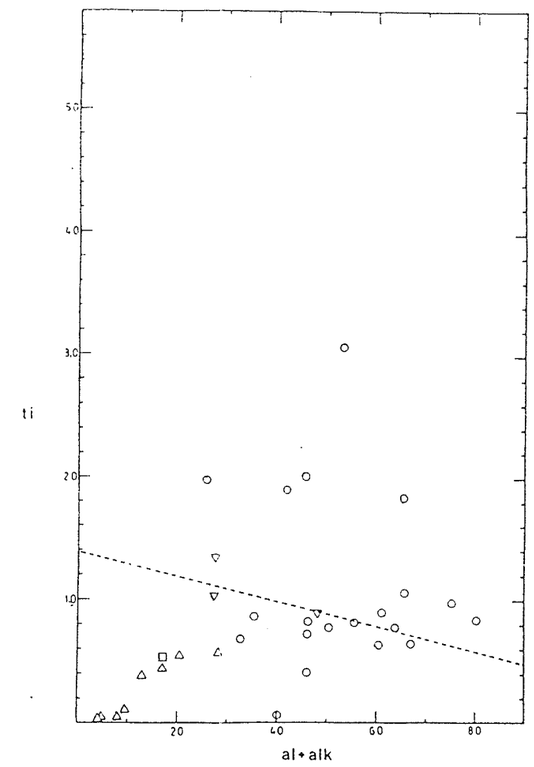

FIGURE 4-84 Niggli ti:al+alk diagram for ore-bearing rocks of the Sillimanite gneiss unit at N. Maysville (after Knight, 1981). Metasbasalts are represented by inverted triangles, sillimanite-bearing rocks by circles, iron formation by triangles, and anthophyllite-bearing rocks by squares.

origin and partially of epiclastic origin. Although rich in Fe and Mg oxides, the Geco iron formation to the North of unit 4 is practically devoid of titanium as was found to be the case with other iron formations studied (Fig. 4-79).

Host gneisses on Yakushavitch Island in the Sherridon area in Northern Manitoba (Fig. 4-82) demonstrate the same clustering observed in the greywacke metasedimentary rocks of the Ear Falls area, to a limited extent. Gneisses which are adjacent to, or directly host, mineralization demonstrate depressed Niggli ti values, however. The lowest values of both Niggli ti and al + alk are observed in the anthophyllite - talc - bearing sulfide - rich gneisses. These same properties are inherent in the extensive blanket-like anthophyllite gneisses of the Sherridon deposit itself (Fig. 4-83). The same elongate field, projecting from the field of "normal" host gneisses towards values of ti = 0 and al + alk = 0, which exists at Geco is again observed in the Sherridon area of Northern Manitoba.

Apart from the mafic gneisses described by Knight (1980) the felsic gneisses at Maysville form a field of moderate to high values of al + alk and Niggli ti values clustering mainly between 0.6 and 1.0 (Fig. 4-84). Again an elongate field projecting towards ti = 0 and al + alk = 0 exists. Those gneisses of probable or possible exhalative sedimentary origin (Knight, 1981) form the part of this field closest to the origin. The postulated mixtures of normal epiclastic (or pyroclastic) sediments and exhalative chemical sediments is supported by the continuity of their respective fields on the Niggli al + alk : ti diagram.

Gneisses hosting the Broken Hill orebody (Main Lode) occupy a relatively disperse field on this type of diagram (Fig. 4-85). Many of

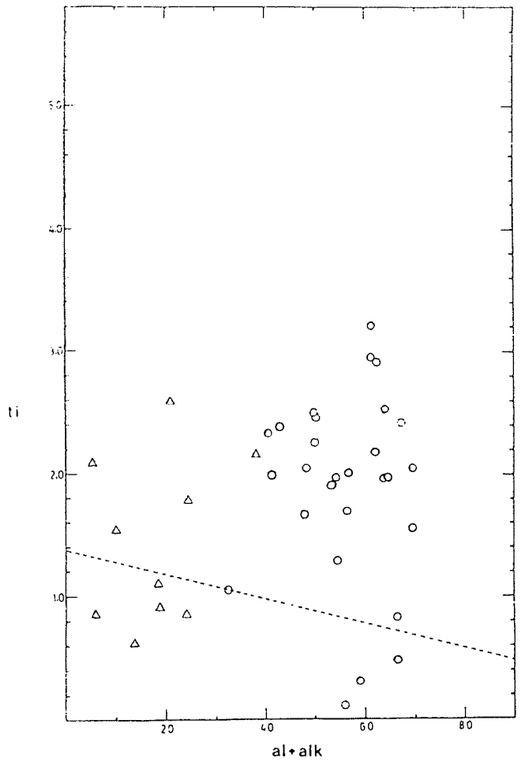

FIGURE 4-85 Niggli ti:al+alk diagram for some representative rocks from the Broken Hill Main Lode, Broken Hill, N.S.W., Australia (analyses from Joplin,1963; see Appendix B). Quartz-feldspar-biotite-(sillimanite) gneisses are represented by circles and iron formations by triangles.

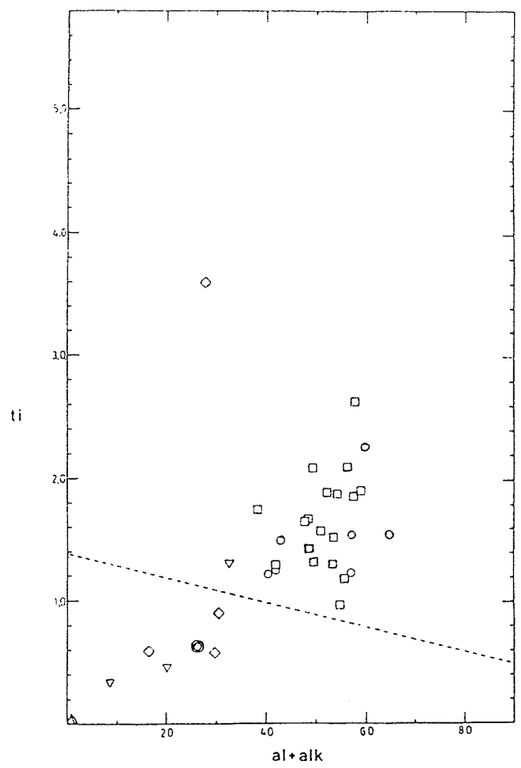

FIGURE 4-86 Niggli ti:al-alk diagram for ore-bearing rocks from the New Calumet deposit, Calumet Island, Quebec. Carbonates are represented by triangles, calc-silicates by inverted triangles, amphibolites by diamonds, quartz-feldspar-biotite-(sillimanite)rocks by circles and quartz-feldspar-biotite rocks by squares. A quartz-rich rusty weathering pyrite-bearing gneiss is represented by a double circle.

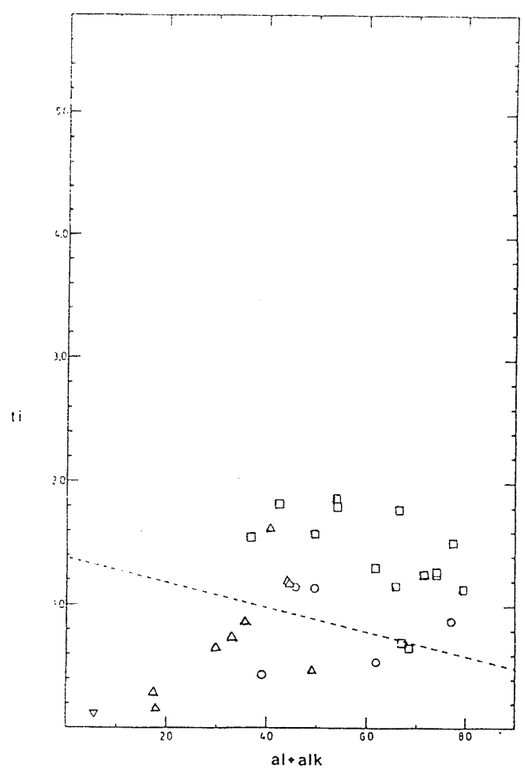

FIGURE 4-87 Niggli ti:al+alk diagram for ore-bearing rocks from the Tetreault Mine and vicinity, Montauban, Quebec. "Leptites" (analyses from Stamatelopoulou-Seymour and MacLean, 1977) are represented by squares, calc-silicates by inverted triangles, sillimanite-bearing rocks by circles and cordierite-anthophyllite rocks by triangles.

the quartz - feldspar wall rocks have Niggli ti values higher than normal igneous rocks of intermediate composition and are displaced towards the high ti values exhibited by sedimentary rocks containing bedded concentrations of titaniferous resistate minerals.

Banded iron formations at Broken Hill are anomalous. Niggli ti values are all > 0.6 and some values in excess of 2.0 occur. This puts them into a category apart from "normal" iron formations. Although titanium is reported to be immobile under the fairly extreme conditions of hydrothermal activity, metamorphic mobilization may occur under granulite facies metamorphism (Ramberg, 1948). Since metamorphism at Broken Hill has attained granulite facies, this mobilization may have produced the local titanium concentrations which are observed in the iron formations. Generally, a behaviour paralleling the behaviour of anomalous rock types associated with mineralization at Geco and Maysville was not observed.

Felsic gneisses from the ore zone at New Calumet generally fall within the field occupied by intermediate igneous rocks (Fig. 4-86). Although an elongate sub - field projecting from this field towards the origin does occur, it reflects mainly carbonates and calc - silicate rocks. This field also extends down from higher ti and al + alk values at a steeper slope. Two samples of amphibole - rich gneiss fall below the igneous field within the elongate carbonate/calc - silicate field. They very likely represent metamorphosed, though rather impure, carbonates. Osborne (1944) and Moorhouse (1941) have reported that amphibolites within the vicinity of the orebody are likely of sedimentary origin. Some high ti amphibolites do also exist within the same area and this would indicate that they are likely of mafic igneous

origin.

Although not observed, anthophyllite - bearing gneiss is reported to occur (Moorhouse, 1941) as a discontinuous irregular unit separated from the footwall amphibolites by rusty weathering gneisses. The "rusty gneiss" is represented in Fig. 4-86 by a double circled data point in the low ti carbonate/calc - silicate field. Due to the cherty nature and low Niggli ti value, this rusty - weathering pyritic felsic gneiss is interpretted to be at least partially of exhalative sedimentary origin. Although data is lacking, the anthophyllite gneisses at New Calumet may represent a lithologic hybrid composed of both chemical and clastic sediments, as is interpreted to be the possible origin of anthophyllite - bearing gneisses at Geco, Sherridon and N. Maysville.

Metamorphosed felsic volcanics ("leptites" of Stamatelopoulou - Seymour and MacLean, 1977), fall within the intermediate - felsic igneous field in the Niggli ti : al + alk diagram (Fig. 4-87). Sillimanite schists and cordierite - anthophyllite - sillimanite schists, however, demonstrate a skewing towards lower Niggli ti and al + alk values in comparison with the leptites to the west of the orebody. The most depressed ti values are found in the anthophyllite - bearing schists in analogy with those of Geco, Sherridon and Maysville.

4.8.3 Discussion of Results Based on the Niggli ti vs. al + alk Discrimination Method

This method partly supports the genetic interpretation of many of

the metamorphosed rocks hosting the orebodies studied here. Metasedimentary rocks considered of exhalative origin (such as the iron formations depicted in Fig. 4-79), are characterized by low Niggli ti values. Physical mixtures of exhalative chemical sediments and epiclastic and/or pyroclastic sediments should give ti values intermediate between the near zero values of iron formations and the values demonstrated by normal volcanic and sedimentary rocks (Fig. 4-78). The same end may be achieved if a normal sediment or solid rock is altered by Mg-Fe metasomatism and alkali leaching through a mechanism similar to that which produced the alteration pipes observed in many volcanogenic massive sulfide deposits (if titanium is also leached). Alteration or modification of a "normal" sediment would give a similar final product. This is dealt with in more detail in chapter 5.

Figure 4-88 demonstrates the prograde alteration which occurs within the alteration pipes at the Millenbach and Mattagami Lake Mines. The same trend towards low ti and al + alk values is repeated here. Although Niggli ti values dip below 1.0, actual TiO_2 concentrations do not fall below 0.20%. Many of the anthophyllite - cordierite bearing schists at Geco, Maysville, the Sherridon area and Montauban, however, show TiO_2 concentrations below 0.20% and often even below 0.10% (appendix A). If original titanium is being diluted through addition of Mg, Fe and silica during alteration, these very low TiO_2 concentrations would require a dilution, by the introduced components, of at least 1:1. If we are dealing with post - depositional alteration, this would pose a volumetric problem (ie. it would require substantial expansion of existing rocks to accomodate added components).

The effects of hydrothermal alteration involving leaching of

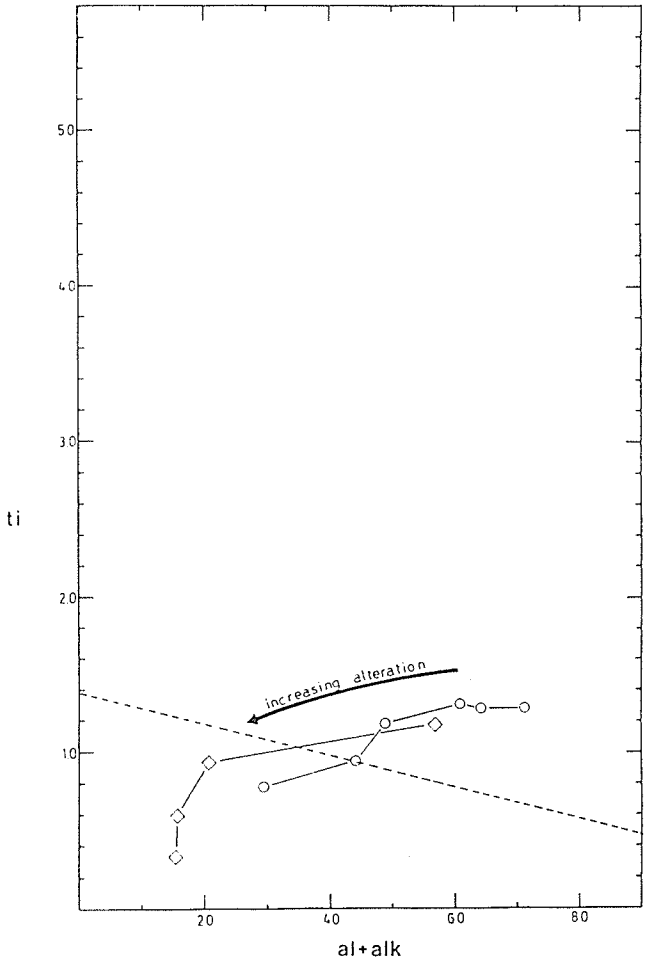

FIGURE 4-88 Niggli ti:al+alk diagram for hydrothermally altered rocks at the Millenbach Mine, Noranda area, Quebec (analyses from Riverin and Hodgson, 1980; see Appendix B-8) represented by circles; and at the Mattagami Lake Mine, Quebec (analyses from Roberts and Reardon, 1978; see Appendix B-9) represented by diamonds. The arrow indicates increasing alteration towards the cores of the alteration zones.

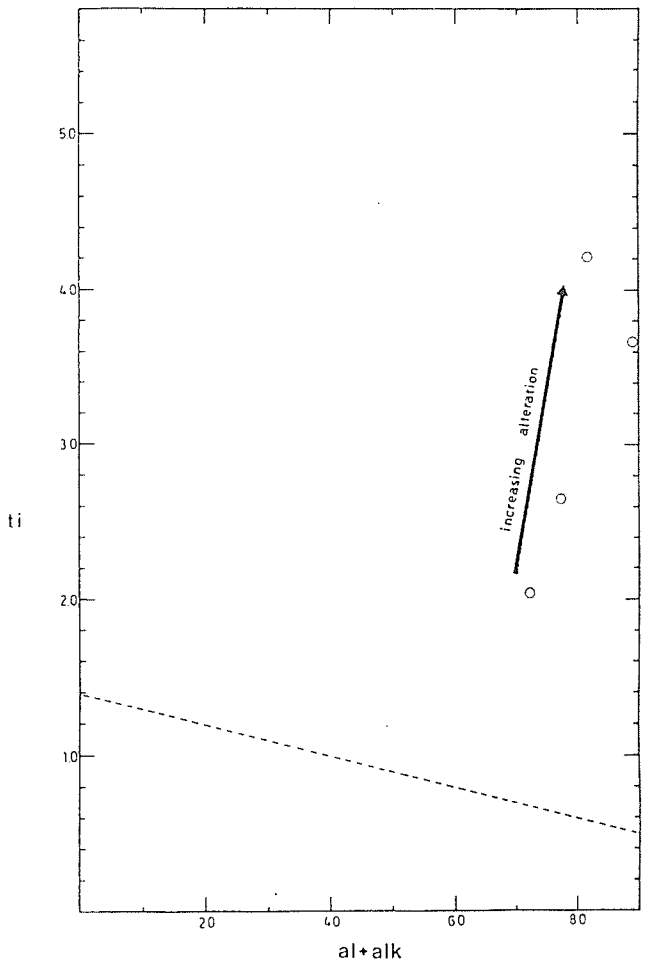

FIGURE 4-89 Niggli ti:al+alk diagram for hydrothermally altered quartz monzonite at Roosvelt Hot Springs, Utah. The arrow indicates increasing intensity of alteration.

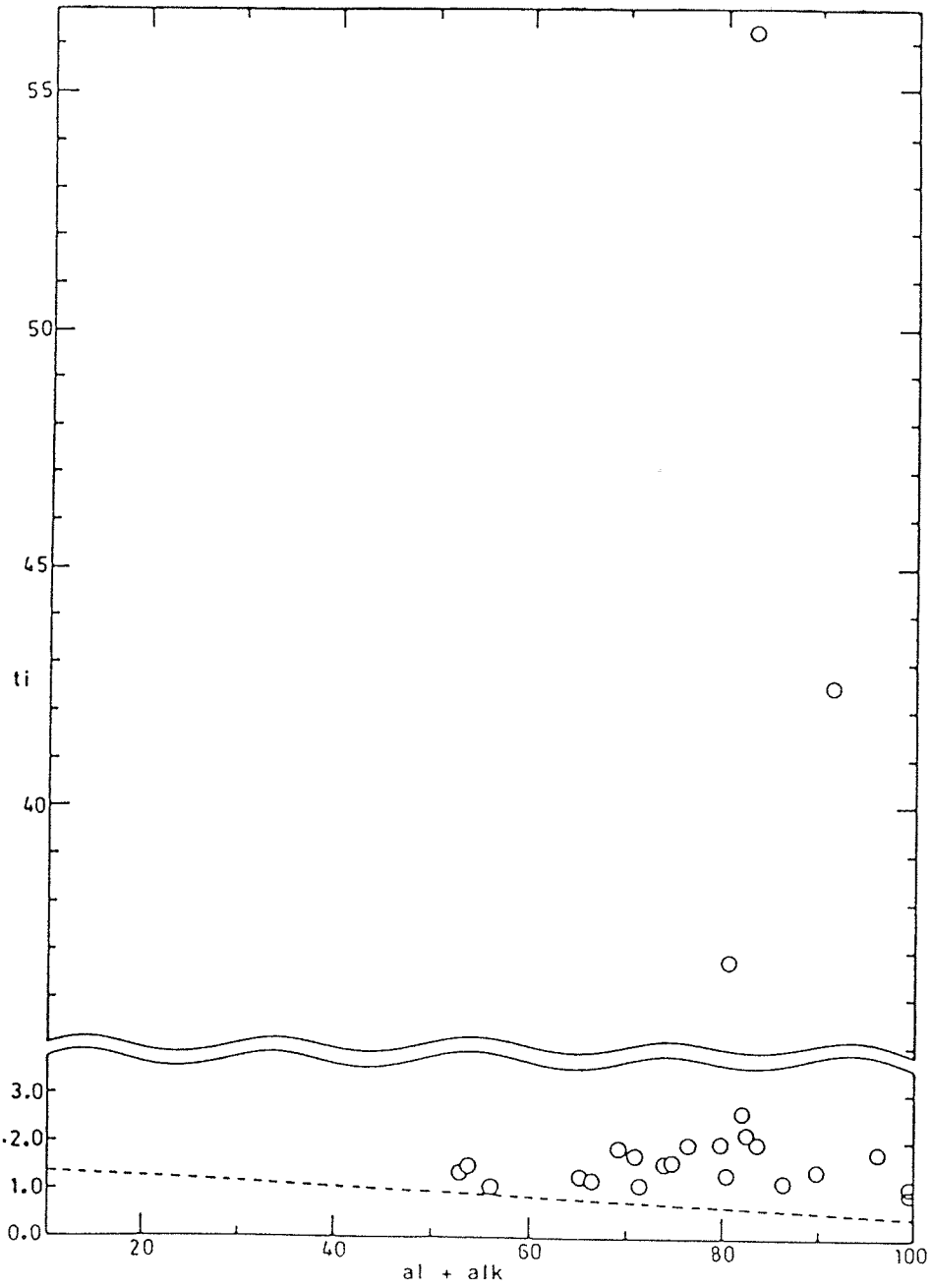

FIGURE 4-90 Niggli ti:al+alk diagram for hydrothermally altered felsic and intermediate igneous rocks at Steamboat Springs, Nevada.

alkalies and iron from intrusive igneous rocks of intermediate composition at Roosevelt Springs Utah and Steamboat Springs Nevada are demonstrated by the Niggli ti vs. al + alk method in Figs. 4-89 and 4-90, respectively. A very noteworthy contrast between this type of hydrothermal leaching and the type of alteration or modification which produced the cordierite - anthophyllite gneisses at Geco, Montauban, etc. is readily observed. At both Hot Springs leaching of alkalies, iron and magnesium has led to the formation of a product composed of the more chemically resistive elements. Hence Niggli ti values are displaced upwards due to titanium's chemical immobility. Even the sillimanite bearing host rocks at Geco, Maysville, Montauban, and New Calumet show depressed Niggli ti values rather than elevated ones. It is therefore unlikely that the type of alteration which occured at Roosevelt Springs and Steamboat Springs played any part in the production of the sillimanite gneisses studied here.

CHAPTER 5

SUMMARY AND CONCLUSIONS

5.1 General Results of Plotting Techniques

The Garrels and MacKenzie (1971) diagram, La Roche's (1974) silicoaluminate diagram and some of the plots utilizing Niggli values produce distinct fields for common igneous and sedimentary rocks. These diagrams also substantiate the findings of others (Engel and Engel, 1960; Stanton, 1984; Stanton, 1979; Taylor, 1955) with regard to the effects of progressive metamorphism on the bulk chemical composition of rocks. It appears that progressive regional metamorphism up to amphibolite facies produces only minor changes in the elements being considered.

Sillimanite - bearing gneisses and schists, and cordierite - anthophyllite rocks often plot outside the fields of common sedimentary and igneous rocks. Table 5-1 is a summary of the results of the manipulation of chemical data from the six localities investigated (presented in Chapter 4). Interpretation of rock types is based on fields outlined by other workers or by the results of plotting various common igneous and sedimentary rocks and outlining the fields produced.

TABLE 5-1 A summary of protolith interpretation based on the chemical data manipulation described in Chapter 4.

LOCATION	ROCK TYPE	INTERPRETATION BASED ON :						
		method of Garrels & Mackenzie (1971)	"silico-aluminate" diagram LaRoche(1974)	niggli k:mg	niggli al+alk:c	niggli ti:al+alk	log(Ni) : niggli mg	Co content & Co/Ni ratio
EAR FALLS AREA	qtz-fldspr-biot-(hbde) gneiss	greywacke	greywacke	greywacke or intermediate igneous	greywacke or intermediate igneous	greywacke or intermediate igneous	shale	shale-sandstone mixture
	ferruginous qtz-fldspr-biot-(garn) gneiss	siliceous sediment	iron formation	iron formation	iron formation or altered volc*	iron formation?	iron formation	same field as Geco iron formation
GECO MANITOUWADGE	Grey Gneiss Gp rocks south of orebody	intermediate to mafic igneous or shale	greywacke or intermediate igneous	greywacke or intermediate to mafic igneous	greywacke or intermediate to felsic igneous	greywacke or felsic to mafic igneous	greywacke or intermediate to mafic igneous	argillite or intermediate to mafic igneous
	qtz-fldspr-biot-sill gneisses of the Sericite Schist Gp	? altered felsic igneous	?	mostly pelitic	subcalcic pelite or altered felsic to intermediate igneous	?	low Ni greywacke or intermediate to mafic igneous	felsic igneous
	cord-anth rocks at the base of the 4/2 ore zone	siliceous sediment	iron formation or altered volc*	no distinction possible data too dispersed	iron formation or altered volc*	iron formation or altered volc*	low Ni greywacke or intermediate to mafic igneous	felsic igneous
	iron formation of the Grey Gneiss Gp (Milne,1969)	siliceous sediment	iron formation	iron formation	iron formation	iron formation	iron formation	?
YAKUSHAVITCH ISLAND, SHERRIDON AREA	qtz-fldspr-biot-(sill) gneisses	greywacke or argillite	greywacke or shale	greywacke-shale or intermediate igneous	greywacke-shale; mineralized gneiss in field of subcalcic pelites	greywacke or intermediate igneous	shale	sandstone-shale mixture
	qtz-fldspr-biot-anth-(sill)-(talc) gneiss/schist	greywacke or mafic igneous or siliceous sediment	? altered volc	greywacke-shale or intermediate igneous	iron formation or altered volc*	low Ti version of host gneiss	low Ni shale ?	?
MONTAUBAN	"leptites" of Stam-Seymour & MacLean (1977)	greywacke	greywacke or felsic igneous	data too dispersed	felsic igneous	felsic to intermediate igneous & greywacke	no data	no data
	qtz-fldspr-biot-sill gneisses	? altered greywacke or intermediate igneous	? same field as sill gneisses at Geco	? data displaced to the high mg & k field to the right of the pelite field	subcalcic shale or greywacke	low Ti greywacke or intermediate igneous	shale-carbonate	felsic igneous ?
	cord-anth rocks	? argillite or altered felsic igneous	iron formation or altered volc*	? same field as high k & mg sill gneisses	iron formation or altered volc*	greywacke & iron formation or altered volc*	shale-carbonate	felsic igneous ?
NEW CALUMET	hbde gneisses	carbonate &/or mafic igneous	mafic igneous	mafic igneous	mafic igneous	inconsistent with mafic igneous origin (Ti too low)	some mafic igneous & some shale-carbonate	mafic igneous
	qtz-fldspr-biot-(sill) gneisses	regular & altered intermediate to felsic igneous or argillite	some shales; sill gneisses occupy same field as sill gneisses at Geco	high mg pelites	greywackes & sill gneisses in subcalcic shale-greywacke field	greywacke or intermediate igneous	most are shale-carbonate	felsic to intermediate igneous ?
NORTH MAYSVILLE	qtz-fldspr-biot-(garn)-(sill) gneisses	mainly felsic igneous	? same field as sill gneisses at Geco	some pelites, & some greywacke or altered intermediate igneous	subcalcic pelite or altered igneous rock	? same field as sill gneisses at Geco	insufficient data	insufficient data
	fibrous amph. bearing gneiss (Knight,1981)	siliceous sediment or argillite	iron formations or altered volc*	data too dispersed	iron formation or altered volc*	? same field as sill gneisses at Geco	insufficient data	insufficient data

* as per rocks in the cores of alteration pipes of volcanogenic massive sulfide deposits of the Noranda Camp

5.2 Some Geochemical Characteristics of Sillimanite - Bearing Host Rocks Revealed in Chemical Data Manipulation

Potassium - enriched, calcium and sodium - depleted sillimanite gneisses and/or schists of amphibolite facies metamorphism are common to all of the five localities considered.

On the Garrels and MacKenzie (1971) diagram (Sec. 4.2) sillimanite - bearing gneisses generally produce an anomalous field demonstrating enrichment of K_2O over Na_2O and CaO. Hydrothermally altered felsic and intermediate igneous rocks at Steamboat Springs, Nevada (Fig. 4-15) and Roosevelt Hot Springs, Utah (Fig. 4-16) plot within the same general potassic field. Similar but less dramatic potash enrichment is observed on the outer margins of some volcanogenic massive sulfide alteration pipes (Fig. 4-17).

Sodium depletion in the sillimanite gneisses is also demostrated in the La Roche (1974) "silicoaluminate" diagram (Sec. 4.3). Similarity to hydrothermally altered felsic and intermediate igneous rocks at Steamboat Springs, Nevada (Fig. 4-28) and Roosevelt Hot Springs (Fig. 4-29) is again observed, as well as similarity to the less intensely modified rocks from the alteration zones of some volcanogenic massive sulfide deposits (Millenbach Mine, Noranda, Quebec and Mattagami Lake Mine, Quebec) (Figs. 4-30 and 4-31).

Calcium depletion of the sillimanite gneisses and schists is well illustrated by the Niggli al + alk : c method (Sec. 4.6). Sillimanite - bearing rocks plot as subcalcic pelitic or greywacke sediments, or subcalcic felsic to intermediate volcanic rocks. Calcium depletion of

the hydrothermally altered rocks at Steamboat Springs, Nevada or Roosevelt Hot Springs, Utah (Figs. 4-68, 4-69 and 4-70), and occasional calcium enrichment may be observed. In analogy with the sillimanite - bearing rocks, the outer margins of the alteration zones of some volcanogenic massive sulfide deposits (i.e. Millenbach Mine, Noranda, Quebec and Mattagami Lake Mine, Quebec) generally show calcium depletion.

With the exceptions of Geco, Manitouwadge, Ontario and N. Maysville, Colorado (Knight, 1981) which demonstrate low and dispersed levels of nickel, the sillimanite gneisses are generally consistent with either a pelitic or greywacke sedimentary origin or an intermediate igneous origin (Van de Kamp, 1970; Rankama and Sahama, 1952). Cobalt : nickel ratios for sillimanite - bearing rocks, although often consistent with argillaceous or felsic igneous rocks, demonstrate considerable fluctuations and, in the case of Geco, may occur over relatively short distances (1-2 metres). Whether this is an original characteristic of these rocks or whether it is a syndepositional or postdepositional alteration effect is uncertain. The same effect, associated with mineralization, is observed in the diamond drill holes on Yakushavitch Island and it may be a reflection of cobalt's tendency to concentrate in hydrothermally precipitated pyrite (Rankama and Sahama, 1952).

Sillimanite - bearing rocks at Geco, Sherridon, N. Mayville and Montauban demonstrate anomalously low titanium contents (and hence low Niggli ti values). This is discussed in greater detail in section 5.4. Another feature of the felsic gneisses encountered is the antipathetic occurrence of plagioclase and sillimanite. Sillimanite - bearing rocks which are depleted in CaO and Na_2O contain little or no plagioclase. An

example of this behaviour involving felsic gneisses at North Maysville is demonstrated in Fig. 5-1. Petrographic analysis of felsic gneisses at the New Calumet deposit, Calumet Island, Quebec has indicated that when plagioclase does occur, it appears as fractured, altered laths in an unequigranular groundmass. Sillimanite - bearing gneisses, which are adjacent to the sillimanite - deficient ones, on the contrary, are often well recrystallized, clean, equigranular, lepidoblastic rocks with polygonal or granoblastic textures. Owing to the stability of plagioclase under the metamorphic conditions involved (Winkler, 1976) any plagioclase present is likely relict and an absence of plagioclase would indicate that it was probably not present prior to the metamorphism. Assuming a genetic relationship between the sillimanite - bearing and sillimanite - deficient felsic gneisses, the precursor to the sillimanite - bearing variety could be an altered version of the sillimanite - free variety. The sillimanite - free felsic gneisses at Geco, on Yakushavitch Island, at N. Maysville (Knight, 1981), Montauban (Stamatelopoulou - Seymour and MacLean, 1977) and New Calumet plot chemically as common felsic to intermediate volcanic rocks or greywacke sedimentary rocks. The sillimanite - bearing rocks at these localities may therefore be the metamorphic equivalent of altered and/or chemically modified versions of these felsic to intermediate volcanic or greywacke sedimentary rocks. Stanton (1979 and 1984) has discussed the derivation of sillimanite by the metamorphism of kaolin, gibbsite, and other hydrothermal clay minerals and in microprobe studies has successfully identified persisting "Al_2O_3 -SiO_2 " materials at Geco. It is still ambiguous, however, whether these hydrothermal clay - rich sediments were:

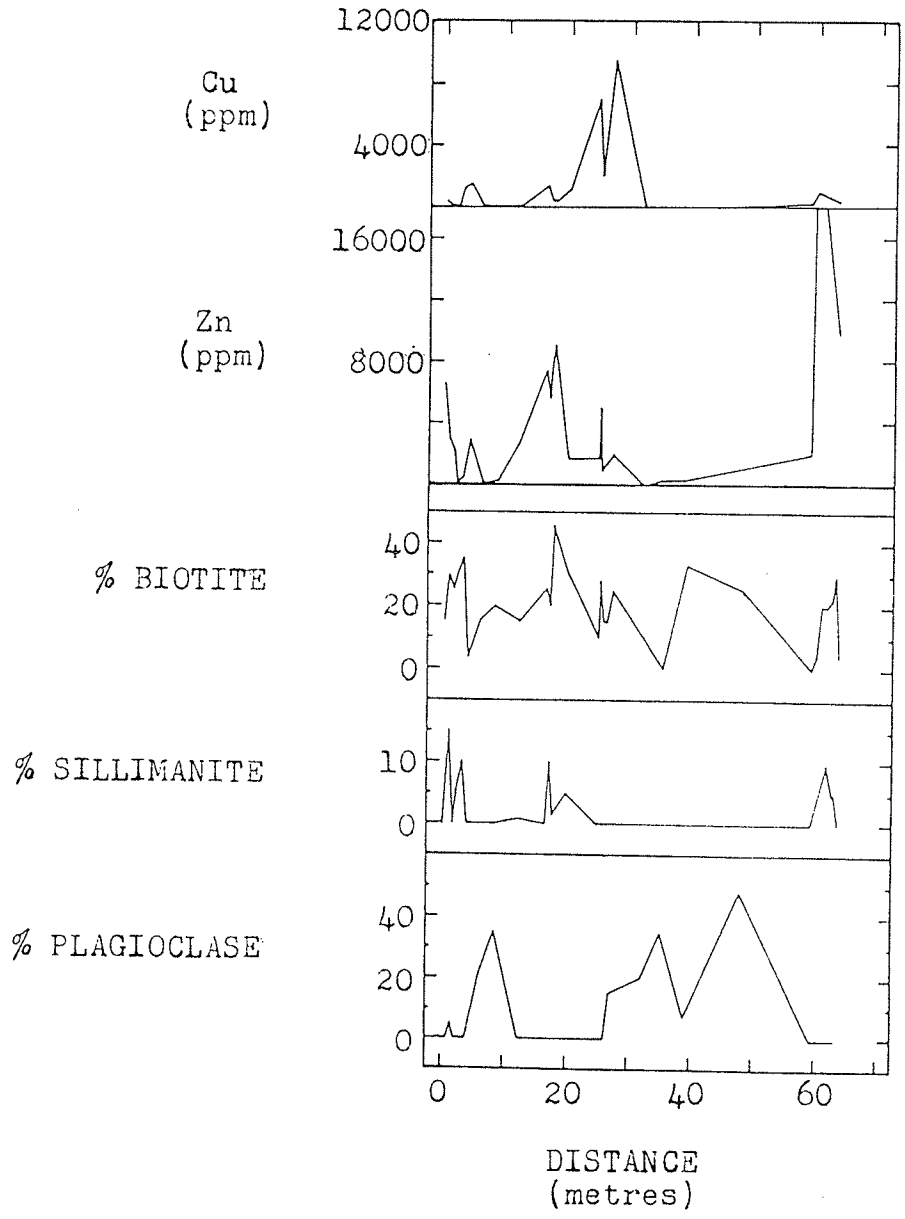

FIGURE 5-1 Interdependence of biotite, sillimanite, and plagioclase across the Sillimanite Gneiss Unit at N.Maysville, Colorado. Copper and zinc levels are also depicted. Distance = 0 corresponds to the west contact of the Sillimanite Gneiss Unit and distances are measured eastward (data from Knight,1981).

1) directly precipitated from a solution;

2) produced by hydrothermal alteration of a tuff prior, during or shortly after deposition (e.g. within a brine pool);

3) produced by hydrothermal alteration of a tuff or greywacke after deposition (by a mechanism similar to that involved in the formation of volcanogenic massive sulfide alteration pipes).

5.3 Some Geochemical Characteristics of the Cordierite - Anthophyllite Host Rocks Revealed in Chemical Data Manipulation

In addition to sillimanite - bearing rocks, cordierite - anthophyllite rocks are integral members of the stratigraphies at five out of the six localities under consideration.

The diagram of Garrels and MacKenzie (1971) indicates that some cordierite - anthophyllite rocks at Geco, Montauban, N. Maysville and on Yakushavitch Island plot in the siliceous sediment field occupied by iron formations (Fig. 4-3). This indicates enrichment of SiO_2 over Al_2O_3 which is not observed in altered rocks from the cores of the alteration pipes at the Millenbach Mine (Fig. 4-17) or the Mattagami Lake Mine (Fig. 4-17). Other cordierite - anthophyllite rocks from Geco, Montauban, N. Maysville and on Yakushavitch Island are dispersed within the same field occupied by enveloping sillimanite gneisses or within the pelitic field outlined by Garrels and MacKenzie (1971).

All cordierite - anthophyllite rocks plot near or at the MgO apex of the La Roche (1974) "silicoaluminate" diagram. This field is also

occupied by iron formations (Fig. 4-19) and the intensely altered rocks from the cores of the alteration pipes at the Millenbach and Mattagami Lake Mines (Figs. 4-30 and 4-31).

Apart from Yakushavitch Island, anthophyllite - bearing rocks do not possess Niggli mg values much greater than those of their enveloping sillimanite - bearing rocks. Niggli k values are also similar even though all alkalies and calcium contents of the anthophyllite - bearing rocks are considerably lower than those of the sillimanite - bearing rocks.

Due to greater MgO and iron oxide contents, cordierite - anthophyllite rocks display lower values of Niggli al + alk than their enveloping sillimanite - bearing rocks. They do, however, possess similar low values of Niggli c and therefore plot, on the Niggli al + alk : c diagram, in a field which hugs the al + alk axis. Although the rocks at the Millenbach Mine demostrate a reduction in Niggli c towards the more intensely altered core of the alteration pipe (Fig. 4-66), the Mattagami Lake Mine does not demonstrate such a marked reduction (Fig. 4-67). Roberts and Reardon (1978) have reported an increase in calcium oxide content towards the more intensely altered core of the Mattagami Lake Mine alteration zone. Knuckey et al. (1982) reported little change in the centre of the Millenbach alteration pipe. Due to the pronounced Mg-Fe metasomatism this increase in CaO content towards the core of the alteration pipe fails to produce an increase in Niggli c, and may even result in a slight decrease. At Geco, N. Maysville, Montauban, Sherridon and on Yakushavitch Island, CaO contents vary from levels observed in rocks from the core of the Mattagami Lake Mine alteration zone down to levels well below those present in common felsic igneous

rocks. On this basis, a genetic relationship between the origin of these cordierite - anthophyllite rocks and the rocks from the cores of volcanogenic massive sulfide alteration zones is still ambiguous.

Cordierite - anthophyllite rocks at Geco and some of the anthophyllite - bearing rocks on Yakushavitch Island display nickel depletions comparable to those observed in sillimanite - bearing rocks at Geco. Cobalt : nickel ratios are again often consistent with a felsic igneous origin but display drastic fluctuations at all of the locations (where cordierite - anthophyllite rocks were sampled). As speculated for the sillimanite - bearing rocks, this may reflect the presence of higher cobalt values in the hydrothermally precipitated pyrite (Rankama and Sahama, 1952).

Niggli ti values in the cordierite - anthophyllite rocks at all the locations display reduced values which are comparable to the ferruginous metasedimentary rocks of the "Ear Falls area" (Fig. 4-80) or to altered rocks from the cores of the alteration zones at the Millenbach and Mattagami Lake Mines (Fig. 4-88). This is discussed in greater detail in section 5.4.

A relationship appears to exist between the sillimanite - bearing and cordierite - anthophyllite - bearing rocks, due to the gradual nature of the contact at Geco, N. Maysville (Knight, 1981) and on Yakushavitch Island. There is also a graduation observed between the respective fields of the two rocks in many of the chemical plots. Whether this relationship is a syndepositional effect of mixing of the two respective progenitors or an effect of subsequent alteration similar to that observed in the cores of volcanogenic massive sulfide alteration pipes is still enigmatic.

5.4 Niggli ti Values and a Comparison of Gneiss - Hosted and Greenstone - Hosted Massive Sulfide Deposits

Both the sillimanite gneisses and cordierite - anthophyllite gneisses at Geco (Fig. 4-81), Yakushavitch Island (Fig. 4-82), Sherridon (Fig. 4-83), North Maysville (Fig. 4-84), New Calumet (Fig. 4-86) and Montauban (Fig. 4-87) possess Niggli ti values and $\%TiO_2$ levels (Appendix A) below those of the most felsic igneous rocks. If these low titanium levels reflect the original precursor levels and titanium is assumed to indeed be immobile (Finlow - Bates and Stumpfl, 1981; Roberts and Reardon, 1978), it is obvious that some dilution of original titanium with a low or zero titanium component has occurred. This component may have been added in one of two ways:

1) co - deposition of a possibly altered felsic volcaniclastic or greywacke sedimentary rock and a chemical precipitate (a ferruginous chert or iron montmorillonite clay);
2) post - depositional hydrothermal alteration (i.e. Mg/Fe metasomatism) paralleling the formation of volcanogenic massive sulfide alteration pipes.

If one attempts to apply the volcanogenic massive sulfide alteration model (#2) to gneiss - hosted massive sulfide deposits, difficulties are encountered. One can not, using the al + alk : ti

method, adequately draw a parallel between the potassic sillimanite - bearing rocks of the gneiss - hosted deposits and the potassium enriched rocks from the outer margins of the alteration zones at the Millenbach and Mattagami Lake volcanogenic massive sulfide deposits (Fig. 4-88). Reduction in Niggli ti does not become pronounced until the cores of the alteration zones are reached, whereas marked Niggli ti reduction is observed in most sillimanite - bearing gneisses of the five localities considered. The prograde hydrothermal alteration of rocks at the Millenbach and Mattagami Lake Mines, therefore, produces a pattern or pathway which is concave down towards the origin on the al + alk : ti diagram (Fig. 4-88). The gradational patterns produced between sillimanite - bearing rocks and cordierite - anthophyllite - bearing rocks at Geco, Montauban, N. Maysville and on Yakushavitch Island, however, are concave up or linear towards the origin and more closely resemble the pattern which is produced by ferruginous chemical metasedimentary and hosting greywacke metasedimentary gneisses in the "Ear Falls area".

Large (1977) has proposed a chemical mechanism involving Mg-Fe metasomatism of K-feldspar to produce chlorite under the conditions existing in the center of a volcanogenic massive sulfide alteration pipe:

$$KAlSi_3O_8 + 3Fe^{2+} + 14H_2O \rightleftharpoons Mg_2Fe_3Al_2Si_3O_8(OH)_8 + 2K^+ + 3H_4SiO_4 + 8H^+$$

Upon balancing components added and components removed, this reaction is found to produce a net weight loss of 2.45 grams per 29.57 grams of K-feldspar converted. This small weight change would have practically no effect on $\%TiO_2$, but since Mg and Fe are added, Niggli ti and the molecular ratio of Ti : (Mg + Fe + Mn + Ti), is reduced. This indeed is what is observed at the Millenbach and Mattagami Lake Mines. In the gneiss - hosted orebodies (e.g. Geco), however, some cordierite - anthophyllite rocks contain less than 0.15% TiO_2 and often less than 0.10% (as opposed to 0.25% for the most intensely altered rocks at the Millenbach Mine, see Appendix B). As was revealed in Chapter 4, TiO_2 contents of 0.10% could be produced only by a dilution of at least 1:1 with a non-titaniferous component. This poses a volumetric problem if one is to assume the volcanogenic massive sulfide alteration model.

5.5 A Chemical Modelling Experiment Based on Intermixing of Clastic and Chemical Sedimentary Material

One can artificially produce a hybrid mixture of chemical and volcaniclastic sediments and analyze the effects produced on the chemical plots utilized earlier (Chapter 4). Table 5-2 is a breakdown of the types of starting materials and types and amounts of chemical components added to produce the different hybrids. Data points E1 and E2 demonstrate the effects of addition of non - titaniferous hydrothermal illite plus silica to a normal granitic (or rhyolitic) rock. Both data points also represent some leaching of soda and CaO.

TABLE 5-2 A chemical modelling experiment involving the hypothetical alteration of a "normal" granite (LT-102) and a "normal" basalt (LT-100).

SAMPLE NUMBER	INITIAL COMPONENTS	RESULTANT CHEMICAL COMPOSITION								
		SiO_2	Al_2O_3	FeO	MgO	CaO	Na_2O	K_2O	TiO_2	P_2O_5
LT-102		73.86	13.75	1.79	0.3	0.7	3.51	5.13	0.20	0.14
LT-100		49.9	16.0	11.45	6.3	9.1	3.2	1.6	1.4	0.5
E1	100g of LT-102 + 10g SiO_2 + 20g Kaolinite * - 1.5g Na_2O - 0.2g CaO	74.16	17.2	1.44	0.2	0.4	1.59	4.09	0.16	0.11
E2	100g of LT-102 + 10g SiO_2 + 25g illite * - 1.5g Na_2O - 0.2g CaO	67.06	13.72	5.50	6.0	0.4	1.45	4.42	0.15	0.10
E3	100g of LT-102 - 0.3g Fe_2O_3 - 0.8g FeO - 0.1g MgO - 0.6g CaO - 3.0g Na_2O	77.6	14.3	0.81	0.2	0.1	0.54	5.39	0.21	0.15
E4	100g of LT-102 -0.5g Al_2O_3 + 10g FeO +15g MgO -0.5g CaO - 3.0g Na_2O -4,5g K_2O	58.16	10.4	9.45	12.0	0.2	0.4	0.5	0.16	0.11
E5	100g of LT-100 + 15g SiO_2 -0.5g Al_2O_3 + 10g FeO + 10g MgO - 8.5g CaO - 2.8g Na_2O - 1.0g K_2O	53.2	12.9	17.8	13.6	0.5	0.3	0.5	1.16	0.4

* chemical composition of kaolinite as per AGI glossary (1977) : $Al_2Si_2O_5(OH)_4$

* chemical composition of illite as per AGI glossary (1977) : $(H_3O,K)_y\ (Al_4Fe_4Mg_4Mg_6)\ Si_{8-y}Al_yO_{20}(OH)_4$

The resultant hybrids are found to plot similarly to the sillimanite gneisses of gneiss - hosted massive sulfide ore bodies (Figs. 5-2, 5-3, 5-4 and 5-5). Similarly, addition of iron and magnesium hydroxides or hydrothermally precipitated chlorite to the same starting material (data points E3, E4 and E5) produces a resultant hybrid chemically similar to the anthophyllite - bearing rocks of gneissic massive sulfide deposits. Deposition of magnesium carbonate and magnesium hydroxide - containing chemical sediments was more prevalent in the Archean than today (Garrels and MacKenzie, 1971) and so the concept of $Mg(OH)_2$ deposition during the formation of gneiss - hosted massive sulfide deposits is a distinct possibility.

Dilution of titanium may also be brought about by co-deposition of chemically precipitated products (SiO_2 , Fe_2O_3 , $Al(OH)_3$, etc.) and epiclastic material derived by eruption of hydrothermally - altered material from a hydrothermal vent. This mechanism has been suggested for the formation of rocks from the core of volcanogenic massive sulfide alteration pipes.

5.6 Strata - Bound Massive Sulfide Deposits in Gneissic Terrains and their Relationship with those of Greenstone Terrains

In keeping with Hutchinson (1973) who has subdivided volcanogenic massive sulfide deposits on the basis of ore metal composition, one may similarly subdivide massive sulfide deposits in gneissic terrains as follows:

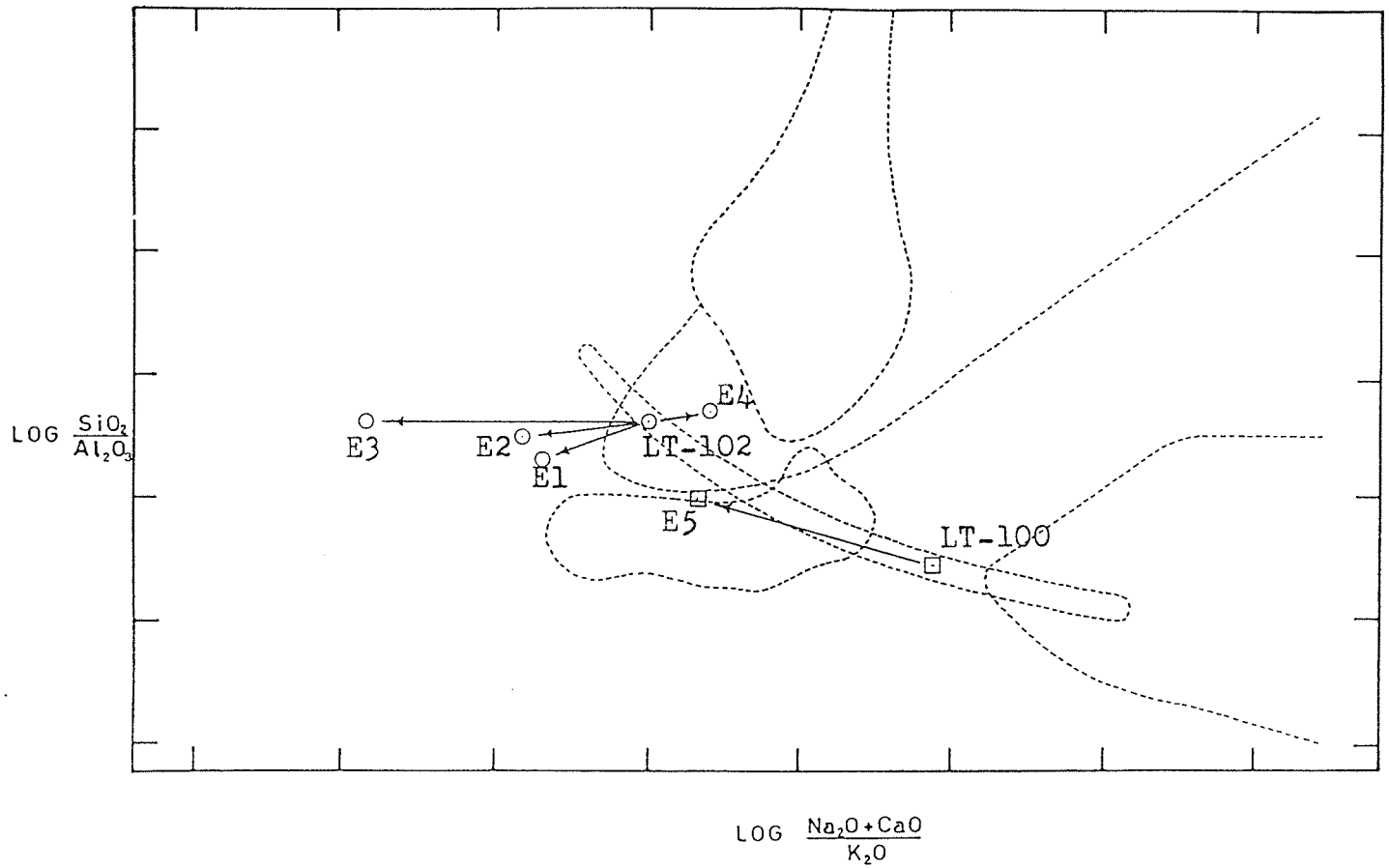

FIGURE 5-2 Garrels and MacKenzie (1971) diagram for hybrid rocks artificially produced in Table 5-2. E1, E2, and E3 resemble the sillimanite gneisses of gneiss-hosted massive sulfide deposits, whereas E4 most closely resembles the cordierite-anthophyllite rocks.

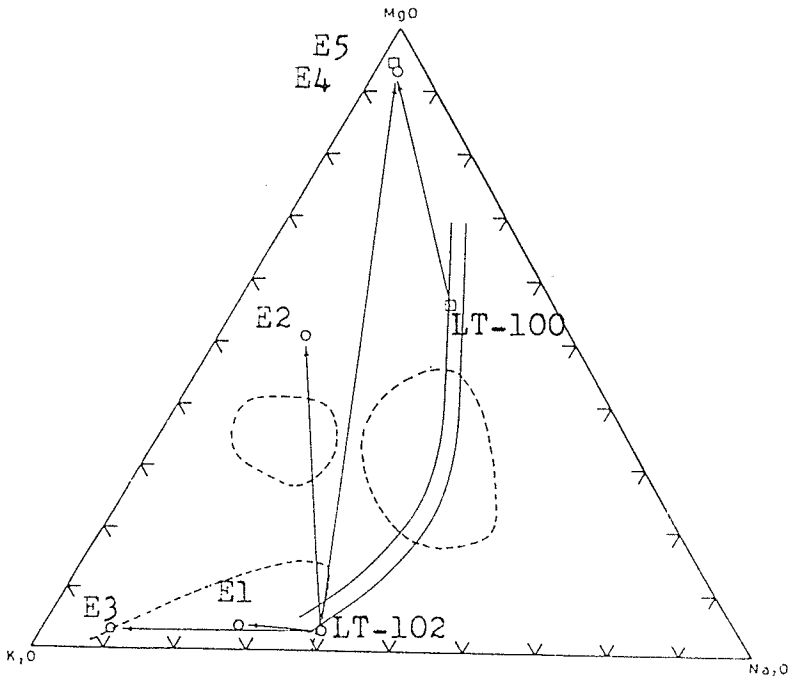

FIGURE 5-3 Siliccaluminate diagram (La Roche,1974) for hybrid rocks artificially produced in Table 5-2. E2 most closely resembles the sillimanite gneisses of gneiss-hosted massive sulfide deposits, whereas E4 and E5 resemble the cordierite-anthophyllite rocks.

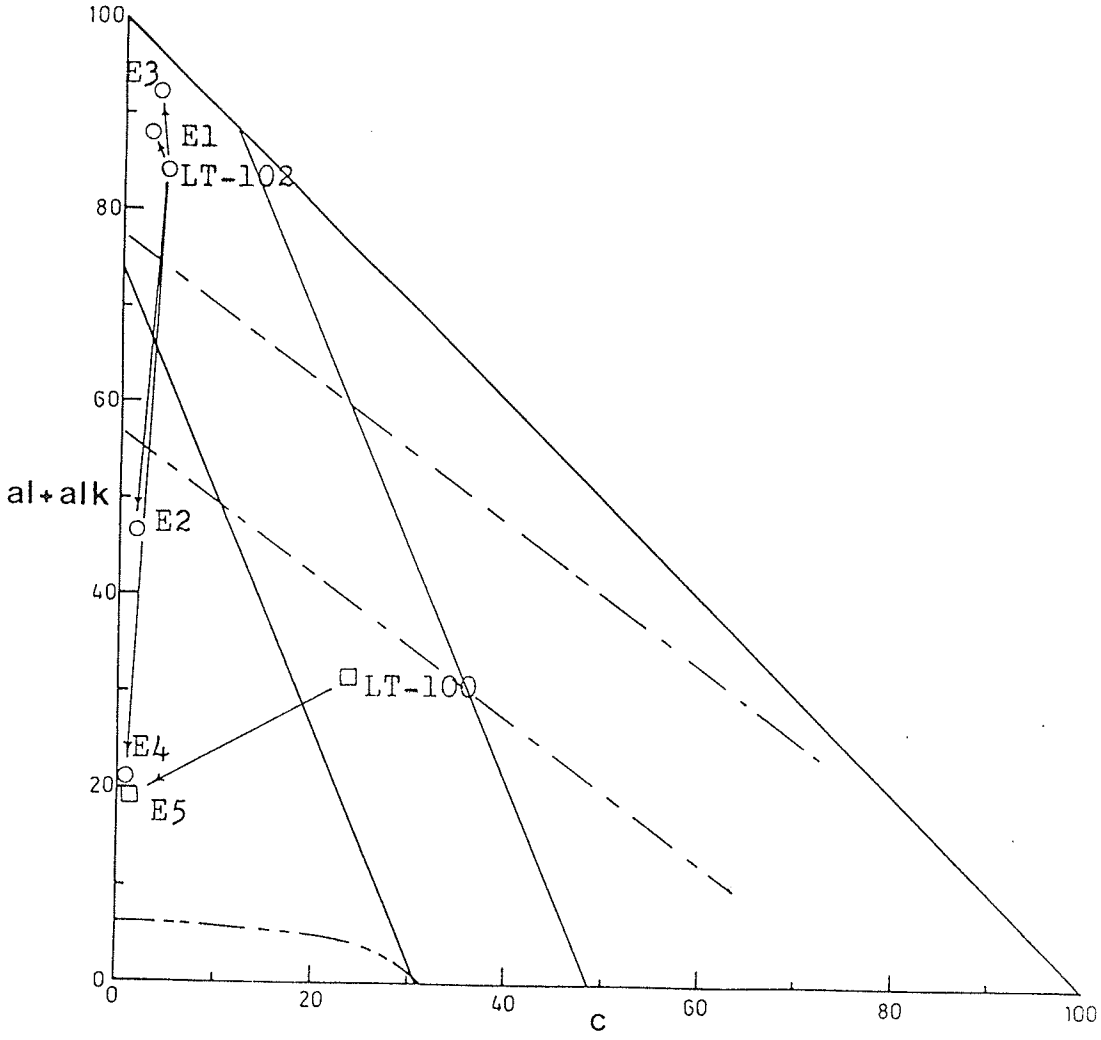

FIGURE 5-4 Niggli al+alk:c diagram for hybrid rocks artificially produced in Table 5-2. E2 most closely resembles the sillimanite gneisses of gneiss-hosted massive sulfide deposits, whereas E4 and E5 resemble the cordierite-anthophyllite rocks.

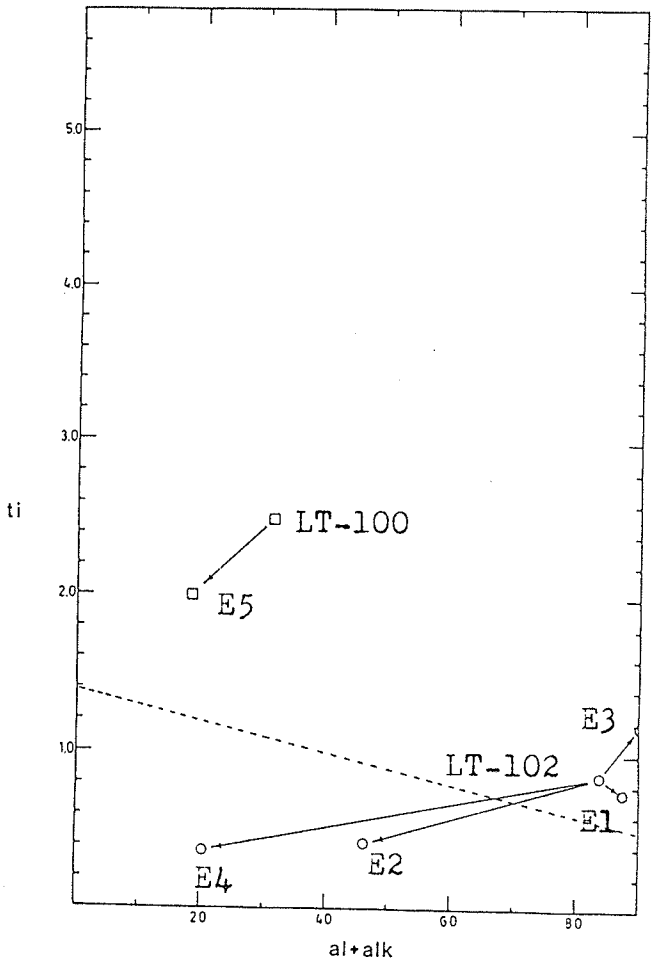

FIGURE 5-5 Niggli ti:al+alk diagram for hybrid rocks artificially produced in Table 5-2. E2 most closely resembles the sillimanite gneisses of gneiss-hosted massive sulfide deposits, whereas E4 resembles the cordierite-anthophyllite rocks.

1) Fe-Cu (Au) type;

2) Fe-Cu-Zn-(Pb) (Au, Ag) type;

3) Fe-Pb-Zn-(Cu) (Ag) type;

(where metals in brackets denote minor components). The evidence suggests that the complexity of ore metal composition is related to the degree of crustal evolution (Mitchell and Bell, 1973). Fig. 5-6 shows the general breakdown of massive sulfide deposits according to geotectonic regime. Table 5-3 indicates the possible types of strata - bound massive sulfide mineralization that may occur during development of an island arc, while Table 5-4 and Table 5-4b lists some of the characteristics of each type of mineralization depicted in Table 5-3. Maynard (1983) utilized a similar scheme for the genetic subdivision of volcano-sedimentary ores.

Although they bear some resemblance to volcanogenic massive sulfide deposits of greenstone terrains, the deposits investigated in this study also bear some resemblance to the large metasedimentary - hosted Pb-Zn deposits such as Broken Hill, N.S.W., Sullivan, B.C. and Bathurst, N.B. The continuity of their ore lenses, their general stratigraphy and metamorphic grade, for example, are similar to deposits such as Broken Hill. They, however, do not possess the size, or the characteristic manganese halo of the Broken Hill deposit, Gamsberg deposit, metaliferous sediments of the Red Sea deeps, or other similar sediment - hosted massive sulfide deposits (Stumpfl, 1979). They also do not possess the multitudinous tabular ore bodies characteristic of Broken Hill, being single lens orebodies like most volcanogenic massive sulfide deposits. Although lead is fairly abundant at the New Calumet and Montauban deposits, the gneissic deposits generally possess metal

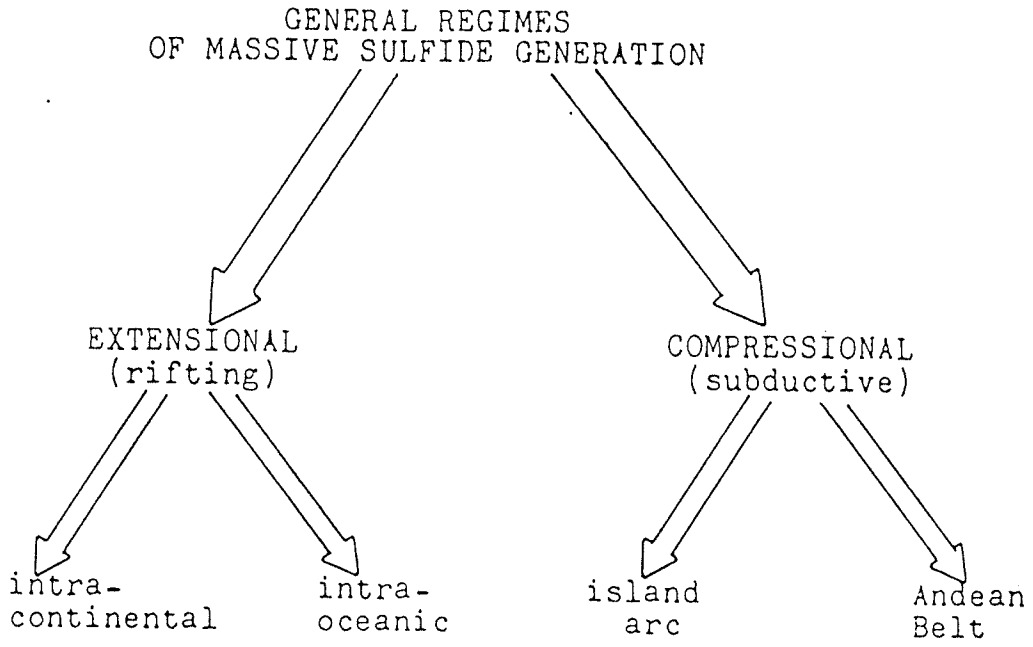

FIGURE 5-6 Geotectonic regimes of massive sulfide generation; summarized from Sawkins (1984), Mitchell and Garson (1981).

TABLE 5-3 ISLAND ARC DEVELOPMENT AND ASSOCIATED STRATIFORM BASE METAL MINERALIZATION; MODIFIED AFTER MITCHELL AND BELL 1973.

	STAGE	MINERALIZATION
I.	Pre-arc generation of oceanic crust and upper mantle (continuous generation of igneous rocks along axial ridge followed by lateral movement and burial). (Note: This process begins at a divergent plate boundary)	CYPRUS TYPE (Fe,Cu)
II.	Submarine island arc tholeites begin to be generated by submarine volcanism in the initial stages of arc development.	None known but some stratiform sulfide deposits occur in ocean crust tholeites
III.	Interbedded shallow marine sediments, subaerial flows and tuffs accumulate rapidly. Isostatic re-equilibration leads to rapid erosion, the development of lahars and turbidites. Deep burial of sediments leads to high temperature regional metamorphism. Volcanism is still chiefly mafic.	BESSHI TYPE (Fe,Cu(Zn))
IV.	Plutonic activity, waning volcanism, and arc rifting.	No statiform or stratabound sulfides
V.	Arc reversal and the development of a new volcanic arc. Attempted subduction of a continental island arc or oceanic island crust leads to arc reversal. The old trench fills with sediments and rises isostatically leading to the development of flysh type associations.	VOLCANIC EXHALATIVE (Fe,Cu,Zn(PB)) (associated with phreatic eruptions accompanying dome emplacement KUROKO TYPE (Fe,Cu,Zn,Fb, barite)
VI.	Collision of arcs. Arc reversal and less marginal basin crust along a younger Benioff zone may result in the approach of remnant and active arcs and their eventual collision.	CYPRUS TYPE (these may occur in obducted slices of ocean floor basalts or melanges)
VII.	Repeated arc rifting, marginal basin spreading and arc reversals lead to successive magmatic arcs, flysch belts and paired metamorphic belts.	Leads to the repetition of the volcanic exhalative, Kuroko and Cyprus types.

TABLE 5-4 General features of the main types of massive sulfide deposits recognized in the literature; summarized from Franklin et al. (1981); Mitchell and Bell (1973); Mitchell and Garson (1981); Sawkins (1984).

TYPE	LITHOLOGY	TECTONIC SETTING	SHAPE OF OREBODY	TYPICAL SIZE TONNES	ORE MINERALS	ALTERATION
Fe, Cu CYPRUS TYPE	The Cyprus orebodies are hosted by pillowed basalts which surround a central core of ultramafic and mafic intrusive rocks. The thick volcanic sequence is overlain by a postvolcanic sequence of maganiferous shales, bentonite, cherts and pyritic sediments.	divergent plate boundaries	irregular lenticular pod-like extended in one dimension. Often convex with protuberances	20M	pyr, ccp with minor sph and only traces of gal	lavas are saussuritized. chloritization clay minerals silicification pyritization
Fe,Cu(Zn) BESSHI TYPE	The besshi deposits of the Sambagawa metamorphic belt of Japan occur within a sequence of andesitic and basaltic volcanic rocks with appreciable carbonaceous mudstone, clastic limestone, quartz-rich sediments or clastic rocks showing evidence of deep water accumulation. Quantities of volcanics and sediments are roughly equal.	convergent plate boundaries (initial stages of island arc development)	lenticular or bedlike elongate	total production of all deposits to 1970 was 28M	pyr, ccp sph	chloritization tourmalinization epidotization silicification carbonatization
Fe,Cu,Zn(Pb) VOLCANIC EXHALATIVE TYPE	Millenbach Mine of the Noranda area. Massive sulfides occur in the thickened centres of felsic to intermediate volcanic piles in the Archean Abitibi Greenstone Belt of the Superior structural province of the Canadian Shield. Rocks are typically submarine tholeitic to calc-alkaline volcanics. Massive sulfides are associated with the phreatic eruptions of felsic dome emplacement. Sulfides are typically underlain by a pipe-like alteration zone with stringer sulfides. At least part of the deposit is of syngenetic sedimentary origin.	convergent plate boundaries (somewhat more advanced stages of island arc development)	lenticular or mushroom shaped	1 M to 50 M	ccp, sph, pyr, po and minor gal	leaching of alkalies, Mg-Fe metasomatism sericitization chloritization
Fe,Cu,Zn,Pb, barite KUROKO TYPE	The Kuroko deposits are associated dominantly with clastic dacitic or more rarely andesitic volcanic rocks of a shallow marine environment plus associated sedimentary rocks. Volcanic rocks are dominant, however. The orebodies are typically located above a persistent unit of felsic fragmental rock. Orebodies usually occur in clusters. Alteration pipes with stringer sulfides may occur	convergent plate boundaries (more advanced stages of island arc development)	stratiform lenticular	median size is 1.3 M but may exceed 10 M	pyr, ccp, sph, gal, tetrahedrite, barite, gypsum anhydrite	silicification chloritization clay minerals feldspathization zeolites carbonatization

TABLE 5-4b Examples of Published Genetic Interpretations of Some Selected Massive Sulfide Orebodies

TYPE	LOCALITY	REFERENCE
Fe, Cu CYPRUS TYPE	Ophiolite deposits in the Red Sea Region	Mitchell & Garson (1981)
	Betts Cove, Newfoundland, Canada	Maynard (1983)
Fe, Cu, (Zn) BESSHI TYPE	Hixbar and Bagacay deposits of the Phillipines	Mitchell & Bell (1973)
	Bathurst Newcastle area of New Brunswick, Canada	Mitchell & Bell (1973)
	Captains Flat, New South Wales, Australia	Mitchell & Bell (1973)
	Stekenjokk and Menstrask, Sweden	Mitchell & Bell (1973)
	The Wim and Osborne deposits of Manitoba, Canada	Gale et al. (1980)
Fe, Cu, Zn, (Pb) VOLCANIC EXHALATIVE TYPE	The Flin Flon and Fox deposits of Manitoba, Canada	Gale et al. (1980)
	The Ruttan, Chisel, Anderson, Stall, and Rod deposits of Manitoba, Canada	Gale et al. (1980)
	The Coronation deposit of Saskatchewan, Canada	Gale et al. (1980)
	Geco, Manitouwadge, Canada	Gale et al. (1980)
	deposits of the Noranda Camp, Canada	Sangster (1972)
	Crandon, Wisconsin, U.S.A.	Franklin et al. (1981)
	Jerome, Arizona, U.S.A.	Franklin et al. (1981)
	Pyhasalmi-Pielavesi, Finland	Franklin et al. (1981)
Fe,Cu,Zn, Pb, barite KUROKO TYPE	Buchans, Newfoundland, Canada	Maynard (1983)
	some of the Bathurst deposits of New Brunswick, Canada	Maynard (1983)
	The Horne and Delbridge deposits of the Noranda Camp, Canada	Mitchell & Bell (1973)

zonations which would place them under the category of the "Type 1" massive sulfides discussed by Hutchinson (1973), i.e.:

pyritic tuffite (exhalite)

py-sp

py-sp-ccp

po-py-ccp-sp

po-ccp+mgt+py

Although their metal zonation resembles that of typical volcanic - hosted deposits, these orebodies are characteristically thinner and much more extensive. Sherridon, for example, consists of two tabular orebodies, each less than 5 metres thick, with a combined strike length of approximately 5 km (Goetz, 1980).

High temperature, sulfur-rich brines of volcanogenic and Kuroko type orebodies readily precipitated sulfides at the seawater interface often producing orebodies on the flanks of a volcanic pile (Hodgson and Lydon, 1977). Henley and Thornley (1979) have stated that the high power and rate of hydrothermal discharge in the case of Kuroko or Archean polymetallic deposits may have been sufficient to fluidize ore particles and lead to transport and sedimentation at a more distal environment. The chemical evidence developed in Chapter 4 would appear to indicate that the host rock associations at the localities considered are volcanosedimentary to sedimentary in origin (i.e. mainly felsic to intermediate tuffaceous volcanics and greywacke sediments with minor volcanic flow-rocks). Host rocks could therefore be classified in the volcano-sedimentary category proposed by Gale et al. (1980).

Since metallic zonation, alteration and size (in terms of tonnes of ore) of the gneissic orebodies considered are similar to those of volcanogenic massive sulfide deposits and provided one accepts the proposal that greenstone and gneissic terrains developed contemporaneously (Bailes and McRitchie, 1978; Ayres, 1978; Goodwin et al., 1972; McKasey et al., 1974; Gale et al., 1980), a genetic relationship between volcanogenic massive sulfides of greenstone terrains and gneissic massive sulfides such as portrayed in Fig. 5-7 may exist. A similar relationship has been proposed by MacGeehan (1978) for the Garon Lake Mine at Mattagami, Quebec. In the model proposed in Fig. 5-7 turbidite flows (initiated by dense ore - bearing brines or by submarine ash flows) may carry:

1) ore - bearing solutions or suspended ore particles;
2) altered volcaniclastic material (which may be partly derived by expulsion of hydrothermally altered material from the hydrothermal edifice); and
3) terrigenous epiclastic material (derived from sources other than the volcanic pile)

variable distances away from the volcanic centre. Such flows would produce continuous units of even-thickness which would be associated with mineralization (Sangster, 1972). Ore deposition may take place in the near transitional regime of Gale et al. (1980), where volcanic rocks may still be fairly prominent (e.g. Geco), or further transport of materials to the more distal transitional regime or to the sedimentary regime would lead to the formation of orebodies such as Sherridon (Gale et al., 1980). A broad spectrum of deposits may exist (from the strictly volcanic - hosted varieties to the mainly sediment - hosted

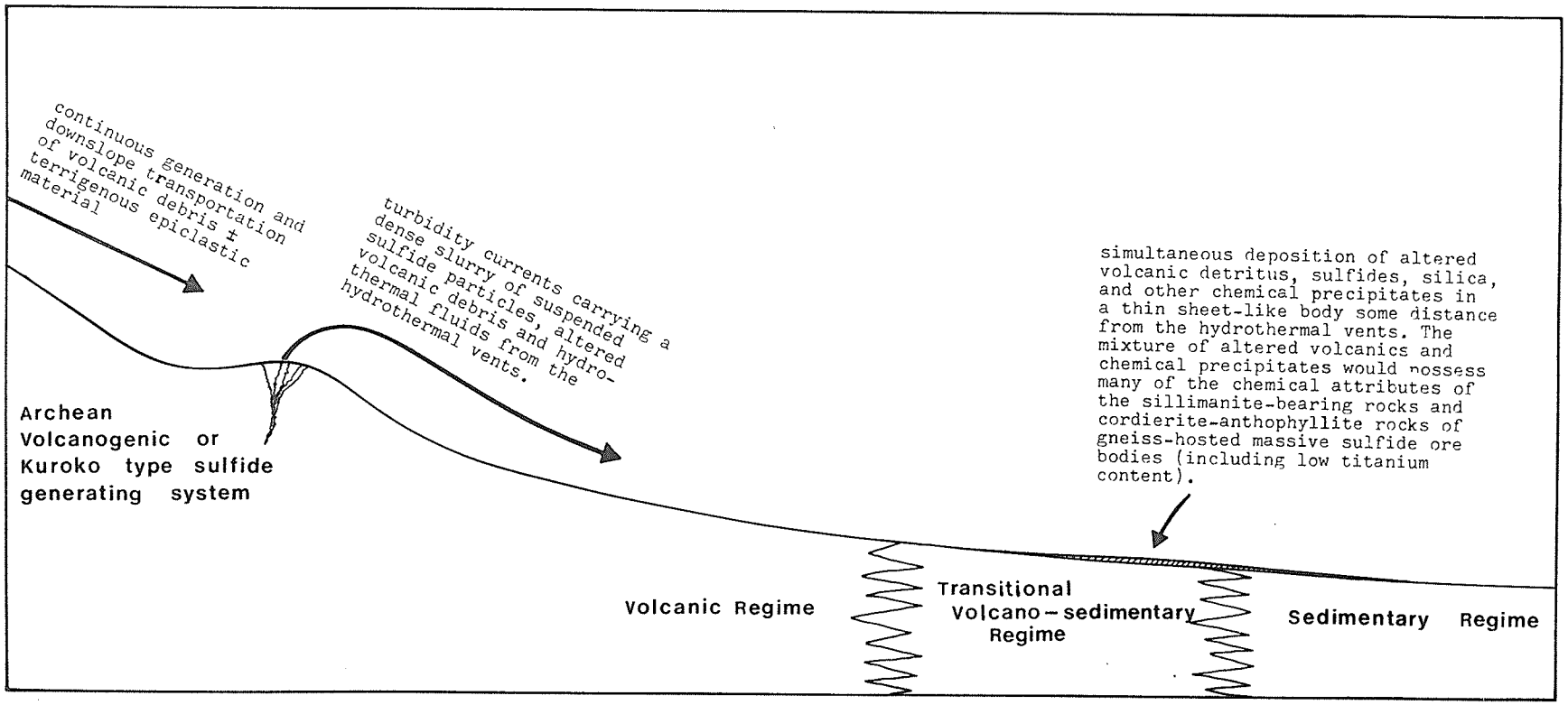

FIGURE 5-7 Schematic model for the generation and deposition of sulfide ores and host rocks which would possess the attributes of gneiss-hosted massive sulfide deposits. Based on the ideas of Beakhouse (1985), Gale et al. (1980), Bailes and McRitchie (1978), Goodwin et al. (1972), and MacKasey et al. (1974); it is suggested that following metamorphism, rocks of the Volcanic Regime would develope into greenstone terrain, rocks of the Sedimentary Regime would develope into gneissic terrain and those of the Transitional Regime would develope into a terrain transitional between gneissic and greenstone terrains.

varieties), influenced by the distance of transport away from the source of volcanics and hydrothermal vents.

5.7 Application of Geochemical Discrimination Techniques to Exploration for Massive Sulfide Deposits in High - Grade Metamorphic Terrains

High - grade metamorphic areas (e.g. Fig. 5-8) in which quartz - feldspar - biotite - sillimanite gneisses and schists, cordierite - anthophyllite rocks, calc - silicate gneisses, quartzites and amphibolites occur, bulk chemical discrimination techniques could be used to predict the favourability of these rocks to host massive sulfide ores. This would entail an investigation of the sillimanite - bearing rocks for K_2O enrichment and CaO-Na_2O depletion. K_2O enrichment and Na_2O depletion is best portrayed by La Roche's (1974) silicoaluminate diagram (section 4.2) while CaO depletion is demonstrated by the Niggli al + alk : c diagram (section 4.6). On both of these diagrams sillimanite - bearing and cordierite - anthophyllite rocks occupy fields, outlined in sections 4.2 and 4.6, which are gradational one into the other.

Anomalously low TiO_2 concentrations and Niggli ti values should by an inherent property of both the sillimanite - bearing and cordierite - anthophyllite rocks (section 4.8).

Another property of some predictive value, but requiring support by the other techniques, is nickel content and Co/Ni ratios. Sillimanite - bearing rocks containg highly variable nickel contents with values of

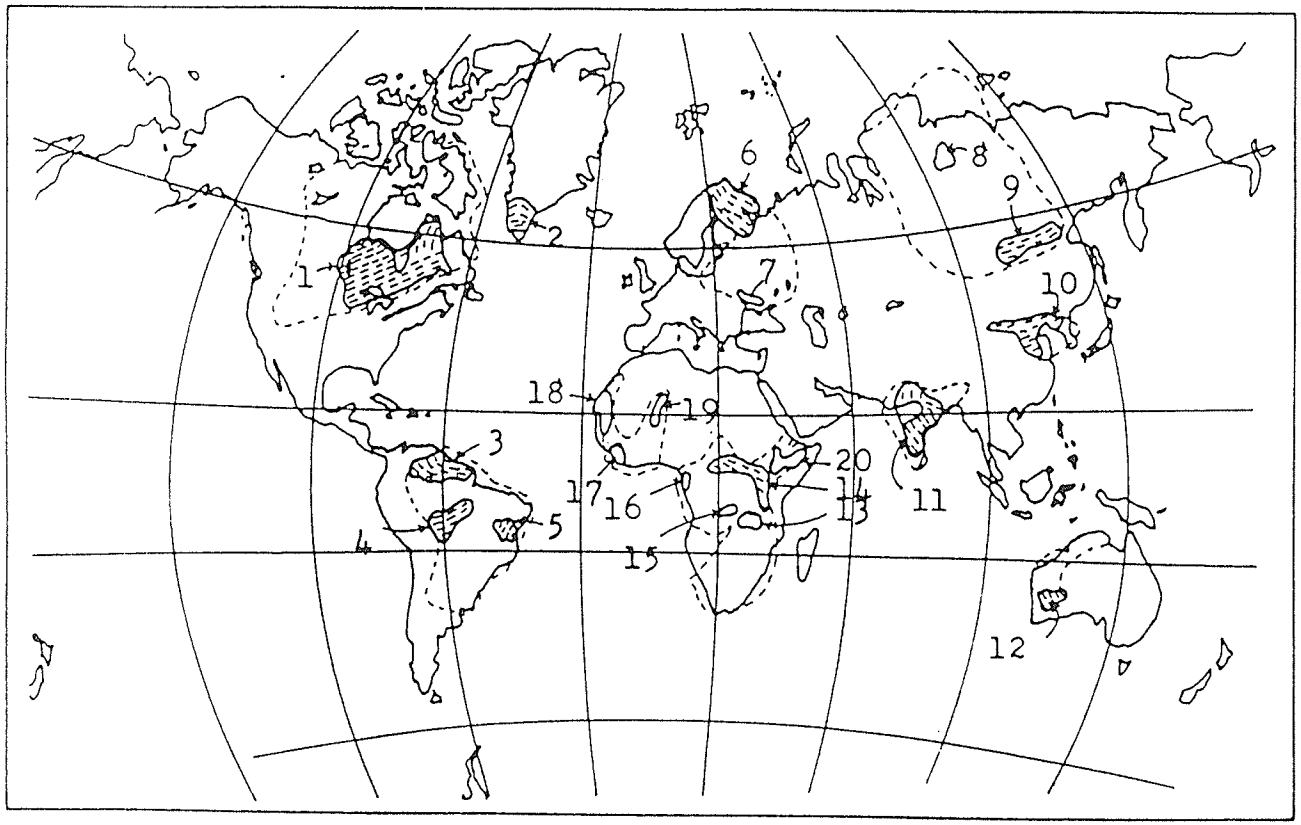

FIGURE 5-8 Location of selected Archean structural provinces of the world which contain high metamorphic grade gneisses
Key to major provinces; 1= Superior, 2=Southern Greenland 3= Guiana, 4= Guapore, 5= Sao Francisco, 6= Kola, 7= Ukranian, 8= Anabar, 9= Aldan, 10= Chinese, 11= Indian, 12= Yilgarn, 13= Zambian, 14= Central African, 15= Kasai, 16= Cameroons, 17= Liberian, 18= Mauritanian, 19= Ouzzalian, 20= Ethiopian Modified after Kroner (1981)

log {Ni} often < 1.0. Similarly Co/Ni ratios in sillimanite - bearing and cordierite - anthophyllite rocks display drastic fluctuations with values extending up to in excess of 3.0. The occasional low values of log {Ni} < 1.0 should aid in filtering out sillimanite - bearing rocks of "normal" pelitic origin, which, according to Rankama and Sahama (1952), should be carrying nickel contents >= 100 ppm (i.e. log {Ni} > 2.0).

Although not investigated in this study, the immobility of zirconium (Finlow-Bates and Stumpfl, 1981) may prove to be of use equal to titanium in characterization of sillimanite - bearing and cordierite - anthophyllite rocks favourable to hosting ore.

REFERENCES CITED

Agron, N. and Bentor, Y.K., 1981. The volcanic massif of Biq at Hayareah (Sinai-Negev): a case of potassium metasomatism; Jour. of Geol., v. 89, pp 479-495

Alexandrov, E.A., 1973. Iron formations of the USSR; Econ. Geol., v. 68, pp 1035-1062

Althaus, E., 1968. Ders Einfluss des Wossers auf Metamorph Mineralreaktionen; Neues Jaharb. Mineral Monatsh #9, pp. 289-306.

Althaus, E., 1967. The triple point andalusite - sillimanite - kyanite; an experimental and petrologic study; Contr. Mineral. Petrol., v16, pp. 29-44.

American Geological Institute, 1977. Glossary of Geology, 2nd ed., Washington, D.C., 805 pages.

Anhaeusser, C.R., 1971. Cyclic volcanicity and sedimentation in the evolutionary development of Archean greenstone belts of shield areas; Spec. Publ. Geol. Soc. Aust., V. 3, pp 57-70

Anhaeusser, C.R., and Button, A., 1976. A review of southern African stratiform ore deposits -- their position in time and space. In Wolf, K.H., (ed.) Handbook of strata - bound and stratiform ore deposits, v. 5, Amsterdam, Elsevier, pp 257-319.

Appel, P.V., 1979. Stratabound copper sulfides in banded iron formation and in basaltic tuffs in the early Precambrian Isua supracrustal belt, western Greenland; Econ. Geol., V. 74, pp 45-52.

Ayres, L.D., 1978. Metamorphism in the Superior province of northwestern Ontario and its relationship to crustal development. In Fraser, J.A. and Haywood, W.W., Metamorphism in the Canadian Shield; Geol. Surv. Can. Paper 78-10, pp 25-36.

Bagley, R.W. and James, H.L., 1973. Iron formations of the U.S.; Econ. Geol., V. 68, pp 934-959.

Bailes, A.H., 1979. Sedimentology and metamorphism of the Proterozoic volcaniclastic, turbidite suite that crosses the boundary between the Flin Flon and Kisseynew belts, File Lake, Manitoba, Canada. U of Man. Ph.D. Thesis (unpublished) 154 pages.

Bailes, A.H. and McRitchie, W.D., 1978. The transition from low to high grade metamorphism in the Kisseynew sedimentary gneiss belt, Manitoba; in: Metamorphism in the Canadian Shield, Geol. Surv.

Can. Paper 78-10 pp 155-178.

Barnes, H.L., 1979. Geochemistry of hydrothermal ore deposits. 2nd ed., Wiley - Interscience, 798 pages.

Barnes, R.G., 1979. Types of mineralization and their relationship to stratigraphy. In Stevens, B.P.J., ed., A Guide to stratigraphy and mineralization in the Broken Hill Block, New South Wales. N.S.W. Dept. of Mineral Resources and Development 1979, pp 31-66.

Bateman, J.D., and Harrison, J.M., 1946. Sherridon, Manitoba; Geological Servey of Canada Map 862A with descriptive notes.

Beakhouse, G.P., 1985. The relationship of supracrustal sequences to a basement complex in the western English River Subprovince. In: Evolution of Archean supracrustal sequences, Geol. Assoc. Can. Special Paper 28, pp 169-178.

Beukes, N.J., 1973. Precambrian iron formations of South Africa; Econ. Geol., v. 68, pp 960-1004.

Bischoff, J.L., Radtke, A.S. and Rosenbauer, R.J., 1981. Hydrothermal alteration in a Tertiary saline lake; Wagon Bed Formation, Wyoming. Am. Jour. of Sci., v. 279, pp 832-853.

Bond, W.D., Breaks, F.W., Desnoyers, D.W., Stone, D., Harris, N., and assistants, 1976. Operation Kenora - Ear Falls, Bruce - Bluffy Lakes Sheet, Ont. Dept Mines Preliminary map number p 1199.

Both, R.A. and Rutland, R.W.R., 1976. The problem of identifying and interpreting stratiform ore bodies in highly metamorphosed terrains; the Broken Hill example. In Wolf, K.H., ed., Handbook of strata - bound and stratiform ore deposits, v. 4, Amsterdam, Elsevier, pp 261-326.

Bradshaw, L., 1978, Report to American Selco Inc.

Burri, C., and Niggli, P., 1945. Die jungen Eruptivgesteine des Mediteranean Orogens. Zurich, Schweizer Spiegel.

Carmichael, D.M., 1969. On the mechanism of prograde metamorphic reactions in quartz bearing pelitic rocks; Contrib. Mineral. Petrol., v. 20, pp 244-257.

Condie, K.C., 1981. Archean greenstone belts. In Condie, K.C., ed., Developments in Precamabrian Geology; v. 3, Amsterdam, Elsevier.

Costa, V.R., Fyfe, W.S., Nesbitt, H.W., and Kerrich, R., 1980. Archean sedimentary talc: evidence for an ancient greenhouse (abs.): E.O.S., v. 61, n. 17, p 386.

Daly, R.A., 1933. Igneous rocks and the depths of the earth; McGraw-Hill, 508 pages.

Davies, J.F., Bannatyne, B.B., Barry, G.S. and McCabe, H.R., 1962. Geology and mineral resources of Manitoba; Province of Manitoba, Dept. of Mines and Natural Resources, 190 pages.

Desnoyers, D.W., 1982. Selco Ltd., company report of activities on Sherridon project.

Dietvorst, E.J.L., 1980. Biotite breakdown and the formation of gahnite in metapelitic rocks from Kemio Southwest Finnland; Contrib. Mineral. Petrol., v. 75, pp 327-337.

Dings, M.G., and Robinson, C.S., 1957. Geology and ore deposits of the Garfield Quadrangle, Colorado; U.S. Geol. Surv. Prof. Paper 289, 110 pages.

Douglas, R.J.W., ed., 1976. Geology and Economic Minerals of Canada, Part A; Geol. Surv. of Can., Economic Geology report #1, 838 pages.

Edmund, J.M., Measures, C., Magnum, B., Grant, B., Sclater, E.R., Collier, R. and Hudson, A., 1979. On the formation of metal rich deposits at ridge crests; Earth and Planet. Sci. Letters, V. 46, pp 19-30.

Engel, A.E.J., and Engel, C.J., 1953. Grenville Series in the northwest Adirondack Mountains; Part I; General features of the Grenville Series; Bull. Geol. Soc. Am., v. 64, pp 1013-1097.

Engel, A.E.J., and Engel, C.G., 1958. Progressive metamorphism and granitization of the major paragneiss, northwest Adirondack mountains, N.Y., Bull. Geol. Soc. Am., v. 69, pp 1369-1414.

Engel, A.E.J., and Engel, C.G., 1960 a. Progressive metamorphism and granitization Adirondack Mountains, N.Y.; Bull. Geol. Soc. Am., v. 71, pp 1-58.

Engel, A.E.J., and Engel, C.J., 1960 b. Migration of elements during metamorphism in the northwest Adirondack Mountains, N.Y.; U.S. Geol. Surv. Prof. Paper 400 B465-470.

Engel, A.E.J., Engel, C.G., Havens, R.G., 1965. Chemical characteristic of oceanic basalts and the upper mantle; Geol. Soc. Am. Bull., v. 76, pp 719-734.

Finlow - Bates, T., 1979. Chemical mobilities in a submarine exhalative hydrothermal system; Chemical Geol., v. 27, pp 65-83.

Finlow - Bates, T., and Stumpfl, E.F., 1981. The behaviour of so called immobile elements in hydrothermally altered rocks associated with submarine exhalative ore deposits; Mineral. Deposita, v. 16, pp 319-328.

Franklin, J.M., Kasarda, J., Poulsen K.H., 1975. Petrology and chemistry of the alteration zone of the Mattabi massive sulfide deposit; Econ. Geol., v. 70, pp 63-79.

Franklin, J.M., Lydon, J.W., and Sangster, D.F., 1982. Volcanic - associated massive sulfide deposits: 75th Anniversary Volume of Economic Geology, Economic Geology Publishing Co. pp 485-627.

Friesen, R.G., Perce, G.A., Weeks, R.M., 1982. Geology of the Geco base metal deposit. In Hutchinson, R.W., Spence, C.D., Franklin, J.M. (eds.). Precambrian sulfide deposits; Geol. Assoc. Can. Spec., Paper 25, pp 343-363

Froese, E., 1969 a. General geology of the Coronation Mine area; Geol. Survey of Can. Paper 68-5, pp 37-55.

Froese, E., 1969 b. Metamorphic rocks from the Coronation Mine and surrounding area; Geol. Survey of Can. Paper 68-5, pp 55-77.

Froese, E., and Goetz, P.A., 1979. Geology of the Sherridon area; Geol. Survey Can. Open File Deposit 623.

Frost, R.B., 1979. Metamorphism of iron formation: Paragenesis in the system Fe-Si-C-O-H; Econ. Geol., v. 74, pp 775-785.

Fryer, B.J., 1977. Trace element geochemistry of the Sokoman Formation; Can. Jour. Earth Sci., v. 14, p 1598.

Gale, G.H., Baldwin, D.A. and Koo, J., 1980. A geological evaluation of Precambrian massive sulfide potential in Manitoba; Manitoba Dept. of Energy and Mines, Minerals Resources Div., Economic Geology Report ER 79-1.

Garrels, R.M., and MacKenzie, F.T., 1971. Evolution of Sedimentary Rocks, 1st ed,; W.W. Dorton and Co. Inc. 397 pages.

Gilmour, P., 1976. Some transitional types of mineral deposits in volcanic and sedimentary rocks. In Wolf, K.H., ed., Handbook of strata - bound and stratiform ore deposits, v. 1, Amsterdam, Elsevier, pp 111-160.

Glen, R.A., Parker, A.J. and Rutland, R.W., 1977. Tectonic relationships between the Proterozoic Gawler and Willyama orogenic domains, Australia; Geol. Soc. Aust. Jour., v. 24, pp 125-150.

Goetz, P.A., 1980. Depositional environment of the Sherridon Group and related deposits near Sherridon Manitoba; Ph D Thesis, Carleton University.

Goetz, P.A. and Froese, E., 1982. The Sherritt Gordon massive sulfide deposit. In Hutchinson, R.W., Spence, C.D., and Franklin,

J.M. (eds.), Precambrian sulfide deposits; Geol. Assoc. Can. Spec. Paper 25, pp 557-567.

Gole, J.M., and Klein, C., 1981. Banded iron formations through much of Precambrian time; Jour. Geol., v. 89, pp 169-183.

Goldschmidt, V.M., 1937. Geochemische Verteilungsgesetze der Elemente. IX. Die Mengenverhaltnisse de elemente und der atom - arten. Skrifter Norske Videnskaps - Akad Oslo, I. Mat. - naturv. Klasse, No 4.

Goodwin, A.M., 1973. Archean iron formations of the Canadian Shield; Econ. Geol., v. 68, pp 915-933.

Goodwin, A.M. et al., 1972. The Superior Province. In Price, R.A. (ed) and Douglas, R.J.W., Variations in tectonic styles in Canada; Geol. Assoc. Can. Spec. Paper 11, pp 527-623.

Graf, J.L. (Jr.), 1977. Rare earth elements as hydrothermal tracers during the formation of massive sulfide deposits in volcanic rocks; Econ. Geol., v. 72, pp 527-548.

Gross, G.A., 1980. A classification of iron formations based on depositional environments; Can. Mineral., v. 18, pp 215-222.

Gustafson, L.B., 1981. Sediment hosted deposits of Cu, Pb and Zn; Econ. Geol. 75th Anniv. Vol, pp 139-178.

Hall, B.V., 1982. Geochemistry of the alteration pipe at the Amulet Upper A deposit, Noranda, Quebec; Canadian Jour. Earth Sci., v. 19, pp 2060-2084.

Hanson, G.N., 1980. Rare earth elements in petrogenetic studies of igneous systems, Ann. Rev. Earth Planet. Sci., v. 8, pp 371-406.

Henley, R.W., and Thornley, P., 1979. Some geothermal aspects of polymetallic massive sulfide formation; Econ. Geol., v. 74, pp 1600-1612.

Hirschberg, A., and Winkler, H.F.G., 1968. Stability relationships between cordierite, chlorite, and almandine during metamorphism; Contrib. Mineral. Petro., v. 18, pp 17-42.

Hobbs, B.E., Ransom, D.M, Vernon, R.H. and Williams, P.F., 1968. The Broken Hill Ore Body, Australia, A review of recent work; Mineral Deposita (Berl.), v. 3, pp 293-316.

Hodgson, C.J. and Lydon, J.W., 1977. Geological setting of volcanogenic massive sulfide deposits and active hydrothermal systems: Some implications for exploration; Can. Inst. Min. Met., v. 70 # 786, pp 95-106.

Huhtala, T., 1979. The geology and zinc - copper deposits of the

Pyhasalmi - Pielavesi District, Finland; Econ. Geol., v. 74, pp 1069 - 1083.

Hutchinson, R.W., 1973. Volcanogenic sulfide deposits and their metalogenic significance; Econ. Geol., v. 68, pp 1223-1246.

Hutchinson, R.W., 1982. Syn-depositional hydrothermal processes and Precambrian sulfide deposits; in Hutchinson, R.W., Spence, C.D., and Franklin, J.M. (eds.), Precambrian sulfide deposits; Geol. Assoc. Can. Spec. Paper 25, pp 761-191.

Irvine, T.W., and Baragar, W.R.A., 1971. A guide to the chemical classification of the common volcanic rocks; Can. Jour. Earth Sci., v. 8, pp 523-543.

Izawa, E., Yoshida, T. and Saito, R., 1978. Geochemical characteristics of hydrothermal alteration around the Fukazawa Kuroko deposit Akita, Japan; Mining Geology, v. 28, pp 325-336.

Jakes, P., and White, A.J., 1971. Composition of island arcs and continental growth; Earth and Planet. Sci. Letters, v. 12, pp 224-231.

James, H.L., 1954. Sedimentary facies of iron formation; Econ. Geol., v. 49, pp 235-293.

James, H.L., 1966. Data of geochemistry, 6th ed., Chapter W, chemistry of iron rich sedimenatary rocks; U.S. Geol. Surv. Prof. Paper 440-W.

James, H.L., 1969. Comparison between Red Sea deposits and older ironstone and iron formation; in Degens, E.T., and Ross, D.A. (eds.), Hot brines and recent heavy metal deposits in the Red Sea; Springer - Verlag, New York, pp 525-532.

Johannes, W., 1969. An experimental investigation of the system MgO - SiO - H O - CO ; Am. Jour. Sci., v. 267, pp 1083-1104.

Joplin, G.A., 1963. Chemical analyses of Australian rocks, Part 1; Igneous and Metamorphic: Commonwealth of Australia, Dept. of National Development, Bureau of Mineral Resources, Geology and Geophysics, Bull #65, 446 pages.

King, P.B., 1976. The evolution of North America; Princeton University Press, Princeton, New Jersey, 197 pages.

Klein, C. and Fink, R.P., 1976. Petrology of the Sokoman iron formation in the Howells River area at the western edge of the Labrador Trough; Econ. Geol., v. 71, pp 453-487.

Knight, D.C., 1981. Stratigraphy and mineralogy of a zinc - rich sillimanite gneiss near Maysville, Chaffee Country, Colorado; MSc thesis, University of Manitoba.

Knuckey, M.G., Comba, C.D.A. and Riverin, G., 1982. Structure, metal zoning and alteration at the Millenbach deposit, Noranda, Quebec; in Hutchinson, R.W., Spence, C.D., and Franklin, J.M. (eds.), Precambrian sulfide deposits; Geol. Assoc. Can. Spec. Paper 25, pp 255-295.

Krauskopf, K.B., 1979. Introduction to Geochemistry, 2nd Ed.; McGraw-Hill Book Co. 617 pages.

Krumbein, W.C., and Garrels, R.M., 1952. Origin and classification of chemical sediments in terms of pH and oxidation - reduction potentials; Jour. Geol., v. 60, pp 1-33.

Laing, W.P., 1979. Stratigraphic interpretation of the Broken Hill Mines area; in Stevens, B.P.J., ed., A guide to stratigraphy and mineralization in the Broken Hill Block, New South Wales; N.S.W. Dept. of Mineral Resources and Development 1979, pp 67-82.

Laing, W.P. Marjoribanks, R.W., and Rutland, R.W.R., 1978. Structure of the Broken Hill Mine area and its significance for the genesis of the ore bodies; Econ. Geol., v. 73, pp 1112-1136.

La Roche, Hubert de, 1965. Sur L' existence de plusiers facies geochemiques dans les schistes Paleozoiques des Pyrenees luchonnaises; Geol, Rundsch., v. 55, pp 274-301.

La Roche, Hubert de, 1974. Geochemical characters of the metamorphic domains, survival and testimony of their premetamorphic history; Sci. de la terr., Nancy, France, t XIX, n. 2, pp 103-117.

Large, R.R., 1977. Chemical evolution and zonation of massive sulfide deposits in volcanic terrains, Econ. Geol. v. 72, pp 549-572.

Leake, B.E., 1964. Chemical distinction of ortho- and para - amphibolites; Jour. of Petrology, v. 5, pp 238-254.

Leake, B.E., 1969. Chemical distinction of ortho and para charnockitic rocks, anorthosites and amphibolites; Indian Mineralogist, v. 10, pp 89-104.

Ledoux, R., and Assad,R., 1979. Field trip B-12, The Montauban - Les - Mines mineralized zone, Portneuf County, Quebec; Dept. de Geologie, Universite Laval.

Lovering, T.S., and Goddard, E.N., 1950. Geology and ore deposits of the Front Range, Colorado; U.S., Geol. Surv. Prof. Paper 223 (319 pages).

Lowe, D.R., 1980. Archean sedimentation, Ann. Rev. Earth Planet. Sci., v. 8, pp 145-167.

MacGeehan, P.J., 1978. The geochemistry of altered volcanic rocks at Mattagami, Quebec; a geothermal model for massive sulfide genesis; Can. Jour. Earch Sci., v. 15, pp 551-570.

MacGeehan, P.J., and MacLean, W.H., 1980 a. Tholeiitic. basalt - rhyolite magmatism and massive sulfide deposits at Mattagami, Quebec; Nature, v. 283, pp 153-157.

MacGeehan, P.J., and MacLean, W.H., 1980 b. An Archean sub - seafloor geothermal system, "calc-alkali" trends, and massive sulfide genesis; Nature, v. 286, pp 767-771.

Magnusson, N.H., 1950. Zn and Pb deposits of central Sweden; 18th Int. Geol. Cong. Great Britain Rept. pt. 7, pp 371-379.

Manson, D., 1912. Geological investigations in the Broken Hill area; Royal Soc. of S. Australia, v. 201, pp 43-80.

Maynard, J.B., 1983. Volcanic sedimentary ores; in, Geochemistry of sedimentary ore deposits, ch. 8, New York, Springer Verlag, pp 205-235.

McAdam, J., and Flanagan, J.T., 1976. The Montauban gold deposits related to base metal mineralization in the Grenville Province; paper presented at the annual general meeting, CIMM, Quebec April 28, 1976.

McKasey, W.O., Blackburn, C.E. and Trowell, N.F., 1974. A regional approach to the Wabigoon - Quetico belts and its bearing on exploration in Northwestern Ontario; Ont. Div. Mines Misc. Paper 58, 30 pages.

Mercer, W., 1976. Minor elements in metal deposits in sedimentary rocks - A review of the recent literature. Reprint from Ch. 1, Wolf K.H., ed., Handbook of Stratabound and stratiform ore deposits, Elsevier, Amsterdam, pp 1-25.

Middleton, R.C., 1973. The geology of Prieska copper Mines (Pty) Limited; Abstr. 15th congr., Geol. Soc. S. Africa, Bloemfontein pp 17-18.

Milne, V.G., 1969. Manitouwadge area, Gemmel twp.; Ontario Dept. of Mines Preliminary Geological Map # p 548.

Mitchell, A.H., and Bell, J.D., 1973. Island arc evolution and related deposits; Jour. Geol., v. 81, pp 381-405.

Mitchell, W.G., and Garson, M.S., 1981. Mineral deposits and global tectonic settings; Academic Press Geology Seves, Academic Press (London) Ltd. (405 pages).

Mookherjee, A., 1976. Ores and metamorphism: Temporal and genetic relationship. In Wolf, K.H., ed., Handbook of strata - bound and stratiform ore deposits, v. 4, Amsterdam, Elsevier, pp

203-260.

Moorhouse, W.W., 1941. Geology of the Zinc - Lead deposit on Calumet Island, Quebec; Bull. Geol. Soc. Am., v. 52, pp 601-632.

Niggli, P., 1954. Rocks and Mineral Deposits; San Francisco, W.H. Freeman and Co, 559 pages.

Nilsen, O., 1971. Sulfide mineralization and wallrock alteration at Rodhammeren Mine, Sor - Trondelag, Norway; Norsk Geol. Tidsskr, v. 51, pp 329-354.

Nilsson, c.A., 1968. Wall rock alteration at the Boliden deposit, Sweden; Econ. Geol., v. 63, pp 472-494.

Nockolds, S.R., 1954. Average composition of some igneous rocks; Geol. Soc. Am. Bull, v. 65, pp 1007-1032.

Nockolds, S.R. and Allen, R., 1954. The geochemistry of some igneous rock series; Geochimica et Cosmochimica acta, v. 5, pp 245-285.

Ohmoto, H., and Rye, R.O. 1974. Hydrogen and oxygen isotopic compostions of fluid inclusions in the Kuroko deposits, Japan; Econ. Geol, v. 69, pp 947-953.

Osborne, F.F., 1936. Lachute map area; Quebec Bureau of Mines Ann. Dept., pt C, pp 1-40.

Osborne, F.F., 1944. Calumet Island area, Pontiac Country; Province of Quebec, Dept. of Mines Geological Report 18, 28 pages.

Ostic, R.G., Russell, R.D., Stanton, R.L., 1967. Additional measurements of the isotopic compostion of lead from stratiform deposits, Can. Jour. Earch Sci., v. 4, pp 245-289.

Park, F.P. (Jr.), and MacDiarmid, R.A., 1970. Ore deposits; 2nd Ed., W.H. Freeman and Co., San Francisco, (521 pages).

Parry, W.T., Ballantyne, J.M., Bryant, N.L. and Dedolf, R.E., 1980. Geochemistry of hydrothermal alteration at Roosevelt Hot Springs thermal area, Utah; Geochimica et Cosmochimica Acta, v. 44, pp 95-102.

Payne, J.G., Bratt, J.A., and Stone, B.G., 1980. Cu Zn sulfide deposit Brittania district B.C.; Econ. Geol., v. 75, pp 700-721.

Phillips, G.N., 1977. Discussion : Broken Hill -- a Precambrian hot spot? -- a comment; Precambrian Research, v. 4, pp 215-220.

Pye, E.G., 1957. Geology of the Manitouwadge area: 66th Annual Report of the Ontario Department of Mines, Part 8, 114 pages.

Pyke, D.R., 1966. The Precambrian geology of the Montauban area,

Quebec; Ph. D., Thesis, McGill Univ. Montreal, P.Q., 181 pages.

Ramberg, H., 1948. Titanic iron ore formed by dissociation of silicates in granulite facies metamorphism; Econ. Geol., v. 43, pp 553-570.

Ramlal, K., 1979. The chemical analysis of silicate rocks; Centre for Precambrian Studies, University of Manitoba Annual Report for 1978, pp 55-59.

Rankama, K., and Sahama, T.G., 1952. Geochemistry, The University of Chicago Press, 911 pages.

Richards, S.M., 1967. The banded iron formations at Broken Hill, Australia, and their relationship to the Pb - Zn orebody; Econ. Geol., v. 61, pp 72-96.

Richardson, S.W., Bell, P.M., Gilbert, M.C., 1968. Kyanite - sillimanite equilibrium between 700 C and 1500 C; Am. Jour. Sci., v.266, pp 513-541.

Richardson, S.W., Gilbert, M.C., and Bell, P.M., 1969. Experimental determination of kyanite - andalusite and andalusite - sillimanite equilibria; the aluminum silicate triple point; Am. Jour. Sci., v.267, pp 259-272.

Riverin, G., and Hodgson, C.J., 1980. Wall rock alteration at the Millenbach Cu - Zn Mine, Noranda, Quebec; Econ. Geol., v. 75, pp 424-444.

Roberts, R.G., and Reardon, E.J., 1978. Alteration and ore forming processes at Mattagami Lake Mine, Quebec; Can. Jour. Earth Sci., v. 15, pp 1-21.

Robertson, D.S., 1953. Batty Lake map-area Manitoba; Geol. Survey of Can. Memoir 271, 55 pages.

Rozendaal, A., 1978. The Gamsberg Zinc Deposit, Namaqualand; Special Publication of the Geological Society of South Africa, v. 4, pp 235-262.

Sangster, D.F., 1972. Precambrian volcanogenic massive sulfide deposits in Canada -- A review; Geol. Surv. Can. Paper 72-22.

Sangster, D.F., and Scott, S.D., 1976. Precambrian strata - bound, massive Cu - Zn - Pb sulfide ores of North America. In Wolf, K.H., Handbook of Strata - Bound and stratiform ore deposits, Vol 6; Amsterdam, Elsevier, pp 129-222.

Sawkins, F.J., 1984. Metal deposits in relation to plate tectonics, Springer - Verlag, Berlin Heidelberg (325 pages).

Shoen, R. and White, D.E., 1965. Hydrothermal alteration in GS - 3 and

GS - 4 drill holes, Main Terrace, Steamboat Springs, Nevada, Econ. Geol., v. 60, pp 1411-1421.

Sigvaldson, G.E., and White, D.E., 1962. Hydrothermal alteration in drill holes GS - 5 and GS - 7 Steamboat Springs, Nevada; U.S. Geol. Survey Prof. Paper 450 D, pp 113-117

Solomon, M., and Walshe, J.L., 1979. The formation of massive sulfide deposits on the sea floor; Econ. Geol., v. 74, pp 797-813.

Speakman, D.S., Chornoby, P,J. Haystead, B.C.W., and Holmes, G.F., 1982. Geology of the Ruttan deposit, northern Manitoba; in Hutchinson, R.W., Spence, C.D, and Franklin, J.M. (eds.), Precambrian sulfide deposits; Geol. Assoc. Can. Spec. Paper 25. pp 525-555.

Spencer, E.W., 1977. Introduction to the structure of the earth; McGraw-Hill Inc., 640 pages.

Stamatelopoulou - Seymour, K. and MacLean, W.H. 1977. The geochemistry of possible metavolcanic rocks and their relationship to mineralization at Montauban - Les - Mines, Quebec; Can. Jour. Earth Sci., v. 14, pp 2440-2452.

Stanton, R.L., 1979. An alternative to the Barrovian interpretation: evidence from stratiform ores. Text of the C.F. Davidson Memorial Lecture given at the Univ. of St. Andrews, Nov. 22, 1977, 86 pages.

Stanton, R.L., 1984. The direct derivation of cordierite from a clay - chlorite precursor; Evidence from the Geco Mine, Manitouwadge, Ontario; Econ. Geol., v. 79, pp 1245-1264.

Stauffer, M.R., Mukherjee, A.C., and Koo, J., 1979. The Amisk Group, an Aphebian island arc deposit; Can. Jour. Earth Sci., v. 12, pp 2021-2035.

Stevens, B.P.J., Stroud, W.J., Willis, IlL., Bradley, G.M., Brown, R.E. and Barnes, R.G., 1979. A stratigraphic interpretation of the Broken Hill Block; in Stevens, B.P.J., ed., A guide to stratigraphy and mineralization in the Broken Hill Block, New South Wales; Dept. of Mineral Resources and Development 1979, pp 7-30.

Stockwell, C.H., 1961. Structural provinces, orogenies, and time classification of rocks of the Canadian Precambrian Shield, Geol. Surv. Can. Paper 61-17, pp 108-118.

Stockwell, C.H., 1972. Revised time scale for the Canadian Shield; Can. Geol. Survey Paper 72-52, 4 pages.

Stumpfl, E.F., 1979. Manganese Haloes surrounding metamorphic stratabound base metal deposits; Mineral. Deposita, v. 14, pp 207-217.

Suk, Milos, 1983. Petrology of metamorphic rocks; Developments in Petrology, v. 9, Amsterdam, Elsevier, 322 pages.

Taylor, S.R., 1955. The origin of some New Zealand metamorphic rocks as shown by their major and trace element composition; Geochimica at Cosmochemica Acta, v. 8, pp 182-197.

Thurston, P.C., and Breaks, F.W., 1978. Metamorphic and tectonic evolution of the Uchi - English River subprovince; in: Metamorphism in the Canadian Shield; Geol. Surv. Can. Paper; 78-10, pp 49-62.

Trendall, A.F., 1973. Precambrian iron formations of Australia; Econ. Geol., v. 69, pp 1023-1034.

Turner, J.S., and Gustafson, L.B., 1978. The flow of hot saline solutions from vents in the sea floor - some implications for exhalative massive sulfide and other ore deposits; Econ. Geol., v. 73, pp 1082-1100.

Vallence, T.G., 1967. Mafic rock alteration and isochemical development of some cordierite - anthophyllite rocks. Jour. Petrol., v. 8, pp 84-96.

Van de Kamp, P.C., 1970. The Green Beds of the Scottish Dalradian Series; Geochemistry, origin and metamorphism of mafic sediments; Jour. Geol., v. 78, pp 281-303.

Van de Kamp, P.C., Leake, B.E., and Senior, A., 1976. The petrography and geochemistry of some Californian arkoses and application to identifying gneisses of metasedimentary origin; Jour. Geol., v. 84, pp 195-212.

Van de Kamp, P.C., 1968. Geochemistry and origin of metasediments in the Haliburton - Madoc area, southeastern Ontario; Can. Jour. Earth Sci., v. 5, pp 1337-1372.

Van de Kamp, P.C., and Beakhouse, G.P., 1979. Paragneisses in the Pakwash Lake area, English River gneiss belt, northwestern Ontario; Can. Jour. Earth Sci., v. 16, pp 1753-1763.

White, D.E., 1968. Environments of generation of some base metal ore deposits; Econ. Geol., v. 63, pp 301-335.

Whithead, R.E.S., and Goodfellow, W.D., 1978. Geochemistry of volcanic rocks from the Tetagouche Group, Bathurst, N.B., Canada; Can. Jour. Earth Sci., v. 15, pp 207-219.

Whitmore, D.R.E., 1968. Geology of the Coronation copper deposits; Geol. Surv. Can. Paper 68-5, n. 3, pp 37-53.

Wilson, H.D.B., Andrews, P., Moxham, R.L., Ramlal, K., 1965. Archean volcanism in the Canadian Shield; Can. Jour Earth Sci., v. 2,

pp 161-175.

Wilson, H.D.B., Morrice, M.G., Zielkhe, D.V. and Beakhouse, G.P., 1976. Development of greenstone - granite and gneissic terrains in Archean Shields; Centre for Precambrian Studies, 1976 Annual Report, University of Manitoba.

Windley, B.F., 1981. Precambrian rocks in the light of the plate tectonic concept; in Kroner, A., ed., Developments in Precambrian Geology; v. 4, Amsterdam, Elsevier, pp 1-20.

Winkler, H.G.F., 1976. Petrogenesis of metamorphic rocks, 4th ed., Springer - Verlag New York Inc., (334 pages)

Wynne - Edwards, H.R., 1972. The Grenville Province, in Price, R.A. and Douglas, R.J.W., eds, Variations in tectonic styles in Canada; Geol. Assoc. Can. Spec. Paper 11, pp 264-334.

Zelt, G.A.D., 1980. Granulite Facies metamorphism in Namaqualand, South Africa; Precambrian Research, v. 13, pp 253-274.

Zwanzig, H.V., 1976. Origin and correlation of the Kisseynew Gneisses; Geol. Assoc. Can. Abstract, 1976 General Meeting, Edmonton.

APPENDIX A

Chemical Analyses and Petrographic Data of Rocks Sampled

A-0: Sample Preparation

All diamond drill core and hand samples were prepared in the same manner. Using a diamond saw, samples were split perpendicular to the foliation to produce two slabs. A thicker slab was crushed and ground for chemical analysis while a thinner slab was prepared for thin sectioning.

Thin sections were examined for relict primary textures and other features as well as metamorphic fabrics. Estimates of mineral abundances were made by means of crude microscopic traverses across the thin section and averaging the mineral abundances in each field of view. Therefore, modal proportions rarely add to 100%.

Crushed and ground samples were analyzed at the University of Manitoba. These were subjected to combustion, acid digested, and the resultant solutions analyzed by titration, X-ray fluorescence spectrometry, and atomic absorption spectrometry according to the procedures described by Wilson, Andrews, Moxham and Ramlal (1965) and Ramlal (1979). Chemical and petrographic data for collected samples are listed in Appendices A-1 to A-5 inclusive. Mineral percentages are optical estimates. Confidence limits and detection limits are listed in Table A-1. Water is quoted as H_2O .

TABLE A-1 Methods, precision and accuracy of chemical analysis of silicate rocks (from Ramlal, 1978).

Constituent	Method(s) Primary	Alternate	Concentration	Instrument precision, σ	Accuracy of replicates, σ
SiO_2	XRF		59.60 wt.%	.12	.20
Al_2O_3	XRF		9.34	.05	.13
Fe_2O_3*	XRF	AAS	10.08	.017	.03
MgO	AAS		4.04	.04	.10
CaO	XRF	AAS	10.22	.02	.07
K_2O	XRF	AAS	2.69	.01	.01
MnO	XRF	AAS	.41	.01	.01
TiO_2	XRF		.48	.02	.02
Na_2O	AAS		4.20	.01	.05
H_2O*	combustion		1.60	.03	.06
CO_2	combustion:acid digestion		1.15	.05	.12
P_2O_5	spectrophotometry		0.20	.01	.01
FeO	titration		10.92	-	0.04
S	combustion	titration	0.185	0.003	0.005
Zr	XRF		0.027	0.003	0.005
Ba	XRF	AAS	0.015	.005	.005
Ag	AAS		4.0 ppm	.02	.04
Cd	AAS				
Cl	gravimetric				
Cr	AAS	XRF	360	2.0	5.0
Cs	AAS		820	5.0	13.0
Co	AAS	XRF	53	1.0	2.0
Cu	AAS	XRF	40	1.0	2.0
Li	AAS		10	.04	.05
Ni	AAS	XRF	77	1.0	3.0
Pb	AAS, flame		34	2.0	3.0
Pb	AAS, flameless		8	.02	.01
Rb	AAS	XRF	228	1.0	2.0
Sr	AAS	XRF	260	5.0	8.0
V	XRF		380	10.0	15.0
Zn	AAS	XRF	108	1.0	2.0

* total concentration expressed as .....

all concentrations expressed in weight percent unless otherwise stated.

Appendix A-1 (Ear Falls area)
(all sample numbers preceded by 'B6')

Sample Number	1	2	3-1	3-2	3-3	3-4	3-5	3-6	3-7	3-8	3-9a	3-9b	3-10	4	5	6	if-1	if-2	if-3
SiO2	69.70	67.40	56.40	67.10	68.60	8.10	71.35	55.10	65.05	52.15	68.20	69.10	68.90	61.50	73.35	69.60	60.10	57.20	57.70
Al203	14.63	14.76	18.87	14.36	14.66	14.62	4.14	20.48	15.58	10.98	14.20	13.90	14.20	17.40	14.68	13.76	8.56	16.83	10.23
Fe203	1.86	1.01	1.32	4.60	1.82	0.82	5.54	1.59	1.30	4.12	0.68	0.32	-0.64	2.23	0.89	2.17	5.59	1.03	3.08
FeO	2.62	4.14	7.52	1.12	3.66	4.44	11.20	7.10	4.40	20.16	4.76	4.28	3.96	5.34	1.70	2.60	20.50	8.08	20.64
MgO	1.72	3.02	3.85	2.46	2.41	2.06	0.90	3.78	2.53	2.10	2.20	2.19	2.60	3.28	1.05	2.70	1.96	3.40	2.09
CaO	2.28	2.50	2.42	2.42	2.92	3.59	2.00	1.17	2.40	6.55	2.14	2.11	2.76	1.68	0.67	1.17	1.93	2.69	4.31
Na20	3.58	2.67	4.03	3.67	2.52	2.98	0.12	3.37	4.80	0.35	3.58	3.68	3.13	2.91	3.08	2.15	0.15	3.42	1.70
K20	1.73	2.19	3.02	2.28	1.62	1.48	0.12	4.98	2.10	0.40	2.04	2.12	1.94	2.92	2.92	4.74	0.16	3.36	0.34
H20	0.87	1.21	1.56	1.03	1.01	0.66	1.86	1.45	0.88	1.09	1.12	1.11	0.97	1.78	0.85	1.30	0.43	1.58	0.69
C02	0.07	0.09	0.04	0.05	0.04	0.24	0.10	0.08	0.04	1.01	0.11	0.15	0.10	0.09	0.20	0.11	0.19	0.07	0.32
TiO2	0.39	0.49	0.76	0.53	0.46	0.44	0.14	0.63	0.50	0.18	0.48	0.47	0.46	0.75	0.24	0.26	0.23	0.86	0.20
P205	0.14	0.15	0.06	0.08	0.12	0.12	0.26	0.12	0.20	0.32	0.10	0.10	0.11	0.08	0.03	0.10	0.13	0.03	0.20
MnO	0.04	0.07	0.09	0.08	0.08	0.10	0.06	0.09	0.09	0.14	0.10	0.07	0.07	0.07	0.01	0.05	0.09	0.05	0.10
S	0.165	0.013	0.015	0.065	0.302	0.213	4.610	0.098	0.023	0.906	0.034	0.024	0.058	0.084	0.001	0.009	0.054	0.012	0.311
Ni (ppm)	25	56	95	23	33	58	63	30	66	36	31	24	32	64	21	33	32	98	52
Cu (ppm)	35	41	12	25	93	65	740	68	31	103	19	20	38	86	11	13	17	8	32
Zn (ppm)	27	68	90	78	70	73	30	85	64	69	65	67	62	83	29	41	39	130	38
Pb (ppm)	58	<10	<10	10	14	<10	15	23		24	<10	<10	<10		18	23		<10	18
Sr (ppm)																			
Cr (ppm)		249																	
V (ppm)	138		140	170	118	65	70	120	168	15	105	37	84	223	38	80	10	50	<10
Co (ppm)	14	25	36	15	16	24	25	25	20	18	12	15	15	29	5	10	11	16	12
Quartz	<=5	<=5	<=5	<=5	<=5	<=5	23			20		5	<5	5	<=5	<5	32	3	16
Biotite	12	20	15	18	17	15		10	8			10	20	10	6	8		25	2
K-feldspar	45	42	50	48	17	10	47		15	20		55			45	5	33	35	22
Microcline								25						40		23			
Plagioclase	35	32	30	26	60	60		63	70			27	70	40	45	55		37	
Muscovite	TR																		
Sillimanite								TR						TR		TR			
Hornblende							10			35									12
Anthophyllite																			
Garnet	TR	5	<=5	3	5	6	8	2	6	25		<=2	5	2			22		45
Gahnite																			
Apatite	<=1	<1		TR	<=1				TR			<1		TR		TR	1		TR
Sphene		TR		TR	TR	TR						TR							
Zircon	TR	TR		TR	TR	TR			TR				TR						
Epidote							TR		TR										
Chlorite					TR					<1									
Sericite			TR																
Carbonate							2										TR		
Cordierite																			
Pyroxene	TR																		
Spinel													TR						
Orthopyroxene																			1
Clinopyroxene																	7		3
Fe Ti oxides	<=1	<1	TR	TR	TR	1%		<1		2					TR	TR	5		1
Sulfides							10%												

Appendix A-1 (Ear Falls area)
(all numbers preceded by 'B6')

Sample Number	IF-5	IF-6	IF-7	IF-8
SiO2	51.00	51.10	55.65	41.30
Al2O3	6.00	6.04	7.90	17.28
Fe2O3	16.53	16.33	8.41	4.05
FeO	22.80	21.92	20.90	22.28
MgO	1.41	1.46	2.11	4.65
CaO	2.34	2.34	2.92	1.10
Na2O	0.07	0.05	0.15	1.20
K2O	0.04	0.01	0.12	2.84
H2O	0.34	0.25	0.50	2.50
CO2	0.20	0.12	0.07	0.77
TiO2	0.15		0.15	0.69
P2O5	0.20	0.24	0.23	0.18
MnO	0.07	0.08	0.07	0.54
S	0.250	0.017	0.959	0.874
Ni (ppm)	14	13	33	164
Cu (ppm)	12	12	3	108
Zn (ppm)	34	34	27	116
Pb (ppm)	33	29		14
Sr (ppm)				
Cr (ppm)				
V (ppm)	ND	<10	10	20
Co (ppm)	<10	<10	8	34
Quartz	20	12	7	<5
Biotite				23
K-feldspar	25	32	35	
Microcline				
Plagioclase				42
Muscovite				
Sillimanite				
Hornblende		3	3	
Anthophyllite				
Garnet	30	20	32	35
Gahnite				
Apatite		<1		
Sphene				
Zircon				
Epidote		TR		
Chlorite		TR		
Sericite				
Carbonate				
Cordierite				
Pyroxene				
Spinel				
Orthopyroxene				
Clinopyroxene	17	23	20	
Fe Ti oxides	8	5	3	
Sulfides		5		

Appendix A-2 (Montauban)
(all numbers preceded by 'MON')

Sample Number	1	2	3	4	5	6	7	8	9	10	11	101	102	103	104
SiO2	64.50	58.92	69.30	77.30	54.40	53.88	65.45	68.45	70.30	66.73	69.87	54.26	84.67	63.27	78.78
Al2O3	15.56	14.37	14.69	12.16	11.60	12.52	15.76	12.14	13.40	13.82	17.05	3.63	5.64	12.31	6.24
Fe2O3	0.08	0.81	0.69	0.36	1.52	0.25	1.12	0.85	0.90	0.73	0.93	0.78	1.77	0.71	1.66
FeO	6.20	4.80	1.90	1.10	0.46	1.20	2.42	2.04	3.34	3.36	3.16	2.78	3.14	6.34	4.54
MgO	4.70	10.26	4.33	2.18	23.10	24.43	7.65	8.73	5.15	9.65	4.83	21.36	2.42	9.14	4.77
CaO	0.33	0.99	0.43	1.57	0.28	0.18	0.30	0.00	0.28	0.08	0.90	12.62	0.18	1.37	0.03
Na2O	0.23	0.34	0.35	1.08	0.33	0.35	0.25	0.21	0.20	0.22	0.37	0.53	0.15	0.69	0.23
K2O	4.96	4.69	5.09	2.82	0.88	0.81	3.48	3.96	2.52	2.24	1.27	0.06	0.63	1.56	2.10
H2O	2.20	2.67	2.46	1.17	6.16	7.35	2.33	3.25	1.95	2.41	0.39	2.01	0.60	2.79	1.13
CO2	0.11	0.74	0.11	0.10	0.02	0.09	0.06	0.17	1.33	0.20	0.71	0.40	0.37	0.59	0.30
TiO2	0.39	0.39	0.19	0.12	0.18	0.11	0.43	0.15	0.33	0.32	0.15	0.09	0.12	0.27	0.13
P2O5	0.171	0.17	0.083	0.077	0.215	0.00	0.184	0.00	0.068	0.01	0.00	0.00	0.00	0.04	0.00
MnO	0.24	0.23	0.54	0.06	0.17	0.35	0.18	0.07	0.12	0.18	0.16	0.77	0.19	0.22	0.22
S	0.008	0.394	0.360	0.250	0.020	0.006	0.060	0.048	0.370	0.018	0.099	0.240	0.030	0.303	0.070
Ni (ppm)	8	35	3	8	3	3	4	13	2	14	30	32	19	18	21
Cu (ppm)	92	60	16	14	9	14	10	31	28	37	108	127	95	41	480
Zn (ppm)	.367%	688	262	59	630	650	104	176	118	175	2025	1013	4500	1538	
Pb (ppm)		215			4		56		3	291	14	179	358	496	
Sr (ppm)		320				180		145		195	385	28	15	58	N/D
Cr (ppm)															
V (ppm)	184		80	93	124		156		150						
Co (ppm)	10	8	4	4	5	N/D	4	2	3	7	4	1	4	12	2
Rb (ppm)		125				32		102		54	40	N/D	17	49	54
Quartz	30	38	50	55	3	7	40	22	22	15	25		20	15	50
Biotite	40	32	10	4	7	3	20	28	17	20	15		5	15	18
K-feldspar	22	7	15	15			15	43	50	18	20		60	15	30
Microcline															
Plagioclase				5								<1		2	
Muscovite	<=1		20	20	5	<=2		2							
Sillimanite	5						5	5	8	5	10	<2		2	
Hornblende															
Anthophyllite		6			50	42				2	1			15	
Garnet	2		2										3	TR	2
Gahnite										1					
Apatite															
Sphene						TR									
Zircon		<=1	<<1			TR									
Epidote															
Chlorite						TR									
Sericite															
Carbonate															
Cordierite							18	<1		40	25		10	35	
Pyroxene			2		5	5					1				
Talc					30	42									
Kyanite							1		1						
Fe Ti oxides		<<1	<<1				<<1		1			<1			
Sulfides											1			1	

Appendix A-3 (New Calumet)
(all numbers preceded by 'Cl#')

Sample Number	1	2	3	4	5	6	7	8	9	10	11	12	13	101	102
SiO2	51.65	50.05	58.65	50.45	48.50	69.25	70.05	67.15	50.30	83.80	35.55	83.10	65.65	75.31	84.01
Al2O3	17.76	17.02	14.82	13.04	11.53	12.34	12.94	14.66	20.86	7.50	13.40	5.89	13.28	5.71	3.58
Fe2O3	1.76	1.79	0.93	3.56	2.09	2.05	1.41	2.70	4.59	1.27	1.22	0.47	1.12	1.40	0.98
FeO	6.72	6.12	7.48	9.32	7.94	5.28	4.58	2.70	1.86	2.08	5.62	3.50	6.44	7.12	6.02
MgO	5.70	8.10	5.10	6.75	10.15	2.70	2.88	3.35	6.03	0.90	9.40	2.23	2.65	3.74	0.17
CaO	11.66	9.35	3.10	8.53	15.76	1.24	0.55	0.60	1.30	0.12	19.70	0.56	1.46	1.01	0.47
Na2O	0.89	1.92	2.30	3.11	1.00	2.12	1.00	0.34	1.46	0.11	0.98	0.12	1.04	0.72	0.89
K2O	1.21	1.34	3.04	1.28	0.28	1.68	3.39	5.13	8.97	1.92	2.36	1.18	3.56	1.42	0.29
H2O	1.79	2.00	1.66	1.57	1.13	0.96	1.46	1.68	2.27	0.99	1.92	0.98	1.53	0.80	1.58
CO2	0.07	0.92	0.40	0.33	0.57	0.07	0.10	0.17	0.13	0.20	8.93	0.76	0.81	0.00	0.24
TiO2	0.31	0.50	0.52	1.82	0.38	0.48	0.52	0.29	0.55	0.35	0.31	0.27	0.51	0.16	0.17
P2O5	0.05	0.27	0.23	0.11	0.15	0.08	0.09	0.11	0.28	0.05	0.19	0.04	0.15	0.00	0.00
MnO	0.182	0.25	0.17	0.201	0.139	0.13	0.10	0.06	0.10	0.03	0.18	0.04	0.09	0.15	0.04
S	0.011	0.21	0.39	0.29	0.17	2.27	1.44	2.17	2.27	0.92	0.06	1.20	2.81	3.34	1.84
Ni (ppm)	32	92	24	33	88	<10	10	11	27	<10	189	10	17	21	39
Cu (ppm)	35	65	115	77	61	85	27	119	91	.144%	45	.08%	89	1525	1025
Zn (ppm)	103	62	80	77	390	88	115	211	348	75	74	212	171	325	650
Pb (ppm)	105			2	116									116	147
Sr (ppm)														50	N/D
Cr (ppm)															
V (ppm)	148			360	128										
Co (ppm)	31	36	28	46	48	11	<10	<10	14	<10	56	10	15	19	38
Rb (ppm)														42	7
Quartz						22	5	5	3	5		12	10	37	
Biotite			35	4		13	18	11	10	3	12	13		7	
K-feldspar	3	3		5		17				75		60	63	35	
Microcline							60	70	63				10		
Plagioclase	60	40	60	50	25	37			7		10			15	
Muscovite									2	5			3		
Sillimanite						5	14	6	12	10		10	7		
Hornblende	17	55		38	57										
Anthophyllite															
Garnet		<<1	2											1	
Gahnite															
Apatite	<<1			<1											
Sphene	TR			1	<1	TR		TR					TR		
Zircon	TR		<<1			TR	TR	TR				TR	TR		
Epidote															
Chlorite						2					TR				
Sericite	TR			<1				5	TR				TR		
Carbonate		<=1		1							43				
Cordierite															
Clinopyroxene	20				18						10				
Amphibole											10				
Spinel												TR			
Fe Ti oxides				<=1	<1						TR				
Sulfides		1	<=1			4	3	3	3	2		5	7	5	

Appendix A-3 (New Calumet)
(all numbers preceded by 'Cla')

Sample Number	14	15	16	17	18	19	20	21	22	23	24	25	26	103
SiO2	67.95	59.85	68.60	72.05	73.40		61.60	57.60	73.00	66.95	69.10	53.15	78.10	43.92
Al2O3	14.80	16.65	14.44	12.94	12.20		17.50	19.20	11.76	13.84	14.22	20.60	8.57	6.68
Fe2O3	3.13	1.89	1.87	0.41	2.08		4.41	2.70	2.79	2.20	4.40	2.47	0.39	2.44
FeO	2.12	5.56	3.20	4.28	1.52	2.66	4.30	5.84	3.40	2.76	1.08	4.80	4.14	3.34
MgO	3.38	3.70	4.20	1.81	2.92	4.45	2.60	4.85	1.06	3.18	5.35	2.73	1.11	25.57
CaO	1.26	0.73	0.23	1.10	1.10	1.15	0.18	0.45	0.55	0.20	0.11	2.50	1.75	9.00
Na2O	0.74	0.86	0.17	1.18	1.21	0.85	0.39	0.50	0.72	0.92	0.87	3.21	1.10	0.91
K2O	2.16	6.39	5.55	4.47	3.20		3.04	3.84	3.29	4.01	3.82	5.60	1.46	0.20
H2O	0.92	2.23	1.88	0.88	1.01	1.48	3.12	1.29	0.97	1.55	1.94	1.30	0.85	3.59
CO2	1.52	1.10	0.32	0.19	0.19	0.23	0.37	1.25	0.68	2.16	0.63	0.45	0.74	1.12
TiO2	0.45	0.68	0.40	0.50	0.43		0.48	0.51	0.42	0.58	0.46	0.95	0.40	0.26
P2O5	0.21	0.27	0.02	0.02	0.04	0.018	0.029	0.03	0.02	0.36	0.10	0.33	0.15	0.31
MnO	0.05	0.16	0.089	0.35	0.053	0.101	0.079	0.073	0.049	0.068	0.092	0.05	0.033	0.51
S	2.27	2.17	0.42	1.22	1.75	1.33	3.88	3.63	2.94	2.01	0.73	2.72	1.73	1.96
Ni (ppm)	14	38	5	13	10	10	9	19	18	44	22	52	93	12
Cu (ppm)	42	87	69	93	20	43	630	278	81	320	46	68	70	740
Zn (ppm)	70	244	111	255	102	291	191	1370	127	163	145	258	400	6500
Pb (ppm)			15	26	14	80	40	133	153	89	2	24	31	562
Sr (ppm)														28
Cr (ppm)														
V (ppm)			118	46	220	116	106	90	64	156	128	226	195	
Co (ppm)	13	<10	12	9	6	7	7	3	14	11	9	23	3	5
Rb (ppm)														2
Quartz	8	5	10	10	10	20	7	5	7	15	5	3	30	
Biotite	10	20	10	5	7	20	11	12	4	20	23	20	5	
K-feldspar	63	40	65	55	60	55	52	55		5			58	
Microcline		15							75		65	25		
Plagioclase				25	15	5		10	3	52		50		
Muscovite		5		1	3		5		2			<1		
Sillimanite	14	10	15	3	4	<=1	10	12	6	2	5	1	2	
Hornblende														
Anthophyllite														
Garnet														
Gahnite														
Apatite			<<1		TR			TR		TR	TR			
Sphene		TR			TR	TR		TR		TR				
Zircon		TR			TR	TR	TR	TR			TR			
Epidote														
Chlorite													<<1	
Sericite				TR					TR		TR		2	
Carbonate									<<1				TR	
Cordierite														
Pyroxene										3		1		
Clay							5							
Fe Ti oxides										2	1		3	
Sulfides	5	5	<1	1	2	<1	10	1	3					

Appendix A-3 (New Calumet)
(all numbers preceded by 'Cla')

Sample Number	27	28	29	30	31	32	33	34	35	36	37	44	48	49
SiO2	63.50	69.00	61.40	73.00	63.70	0.80	1.25	1.00	0.10	45.40	69.50	62.15	60.45	65.70
Al2O3	14.74	14.58	16.10	12.10	14.36	0.44	0.34	0.56	0.28	13.86	13.96	14.67	20.38	15.38
Fe2O3	0.42	1.81	1.66	1.03	1.16	1.36	0.72	0.80	0.44	6.05	1.94	1.28	0.91	1.79
FeO	6.14	3.06	7.32	3.88	6.26	0.90	0.24	23.20	0.20	9.54	4.56	6.74	0.46	4.12
MgO	2.15	1.30	4.00	1.05	3.90	21.12	20.75	32.40	22.45	5.31	0.90	4.15	0.75	2.05
CaO	2.05	1.45	3.15	2.50	3.80	28.60	29.84	0.45	33.04	10.56	0.75	3.00	3.52	0.95
Na2O	3.66	2.41	2.52	3.93	2.58	0.46	0.50	0.45	0.38	2.75	4.53	2.23	2.96	1.80
K2O	3.34	3.28	1.06	0.14	0.23	0.14	0.12	0.09	0.11	0.89	1.86	2.85	7.92	4.74
H2O	1.21	1.50	0.90	0.55	1.08	0.13	0.11	0.32	0.22	0.73	0.90	1.22	0.64	1.98
CO2	0.86	0.22	0.16	1.30	1.68	44.65	45.25	39.77	42.83	0.67	0.23	0.59	0.61	0.38
TiO2	0.52	0.46	0.59	0.32	0.44	0.00	0.00	0.03	0.00	3.64	0.44	0.58	0.96	0.82
P2O5	0.07	0.03	0.06	0.07	0.02	0.08	0.04	0.10	0.01	0.03	0.05	0.06	ND	0.04
MnO	0.05	0.03	0.11	0.08	0.19	0.10	0.10	0.13	0.06	0.29	0.09	0.13	0.02	0.04
S	2.57	1.89	1.48	0.09	1.21	1.62	0.43	0.50	0.04	0.20	0.015	0.36	0.031	0.16
Ni (ppm)	53	5	47	0	16	12	4	4	0	17	0	14	2	22
Cu (ppm)	107	49	77	10	70	13	9	9	7	20	10	77	22	39
Zn (ppm)	171	69	111	63	366	1110	960	219	17	107	85	75	32	85
Pb (ppm)	8	12	1	<1	161	119	31	6	2	ND	ND		10	34
Sr (ppm)														
Cr (ppm)														
V (ppm)	216	48	208	79	195	62	22	12	9	94	247	300	164	160
Co (ppm)	17	50	19	4	16	2	4	2	2	3	10	23	5	14
Rb (ppm)														
Quartz	8		8	4	4	1	<1	<1	<1	2	3			
Biotite	10		8	1	<<1		<=1	<=1		1	15			
K-feldspar			3	27	8					2	7			
Microcline	80													
Plagioclase	3		64	60	60					60	75			
Muscovite	1						<=1	<1	<<1					
Sillimanite														
Hornblende										30				
Anthophyllite														
Garnet										3	<=1			
Gahnite														
Apatite											TR			
Sphene														
Zircon														
Epidote														
Chlorite						TR					TR			
Sericite	TR													
Carbonate	TR					97	96	96	97		TR			
Cordierite														
Orthopyroxene				8	4									
Clinopyroxene			13		20	1	1	1	<1	2				
Fe Ti oxides	3		2	<1	2						<1			
Sulfides						1	<=1	<=1	<=1					

Appendix A-4 (Surface Traverse Geco)
(all numbers preceded by '60-')

Sample Number	1	2	3	4	5	6	7a	7b	7c	8	9	9a	10	10b
SiO2	50.40	55.45	50.68	54.10	65.25	56.10	66.53	64.66	63.65	60.97	66.89	63.40	61.25	61.90
Al2O3	13.98	15.44	14.10	12.76	17.28	15.06	16.97	17.16	18.94	17.44	15.80	16.10	16.36	16.88
Fe2O3	3.33	3.86	3.34	2.01	1.22	2.03	1.21	1.14	1.78	1.00	0.86	1.94	2.16	2.11
FeO	10.36	5.14	9.52	16.28	1.56	6.32	1.56	0.94	2.76	4.52	2.60	3.36	3.18	2.74
MgO	6.25	4.25	4.71	3.95	1.63	6.65	1.43	1.14	2.10	2.98	2.35	2.70	3.45	3.28
CaO	9.40	9.35	9.64	2.85	3.23	7.75	2.47	3.68	2.15	2.47	3.02	4.35	5.00	3.25
Na2O	2.21	3.70	3.62	2.61	5.44	0.67	4.69	6.05	5.35	5.34	4.94	4.38	5.10	5.25
K2O	0.80	0.69	0.89	0.39	2.53	2.82	3.00	2.20	1.44	2.01	1.53	1.51	1.22	1.92
H2O	1.00	0.89	1.24	0.94	1.09	1.04	1.22	1.41	0.87	1.81	0.69	0.78	1.29	1.95
CO2	0.06	0.06	0.18	0.02	0.50	0.04	0.62	0.71	0.25	0.08	0.32	0.13	0.08	0.07
TiO2	1.41	0.80	1.09	3.06	0.39	0.79	0.31	0.32	0.52	0.60	0.35	0.52	0.56	0.46
P2O5	0.02	0.02	0.14	0.26	0.19	0.18	0.15	0.15	0.13	0.25	0.18	3.00	0.07	0.16
MnO	0.22	0.17	0.26	0.35	0.04	0.18	0.09	0.09	0.05	0.07	0.05	0.07	0.07	0.06
S	0.143	0.018	0.295	0.129	0.005	0.081	0.128	0.067	0.102	0.077	0.029	0.009	0.010	0.043
Ni (ppm)	56	125	94	29	35	28	12	18	50	68	37	46	72	59
Cu (ppm)	68	29	214	20	11	20	43	11	48	68	17	18	21	44
Zn (ppm)	102	80	98	525	84	78	50	50	136	70	44	64	67	50
Pb (ppm)	ND	10	<1	2	<1	ND	<1	<1	8	<1	12	2	9	3
Sr (ppm)	145	190	155	40	320	103	395	470	425	360	605	408	778	483
Cr (ppm)	149	250		69		275			124			157	203	208
V (ppm)														
Co (ppm)	61	53	63	43	23	33	11	12	19	29	14	17	23	23
Rb (ppm)	25	5	26	10	58	111	64	52	37	65	35	36	11	37
Quartz	3	3	2	3	5	3	10	5	5	5		5		4
Biotite				4	10	16	7	8	8	30		8		
K-feldspar							30					20		
Microcline					5			5						
Plagioclase	40	75	45	35	10	10	40	58	68	65		60		68
Muscovite					7		4	3	2					
Sillimanite														
Hornblende	6	22	45			45						8		15
Anthophyllite														
Garnet		1		7						1				
Gahnite														
Apatite			TR											
Sphene			TR		<1		<1	<1	<1			TR		
Zircon			TR											
Epidote														
Chlorite									3					10
Sericite	8		5		TR	25	8	15	10	TR				12
Carbonate					<2		<2	5	2					
Cordierite														
Amphibole				50										
Clinopyroxene	36													
Fe Ti oxides	7		3	3	<=1	1	1	1	2	1		<1		
Sulfides														

Appendix A-4 (Surface Traverse Geco)
(all numbers preceded by 'GO-')

Sample Number	11	12	13	14a	14b	14c	15a	15b	15c	15d	15e	15f	15g	15i	15j
SiO2	48.10	64.45	64.23	66.25	77.21	64.00	55.70	56.20	56.45	54.10	51.90	83.00	82.90	49.80	42.50
Al2O3	14.06	15.66	16.92	15.48	9.50	16.00	15.64	14.74	15.30	15.02	9.19	0.44	0.71	3.60	5.29
Fe2O3	3.46	2.35	1.05	1.02	4.80	1.79	1.18	1.28	1.36	2.40	5.04	8.75	7.68	10.62	10.09
FeO	12.00	2.44	3.04	2.64	2.84	2.84	3.26	3.06	3.14	8.08	17.20	2.92	3.62	22.82	28.02
MgO	5.80	2.75	2.77	2.65	3.49	2.60	9.30	9.70	8.65	2.15	1.65	0.26	1.00	1.25	2.85
CaO	8.75	3.45	3.16	4.00	0.14	4.20	8.25	8.95	8.10	3.80	3.00	0.45	1.00	2.10	3.75
Na2O	1.28	4.90	5.23	5.00	0.31	4.40	3.50	3.73	4.05	2.38	0.98	0.01	0.01	0.12	0.25
K2O	1.24	1.42	2.03	1.31	0.26	1.48	2.39	1.05	1.43	5.19	1.40	0.04	ND	0.04	0.34
H2O	2.57	1.59	0.28	1.06	0.61	1.49	1.38	0.48	0.44	0.92	0.72	0.15	0.18	0.86	0.72
CO2	0.15	0.08	0.16	0.19	0.16	0.70	0.18	0.03	0.18	0.20	0.16	0.03	0.03	1.65	0.07
TiO2	2.04	0.48	0.44	0.45	0.28	0.48	0.43	0.47	0.44	0.47	0.26	0.02	0.02	0.05	0.07
P2O5	0.30	0.03	0.29	0.08	0.10	0.02	0.14	0.20	0.20	0.31	0.12	ND	ND	0.03	0.05
MnO	0.24	0.05	0.07	0.06	0.05	0.08	0.09	0.09	0.08	1.44	2.86	0.22	0.39	1.59	1.83
S	0.194	0.026	0.038	0.020	0.010	0.058	0.005	0.003	0.058	1.230	8.169	5.70	4.03	15.12	8.22
Ni (ppm)	54	55	62	50	52	48	280	315	305	11	18	16	12	70	16
Cu (ppm)	79	31	46	26	25	30	9	10	20	23	97	14	16	60	48
Zn (ppm)	161	48	67	55	83	51	76	61	50	107	127	36	61	90	234
Pb (ppm)	ND	3	1	2	2	2	28	30	4	92	14	ND	1	ND	ND
Sr (ppm)	208	603	590	615	530	570	635	790	725	843	298	70	65	30	63
Cr (ppm)	104	181		202		185	475	615	475	136	187	204	202	125	95
V (ppm)															
Co (ppm)	64	18	18	15	16	12	36	37	33	7	19	3	3	18	6
Rb (ppm)	44	32	54	36	61	41	60	31	38	93	55	<5	3	7	6
Quartz		8	8	10	8	7	4	4	5	4	57	86	73	65	40
Biotite		7	17	7	18	6	12	10	6	8	5	<=1		<=1	
K-feldspar			8		6					20					
Microcline				5			8			38					3
Plagioclase		35	65	68	68	60	45	15	45	9	2				
Muscovite												TR			
Sillimanite												TR			
Hornblende		10	1	7		5	30	50	40	12	5	3	13	10	20
Anthophyllite															
Garnet										4	16	<1	4	5	25
Gahnite															
Apatite										1					
Sphene		TR		<=1			1	1	1	1	TR				
Zircon		TR		TR			TR			1	TR				
Epidote															
Chlorite															
Sericite		40		2		20	TR	20	3	1	<1				
Carbonate						1				TR			<<1		
Cordierite															
Fe Ti oxides			<1	<=1		<=1	TR	<1	<1	<1				2	6
Sulfides											15	10	10	18	6

Appendix A-4 (Geco Subsurface Sampling)
(all numbers preceded by '60-')

Sample Number	101	102	103a	103b	104	105a	105b	105c	109	109b	110a	110b	108
SiO2	65.10	77.10	76.15	77.90	40.90	74.05	70.20	79.00	36.90	39.80	85.30	86.20	
Al2O3	17.28	11.60	12.19	10.80	13.58	13.46	17.92	9.24	24.96	23.30	8.96	7.80	
Fe2O3	1.73	2.17	0.04	1.59	20.41	0.91	1.10	2.40	5.21	6.34	0.36	0.92	
FeO	1.54	1.14	2.04	2.38	6.40	0.94	0.86	1.00	4.64	6.68	0.44	0.76	
MgO	1.80	0.85	1.15	1.38	0.85	0.51	0.85	0.43	0.16	0.37	0.13	0.23	
CaO	4.45	0.26	1.50	1.35	0.85	0.51	0.85	0.43	0.16	0.37	0.13	0.23	
Na2O	3.66	2.23	1.82	1.48	0.68	2.23	3.13	1.48	1.00	0.08	0.33	0.40	
K2O	3.29	3.40	3.65	2.10	3.72	3.52	2.48	1.38	3.70	5.88	0.22	1.86	
H2O	0.29	0.30	0.82	0.65	2.39	1.82	1.79	0.95	4.06	1.38	1.19	0.91	
CO2	0.31	0.41	0.40	0.32	0.92	0.07	0.07	0.10	ND	0.06	0.09	0.01	
TiO2	0.21	0.07	0.09	0.10	0.15	0.08	0.09	0.13	0.26	0.44	0.09	0.08	
P2O5	0.143	0.001	ND	ND	0.08	0.05	0.002	ND	0.11	0.27	0.01	0.01	
MnO	0.18	0.03	0.11	0.11	0.09	0.03	0.03	0.02	0.31	0.14	0.01	0.01	
S	0.030	0.074	0.680	0.608	16.50	0.544	0.603	0.971	2.636	2.501	0.168	0.400	
Ni (ppm)	27	45	4	12	2	4	5	2	2	1	6	12	
Cu (ppm)	7	63	13	10	140	1130	600	1780	19300	7600	257	955	
Zn (ppm)	62	141	1270	480	10800	196	218	600	3460	1270	23	53	
Pb (ppm)	5	1	7	7	157	491	15	29	612	195	9	7	
Sr (ppm)	783	145	128	113	145	88	205	103	80	71	29	34	
Cr (ppm)	121	196	228	130	95	192	145	259	33	70	385	225	
V (ppm)													
Co (ppm)	9	3	2	2	9	3	4	3	5	9	<10	4	
Rb (ppm)	55	55	112	137	93	68	62	44	72	112	40	34	
Quartz	20	20			5	25	9	50		2	60	60	20
Biotite	7	4			8	4	3	2	20	55			
K-feldspar	40	20			10	22	5				20	20	
Microcline	8	30											
Plagioclase	20	15				30	50	32			5	5	
Muscovite		10			32	12	30	12			15	15	
Sillimanite						6	3	2					
Hornblende													
Anthophyllite													
Garnet						TR							
Gahnite					1					1			10
Apatite		TR											
Sphene					<1		TR						
Zircon						TR			1				
Epidote													
Chlorite					4					2			5
Sericite	4	TR			10	<1		<=1	10	TR	1	1	10
Carbonate													
Cordierite									45	10			30
Kyanite									10	25			
Anhydrite	1												
Fe Ti Oxide													
Sulfide		1			30	1			15	5	2	2	25

Appendix A-4 (Geco Subsurface Sampling)
(all numbers preceded by '80-')

Sample Number	111a	111b	111c	111c2	111d	112	113a1	113a2	113b	113c	113d1	113d2	114
SiO2	74.95	79.20	60.00	78.00	75.90	77.90	75.00	74.05	82.50	71.30	72.50	70.15	79.45
Al2O3	7.26	3.44	5.30	3.50	6.35	2.60	8.30	8.97	5.95	8.64	8.88	8.36	11.37
Fe2O3	4.30	4.44	9.92	4.52	5.10	5.35	3.36	3.78	2.40	3.78	4.36	3.26	1.22
FeO	3.52	3.28	7.58	10.52	3.62	5.64	6.18	6.32	3.78	7.06	7.24	8.04	1.42
MgO	4.75	2.55	4.15	3.10	4.65	1.45	5.31	4.93	3.80	6.45	4.56	5.95	1.55
CaO	0.38	0.23	1.45	0.23	0.57	0.38	0.13	0.13	0.07	0.13	0.34	0.23	0.02
Na2O	0.22	0.17	0.27	0.08	0.22	0.22	0.08	0.08	0.21	0.50	0.08	0.13	0.28
K2O	0.74	0.27	0.18	0.32	0.83	0.36	0.12	0.13	0.05	0.06	0.06		3.12
H2O	1.60	2.06	1.26	0.30	0.79	0.64	1.16	1.04	0.98	1.36	1.25	2.33	1.35
CO2	0.87	0.02	0.04	1.90	0.05	0.08	0.09	0.04	0.12	0.14	0.17	0.32	0.03
TiO2	0.09	0.08	0.17	0.08	0.10	0.12	0.15	0.16	0.11	0.14	0.15		0.15
P2O5	0.02	0.02	0.03	0.02	0.004	0.02	0.03	0.02	ND	0.04	0.04	0.03	ND
MnO	0.13	0.04	0.14	0.03	0.09	0.02	0.08	0.07	0.05	0.11	0.17	0.19	0.03
S	1.611	3.180	7.415	2.891	2.299	4.304	0.227	0.081	0.010	0.055	0.081	1.392	0.007
Ni (ppm)	6	1	54	11	9	4	5	<10	3	<10	1	18	3
Cu (ppm)	5420	22500	56200	38700	7520	6450	455	115	117	5	9	1270	10
Zn (ppm)	1230	1330	3930	162	1370	1010	145	121	54	166	89	570	85
Pb (ppm)	13	12	111	18	9	5	75	70	37	22	68	71	56
Sr (ppm)	79	50	114	38	79	43	23	31	21	23	25	28	26
Cr (ppm)	170	325	185	205	185	205	305	305	420	140	185	300	255
V (ppm)													
Co (ppm)	7	2	4	9	12	22	3	8	4	7	7	5	7
Rb (ppm)	27	5	5	9	27	9	5	4	<10	2	<10	9	67
Quartz	57	74	80	48	77	90	66	70	63	75	50	58	37
Biotite	10	7	5	2	6	3	2	2		2		3	5
K-feldspar		3											38
Microcline													
Plagioclase													
Muscovite													16
Sillimanite										<1			4
Hornblende													
Anthophyllite	8	3		20	2	<1	17	20	25	8	2	3	
Garnet											25		
Gahnite	1		<1		1								
Apatite													
Sphene													
Zircon							<1		1				
Epidote													
Chlorite	10	4	6	5	7	2	5	3	4		2	8	
Sericite		6	1		4	1	2					1	
Carbonate													
Cordierite	13		5	10			7	4	5	12	15	20	
Staurolite											<1	<1	
Fe Ti Oxides										3	5	6	<<1
Sulfides	1	3	3	15	3	4	1	1	2				

Appendix A-4 (Geco Subsurface Sampling)
(all numbers preceded by '80-')

Sample Number	116	117a	117b	118	119	120	202	203	204	205	206	207	208
SiO2	72.60	82.45	79.00	66.30	79.50	84.90	79.59	82.71	79.01	81.65	7.18	62.27	80.21
Al2O3	12.75	10.83	9.02	16.16	8.96	9.76	10.94	5.80	11.61	9.17	10.42	17.22	11.60
Fe2O3	0.82	0.88	1.64	0.87	1.19	1.16	1.11	1.07	1.39	1.25	1.55	4.17	0.88
FeO	3.00	2.28	3.84	3.12	3.60	1.36	3.18	4.06	2.58	2.92	3.68	3.12	1.88
MgO	1.80	0.90	2.10	2.00	1.65	1.05	2.00	0.17	2.22	1.66	2.41	2.31	1.52
CaO	1.60	0.06	0.07	3.20	0.12	0.08	0.12	0.30	0.16	0.01	0.01	3.10	0.00
Na2O	3.83	0.26	0.16	4.26	0.35	0.13	0.23	0.18	0.52	0.36	0.29	3.42	0.19
K2O	2.14	1.19	2.41	2.04	2.05	0.61	1.20	0.75	1.41	1.29	2.28	2.15	2.31
H2O	0.96	0.67	1.12	0.86	1.24	0.45	0.970	2.009	0.989	0.872	1.444	1.219	1.266
CO2	0.01	0.18	0.16	0.08	0.10	0.04	0.046	0.067	0.007	0.048	0.028	0.005	0.028
TiO2	0.25	0.20	0.21	0.65	0.29	0.16	0.38	0.09	0.09	0.08	0.10	0.57	0.09
P2O5	0.05	0.01	ND	0.29	0.03	0.04	0.14	0.00	0.00	0.01	0.00	0.25	0.01
MnO	0.05	0.03	0.05	0.07	0.05	0.02	0.04	0.05	0.03	0.05	0.07	0.06	0.04
S	0.017	0.261	0.315	0.117	0.869	0.003	0.016	0.334	0.003	0.446	0.551	0.300	0.006
Ni (ppm)	2	4	6	14	1	3	2	5	2	5	8	3	7
Cu (ppm)	22	177	205	5	4670	11	66	194	16	2680	496	79	16
Zn (ppm)	47	83	155	75	107	54	61	62	47	2200	430	109	206
Pb (ppm)	116	71	52	105	63	67	1	2	8	4	5	4	<1
Sr (ppm)	318	4	20	835	51	38	25	138	135	25	13	25	20
Cr (ppm)	105	220	175	130	150	285							
V (ppm)													
Co (ppm)	<10	3	3	12	4	1	2	6	6	8	4	4	4
Rb (ppm)	52	42	99	74	64	17	30	18	25	24	39	48	47
Quartz	18	30	27	10	32	20							
Biotite	9	6	12	13	10	6							
K-feldspar	3	50	43	18	27	60							
Microcline													
Plagioclase	65			57									
Muscovite	4	6	7		14								
Sillimanite	<<1	7	8		14	12							
Hornblende													
Anthophyllite													
Garnet													
Gahnite													
Apatite													
Sphene													
Zircon													
Epidote													
Chlorite			2										
Sericite	TR			2									
Carbonate													
Cordierite													
Fe Ti Oxides	1	1		<<1									
Sulfides			1		3	3							

Appendix A-4 (Geco Subsurface Sampling)
(all numbers preceded by '60-')

Sample Number	210	211	212	213	214	215	216	217	218	219	220	221	222	223
SiO2	83.35	79.89	76.57	79.94	84.26	83.40	83.97	79.80	83.10	82.02	85.74	80.88	78.60	60.67
Al2O3	11.08	11.38	13.40	10.31	9.80	8.97	9.73	12.19	9.60	9.89	8.18	8.56	10.01	12.45
Fe2O3	0.50	0.81	1.12	1.10	0.53	0.66	0.47	0.84	0.73	1.06	0.64	1.57	2.11	3.20
FeO	0.22	2.20	3.28	2.14	1.96	1.92	0.66	0.58	1.22	1.56	0.56	1.70	2.24	12.08
MgO	0.15	2.02	2.33	1.53	0.94	1.29	0.45	0.58	0.73	0.61	0.26	0.97	0.94	5.03
CaO	0.03	0.01	0.00	0.01	0.04	0.00	0.01	0.19	0.07	0.08	0.04	0.08	0.00	0.29
Na2O	0.64	0.04	0.06	0.19	0.38	0.17	0.13	0.93	0.35	0.34	0.14	0.47	0.23	0.09
K2O	2.70	1.93	2.04	3.20	1.17	2.50	2.88	3.27	2.49	2.47	1.99	3.53	3.16	1.28
H2O	1.34	1.18	0.99	1.44	0.79	1.15	1.14	1.55	1.19	1.40	1.05	0.81	1.18	4.56
CO2	0.01	0.02	0.03	0.03	0.01	0.02	0.01	0.01	ND	ND	0.01	0.02	0.04	0.13
TiO2	0.10	0.11	0.15	0.15	0.10	0.09	0.09	0.13	0.12	0.09	0.08	0.10	0.10	0.15
P2O5	0.00	0.01	0.01	0.00	0.00	0.00	0.00	0.03	0.02	0.00	0.00	0.00	0.00	0.02
MnO	0.01	0.02	0.02	0.03	0.03	0.03	0.01	0.02	0.02	0.02	0.01	0.04	0.02	0.10
S	0.019	0.003	0.049	0.097	0.128	0.382	0.243	0.075	0.415	0.900	0.209	1.298	1.853	0.472
Ni (ppm)	6	3	2	3	9	5	6	4	6	2	2	2	ND	3
Cu (ppm)	27	27	350	54	104	430	129	375	423	3610	990	5550	5720	1530
Zn (ppm)	20	44	47	90	68	201	59	61	70	195	23	128	137	256
Pb (ppm)	<1	<1	<1	4	<1	<1	2	7	3	1	5	12	<1	<1
Sr (ppm)	25	14	18	20	13	13	8	48	40	14	14	74	8	101
Cr (ppm)														
V (ppm)														
Co (ppm)	4	4	4	9	6	6	7	ND	1	6	1	2	3	11
Rb (ppm)	37	58	48	64	38	54	55	66	39	36	34	76	62	63

Appendix A-4 (Geco Subsurface Sampling)

Sample Number	Geco 1	Geco 2	Geco 3	Geco 4	Geco 5	Geco 6	Geco 7	Geco 8	Geco 9	Geco 10
SiO2	88.20	77.45	83.00	64.65	79.70	79.60	74.45	79.10	77.20	77.60
Al2O3	6.98	12.04	9.60	17.89	9.40	9.64	10.72	9.20	10.50	7.95
Fe2O3	0.85	1.12	1.10	1.38	1.05	0.79	2.25	1.96	1.75	0.86
FeO	1.40	1.16	0.76	1.22	4.06	1.94	3.74	2.38	3.78	3.00
MgO	0.82	0.90	0.40	1.68	1.59	2.59	0.95	0.34	1.74	0.91
CaO	0.09	0.35	0.11	4.35	0.49	2.16	2.36	0.22	0.09	2.98
Na2O	0.10	3.17	0.43	5.55	0.97	0.38	0.60	0.75	0.09	0.45
K2O	2.38	2.18	2.41	1.53	1.63	3.22	2.65	1.48	1.24	0.86
H2O	0.42	1.28	1.09	0.67	0.84	0.66	1.47	0.77	1.10	1.20
CO2	0.18	0.07	0.49	0.12	0.10	0.49	0.33	1.40	0.98	0.69
TiO2	0.07	0.13	0.02	0.31	0.07	0.07	0.08	0.04	0.07	0.01
P2O5	0.003	0.004	0.001	0.140	0.017	0.003	0.008	0.010	0.003	0.010
MnO	0.009	0.013	0.005	0.034	0.034	0.077	0.260	0.003	0.011	0.074
S	0.284	0.025	0.810	0.036	0.146	0.298	0.218	1.96	1.26	0.58
Ni (ppm)	<10	14	<10	38	<10	<10	<10	41	<10	<10
Cu (ppm)	795	3	520	22	142	155	375	230	7400	61
Zn (ppm)	26	48	1760	48	240	101	96	293	147	102

Appendix A-5 (DDH-11-11-5 Yakushavitch Island)
(all numbers preceded by 'S-')

Sample Number	1	2	3	4	5	6	7	8	9	10	11	12	13	14	15
SiO2	60.80	60.85	62.02	66.86	66.36	61.39	59.65	58.16	65.18	65.28	71.22	74.10	36.90	34.64	66.04
Al2O3	18.70	17.05	17.17	13.78	14.21	17.81	18.01	17.47	11.39	13.96	17.31	10.49	7.19	11.64	13.65
Fe2O3	0.69	0.80	1.08	0.91	1.23	0.98	1.25	1.32	1.09	0.32	1.12	3.19	21.93	8.83	0.92
FeO	5.96	4.98	7.72	6.80	6.24	7.02	6.34	6.52	3.88	3.72	3.08	4.72	9.14	9.98	6.66
MgO	3.26	2.56	3.20	1.99	2.04	2.66	3.46	4.47	3.28	4.66	1.86	1.60	6.48	14.77	3.93
CaO	2.39	3.67	1.75	2.43	2.56	1.47	1.70	4.30	6.38	6.92	0.15	0.18	0.23	4.95	2.92
Na2O	2.39	3.56	1.85	2.50	2.97	1.79	1.60	2.57	1.37	1.23	0.28	0.11	0.57	0.97	1.73
K2O	2.88	2.39	2.65	1.54	1.77	2.76	3.42	2.07	1.44	1.23	2.14	1.55	0.26	0.57	1.18
H2O	1.27	1.88	1.14	1.14	1.01	1.19	1.58	2.04	1.28	1.47	1.68	2.31	2.20	1.27	1.82
CO2	0.47	1.44	0.72	1.65	1.05	0.73	2.17	0.45	3.75	1.06	0.18	0.24	0.00	2.87	0.24
TiO2	0.74	0.64	0.69	0.52	0.51	0.62	0.69	0.55	0.19	0.24	0.24	0.19	0.18	0.20	0.40
P2O5	0.19	0.16	0.14	0.17	0.17	0.15	0.22	0.21	0.00	0.01	0.01	0.00	0.00	0.07	0.21
MnO	0.04	0.05	0.07	0.08	0.06	0.06	0.04	0.09	0.08	0.07	0.03	0.03	0.64	0.27	0.08
S	0.048	0.130	0.020	0.057	0.048	0.043	0.284	0.081	0.038	0.284	0.626	1.334	18.090	6.590	0.213
Ni (ppm)	30	53	66	74	100	61	66	58	17	17	13	11	12	10	19
Cu (ppm)	53	69	68	107	82	95	122	59	55	60	875	2700	11250	9250	177
Zn (ppm)	398	118	41	119	115	59	214	79	104	63	2825	900	1338	11400	146
Pb (ppm)	33	4	<1	<1	<1	<1	1	<1	<1	60	10	4	16	53	2
Sr (ppm)	350	500	255	350	395	165	225	405	180	135	75	65	65	50	210
Cr (ppm)															
V (ppm)															
Co (ppm)	27	29	24	26	18	24	22	31	4	5	6	10	83	29	15
Rb (ppm)	72	55	63	54	70	123	74	47	54	18	53	35	10	13	30
Quartz	5			10	8		10	4			45	75	35	5	
Biotite	12			10	8		15	20				7			
K-feldspar	5			3	5		5					2			
Microcline															
Plagioclase	60			60	75		50	65							
Muscovite	3			3	<1		3	1			2	1			
Sillimanite	3			2			3				20	2			
Hornblende															
Anthophyllite													40	55	
Garnet	7			8	2		9	7						10	
Gahnite															
Apatite															
Sphene	<=1				<1		<1	<1			<1				
Zircon															
Epidote															
Chlorite				1				2			2			3	
Sericite	TR			TR			2	1			30	7	5	3	
Carbonate														4	
Cordierite															
Talc														20	
Fe Ti Oxides	3			2	2		3	<<1			<1		1		
Sulfides												6	20		

Appendix A-5 (DDH-11-11-5 Yakushavitch Island)
(all numbers preceded by 'S-')

Sample Number	16	17	18	19	20	21	22	23	24	25	26	27	28	29	30
SiO2	79.00	73.97	73.62	69.83	73.53	73.65	71.99	72.05	67.88	73.37	63.44	75.19	75.26	74.48	57.01
Al2O3	9.07	12.97	12.64	13.17	11.97	12.45	11.98	11.78	8.05	11.61	12.39	12.16	11.90	12.68	17.75
Fe2O3	3.75	0.53	0.59	1.54	0.58	0.59	0.83	0.53	0.75	1.91	0.50	0.72	0.45	0.61	0.94
FeO	0.24	3.84	3.48	6.36	5.16	5.40	6.28	5.66	4.60	2.84	3.72	3.24	2.92	3.44	7.66
MgO	2.76	3.24	3.23	2.23	2.67	2.93	3.03	3.39	4.88	3.22	3.65	2.11	2.09	2.03	3.72
CaO	2.27	0.61	0.88	0.52	1.70	1.30	1.55	1.94	8.88	1.41	8.48	0.91	1.98	1.03	3.85
Na2O	1.40	0.91	1.17	0.74	1.60	1.29	1.31	1.42	0.56	2.06	0.67	1.30	2.31	1.53	2.17
K2O	0.29	1.80	1.71	1.32	1.13	1.23	1.09	1.02	0.87	1.54	1.49	2.12	0.99	1.93	2.05
H2O	0.87	1.36	2.38	1.79	1.07	1.21	1.12	1.48	1.37	1.75	3.34	1.89	1.45	1.82	3.18
CO2	0.24	0.40	0.19	1.19	0.25	0.27	0.27	0.28	1.89	0.17	2.16	0.18	0.21	0.39	0.52
TiO2	0.14	0.21	0.22	0.26	0.24	0.26	0.24	0.22	0.15	0.27	0.19	0.20	0.19	0.21	0.74
P2O5	0.00	0.00	0.02	0.00	0.01	0.00	0.00	0.00	0.36	0.00	0.01	0.00	0.00	0.02	0.29
MnO	0.03	0.03	0.03	0.03	0.14	0.14	0.15	0.13	0.13	0.05	0.06	0.04	0.04	0.04	0.11
S	0.302	0.037	0.016	2.402	0.021	0.071	0.076	0.076	0.093	0.021	0.020	0.027	0.032	0.010	0.296
Ni (ppm)	24	15	15	48	17	17	20	18	17	17	16	18	18	20	71
Cu (ppm)	97	61	55	232	63	76	86	75	83	65	67	51	38	47	73
Zn (ppm)	53	70	96	156	126	117	86	94	63	104	53	47	50	45	107
Pb (ppm)	20	<1	4	2	<1	1	1	<1	<1	2	<1	1	7	<1	<1
Sr (ppm)	205	155	170	125	205	84	72	92	102	79	5	79	138	107	433
Cr (ppm)															
V (ppm)															
Co (ppm)	4	7	7	15	53	7	5	4	2	3	5	6	4	7	30
Rb (ppm)	4	56	51	48	39	31	25	19	20	31	30	46	24		7
Quartz	62		45		60				47				50		20
Biotite	4		13		12								8		10
K-feldspar															
Microcline															
Plagioclase	23		25		15								40		60
Muscovite			6												
Sillimanite			6		3										
Hornblende															
Anthophyllite	7														
Garnet					7										2
Gahnite															
Apatite															
Sphene															
Zircon															
Epidote															
Chlorite	2														4
Sericite			5		2				3				2		4
Carbonate															
Cordierite					1										
Staurolite	2														
Clinopyroxene									50						
Fe Ti Oxides									<1				<<1		
Sulfides	<1														

Appendix A-5 (DDH-11-11-3 Yakushavitch Island)
(all numbers preceded by 'S-')

Sample Number	31	32	33	34	35	36	37	38	39	40	41	42	44	45	46	47
SiO2	52.59	61.01	64.12	64.66	64.40	78.56	66.71	65.43	61.50	59.17	51.11	65.69	63.06	76.08	67.08	72.22
Al2O3	21.71	16.79	16.33	15.46	16.11	10.73	15.01	15.81	17.49	17.63	20.39	14.55	15.37	10.92	10.15	10.37
Fe2O3	1.59	0.88	0.83	0.68	0.99	4.47	0.78	0.82	1.94	3.08	1.43	0.99	1.38	1.08	3.78	1.25
FeO	8.70	7.18	6.16	5.94	5.86	6.24	6.72	6.56	6.00	4.68	8.32	6.24	6.64	3.08	5.98	4.24
MgO	4.25	2.77	2.20	2.59	2.31	2.44	2.09	2.46	3.72	3.96	4.43	2.43	2.44	2.54	5.92	4.03
CaO	0.74	1.65	2.93	3.21	2.32	0.28	2.22	1.87	1.25	2.06	2.44	2.38	2.47	1.21	0.07	1.78
Na2O	0.36	2.11	3.52	3.17	3.06	0.12	3.01	2.30	1.57	2.53	3.63	2.91	2.74	1.35	0.31	1.67
K2O	4.00	3.03	1.86	1.96	2.31	1.64	1.83	2.49	4.15	4.39	4.60	2.09	2.43	1.51	2.19	0.78
H2O	4.01	2.89	1.06	0.98	0.63	0.67	0.85	0.72	0.85	0.77	1.72	1.13	1.45	1.53	2.00	1.98
CO2	0.97	1.11	0.43	0.27	1.25	0.83	0.42	0.81	0.27	0.08	0.74	0.85	0.98	0.31	0.02	0.03
TiO2	0.87	0.66	0.47	0.50	0.56	0.08	0.51	0.57	0.63	0.60	0.92	0.55	0.63	0.18	0.22	0.22
P2O5	0.20	0.20	0.10	0.24	0.16	0.00	0.12	0.22	0.30	0.29	0.06	0.29	0.12	0.04	0.00	0.11
MnO	0.09	0.06	0.12	0.08	0.06	0.05	0.07	0.06	0.07	0.07	0.14	0.06	0.06	0.03	0.07	0.04
S	0.060	0.010	0.080	0.050	0.013	0.074	0.045	0.060	0.652	0.795	0.903	0.034	0.320	0.120	2.127	1.784
Ni (ppm)	70	58	38	56	48	48	47	46	54	37	66	49	59	19	15	23
Cu (ppm)	69	66	82	58	92	86	54	53	65	130	428	46	90	51	1550	182
Zn (ppm)	126	189	102	75	83	75	57	72	109	145	239	71	103	335	1100	194
Pb (ppm)	<1	<1	13	5	<1	1	8	1	<1	<1	7	<1	<1	<1	84	<1
Sr (ppm)	27	205	289	369	293	340	283	233	64	80	280	280	273	91	30	155
Cr (ppm)																
V (ppm)																
Co (ppm)	24	22	14	22	19	19	18	21	25	15	26	19	20	2	7	6
Rb (ppm)	80	64	55	44	68	55	44	62	75	73	153	44	51	41	47	16

APPENDIX B

Chemical Analyses of Selected Rocks from the literature

Appendix B-1

SAMPLE #	DESCRIPTION	SiO2	Al2O3	Fe2O3	FeO	MgO	CaO	Na2O	K2O	H2O	CO2	TiO2	P2O5	MNO	S	REFERENCE
lt 100	average of 198 basalts	49.90	16.00	5.50	6.50	6.30	9.10	3.20	1.60			1.40	0.50			Daly, 1933
lt 101	average of 72 calc-alkaline granites	72.08	13.86	0.86	1.67	0.57	1.33	3.08	5.46	0.53		0.37	0.18	0.06		Nockolds, 1954
lt 102	average of 48 alkaline granites	73.86	13.75	0.78	1.13	0.26	0.72	3.51	5.13	0.47		0.20	0.14	0.05		Ibid
lt 103	average of 137 granodiorites	66.88	15.66	1.33	2.59	1.57	3.56	3.84	3.07	0.65		0.57	0.21	0.07		Ibid
lt 104	average of 58 quartz diorites	66.15	15.56	1.36	3.42	1.94	4.65	3.90	1.42	0.69		0.62	0.21	0.08		Ibid
lt 105	average of 50 diorites	51.86	16.40	2.73	6.97	6.12	8.40	3.36	1.33	0.80		1.50	0.35	0.18		Ibid
lt 106	average of 38 pyroxene gabbros	50.78	15.68	2.26	7.41	8.35	10.85	2.14	0.56	0.48		1.13	0.18	0.18		Ibid
lt 107	average of 53 divine gabbros	46.83	17.38	1.91	8.20	10.03	11.36	2.03	0.40	0.63		0.97	0.12	0.14		Ibid
lt108	average of 42 alkaline gabbros	43.94	14.87	4.35	7.80	9.31	12.37	2.32	0.92	0.66		2.86	0.44	0.16		Ibid
lt 109	average shale	53.80	15.47	4.03	2.46	2.45	3.12	1.31	3.25	5.02	2.64	0.65		tr.		Garrels and MacKenzie, 197
lt 110	average slate	60.64	17.32	2.25	3.66	2.60	1.54	1.19	3.69	4.13	1.47	0.73				Ibid
lt 111	average low grade pelite	59.93	16.62	3.03	3.18	2.63	2.18	1.73	3.54	4.34	2.31	0.85				Ibid
lt 112	average high grade pelite	63.51	17.35	2.00	4.71	2.31	1.24	1.96	3.35	2.42	0.22	0.79				Ibid
lt 113	average sandstone	77.60	7.10	1.70	1.50	1.20	3.10	1.20	1.30	2.10	2.50	0.40				Ibid
LT 114	Average limestone	0.73	0.00	0.20	1.03	20.48	30.97	0.00	0.00	0.00	47.51	0.00		0.00		Garrels and MacKenzie, 197
LT 98	average of 52 metapelites from Namagualand (cord-garn-sill quartz)	54.73	25.22	4.43	2.96	2.31	0.30	2.12	6.58			1.09	0.07	0.05		Zelt, 1980
LT 99	Average of 51 metapelites from Namagualand (cord-garn-sill)	67.26	14.63	2.03	5.04	4.55	0.45	0.77	3.45			0.80	0.02	0.06		Zelt, 1980
Lt 163	Ocean ridge tholeitic basalt (average)	49.34	17.02	9.56		7.19	11.72	2.73	0.16			1.49	0.16	0.17		Engel et al., 1965.00
LT 164	Alkaline basalt (average)	47.41	18.02	10.61		4.79	8.65	3.99	1.66			2.87	0.92	0.16		Engel et al., 1965.00
LT 165	Ocean ridge tholeitic basalt (average)	50.61	13.24	12.43		2.73	11.10	2.10	0.52			3.02	0.95	0.12		Nockolds and Allen, 1954
LT 166	Island arc tholeitic basalt (average)	51.57	15.91	10.56		6.73	11.74	2.41	0.44			0.80	0.11	0.17		Jakes and White, 1971
LT 167	High Al Island arc basalt (average)	50.59	16.29	9.30		8.96	9.50	2.89	1.07			1.05	0.21	0.17		Jakes and White, 1971
LT 168	Island arc Shoshanite (average)	53.74	15.84	8.63		6.36	7.90	2.38	2.57			1.05	0.54	0.11		Jakes and White, 1971
LT 169	Tholeitic picrite basalt	46.40	8.50	2.50	9.80	20.80	7.40	1.60	0.30			2.00	0.20	0.20		Irvine and Baragar, 1971
LT 170	Olivine tholeite basalt	49.16	13.33	1.31	9.71	10.41	10.93	2.15	0.51			2.29	0.16	0.16		Ibid
LT 171	Tholeite basalt	53.80	13.90	2.60	9.30	4.10	7.90	3.00	1.50			2.00	0.40	0.20		IBID
LT 172	Tholeitic andesite	58.31	13.77	3.37	6.48	2.27	5.58	3.91	1.88			1.71	0.46	0.23		Ibid
LT 173	Icelandite	61.76	15.36	2.35	5.84	1.76	5.04	4.37	1.62			1.27	0.44	0.19		Ibid
LT 174	High Al, calc-alkaline basalt	49.15	17.73	2.76	7.20	6.91	9.91	2.88	0.72			1.52	0.26	0.14		Irvine and Baragar, 1971

SAMPLE #	DESCRIPTION	SiO2	Al2O3	Fe2O3	FeO	MgO	CaO	Na2O	K2O	H2O	CO2	TiO2	P2O5	MnO	S	Reference
LT 175	High Al, calc-alkaline andesite	58.65	17.43	3.21	3.48	3.28	6.26	3.22	1.99			0.79	0.18	0.10		Ibid
LT 176	Calc-alkaline andesite	60.00	16.00	1.89	6.20	3.90	5.87	3.85	0.87			1.04	0.23	0.16		Ibid
LT 177	Calc-alkaline dacite	69.68	15.21	1.08	1.90	0.91	2.70	4.47	3.01			0.36	0.10	0.04		Ibid
LT 178	Calc-alkaline rhyolite	73.23	14.03	0.60	1.70	0.35	1.32	3.94	4.08			0.24	0.05	0.02		Ibid
LT 179	Peralkaline rock Pantallerite	69.80	7.40	2.42	6.15	0.05	0.45	6.70	4.30			0.45	0.15	0.32		Ibid
LT 180	Peralkaline rock Comendite	75.23	11.99	0.90	1.25	0.02	0.27	4.79	4.67			0.13	0.09	0.08		Ibid
LT 181	Alkalic Picrite basalt (Alkaline olivine basalt series)	46.57	8.20	1.20	9.75	19.65	9.43	1.56	1.18			1.85	0.26	0.14		Ibid
LT 182	Ankaranite (alkaline olivine basalt series)	44.10	12.10	3.20	9.60	13.00	11.50	1.90	0.70			2.70	0.30	0.30		Ibid
LT 183	K poor alkaline olivine basalt	45.40	14.70	4.10	9.20	7.80	10.50	3.00	1.00			3.00	0.40	0.20		Ibid
LT 184	K rich alkaline olivine basalt	42.43	14.15	5.84	8.48	6.71	11.91	2.77	2.04			4.11	0.58	0.17		Ibid
LT 185	Trachybasalt (alkaline olivine basalt series)	46.48	16.68	4.12	7.30	4.65	9.40	3.80	3.07			3.10	0.90	0.18		Ibid
LT 186	Hawaiite (alkaline olivine basalt series)	47.90	15.90	4.90	7.60	4.80	8.00	4.20	1.50			3.40	0.70	0.20		Ibid
LT 187	Mugearite (alkaline olivine basalt series)	49.68	16.99	3.45	8.99	2.79	5.46	5.78	1.90			2.13	0.48	0.27		Ibid
LT 188	Tristanite (alkaline olivine basalt series)	55.85	18.98	2.59	3.11	2.04	4.51	5.16	4.08			1.80	0.39	0.12		Ibid
LT 189	Bennorite (alkaline olivine basalt series)	55.64	16.38	3.05	4.91	1.06	2.90	6.07	3.49			0.89	0.66	0.18		Ibid
LT 190	Phonolite (alkaline olivine basalt series)	60.64	18.29	2.75	1.18	0.09	0.83	8.93	5.10			0.04	0.00	0.23		Ibid
LT 191	Trachyite (alkaline olivine basalt series)	60.70	20.50	2.30	0.40	0.20	1.40	6.20	6.70			0.50	0.03	0.20		Ibid
LT 192	Nephelinite	39.70	11.40	5.30	8.20	12.10	12.80	3.80	1.20			2.80	0.90	0.20		Ibid
LT 193	Analicite	49.00	13.00	4.90	4.50	8.30	11.50	3.90	3.00			0.70	1.10	0.10		Ibid
LT 194	Leucitite	46.24	14.42	4.06	4.36	6.99	13.24	1.65	6.37			1.17	0.41	0.00		Ibid
LT 195	Wyomingite	54.09	9.94	3.15	1.48	6.99	4.71	1.36	11.38			2.35	1.79	0.06		Ibid
LT 196	Average of 27 Mesozoic and Cenozoic shales	55.40	13.80	4.00	1.70	2.70	6.00	1.80	2.70		4.60	0.50	0.20	tr.		Blatt et al., 1972.00
LT 197	Average of 51 Paleozoic shales	60.20	16.40	4.00	2.90	2.30	1.40	1.00	3.60		1.50	0.80	0.20	tr.		Ibid
LT 198	Average of 4030 mudrocks, Russia	56.20	15.10	3.40	2.30	2.10	4.40	1.10	2.60		3.30	0.80	0.10	0.10		Ibid
LT 199	Average of 11151 mudrocks, Russia	53.40	16.40	3.40	2.80	2.40	5.80	1.10	2.70		4.30	0.70	0.20	0.10		Ibid

SAMPLE #	DESCRIPTION	SiO2	Al2O3	Fe2O3	FeO	MgO	CaO	Na2O	K2O	H2O	CO2	TiO2	P2O5	MnO	S	Reference
LT 200	Average of 69 slates	58.50	17.30	3.00	4.40	2.60	1.30	1.20	3.70		1.20	0.80	0.10	0.10		Blatt et al., 1972
LT 201	Average of 26 orthoquartzites	95.40	1.10	0.40	0.20	0.10	1.60	0.10	0.20		1.10					Ibid
LT 202	Average of 20 lithic arenites	66.10	8.10	3.80	1.40	2.40	6.20	0.90	1.30		5.00					Ibid
LT 203	Average of 61 greywackes	66.70	13.50	1.60	3.50	2.10	2.50	2.90	2.00		1.20					Ibid
LT 204	Average of 32 arkoses	77.10	8.70	1.50	0.70	0.50	2.70	1.50	2.80		3.00					Ibid
LT 205	Average of 17 greywackes (Hartz)	69.70	14.30	1.90	2.40	1.80	1.30	3.10	1.40		0.90					Ibid
LT 206	Average of 6 sandstones (Charny)	71.50	13.40	1.30	3.60	1.00	1.00	2.80	1.60		0.60					Ibid
LT 207	Average of 4 sandstones (Charny)	69.90	15.10	4.90	1.50	0.80	0.60	2.10	2.90		0.20					Ibid
LT 208	Average of 96 Jurassic sublitharenites	84.01	2.57	0.17	0.26	0.67	5.41	0.17	0.86		4.65	0.05	0.04	0.04		Pettyohn, 1975
LT 209	Average of 10 Oligocene lithic arenites	65.00	9.57	1.59	1.08	0.40	10.10	2.14	1.43		6.90	0.00	0.00	0.00		Ibid
LT 210	Calcareous subgreywacke	56.80	8.48	1.67	0.00	1.24	15.25	1.31	1.46		12.95	0.10	0.00	0.00		Ibid
LT 211	Calcareous subgreywacke	51.52	5.77	2.43	0.00	0.95	16.96	1.32	1.90		13.34	0.32	0.00	0.14		Ibid
LT 212	Mississipian sublitharenite	92.91	3.78	0.00	0.91	0.00	0.31	0.34	0.61		0.00	0.00	0.00	0.00		Ibid
LT 213	Calcareous subgreywacke	47.75	6.41	2.39	0.00	4.48	18.75	1.20	1.02		17.78	0.20	0.10	0.00		Ibid
LT 214	Carboniferous calcareous subgreywacke	40.35	2.43	3.27	0.00	10.28	12.00	0.54	0.93		17.80	0.30	0.00	0.00		Ibid
LT 215	Carboniferous subgreywacke	74.45	10.83	4.62	0.00	1.30	0.35	1.07	1.51		0.00	0.50	0.00	0.00		Ibid
LT 216	Archean Greywacke Ontario	60.51	15.36	0.76	7.63	3.29	2.14	2.50	1.69		1.01	0.87	0.27	0.16		Ibid
LT 217	Average of 3 Archean greywackes (N.W.T. Can)	66.24	15.28	0.70	4.53	2.74	1.70	3.12	1.91		0.38	0.64	0.12	0.06		Ibid
LT 218	Tyler Slate, Wisc. USA Animikean	76.84	11.76	0.55	2.88	1.39	0.70	2.57	1.62		0.00	0.00	0.00	0.00		Ibid
LT 219	Greywacke, Arkansas, USA Carboniferous	74.43	11.32	0.81	3.88	1.30	1.17	1.63	1.74		0.48	0.83	0.18	0.04		Ibid

B-2 Iron Formations

SAMPLE #	DESCRIPTION	SiO2	Al2O3	Fe2O3	FeO	MgO	CaO	Na2O	K2O	H2O	CO2	TiO2	P2O5	MnO	S	Reference
LT 63	Yilgarn Block, Aust. (Archean)	79.07	0.70	18.98	23.65	3.46	2.68	0.11	0.10			0.04	0.16	0.55		Gole and Klein,
LT 64	Montana (Archean)	45.53	1.80	26.91	17.51	3.82	3.01	0.34	0.07			0.06	0.29	0.64		Ibid
LT 65	Maira Mamba (Proterozoic)	49.16	1.64	12.93	25.49	5.03	3.79	0.38	0.43			0.18	0.08	0.13		Ibid
LT 66	Hammerseley Basin Dales Gorge Member (Proterozoic)	46.20	1.03	18.40	23.88	3.15	5.22	0.50	0.81			0.04	0.31	0.18		Ibid
LT 67	Hammerseley Basin Joffre Member (Proterozoic)	43.31	1.72	20.16	22.53	4.86	4.97	0.39	1.15			0.07	0.25	0.36		Ibid
LT 68	Labrador Trough; Unmetamorphosed (Proterozoic)	47.81	0.62	19.96	21.69	4.00	4.30	0.17	0.20			0.04	0.04	1.15		Ibid
LT 69	Labrador Trough; Metamorphosed (Proterozoic)	44.33	0.74	16.87	23.68	6.25	6.55	0.21	0.10			0.10	0.06	1.01		Ibid
LT 70	Biwabik Proterozoic	50.62	1.13	20.28	21.43	3.17	1.98	0.06	0.17			0.06	0.09	0.73		Ibid
LT 71	Carter Ck. Ruby Range, Montana	44.02	0.66	32.29	17.14	3.21	1.37	0.06	0.02		0.15	0.01	0.55	0.04		Bagley and James, 1973
LT 72	Carter Ck. Ruby Range, Montana	45.20	0.73	38.05	10.99	2.14	1.22	0.58	0.21		0.01	0.01	0.51	0.06		Ibid
LT 73	Kelly, Ruby Range, Montana	40.00	1.95	32.91	18.87	2.47	1.87	0.12	0.56		0.15	0.08	0.10	0.73		Ibid
LT 74	Kelly, Ruby Range, Montana	39.58	2.47	32.07	19.22	2.41	1.90	0.09	0.85		0.16	0.10	0.09	0.75		Ibid
LT 75	Black Butte, Ruby Range, Montana	51.42	1.75	18.24	22.00	2.97	2.15	0.17	0.05		0.05	0.08	0.08	0.13		Ibid
LT 76	Black Butte, Ruby Range, Montana	50.80	1.04	25.66	16.64	2.07	2.65	0.12	0.02		0.00	0.03	0.05	0.07		Ibid
LT 77	Hotazel bedded iron formation, S. Africa	53.00	0.13	45.20	0.43	0.02	0.48	0.09	0.06		0.20					Beukes, 1973
LT 78	Smartt bedded iron formation, S. Africa	55.00	0.33	39.80	1.11	0.10	0.20	0.08	0.14		2.09					Ibid
LT 79	Black Rock, S. Africa	47.00	0.45	48.90	0.22	0.01	0.17	0.12	0.53		0.34					Ibid
LT 80	Average of 10 Mn ore samples, Hotazel	7.75	0.72	10.51		1.47	1.83	0.07	0.77		0.40					Ibid
LT 81	Silicate-Sulfide IF, Isua belt, W. Greenland	56.60	2.91	12.07	3.67	10.78	6.16	1.22	0.07		0.02	0.45	0.06	0.30		Appel, 1979
LT 82	Gogebic, US siderite facies	39.26	2.88	0.63	29.94	4.62	4.62	0.00	0.00		20.46	0.07	0.11	1.23		Bagley and James, 1973
LT 83	Gogebic, US Jasper-magnetite facies	34.44	0.85	30.54	22.06	2.30	1.72	0.00	0.13		7.36	0.02	0.07	0.21		Bagley and James, 1973
LT 84	Riverton, US carbonate facies	32.20	1.50	0.60	31.60	2.80	1.60	0.00	0.20		24.80	0.00	0.80	1.90		James, 1954

SAMPLE #	DESCRIPTION	SiO2	Al2O3	Fe2O3	FeO	MgO	CaO	Na2O	K2O	H2O	CO2	TiO2	P2O5	MnO	S	Reference
LT 85	Schistose Itabrite Damara Supergroup, S. Africa	22.00	0.10	65.20		4.20	5.75	0.10	0.01			0.06	1.40			Beukes, 1973
LT 86	Itabrite, Damara Supergroup, S. Africa	42.30	0.30	55.30		0.16	0.17	0.00	0.01			0.12	0.74			Beukes, 1973
LT 87	IF, Marquette Range, U.S.	42.37		1.09	31.41	2.48	0.50	0.00			21.80					James, 1954
LT 88	IF, Marquette Range, U.S.	26.97	1.30	2.31	39.70	1.84	0.66	0.00	0.00		26.20			0.29		James, 1966
LT 89	Sokoman Formation, Labrador Trough (lower IF)	40.90	0.48		20.70	5.14	8.67	0.006	0.17		23.10	0.066	0.066	0.50		Klein and Funk, 1976
LT 90	Sokoman Formation, Labrador Trough (lower IF)	29.60	0.78	11.70	32.00	3.62	2.73	0.006	0.25		18.10	0.045	0.06	0.85		Ibid
LT 91	Sokoman Formation, Labrador Trough (average of 2 analyses of lower fa)	29.80	1.16	9.46	33.20	3.98	1.33	0.061	0.33		18.10	0.133	0.085	0.90		Ibid
LT 92	Sokoman Formation, Labrador Trough (average of 3 analyses of lean iron formation)	30.70	0.50	10.71	35.13	3.40	5.19	0.034	0.22		9.73	0.075	0.11	1.32		Ibid
LT 93	Sokoman Formation, Labrador Trough, lower green-red chert	14.00	0.90	37.00	21.50	4.35	4.35	0.052	0.25		15.70	0.029	0.09	2.13		Ibid
LT 94	Sokoman Formation, Labrador, lover green-red-chert	36.00	0.38	33.40	20.70	1.38	1.98	0.004	0.16		5.70		0.027	0.66		Ibid
LT 95	Sokoman Formation, Labrador, pink-grey chert	48.90	0.39	3.58	19.40	2.10	6.84	0.007	0.13		17.20	0.053	0.005	1.75		Ibid
LT 96	Sokoman Formation, green chert	82.60	0.52	1.08	7.67	1.19		0.004	0.077		4.20		0.003	1.80		Ibid
LT 97	Sokoman Formation, Labrador, Jasper of Upper iron formation	46.70	0.07	19.80	9.36	3.82	7.83	0.009	0.09		11.30		0.014	1.70		Ibid

Appendix B-3 Broken Hill rocks (N.S.W., Australia)

SAMPLE #	DESCRIPTION	SiO2	Al2O3	Fe2O3	FeO	MgO	CaO	Na2O	K2O	H2O	CO2	TiO2	P2O5	MnO	S	Reference
LT 6	Platey gneiss (granitic composition)	68.13	15.99	0.18	4.42	0.43	4.88	0.67	4.56		0.02	0.62		0.23		Joplin, 1963
LT 7	granulite (granitic composition)	67.24	13.67	2.93	5.00	1.81	4.25	1.04	2.04		0.12	0.67		1.03		Ibid
LT 8	granulite (granitic composition)	67.09	14.57	0.17	6.33	0.96	4.10	0.35	4.03		0.04	0.65		0.99		Ibid
LT 9	Footwall gneiss (granitic composition)	66.38	16.60	1.43	5.27	0.64	5.00	0.91	1.23		0.10	0.53		0.50		Ibid
LT 10	Flaser gneiss (granitic composition)	68.97	16.45	0.36	3.38	1.00	4.32	3.14	1.28			0.10	0.26	0.03	0.01	Ibid
LT 11	granulite (dioritic composition)	60.34	19.10	0.64	7.89	0.62	4.86	0.26	3.83		0.04	0.93		0.93		Ibid
LT 12	granulite (dioritic composition)	64.10	14.23	0.17	8.71	1.15	5.20	0.21	3.34		0.03	0.82		0.83		Ibid
LT 13	Footwall gneiss (dioritic composition)	58.22	19.02	2.90	5.85	1.58	5.04	2.95	1.91			0.92	0.10	0.28		Ibid
LT 14	Non-calcareous pelite	79.20	11.50	0.28	3.48	0.25	2.89	0.65	1.20		0.06	0.26		0.18		Ibid
LT 15	Garn-sill-cord gneiss	71.68	14.20	2.40	3.92	2.37	1.25	1.18	1.44		0.09	0.68		0.18		Ibid
LT 16	Garn-or. rock	59.12	14.66	0.30	8.66	1.20	0.56	0.34	5.60			0.93	0.20	7.79		Ibid
LT 17	Biot-or. rock	59.16	17.83	0.03	5.67	0.81	0.57	0.64	8.74			0.66	0.54	0.68		Ibid
LT 18	Garn-sill-cord gneiss	62.56	19.41	0.70	7.20	2.12	2.22	1.86	2.41		0.02	0.72	0.07	0.29		Ibid
LT 19	Garn-feldspar rock	53.88	15.80	5.00	16.30	2.73	1.34	0.66	2.28		0.14	0.50	0.05	0.59		Ibid
LT 20	Sill gneiss	59.76	20.08	2.20	7.38	2.32	0.40	0.99	3.76		0.01	1.05	0.19	0.18		Ibid
LT 21	Garn-cord-sill gneiss	59.18	24.02	0.50	6.26	1.67	0.56	1.07	4.83		0.05	0.88		0.08		Ibid
LT 22	Sericite schist	58.88	21.83	4.60	2.25	1.03	0.54	0.66	5.94		0.01	0.52	0.18	0.03		Ibid
LT 23	Sericite schist	57.92	21.30	1.60	5.67	1.91	0.58	1.08	5.41			0.70	0.11	0.10		Ibid
LT 24	Schist	57.70	21.48	1.75	5.58	1.82	0.46	1.09	5.39			0.70	0.16	0.10		Ibid
LT 25	Garn-biot-ser schist	56.63	22.25	0.57	6.87	1.54	0.65	0.24	6.84			0.93	0.17	0.71		Ibid
LT 26	Garn-cord-sill gneiss	54.02	27.24	1.45	7.56	2.13	0.62	0.60	4.21		0.06	1.20		0.20		Ibid
LT 27	Schist	60.46	25.93	0.11	6.76	0.50	1.27	0.64	3.54		0.21	0.31		0.24		Ibid
LT 28	Garn-cord-sill gneiss	60.30	23.60	0.30	7.20	1.60	1.30	1.10	3.20		0.03	0.80		0.30		Ibid
LT 29	Garn-cord-sill gneiss	60.02	22.82	0.46	7.35	0.75	2.32	0.73	3.21		0.06	1.52		0.05		Ibid
LT 30	Garn-cord-sill gneiss	58.72	22.44	0.18	8.88	2.02	1.35	0.32	4.50		0.05	0.66		0.54		Ibid
LT 31	Garn-cord-sill gneiss	57.49	22.99	0.37	8.42	0.90	1.57	2.24	3.01		0.05	1.21		0.20		Ibid
LT 32	Garn-sill schist	53.36	25.36	0.70	7.83	2.11	1.22	0.76	4.75		0.05	1.20	0.14	0.20		Ibid
LT 33	Ba-rich rock	55.12	20.72	0.75	0.36		10.08	1.13	0.39			0.65	0.25			Ibid
LT 34	Ba-rich gneiss	49.10	25.43	0.04	0.19		7.65	1.68	0.73			0.17	0.06		0.04	Ibid
LT 35	Almandine-spessartine iron formation (lean)	31.34	8.34	32.60	6.75	0.94	7.54	0.11	0.05			0.40	4.68			Ibid
LT 36	Magnetite-spessartine actinolite schist	27.29	5.21	7.30	37.64	2.81	6.06	0.01				1.43	0.31			Ibid
LT 37	Garn-qtz-mgt rock	53.73	11.57	13.15	14.41	2.11	1.79	0.15				1.14	0.53			Ibid
LT 38	Garn-mgt schist	57.78	12.02	7.35	4.98	1.79	2.85	1.70	1.47			0.73	1.16			Ibid
LT 169	iron formation	17.25	6.76	44.87	24.17	0.79	2.24					0.73	1.36	1.20		Richards, 1966
LT 170	iron formation			27.25	19.75									3.55		Ibid
LT 171	iron formation	42.29	10.63	15.48	17.77	1.51	3.67					0.38	1.93	6.32		Ibid
LT 172	iron formation	38.37	14.46	12.79	17.38	1.67	4.06					0.68	2.11	6.88		Ibid
LT 173	iron formation	44.12	13.19	9.16	18.99	1.44	4.44					0.50	2.57	3.80		Ibid
LT 174	iron formation	56.68	12.71	4.06	11.80		4.54					0.36	2.03	6.37		Ibid
LT 175	iron formation	33.52	19.17	4.53	31.34		4.05					1.11	1.77	0.95		Ibid

Appendix B-4 Rocks from Montauban
(from Stamatelopoulou-Seymour + MacLean, 1977)

SAMPLE Number	Comments	SiO2	Al2O3	Fe2O3	FeO	MgO	CaO	Na2O	K2O	TiO2	P2O5	MnO
A 31	Leptite	75.33	11.35	4.30		1.97	4.61	0.81	1.03	0.47	0.14	
A 38	Leptite	67.35	14.91	6.72		1.38	3.83	3.29	1.66	0.61	0.25	
A 39	Leptite	65.01	16.71	6.31		0.99	2.81	2.93	4.81	0.43	0.00	
A 69	Leptite	76.91	10.31	3.37		2.23	5.54	0.44	0.61	0.39	0.20	
A 70	Leptite	71.69	13.89	4.05		1.53	4.97	0.74	2.46	0.45	0.18	
A 77	Leptite	74.71	12.55	3.08		0.73	1.11	2.97	4.45	0.30	0.08	
A 80	Leptite	69.65	15.22	4.48		1.74	2.52	3.84	2.02	0.40	0.11	
A 84	Leptite	75.26	13.21	3.69		0.98	1.74	2.14	2.32	0.62	0.03	
A 88	Leptite	76.93	12.34	2.10		1.19	2.02	2.04	3.16	0.16	0.06	
A 89	Leptite	68.74	15.57	3.84		2.30	1.59	4.90	2.49	0.37	0.14	
A 90	Leptite	64.56	16.48	6.43		3.75	1.80	2.04	4.28	0.65	0.00	
A 121	Leptite	75.14	13.09	3.70		0.60	1.32	4.12	1.66	0.30	0.07	
A 33	Leptite	86.44	7.53	1.41		0.44	0.78	2.48	0.69	0.17	0.06	
A 34	Leptite	80.27	10.93	1.74		0.54	0.65	4.41	1.23	0.21	0.00	
A 35	Leptite	85.66	8.74	1.95		0.51	1.04	0.85	1.01	0.24	0.00	
A 123	Leptite	89.34	6.55	0.42		0.26	1.64	1.31	0.36	0.07	0.04	
A 101	Cord. Gneisses	82.76	7.18	5.51		3.16	0.29	0.02	0.87	0.17	0.03	
A 133	Cord. Gneisses	70.43	12.54	0.70	4.89	5.68	1.25	0.32	3.59	0.54	0.25	0.21
A 10	Composite Gneisses	50.23	17.08	10.52		7.70	9.43	3.56	0.57	0.69	0.22	

Appendix B-5 Additional Analyses for Sherridon, Man. (from Goetz, 1980)

SAMPLE Number	Comments	SiO2	Al2O3	Fe2O3	FeO	MgO	CaO	Na2O	K2O	H2O	CO2	TiO2	P2O5	MnO
LT 115	Biotite gneiss (Sherridon) Unit 5 (average of 33 samples)	74.43	11.77	0.46	3.05	1.92	2.24	1.74	2.36	1.13	0.52	0.21	0.08	0.09
LT 116	Lithic arenite (Missi 6p; File L.) (average of 4 samples)	77.22	10.56	1.46	2.21	1.05	1.67	1.52	2.53	0.77	0.22	0.41	0.07	0.05
LT 117	Felsic Volcanics (Sherridon) Unit 15 (average of 5 samples)	67.74	14.68	0.12	1.40	2.62	5.89	3.92	1.69	0.68	0.64	0.70	0.59	0.02
LT 118	Hornblende Parageneisses (Sherridon) Unit 11 in part (average of 7 samples)	55.76	14.96	1.93	9.41	4.34	7.61	1.90	1.37	1.47	0.64	0.78	0.32	0.20
LT 119	Fragmental amphibolites (Sherridon) Unit 13/13a (average of 17 samples)	52.01	16.15	1.79	9.26	5.46	8.94	2.57	0.70	1.39	1.59	0.56	0.14	0.19
LT 120	Massive low TiO2 amphib. (Sherridon) (parts of Unit 14) (average of 12 samples)	51.73	15.47	2.92	9.32	6.28	9.10	1.92	0.46	1.32	0.83	0.64	0.14	0.21
LT 121	Massive high TiO2 AMPHIB. (sherridon) (parts of Unit 14) (average of 6 samples)	44.65	15.57	3.13	12.82	6.07	9.36	1.75	0.37	1.60	1.62	2.32	0.26	0.25
LT 122	All massive Amphibolites (Sherridon) (Unit 14) (average of 18 samples)	49.37	15.50	2.99	10.49	6.21	9.19	1.87	0.43	1.42	1.09	1.20	0.18	0.22
LT 123	Basalt (Flin Flon area - Stauffer et al., 1975) (average of 12 samples)	54.35	16.07	3.09	9.68	5.15	7.01	2.83	0.57			0.70	0.17	0.20
LT 124	Sill. biot. gneiss (Sherridon) (average of 5 samples)	77.08	11.04	0.18	3.04	2.09	1.46	0.86	1.75	1.30	0.26	0.19	0.06	0.04
LT 125	Qtz.-feldspar gneiss (Sherridon) (average of 7 samples)	80.40	10.70	0.13	0.81	0.70	2.14	1.96	2.19	0.74	0.31	0.16	0.06	0.04
LT 126	Mafic biot. gneiss (Sherridon) (average of 10 samples)	67.64	14.00	1.14	4.82	2.07	3.22	1.86	3.07	1.10	0.44	0.37	0.13	0.12
LT 127	Biot. gar. schist (Sherridon) (average of 3 samples)	62.47	16.67	0.63	5.73	2.87	3.69	2.47	2.24	1.13	0.23	0.63	0.51	0.08
LT 128	Nokomis Gneiss (Fife L.) (average of 18 samples)	65.65	11.53	1.37	3.84	2.25	5.07	1.42	2.17	0.90	1.11	1.08	0.16	0.30
LT 129	Cummingtonite Gneiss (Sherridon)	52.61	16.06	2.09	9.82	6.62	5.61	2.91	0.77	1.41	0.75	1.02	0.26	0.19
LT 130	Low Ti Basaltic flows	51.73	15.47	2.92	9.32	6.28	9.10	1.92	0.46	1.32	0.83	0.64	0.14	0.21
LT 131	Pale-regolith on Basaltic flows (Flin Flon)	52.98	16.42	5.48	6.42	4.17	3.05	2.27	1.70	2.67	2.63	0.75	0.10	0.17
LT 132	Anthophyllite gneiss (Sherridon)	49.05	16.72	1.35	9.87	15.16	0.87	0.27	1.31	4.12	0.25	0.46	0.06	0.12
LT 133	Cordierite-Anthophyllite gneiss (Coronation Mine) from Byers, 1969	53.10	14.90	3.40	15.48	7.30	0.35	0.44	0.40	4.60	0.11	0.31	0.06	0.14
LT 134	Chlorite (Shakani Mine, Japan) from Shirozu, 1974	24.61	23.36	2.72	20.93	14.15	0.10	0.28	0.36	11.93				2.06

SAMPLE Number	Comments	SiO2	Al2O3	Fe2O3	FeO	MgO	CaO	Na2O	K2O	H2O	CO2	TiO2	P2O5	MnO
LT 139	Sample #34, sill-biot. gneiss unit 5a	73.00	13.90	0.30	1.90	2.21	2.82	1.50	1.10	2.40	0.80	0.24	0.10	0.04
LT 140	Sample #81, sill-biot. gneiss unit 5a	75.80	12.00		2.00	2.54	2.68	1.80	1.23	1.60	0.40	0.13	0.05	0.04
LT 141	Sample #126, sill-biot. gneiss unit 5a	75.60	10.50		3.60	3.28	0.79	0.80	3.00	1.10		0.16	0.07	0.04
LT 142	Sample #123, sill-biot. gneiss unit 5b	83.20	8.40	0.60	1.60	1.76	0.80	0.20	2.30	0.70	0.10	0.16	0.04	0.03
LT 143	Sample #131, sill-biot. gneiss unit 5b	77.80	10.10		6.10	0.66	0.19		1.14	0.70		0.26	0.04	0.05
LT 144	Sample #115, AT-GA Gneiss, Unit 10	43.60	16.20	1.90	12.90	17.50	0.47	0.10	2.97	4.20		0.49	0.07	0.17
LT 145	Sample #130 AT-GA Gneiss, Unit 10	63.40	12.60	0.60	10.40	8.36	0.49	0.20	0.86	1.40	0.20	0.24	0.04	0.10
LT 146	Sample #141 AT-GA Gneiss, Unit 10	51.76	17.20	0.90	10.10	12.70	2.38	0.80	0.52	2.70	0.80	0.77	0.10	0.12
LT 147	Sample #154 AT-GA Gneiss, Unit 10	37.60	20.90	2.00	6.10	22.10	0.12		0.88	8.20		0.34	0.04	0.08

Appendix B-6 Hydrothermally altered rocks at Steamboat Springs, Nev. (from Sigvaldson + White, 1962)

SAMPLE Number	Comments	SiO2	Al2O3	Fe2O3	FeO	MgO	CaO	Na2O	K2O	H2O	CO2	TiO2	P2O5	MnO
LT 48	granodiorite; depth 20' christobalite, (anatase + barite)	95.40	0.68	0.06	0.00	0.01	0.14	0.18	0.08	3.80	<.05	0.38	0.00	0.00
LT 49	granodiorite; depth 68' opal (py, anatase)	92.00	0.76	0.00	0.00	0.01	0.04	0.18	0.14	2.20	0.07	0.44	0.01	0.01
LT 50	granodiorite; depth 111' opal (py, marcasite, antase, barite)	90.50	0.58	0.00	0.00	0.00	0.21	0.18	0.16	1.90	0.06	56.00	0.02	0.00
LT 51	granodiorite; depth 114' alunite, opal (py, marc, anat.)	56.90	15.10	0.00	0.00	0.03	0.04	0.20	4.10	6.90	0.23	0.28	0.16	0.00
LT 52	granodiorite; depth 120' alunite (opai, py, marc, kaol.)	21.80	29.00	0.00	0.00	0.00	0.12	0.31	7.90	11.40	0.18	0.26	0.42	0.01
LT 53	granodiorite; depth 127' alunite, kaol (marc, py)	26.80	27.90	0.00	0.00	0.00	0.08	0.32	7.40	10.50	0.08	0.30	0.30	0.00
LT 54	granodiorite; depth 133' mont, kaol (alun., py)	69.40	15.60	0.00	0.00	2.10	0.53	0.22	3.00	7.30	0.12	0.32	0.06	0.09
LT 55	granodiorite; depth 145' mont, kaol (ill, marc py)	69.60	12.00	0.00	0.00	2.60	0.62	0.28	2.20	8.70	<.05	0.22	0.04	0.12
LT 56	granodiorite; depth 170' mont, kaol, ill, Mn-cc, (py)	61.30	12.50	0.00	0.50	1.60	4.50	0.40	3.60	8.10	2.90	0.26	0.06	0.25
LT 57	granodiorite; depth 217' mont, kaol, ill (py)	66.90	14.60	0.00	0.00	2.00	1.40	1.20	4.10	7.50	0.07	0.30	0.07	0.13
LT 58	andesite dike; depth 264' mont, Kspar, ill (py, cc)	58.00	17.80	0.50	0.16	1.90	2.20	0.64	3.20	13.80	0.18	0.46	0.20	0.06
LT 59	andesite dike; depth 281' mont, Kspar, ankerite, chl. (py)	54.20	17.10	0.40	1.20	2.90	5.00	1.80	3.00	8.50	0.73	0.50	0.36	0.73
LT 60	granodiorite; depth 335' ill, mont, chl, seric. (py)	68.60	15.40	0.40	1.20	1.80	0.71	0.35	5.30	5.30	0.04	0.37	0.07	0.04
LT 61	granodiorite; depth 358' ill, mont, chl (py, cc)	68.80	14.80	0.40	1.60	1.20	2.20	3.60	3.90	1.40	0.04	0.30	0.06	0.04
LT 62	granodiorite; depth 385' ill, mont (chl, ser, py)	69.70	15.20	0.80	0.10	1.00	1.60	2.30	4.10	4.40	0.02	0.31	0.07	0.02
LT 39	altered Arkose; depth 109'	97.20	10.30	0.40	0.50	0.25	0.92	1.10	5.60	1.61	<.05	0.34	0.02	0.01
LT 40	altered granodiorite; depth 155' qtz, ill, mont, (Kspar, cc, py + hem.)	81.00	9.60	0.30	0.30	0.31	0.45	0.66	4.30	1.30	<.15	0.16	0.00	0.00
LT 41	altered granodiorite; depth 306' ill, chl, Kspar (albite, py)	69.90	14.60	0.00	0.00	0.44	0.93	2.40	5.80	1.20	<.05	0.30	0.07	0.01
LT 42	altered granodiorite depth 450' ill, mont, ser, alb, chl, cc + py	65.40	13.60	0.10	0.30	1.00	4.20	2.00	4.40	2.00	2.60	0.30	0.08	0.10
LT 43	andesite dike; depth 482' ill, mont, qtz, chl, alb, py	65.40	16.40	0.40	0.80	0.70	0.65	0.66	4.20	5.20	<.05	0.52	0.20	0.06
LT 44	andesite dike; depth 512' ill, mont, qtz, chl, alb, py	66.60	16.10	0.00	0.30	1.40	0.31	0.54	4.20	3.40	<.05	0.47	0.23	0.00
LT 45	trachy-andesite dike; depth 532' ill, mont, qtz, alb, chl (py, cc)	64.00	16.50	0.70	0.70	1.10	0.94	2.80	4.00	4.20	0.08	0.49	0.09	0.03
LT 46	granodiorite; depth 562' ill, mont, chl (cc, ser, py)	68.00	16.00	0.80	2.10	0.61	2.50	3.20	3.50	1.30	0.68	0.47	0.12	0.10
LT 47	granodiorite; depth 574' ill, mont, chl, alb, cc, hem	67.10	14.50	0.40	1.90	0.68	1.40	3.20	4.60	2.80	0.67	0.49	0.08	0.11

Appendix B-7 Hydrothermally altered quartz monzonite at Roosevelt Hot Springs, Utah
(from Parry et al., 1980)

SAMPLE Number	Comments	SiO2	Al2O3	Fe2O3	FeO	MgO	CaO	Na2O	K2O	H2O	CO2	TiO2	P2O5	MnO
LT 135	intensely altered qtz monz 22.9m down, DDH 76-1	79.30	14.50	0.46		0.39	0.34	0.00	3.90			0.60		
LT 136	intensely altered qtz monz 32m down, DDH 76-1	66.20	22.20	2.10		0.50	0.98	0.00	5.00			1.10		
LT 137	moderately altered qtz monz 39.6m down, DDH 76-1	65.50	16.60	3.30		0.68	1.60	3.80	7.50			0.82		
LT 138	moderately altered qtz monz 57.9m down, DDH 76-1	62.00	20.20	3.90		1.20	2.30	4.10	5.50			0.72		

Appendix B-8 Hydrothermal alteration at the Millenbach Mine, Que.
(from Riverin and Hodgson, 1980)

SAMPLE Number	Comments	SiO2	Al2O3	Fe2O3	FeO	MgO	CaO	Na2O	K2O	H2O	CO2	TiO2	P2O5	MnO
LT 148	QFP Tuff, fresh ave. 9 analyses	76.56	12.08		2.22	1.18	1.10	3.64	2.30	0.61		0.29	0.03	
LT 149	QFP Tuff, weakly altered. ave. 6 analyses	76.23	12.06		2.62	1.92	0.64	1.68	2.96	1.57		0.28	0.03	
LT 150	QFP Tuff, spotted ave. 12 analyses	76.96	12.01		3.21	1.97	0.28	0.75	2.60	1.94		0.27	0.02	
LT 151	QFP Tuff, giant spots, ave. of 17 analyses	74.47	11.41		5.54	2.74	0.39	0.59	2.39	2.20		0.26	0.03	
LT 152	QFP Tuff, silicified ave. of 5 analyses	77.84	9.84		5.54	2.54	0.30	0.55	1.03	2.15		0.20	0.01	
LT 153	QFP Tuff, core ave of 10 analyses	68.36	10.68		10.80	4.99	0.42	0.64	0.39	3.42		0.25	0.05	

note; QFP = quartz-feldspar porphyry

Appendix B-9 Hydrothermally altered rocks from the Mattagami Lake Mine, Que.
(from Roberts + Reardon, 1978)

SAMPLE Number	Comments	SiO2	Al2O3	Fe2O3	FeO	MgO	CaO	Na2O	K2O	H2O	CO2	TiO2	P2O5	MnO
LT 158	Composite A 'unaltered' rhyodacitic tuff	75.20	10.25		5.61	1.06	0.63	2.80	1.07			0.26		0.11
LT 159	Composite B altered rhyodacitic tuff	75.09	6.62		7.18	6.14	0.09	0.03	0.29			0.24		0.10
LT 160	Composite C altered rhyodacitic tuff	59.37	8.14		14.19	6.91	3.56	0.19	0.17			0.24		0.22
LT 161	Composite D altered rhyodacitic tuff	45.00	12.10		15.46	16.87	1.15	0.07	0.44			0.21		0.32
LT 162	Composite E talc actinolite schist	58.00	1.10		12.30	21.30	2.10	0.07	0.07			0.02		0.34

Appendix B-10 Other altered rocks
(taken from literature)

SAMPLE #	DESCRIPTION	SiO2	Al2O3	Fe2O3	FeO	MgO	CaO	Na2O	K2O	H2O	CO2	TiO2	P2O5	MnO	Reference
LT 4	Average of 5 unaltered rhyolite porphyries	75.84	11.73	3.29	0.20	0.15	0.05	3.33	4.98			0.25	0.03	0.14	Agron and Bantor, 1981
LT 5	Average of 8 altered rhyolite porphyries	77.70	10.83	2.67	0.12	0.13	0.05	0.22	7.89			0.18	0.03	0.15	Ibid.
LT 1	Fresh Greywacke	55.50	16.30	7.82		5.40	3.17	1.51	3.20			0.90	0.13	0.08	Bischoff et al., 1981
LT 2	Greywacke altered by brine	56.90	16.60	7.03		7.42	0.86	2.19	1.98			0.94	0.14	0.03	Ibid.
LT 3	Greywacke altered by seawater	55.50	16.10	7.69		7.08	0.98	1.73	2.50			0.91	0.14	0.06	Ibid.

Appendix B-11 N. Maysville

Sample Ident. Number	SiO2	Al2O3	Fe2O3	FeO	MgO	CaO	Na2O	K2O	H2O	CO2	TiO2	P2O5	MnO	S	Ni	Cu	Co	Zn	Pb
DK-6109	57.75	14.97	6.72	1.32	3.35	1.2	3.3	4.18	4.31	0.73	1.12	0.55	0.15	0.006	71	123	22	247	<10
DK-6201	57.8	20.88	1.37	3.04	2.88	3.78	4.97	2.9	1.45	0.01	0.38	0.07	0.14	0.002	<10	<10	<10	319	46
DK-6202	77.5	11.32	0.56	0.96	1.15	0.46	1.28	4.52	1.39	0.15	0.19	0	0.11	0.001	<10	43	<10	2700	64
DK-6203	45.05	2.9	13.78	8.12	17.2	5.42	0.2	0.37	3.08	0.29	0.04	0.057	2.09	0.038	<10	1470	12	7300	1950
DK-6204	47.05	5.18	4.85	12.7	19	2.82	0.23	2.53	2.82	0.44	0.99	0.064	1.77	0.006	<10	244	12	5600	208
DK-6205	75.1	11.52	1.38	1.48	1.72	0.3	0.68	3.32	2.33	0.12	0.16	0.012	0.36	0.002	<10	252	11	1.00%	1860
DK-6206	54.2	16.1	2.63	7.42	7.9	0.086	0.23	6.58	2.47	0.03	0.22	0.036	0.7	0.003	<10	197	<10	9200	98
DK-6207	74.75	10.66	4.1	3.28	1.75	0.12	0.13	2.16	1.75	0.13	0.19	0.027	0.42	0.008	<10	640	<10	1700	<10
DK-6208	48.9	3.2	39.51	4.74	0.1	0.25	0.0042	0.01	1.76	0.36	0.07	0.067	0.08	0.014	<10	6200	<10	1100	<10
DK-6208b	42.6	10.1	23.27	10.28	3.4	3.02	0.22	1.61	2.41	0.16	0.26	0.085	1.27	0.01	<10	7600	14	2400	41
DK-6209	62.5	10.04	9.16	5.92	3.78	1.38	0.042	2.52	2.47	0.1	0.21	0.024	0.68	0.005	<10	3350	12	4900	36
DK-6210	88.9	1.61	5.78	1.8	0.3	0.22	0.026	0	0.9	0.18	0.04	6E-04	0.09	0.009	<10	2500	<10	800	<10
DK-6101	73.4	11.86	3.23	2.08	1.6	0.04	0.35	3.76	1.34	0.14	0.14	0.006	0.12	0.002	<10	354	<10	1.699%	98
DK-6102	78.6	10.96	0.91	1.24	1.42	0.48	1.22	3.12	1.31	0.17	0.14	0.005	0.14	0.001	<10	37	<10	3100	48
DK-6103	75.5	11.58	1.66	2.18	2.4	0.74	1.08	2.49	1.66	0.26	0.19	0.016	0.14	0.001	<10	105	<10	2200	36
DK-6104	79	9.1	2.4	4.54	1.22	0.074	0.096	1.78	1.19	0.1	0.14	0.034	0.21	0.006	<10	83	<10	247	<10
DK-6105	70.85	10.96	3.01	6.08	2.9	0.13	0.15	3.26	2.34	0.19	0.53	0.099	0.14	0.005	<10	1150	<10	560	47
DK-6106	6.5	4.4	62	24	0.32	0.066	0.33	0.11	0.72	0.12	0.07	0.5	0.36	0.001	<10	1540	12	2800	<10
DK-6107	72	12.46	3.81	0.48	1.28	0.36	1.58	3.45	3.12	0.76	0.41	0.082	0.1	0.003	<10	42	<10	205	<10
DK-6211	53.8	9.16	21.55	3.46	2.1	1.15	0.04	1.27	2.97	0.36	0.26	0.069	0.58	0.054	5	1.53	11	1.02%	58
DK-6212	62.05	13.1	3.53	7.18	2.65	0.7	0.73	3.36	3.08	0.73	0.66	0.13	0.5	0.013	<10	9600	11	1900	107
DK-6213	80.8	10.31	1.72	0.4	0.32	0.66	4.32	0.46	0.7	0.28	0.15	0.036	0.035	0.003	<10	22	<10	54	27
DK-6215	45.65	15.24	4.25	7.56	8.25	10.5	1.83	1.4	3.16	0.46	1.2	0.15	0.28	0.004	94	64	48	343	<10
DK-6216	47.85	15.95	3.3	6.86	8.8	10.1	1.98	1.44	2.5	0.03	0.62	0.12	0.29	0.003	120	18	42	254	<10
DK-6217	47	15.76	4.17	6.52	8.25	10.1	1.52	2.16	2.96	0.21	0.8	0.15	0.32	0.002	110	15	44	289	<10
DK-6307	46.5	6.16	3.26	6.38	15.55	10.65	0.28	0.06	5.13	1.2	0.04	0.078	3.9	0.16	<10	367	10	2050	4100
DK-6306	32	9.74	9.64	7.26	9.9	0.18	0.07	0.11	9.43	0.57	0.25	0.17	0.58	0.007	<10	1020	64	16.0%	1660
DK-6305	73.4	13.07	1.43	1	3.08	1.83	0.57	3.24	1.89	0.07	0.21	0.032	0.15	0.002	1	28	2	1810	135
DK-6304	71.65	13.98	2.35	2.32	1.83	0.88	1.37	1.4	1.68	0.15	0.22	0.048	0.1	0.088	6	1655	3	1.20%	170
DK-6303	62.9	13.58	5.21	5.86	3.64	0.94	0.32	3.04	2.33	0.1	0.29	0	0.43	0.014	2	1290	18	8675	81
DK-6302	53.6	15.65	7.71	4.08	3.22	0.75	0.28	2.4	3.41	0.31	0.36	0.007	0.23	0.017	4	1.66%	17	2.92%	110
DK-6301	86.5	6.1	1.7	1.68	1.08	0.018	0.037	0.6	0.66	0.11	0.01	0.007	0.037	0.019	<10	305	<10	9700	30
DK-6799:1	79.6	10.72	1.94	0.36	1.62	0.056	0.25	2.53	1.95	0.45	0.18	0.052	0.05	0.004	<10	8	<10	73	57

APPENDIX C Formulas for the Calculation of Parameters Used in Plotting Exercises (all oxides are in weight percentages).

Niggli Values:

$$\text{Let } Z = \left\{ \frac{Al_2O_3}{102} + \frac{2(Fe_2O_3)}{160} + \frac{FeO}{72} + \frac{MnO}{71} + \frac{MgO}{40} + \frac{Na_2O}{62} + \frac{CaO}{56} + \frac{K_2O}{94} \right\}$$

$$al = \left[\frac{\frac{Al_2O_3}{102}}{Z} \right]$$

$$si = \left[\frac{\frac{SiO_2}{60}}{Z} \right]$$

$$c = \left[\frac{\frac{CaO}{56}}{Z} \right]$$

$$alk = \left[\frac{\frac{Na_2O}{62} + \frac{K_2O}{94}}{Z} \right]$$

$$ti = \left[\frac{\frac{TiO_2}{80}}{Z} \right]$$

$$p = \left[\frac{\frac{P_2O_5}{147}}{Z} \right]$$

$$k = \left[\frac{\frac{K_2O}{94}}{\frac{K_2O}{94} + \frac{Na_2O}{62}} \right]$$

$$fm = \left[\frac{\frac{2(Fe_2O_3)}{160} + \frac{FeO}{72} + \frac{MnO}{71} + \frac{MgO}{40}}{Z} \right]$$

$$mg = \left[\frac{\frac{MgO}{40}}{fm} \right]$$

Parameters for the Method of Garrels and MacKenzie (1971):

$$\text{"y" coordinate} = \log_{10}\left(\frac{SiO_2}{Al_2O_3}\right)$$

$$\text{"x" coordinate} = \log_{10}\left(\frac{Na_2O + K_2O}{K_2O}\right)$$

Parameters for the Method of La Roche (1974):

$$\text{"MgO"} = \left(\frac{MgO}{MgO + Na_2O + K_2O}\right) 100\%$$

$$\text{"Na}_2\text{O"} = \left(\frac{Na_2O}{MgO + Na_2O + K_2O}\right) 100\%$$

$$\text{"K}_2\text{O"} = \left(\frac{K_2O}{MgO + Na_2O + K_2O}\right) 100\%$$

APPENDIX D LIST OF ABBREVIATIONS

qtz	quartz
fldspr	feldspar
biot	biotite
musc	muscovite
sill	sillimanite
garn	garnet
ser	sericite
mgt	magnetite
epid	epidote
amph	amphibole
cord	cordierite
anth	anthophyllite
alm	almandine
staur	staurolite
ab	albite
kspr	K-feldspar
plag	plagioclase
or	orthoclase
IF	iron formation
fm	formation
mont	montmorillonite
chl	chlorite
py	pyrite
ill	illite
cc	calcite
kaol	kaolinite
hem	hematite
alun	alunite
marc	marcosite
monz	monzonite